An ACI Technical Publication

SYMPOSIUM VOLUME

Evaluation of Concrete Bridge Behavior through Load Testing – International Perspectives

Editors:
Eva Lantsoght and Pinar Okumus

SP-323

American Concrete Institute
Always advancing

Evaluation of Concrete Bridge Behavior through Load Testing – International Perspectives

Editors:
Eva Lantsoght and
Pinar Okumus

American Concrete Institute
Always advancing

SP-323

First printing, May 2018

On the cover: Load test of a cable stayed bridge over Wisłok River, Poland. Photograph by Dr. K. Wilde.

Printed in the United States of America

Editorial production: Susan K. Esper

ISBN-13: 978-1-64195-007-7

Preface

Load testing of concrete bridges is a practice with a long history. Historically, and particularly before the unification of design and construction practices through codes, load testing was performed to show the travelling public that a newly built bridge was safe for use. Nowadays, with the aging infrastructure and increasing loads in developed countries, load testing is performed mostly for existing structures either as diagnostic or proof tests. For newly built bridges, diagnostic load testing may be required as a verification of design assumptions, particularly for atypical bridge materials, designs, or geometries. For existing bridges, diagnostic load testing may be used to improve analysis assumptions such as composite action between girders and deck, and contribution of parapets and other nonstructural members to stiffness. Proof load testing may be used to demonstrate that a structure can carry a given load when there are doubts with regard to the effect of material degradation, or when sufficient information about the structure is lacking to carry out an analytical assessment.

In recent years, both researchers and practicing engineers worldwide have been refining load testing methods to balance accuracy, cost, effort, and time, and have been addressing increasingly complex structures and situations. To exchange international experiences among a global group of researchers and compare load testing methods used internationally, ACI Committee 342 organized two sessions titled “Evaluation of Concrete Bridge Behaviour through Load Testing – International Perspective” at the 2017 ACI Fall Convention in Anaheim, CA. This Special Publication contains several technical papers from experts who presented their work at these sessions, in addition to papers submitted for publication only.

This Special Publication combines contributions from different regions of the world, and in particular from Denmark, Germany, the Netherlands, Poland, Spain, Sweden, and from different regions in the United States. The technical papers consider both theoretical and practical aspects of load testing, discuss different levels of bridge behaviour assessment such as visual inspections, modelling, and load testing. They introduce the reader to the codes and guidelines that may only be available in some countries. The impact of differences in live loads, design codes, reserve capacities, age of structures, construction practices between Europe, and North America on assessment of concrete bridges is reflected by case studies. Recent developments with regard to codes and standards around the world for load testing are discussed, and open questions for future developments are highlighted by the authors.

The wide variety of concrete bridge structures investigated included short-span reinforced concrete slab bridges, older reinforced concrete earth-filled arch bridges, bridges that have been damaged and/or retrofitted, and modern prestressed concrete bridges with new materials. Reasons why load testing is required also vary and include apparent damage, opportunities created by decommissioned bridges, necessity to carry super heavy vehicles, use of unique materials or geometry, and absence of design plans. Results of testing bridges under static or dynamic service loads create knowledge on expected service

performance and allow load ratings, while testing decommissioned bridges to near collapse or collapse reveals true capacity and the level of conservatism in design assumptions. Several papers highlight vehicles or rigs designed specifically for reuse in standardized load testing. Others use recent technology such as 3-D scanning or digital image correlation to collect data, in addition to traditional methods such as strain gauges. As such, this Special Publication provides a global perspective on strategies for assessing the in-service performance of concrete bridges, and an overview of the state-of-the-art with regard to load testing internationally.

Overall, in this Special Publication, authors from different backgrounds and geographical locations share their experiences and perspectives on load testing and its impact on understanding concrete bridge behaviour. The coeditors, Dr. Pinar Okumus and Dr. Eva Lantsoght, are grateful for the contributions of the Special Publication authors and sincerely value the time and effort of the authors in preparing the papers in this volume.

Eva Lantsoght and Pinar Okumus
Co-Editors

TABLE OF CONTENTS

ASSESSMENT OF SLAB BRIDGES THROUGH PROOF LOADING IN THE NETHERLANDS

Eva O. L. Lantsoght, Cor van der Veen, Ane de Boer and Dick A. Hordijk

Synopsis: A large subset of the Dutch bridge stock consists of reinforced concrete slab bridges, for which assessment often results in low ratings. To prioritize the efforts of the bridge owner, more suitable assessment methods for slab bridges are necessary. Research efforts over the past years resulted in the development of several methods, at levels requiring increasing costs, time, and effort for increasing accuracy. The last option, when an analytical assessment is not possible due to uncertainties, is to use proof load testing to evaluate the bridge directly. To develop recommendations for the proof load testing of reinforced concrete slab bridges for the Netherlands, different methods are combined: pilot proof load tests on bridges with and without material damage, a collapse test, tests on beams taken from an existing bridge and new beams with similar dimensions cast in the laboratory, and an extensive literature review. The result of this study is a set of recommendations that describe how to prepare and execute a proof load test, and how to analyze the results. This paper summarizes the research program about proof load testing from the Netherlands and gives an overview of the currently developed recommendations and topics for further research.

Keywords: field testing; flexure; measurements; proof load testing; reinforced concrete; shear; slab bridges

ACI member **Eva O. L. Lantsoght** is a full professor at Universidad San Francisco de Quito, a structural engineer at Adstren and a researcher at Delft University of Technology. She is a member of ACI 445-0D Shear Databases and of ACI-ASCE 421, Design of Reinforced Concrete Slabs, and an associate member of ACI 342, Evaluation of Concrete Bridges and Bridge Elements, ACI 437, Strength Evaluation of Existing Concrete Structures, and ACI-ASCE 445, Shear and Torsion.

Cor van der Veen is an associate professor at Delft University of Technology, Delft, The Netherlands. He received his M.Sc. and Ph.D. from Delft University of Technology. He is a member of various National Committees. His research interests include (very) high strength (steel fiber) concrete, concrete bridges and computational mechanics.

Ane de Boer is a senior advisor at Rijkswaterstaat, the Ministry of Infrastructure and the Environment, Utrecht, The Netherlands. He received his M.Sc. and Ph.D. from Delft University of Technology. He is a member of some National Committees, *fib* COM3 and member of an IABSE Working Committee. His research interests are remaining lifetime, existing structures, computational mechanics, traffic loads and composites.

Dick A. Hordijk is a full professor at Delft University of Technology, Delft, the Netherlands. He received his M.Sc. and Ph.D. in civil engineering from Delft University of Technology, Delft, the Netherlands, in 1985 and 1990, respectively. His research interests include concrete fracture mechanics, assessment of existing structures, structural application of new concrete types and forensic engineering.

INTRODUCTION

Existing bridges in the Netherlands

The expansion of the Dutch road network after the Second World War included the construction of a large number of bridges. These bridges are now approaching the end of their originally devised service life of 80 years. To evaluate if extension of the service life of these bridges is possible, and if they are suitable for carrying the current traffic, assessment of these structures is required.

A large subset of the Dutch bridge stock consists of reinforced concrete slab bridges. Of the bridges built during the 1960s and 1970s, 50% are reinforced concrete slab bridges. In later periods, the majority of bridges were prestressed prefabricated girder bridges. The reinforced concrete slab bridges are typically short span bridges in or over the highway, and can be a single span or multiple spans. A first assessment, based on the code provisions for the design of new structures (Vergoossen et al., 2013), showed that about 600 of these bridges do not fulfil these code requirements. In many cases, the shear capacity was insufficient. This observation resulted from the fact that the applied live loads according to NEN-EN 1991-2:2003 (CEN, 2003) are heavier than those used in the past, and that the shear provisions described in NEN-EN 1992-1-1:2005 (CEN, 2005) generally lead to lower shear capacities than the previously governing national code NEN 6720:1995 (Code Committee 351001, 1995).

Assessment based on Levels of Approximation

The *fib* Model Code 2010 (fib, 2012) introduced the Levels of Approximation concept for the first time. A low Level of Approximation is a conservative method that can be used, for example, for preliminary design. If the assessment requires a more accurate answer, a higher Level of Approximation is necessary. This higher Level of Approximation will require more time to set up the model, and increased computational time and effort as compared to a lower Level of Approximation. Belletti et al. (2015) recommend different Levels of Approximation for the shear and punching provisions (Belletti et al., 2015), as used in the *fib* Model Code 2012 (fib, 2012). Figure 1 illustrates the concept of using Levels of Approximation.

For the assessment of the shear capacity of reinforced concrete slab bridges, a method with Levels of Approximation was developed as well (Lantsoght et al., 2017a), called Levels of Assessment. In total, four Levels of Assessment were identified:

1. Level of Assessment 1 – Quick Scan method: the Quick Scan method (Lantsoght et al., 2013b; Lantsoght et al., 2016f) is a fast, spreadsheet-based calculation that mimics a hand calculation. The provisions of the Eurocodes NEN EN 1991-2:2003 (CEN, 2003) and NEN-EN 1991-2-2:2005 (CEN, 2005) are followed and extended with recommendations based on slab experiments (Lantsoght et al., 2013c; Lantsoght et al., 2014b; Lantsoght et al., 2015a; Lantsoght et al., 2015c). The result is a Unity Check: the ratio of the shear stress caused by the loads (self-weight, superimposed dead load, and live loads) to the shear capacity. If the Unity Check is smaller than or equal to one, no further refinement of the assessment method is required and the code requirements for the bridge are fulfilled. If the Unity Check is larger than 1, a higher Level of Assessment is necessary.

2. Level of Assessment 2 – Linear finite element models: at Level of Assessment 2, the shear stresses caused by the loads (self-weight, superimposed dead load, live loads consisting of distributed lane loads and concentrated truck loads) is determined by making a linear finite element model of the superstructure. The resulting peak shear stress is then distributed transversely over a width of $4d_l$, with d_l the effective depth to the longitudinal reinforcement (Lantsoght et al., 2013a; Lantsoght et al., 2014a). This averaged shear stress is then compared to the shear capacity from the provisions of NEN-EN 1992-1-1:2005 (CEN, 2005) to determine the Unity Check based on Level of Assessment 2. If the Unity Check is smaller than or equal to 1, the structure fulfills the code requirements. If the Unity Check is larger than 1, the assessment needs to be continued at a higher Level of Assessment.
3. Level of Assessment 3 – nonlinear finite element models and probabilistic analyses. Recommendations (Rijkswaterstaat, 2016) were developed for the use of nonlinear finite element models, and the required safety formats have been described (Belletti et al., 2010; Belletti et al., 2013). The result of such a calculation is an estimate of the full behavior of the bridge from initial loading to the ultimate limit state. As such, the model gives insight in the capacity beyond the code provisions. If the applied loading results in an action that is lower than the determined capacity, the structure fulfils the requirements. This Level of Assessment can also include probabilistic calculations (Lantsoght et al., 2015b; Lantsoght et al., 2016e). Recommendations for this application can be found in the Probabilistic Model Code (JCSS, 2001; Vrouwenvelder et al., 2002).
4. Level of Assessment 4 – field testing. If the calculations at lower Levels of Assessment show that the structure does not have sufficient capacity to carry the prescribed loads, but when there are reasons to expect additional capacity, the assessment can be based on a field test. A proof load test, in which the bridge is loaded with a load representative of the factored live loads, can lead to an experimental approval of the bridge. A diagnostic load test, in which the bridge is loaded with a lower load and the structural response is measured, can be used to update the models developed with Level of Assessment 2 or 3. Field testing only brings new information when the uncertainties are large (Lantsoght et al., 2017b), and when it has been defined prior to the test what are the objectives, and what needs to be measured to fulfill these objectives. Load testing is significantly more expensive than the other Levels of Assessment, and therefore a solid preparation of a load test is always required. This preparation should explore the possible benefits of a load test, and weigh these benefits against the cost of testing and/or strengthening or replacing of the considered bridge.

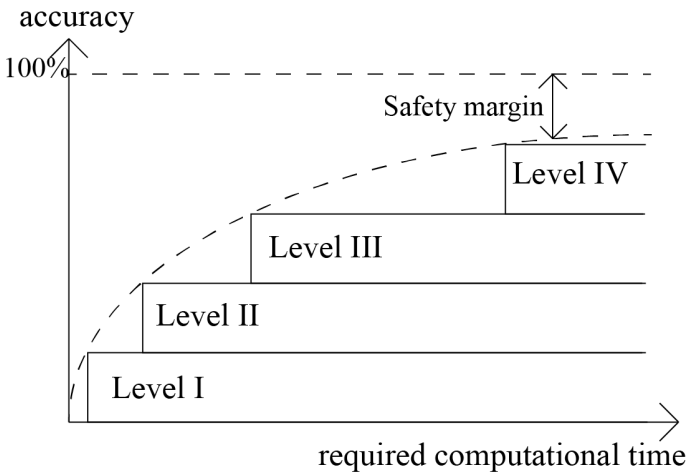

Figure 1 — Principle of Levels of Approximation (fib, 2012).

RESEARCH SIGNIFICANCE

Load testing is not a new practice, and extensive research from the past about load testing is available. However, many load testing guidelines and codes prescribe practices that are based on rules of thumb. The presented research combined field testing, a collapse test, and additional laboratory testing to develop evidence-based recommendations for the determination of the target proof load, for the loading protocol, and for the threshold values of the measurements to be used during proof load testing. As such, these results and the experience gathered in the Netherlands can be valuable for the international community of bridge engineers, to improve the current practice of proof load testing.

LITERATURE REVIEW

Two different types of load tests exist: diagnostic load tests and proof load tests. In a diagnostic load test (Fu et al., 1997; Matta et al., 2008; Moses et al., 1994; Olaszek et al., 2014; Russo et al., 2000; Sanayei et al.,

2016; Velázquez et al., 2000) a low load is applied and the structural response is measured. These measurements then lead to updating of the analytical model, often a finite element model. The updated model can subsequently be used to improve the assessment of the structure. The field measurements can give information about the transverse flexural distribution, the stiffness of the structure and the effect of non-structural members such as parapets and barriers on the stiffness of the system, and the effect of frozen bearings on the distribution of forces.

In a proof load test (Anay et al., 2016; Arangjelovski et al., 2015; Casas and Gómez, 2013; Faber et al., 2000; Olaszek et al., 2012; Saraf et al., 1996; Stewart and Val, 1999), the bridge is loaded with a load that is representative of the factored live load. If the bridge can carry this load level without signs of distress, the test shows that the structure fulfills the code requirements. Since a proof load test involves high loads, the applied sensors become important to evaluate if further loading may lead to irreversible damage to the structure. For this purpose, the measurements from the sensors are compared to thresholds, the so-called "stop criteria." If a stop criterion is exceeded, further loading is not permitted and the proof load test needs to be terminated, even when the target proof load has not been achieved yet. The structure may then perhaps fulfil lower requirements, depending on how high the load was at exceedance of the stop criterion. This concept for proof load testing is shown in Figure 2, in which G_1 is the effect of the permanent loads, $effR_u$ is the capacity of the structure, F_{lim} is the load for which a stop criterion is exceeded, $ext.F_{lim}$ is the load above the permanent loads G_1 for which a stop criterion is exceeded, G_{dj} is the additional permanent loads, Q_d are the live loads, $ext.F_{target}$ is the proof load that should be applied in the test in addition to the already present load G_1, and F_{target} is the total target proof load. Additionally, the measurements can be interesting for comparison to the output of a calculation carried out at Level of Assessment 3.

The prescribed stop criteria depend on the considered failure mode. The existing codes for proof load testing of concrete bridges from France (Cochet et al., 2004), Poland (PN-S-10040/99, 1999), and the Czech Republic and Slovakia (Frýba and Pirner, 2001) include stop criteria for flexure that are based on a maximum deflection and crack width. Other guidelines, such as the AASHTO LRFR Manual for Bridge Evaluation (AASHTO, 2016) mention in a more general way that the proof load test shall not result in non-linear behavior of the structure and/or irreversible damage.

A full literature review on the topic was developed as part of this research program (Lantsoght, 2016; Lantsoght et al., 2017h).

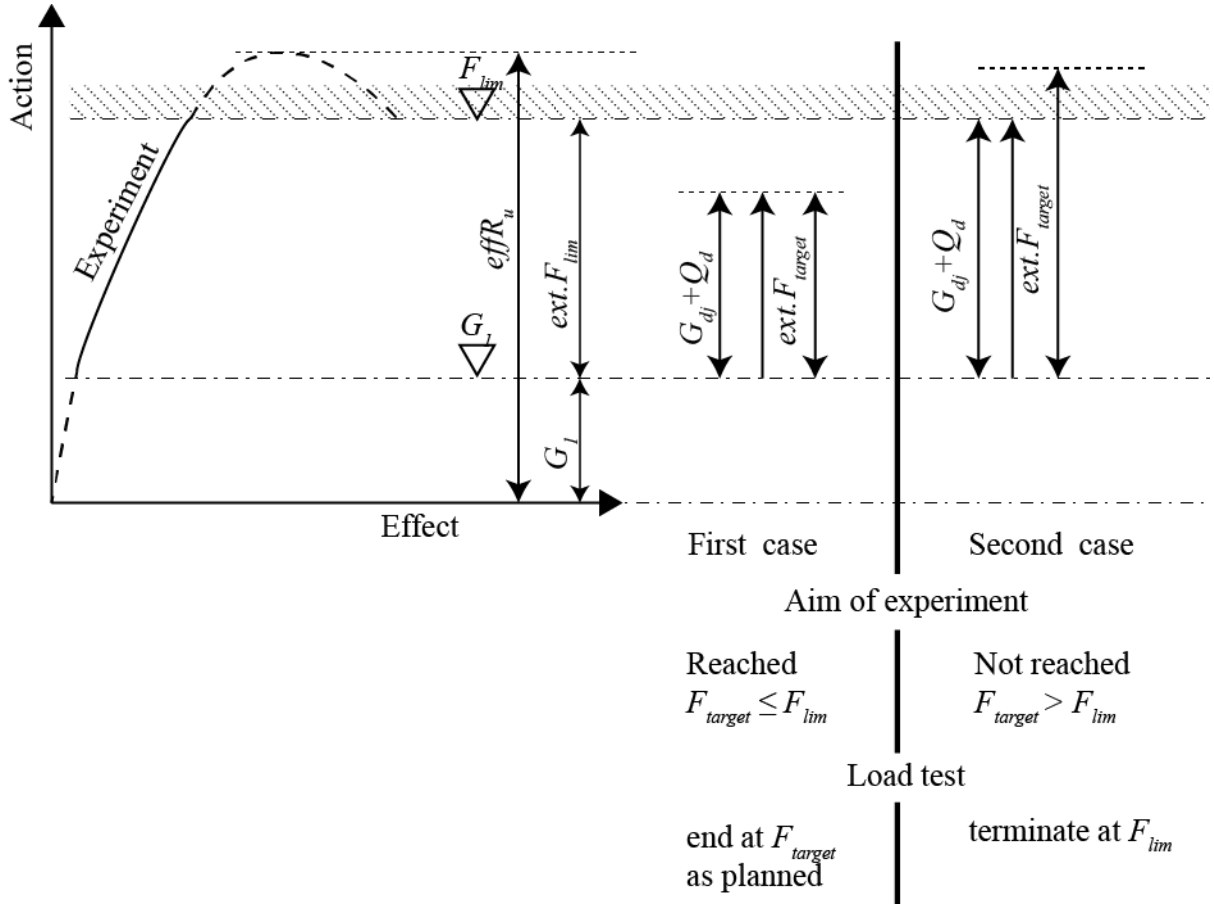

Figure 2 — Safety philosophy for proof load testing, originally proposed in the German guidelines for proof load testing (Deutscher Ausschuss für Stahlbeton, 2000).

PROOF LOAD TESTING RESEARCH IN THE NETHERLANDS

Pilot proof load tests

Over the past decade, a number of pilot proof load tests have been carried out in the Netherlands (Lantsoght et al., in press-b). The first pilot test was carried out on the viaduct Heidijk in 2007 (Dieteren and den Uijl, 2009), a continuous reinforced concrete slab bridge. This viaduct suffered material damage caused by alkali silica reaction (ASR), which resulted in an insufficient shear capacity upon assessment, as in the Netherlands the shear capacity of elements with ASR damage is assumed to be 75% of the capacity according to the code provisions (den Uijl and Kaptijn, 2004). The load in this test was applied by using a loading frame, ground anchors, and jacks. The maximum applied load was 640 kN (144 kip), which resulted in the conclusion that the viaduct could carry vehicles of 30 metric tons (66 kip).

The second test was carried out in 2009 on viaduct Medemblik, which is a girder bridge with damage caused by reinforcement corrosion. For this case, the BELFA vehicle from Germany (a special vehicle used for load testing) (Bretschneider et al., 2012) was used. The maximum applied load was 545 kN (123 kip) and the conclusion was that the viaduct could carry one lane of vehicles of 30 metric tons (66 kip).

The first two pilot proof load tests were carried out with minimal involvement of Delft University of Technology. In the subsequent tests, the involvement of Delft University of Technology became more important, and the goals of the proof load tests shifted from the evaluation of isolated cases to a broader research program.

The first pilot proof load test that had partial involvement of Delft University of Technology was the test on the viaduct Vlijmen Oost in 2013 (Fennis et al., 2014), see Figure 3a. This viaduct is a continuous reinforced concrete solid slab bridge with material damage caused by ASR. The BELFA vehicle applied the load, and the maximum applied load was 900 kN (202 kip). A difficulty in this test was that one lane had to remain available for traffic, whereas only two lanes were available for testing (one lane with the BELFA and one lane with a crane to provide additional counterweight). As a result, the level of noise on the measurements was rather large.

In 2014, the Halvemaans Bridge (Fennis and Hordijk, 2014), see Figure 3b, was tested. This single-span reinforced concrete slab bridge from 1939 was evaluated for flexure. In the proof load test, a system with a load spreader beam, counterweights, and hydraulic jacks applied the load in a cyclic manner. The maximum applied load was 900 kN (202 kip), which showed that the bridge fulfils the requirements of the Dutch guidelines for the assessment of bridges (Richtlijn Beoordelen Kunstwerken, RBK, RTD 1006:2013 1.1) (Rijkswaterstaat, 2013) at the Reconstruction level.

Figure 3 — Overview of bridges tested by Delft University of Technology in proof load testing program: (a) Viaduct Vlijmen Oost; (b) Halvemaans Bridge; (c) Viaduct Zijlweg; (d) Viaduct De Beek.

In June 2015, the viaduct Zijlweg (Koekkoek et al., 2015; Lantsoght et al., 2017b), see Figure 3c, was proof load tested. This continuous reinforced concrete slab bridge has material damage caused by ASR. As a result, there were concerns with regard to the shear capacity of the bridge. The first span was tested at two positions: a shear-critical and a flexure-critical position by using a combination of a steel spreader beam, counterweights, and hydraulic jacks. A cyclic loading protocol was used. The maximum loads were 1368 kN (308 kip) for the bending moment test and 1377 kN (310 kip) for the shear test. With these loads, the conclusion is that the viaduct fulfils the requirements of the RBK at the Design level.

In November 2015, the viaduct De Beek (Koekkoek et al., 2016; Lantsoght et al., 2017f; Lantsoght et al., in press-a), see Figure 3d, was proof load tested. This continuous reinforced concrete slab bridge has significant flexural cracking. It was found upon assessment that the flexural capacity of the bridge is insufficient. As a result, the two lanes available on the bridge were reduced to a single lane. Two positions in the first span were tested: a shear-critical and a flexure-critical position. Again, a combination of a steel spreader beam, counterweights, and hydraulic jacks, and a cyclic loading protocol loaded the bridge. The maximum loads were 1751 kN (394 kip) for the bending moment test and 1560 kN (351 kip) for the shear test. With these loads, it the first span fulfills the requirements of the RBK at the Design level for two lanes of traffic. However, testing the second span was not possible, because this would require closing of the highway. This span had an even higher Unity Check than the first span. For the second span, an assessment assuming plastic redistribution was carried out, for which it was found that two lanes of traffic can be permitted, provided that no corrosion damage has occurred which would further reduce the available amount of flexural reinforcement.

Collapse test

In addition to the pilot proof load tests, a collapse test was carried out on two spans of the Ruytenschildt Bridge (Lantsoght et al., 2016a; Lantsoght et al., 2016b; Lantsoght et al., 2016c; Lantsoght et al., 2016e; Lantsoght et al., 2017e) in August 2014. The Ruytenschildt Bridge, see Figure 4, was a five-span continuous reinforced concrete slab bridge. A new structure for functional reasons now replaces the previous Ruytenschildt Bridge. Therefore, the old bridge could be tested to collapse for research purposes. A steel spreader beam, counterweights, and hydraulic jacks, which permitted the use of a cyclic loading protocol, loaded the bridge. The maximum applied load in the first span was 3049 kN (685 kip), which was the maximum available counterweight. The cross-section did not fail, but showed signs of flexural distress. For the test in the second span, additional counterweight was ordered, and the maximum load was 3991 kN (897 kip). This load caused yielding of the flexural reinforcement, large cracking, and a settlement of the pier.

The results of the collapse tests give information for the verification of proposed calculation methods for reinforced concrete slabs, such as the Extended Strip Model (Lantsoght et al., 2016d; Lantsoght et al., 2017c; Lantsoght et al., 2017d). The results have also been used to evaluate the margin of safety (Lantsoght, 2017a) provided by the stop criteria from existing codes and guidelines such as the German guidelines (Deutscher Ausschuss für Stahlbeton, 2000) and ACI 437.2M-13 (ACI Committee 437, 2013), as well as stop criteria proposed as part of this research (Lantsoght et al., 2017g). As such, the results of the tests on the Ruytenschildt Bridge have been important for the development of the recommendations for proof load testing of reinforced concrete slab bridges.

Figure 4 — Ruytenschildt Bridge in 2014.

Laboratory testing

Two sets of laboratory experiments have been carried out and analyzed to develop recommendations for proof load testing. The experiments consist of testing reinforced concrete beams without shear reinforcement in a cyclic manner. The first set of experiments consists of five tests on three beams sawn from the Ruytenschildt Bridge (Lantsoght et al., 2016b). Four of the experiments resulted in a flexural failure, and one test resulted in a flexural shear failure. Figure 5 shows the observed failure modes. All experiments were carried out in a cyclic manner, so that they could be used to evaluate the margin of safety of the stop criteria from the German guidelines and from ACI 437.2M-13 (Lantsoght et al., 2016g). This analysis could then be used to develop and improve recommendations for stop criteria for proof load testing (Lantsoght, 2017c).

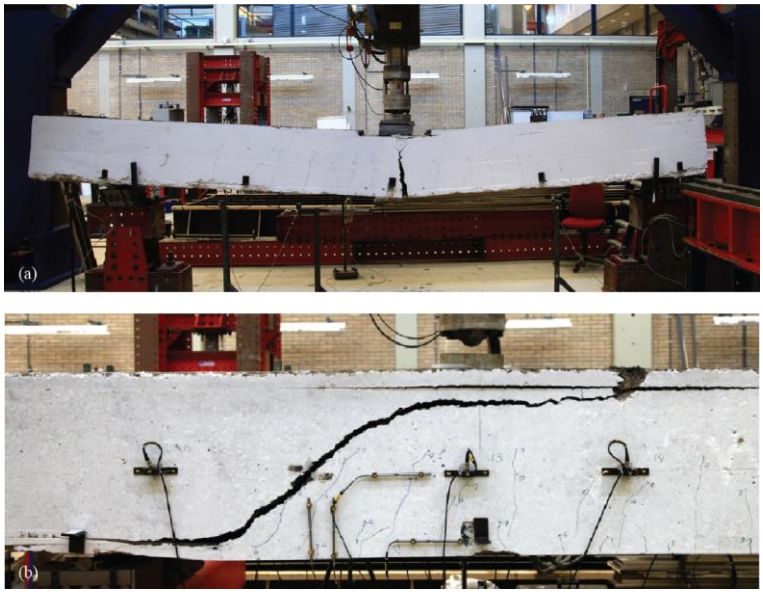

Figure 5 — Failure modes observed in the beams sawn from the Ruytenschildt Bridge: (a) flexural failure, RSB01; (b) shear failure, RSB03A (Yang, 2015).

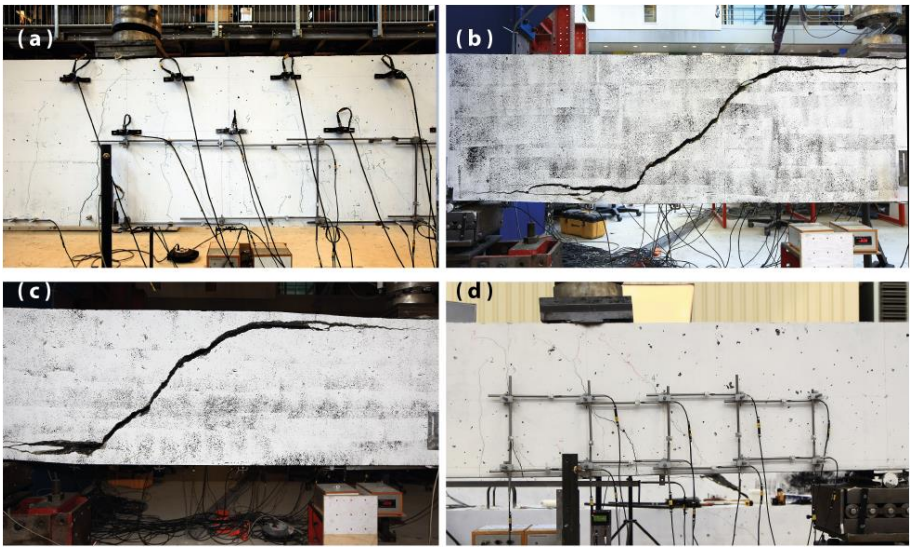

Figure 6 — Failure modes observed experiments on beams cast in the lab: (a) flexural failure of a beam without flexural cracks, P804A1; (b) shear failure of a beam with flexural cracks, P804A2; (c) shear failure of a beam without flexural cracks, P804B; (d) flexural failure of a beam with flexural cracks, P502A2.

The second set of experiments consists of four tests on two beams reinforced with plain bars, and cast in the laboratory (Lantsoght et al., 2017g). These tests studied the following parameters to develop recommendations for the loading protocol:

- loading speed
- number of cycles

- length of loading at the peak of a load cycle
- length of resting period between load cycles
- load levels

Additionally, the results were used to evaluate the margin of safety of the stop criteria from the German guidelines and from ACI 437.2M-13, as well as to develop new recommendations for stop criteria. Two experiments resulted in a flexural failure, and two experiments resulted in a shear failure. The presence of flexural cracks was found to have an effect on the margin of safety provided by the stop criteria. Therefore, this research resulted in the recommendation that for the stop criteria, four different cases need to be distinguished:

1. Flexural failure of an element without flexural cracks, see Figure 6a.
2. Flexural failure of an element with flexural cracks, see Figure 6d.
3. Shear failure of an element without flexural cracks, see Figure 6c.
4. Shear failure of an element with flexural cracks, see Figure 6b.

Note that the terms without and with flexural cracks refer to the state of the element at the beginning of the test. A test on a member that is precracked by a previous experiment is denoted as a test on a member with flexural cracks, whereas a test on a virgin specimen is denoted as a test on a member without flexural cracks.

RESULTING RECOMMENDATIONS FOR PROOF LOAD TESTING

Recommendations for the preparation of proof load tests

In the Netherlands, the procedure of using the Levels of Assessment is started when an inspection leads to the observation of material damage (such as damage caused by ASR), or when it is expected that the bridge does not fulfil the current requirements. These inspections are carried out once every six years. If regular assessment calculations show that the capacity is insufficient, linear or nonlinear finite element models are developed. These calculations are often complimented with the determination of the concrete compressive strength from core samples. If uncertainties about the structural behavior or the effect of material degradation remain, proof load testing of the bridge can become a viable assessment option.

The first step in the preparation of a proof load test is to consider if the structure is suitable for proof load testing. The engineer should gather he available information of the structure, and discuss the goals of the proof load test with the bridge owner. In order to approve a bridge experimentally through a proof load test, there must be uncertainties on the analytical assessment. The outcome of the proof load test then removes these uncertainties. The engineer should evaluate if proof load testing is the right method to address these uncertainties, or if diagnostic load testing can be sufficient for the case under consideration. Cases where proof load testing is recommended are when crucial information about the structure is missing (Aguilar et al., 2015), or when the effect of material deterioration on the capacity is unknown (Lantsoght et al., 2017b).

When it is determined that the structure is suitable for proof load testing, the test needs to be prepared. The first step in the preparation of a proof load test is an inspection of the bridge and its surroundings. In such an inspection, the engineer should identify if there are limitations in the access to the bridge site for the application of the load and the measurements. The engineer should note changes to the bridge as compared to the as-built drawings (widening of the superstructure, an increase in the thickness of the layer of asphalt, an overlay with high strength concrete to strengthen the bridge deck, or changes in lane layout). The effect of these changes on the assessment should be checked. The conditions of the joints and bearings must be inspected. If these conditions can have an effect on the distribution of forces in the structure, they should be taken into account for the assessment calculations and the preparatory calculations for the test. The inspection should also include a study of the cracks that are present on the bottom face of the deck and on the side faces. Inspection of the top face is only possible if no asphalt layer is present. The inspection of the cracks leads to the drawing of a map of the cracks. The position of the cracks determines the position of sensors that measure the increase in crack width during the proof load test.

After the inspection, preparatory calculations of the capacity are required. It is recommended (Lantsoght et al., in press-b) to use the mean material properties to estimate the expected value of the bending moment capacity, the shear capacity, and the punching capacity of the deck. If possible, the mean material properties should be determined by drilling concrete cores to find the mean concrete compressive strength and by taking samples of the reinforcement steel to find the average value of the yield strength of the steel. The engineer should calculate the expected deflections during the proof load test to select the correct measurement range for the sensors. The moment-curvature diagram and load-displacement diagram of the slab can be prepared based on hand calculations, to have a first idea of the expected behavior during the test. If it is not possible to approximate the behavior of the slab bridge during the experiment with simple hand calculations, then sometimes it may be necessary to model the bridge with nonlinear finite element models.

The next step in the preparation of a proof load test is to make a linear finite element model of the slab to determine the position and magnitude of the proof load. Since this model is only used to study the loading side of the equation, it is sufficient to use shell elements and to assume a Poisson's ratio of 0.2 and the Young's modulus of uncracked concrete. The model uses the following loads:

1. The self-weight of the superstructure. If the model is a simplified representation of the geometry, the model should include the equivalent load of the omitted parts. For concrete, a distributed load of 25 kN/m^3 (159 lb/ft^3) can be assumed.
2. The superimposed dead load. If asphalt is used, a distributed load of 23 kN/m^3 (146 lb/ft^3) can be assumed.
3. The live loads. The assessment of the bridges in the Netherlands is according to the loads prescribed by NEN-EN 1991-2:2003 (CEN, 2003) Load Model 1. This live load model uses a distributed load in all lanes, with a heavier distributed load in the first lane. Each lane holds a design tandem. The value of the applied load on the axles of the design tandem is different for each lane. Since the model uses shell elements, the concentrated loads can be distributed to mid-height of the slab, assuming a vertical load distribution of 45°, so that the resulting wheel print is larger than at the surface of the slab.

The load factors that are used to make the load combination are defined by the RBK (guidelines for the assessment of existing bridges) (Rijkswaterstaat, 2013) for all bridges that are owned by the Dutch Ministry of Infrastructure and the Environment. These bridges are highway bridges of Eurocode Consequences Class 3 as defined in NEN-EN 1990:2002 (CEN, 2002). For assessment, the minimum safety level from the RBK that a bridge has to fulfill is the "Usage" level. For this level, the load factors correspond to a reliability index of 3.3 and a reference period of 30 years. This required reliability index is high as compared to the target reliability index for the AASHTO LRFR (AASHTO, 2016) operating rating level with β = 2.5. For the pilot proof load tests, the evaluation includes all safety levels described in the RBK. Table 1 shows these safety levels, in which γ_{sw} is the load factor for the self-weight, γ_{sd} is the load factor for the superimposed dead load, and γ_{ll} is the load factor for the live loads. In the RBK, the same value for γ_{sw} and γ_{sd} is used. However, in combination with proof load testing, the geometry of the structure is not a random variable anymore, so that a reduction of the load factor for the self-weight to its model factor of 1.10 is possible.

Table 1 – Safety levels described by RBK and associated load factors as used in combination with proof load testing (Rijkswaterstaat, 2013)

Safety level	β	Reference period	γ_{sw}	γ_{sd}	γ_{ll}
RBK Design	4.3	100 years	1.10	1.25	1.50
RBK Reconstruction	3.6	30 years	1.10	1.15	1.30
RBK Usage	3.3	30 years	1.10	1.15	1.25
RBK Disapproval	3.1	15 years	1.10	1.10	1.25

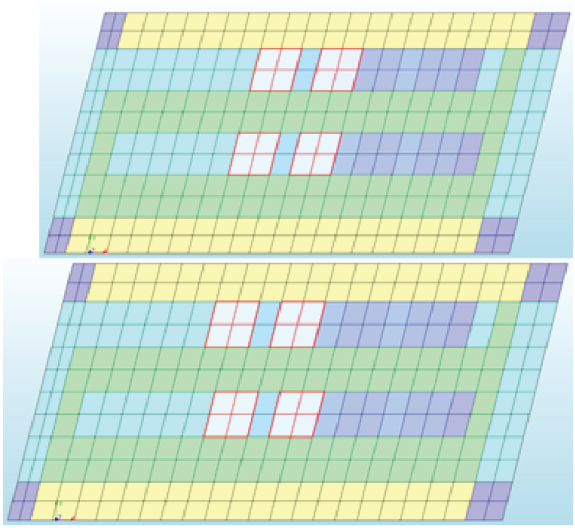

Figure 7 — Moving of the design tandem in its lane, for a one-lane bridge (viaduct Zijlweg).

With the prescribed finite element model, the critical position of the design tandems is determined. For the failure mode of bending, the design trucks are moved in their respective lanes until the position is found for which the resulting bending moment is the largest. This position is then the critical position for flexure. Figure 7 illustrates this procedure. Note that this procedure only considers the loading side of the load and resistance equation. If the capacity changes, for example because the height of the cross-section changes, or because the reinforcement layout changes, it may be better to determine the critical position as the cross-section with the highest Unity Check (ratio of considered load effect to capacity). When the studied failure mode is shear, it is assumed that the critical position on the slab is at a distance between the face of the support and the face of the first axle of 2.5d_l, with d_l the effective depth to the longitudinal reinforcement (Lantsoght et al., 2013b).

After the determination of the critical position and the largest bending moment or shear caused by the loads prescribed by the code, the live loads are removed and replaced by the proof loads. For bridges with a small width (maximum three lanes), a single tandem can be used for proof load testing. The name of this tandem is the "proof load tandem." The proof load tandem is placed at the critical position. Then, the load on the proof load tandem is increased until the same sectional moment or shear is found as with the loads prescribed by the code in the load combination prescribed by the RBK. The load factor on the proof load is γ_{proof} = 1.0. For the comparison of the sectional moment, the average moment over a width of $2d_l$ can be used and for the comparison of the sectional shear, the average shear over a width of $4d_l$ can be used (Lantsoght et al., 2013a). For skewed slabs, the critical position for shear of the proof load tandem needs to be taken in the obtuse corner (Cope, 1985).

The last step in the preparation of a proof load test is the determination of the sensor plan. Based on the map of cracks developed during the inspection of the cracks in the field, the cracks for monitoring during the test can be identified. The position of the proof load tandem determines the positions of the deflection measurements. The following minimum measurements are recommended for a proof load test:

- deflection in the longitudinal direction at five positions
- deflection in the transverse direction at three positions
- deflection of the supports on both sides of the tested span
- strain on the bottom of the slab for at least one position (i.e. under the proof load tandem)
- reference strain measurement to evaluate the effect of the environmental conditions
- crack width for at least one existing crack if bending cracks are present prior to the test

Other critical parameters, identified during the inspection, should be measured during the test. Measuring the applied load is necessary. If hydraulic jacks apply the load, load cells can measure its value. Figure 8 shows an example of a sensor plan.

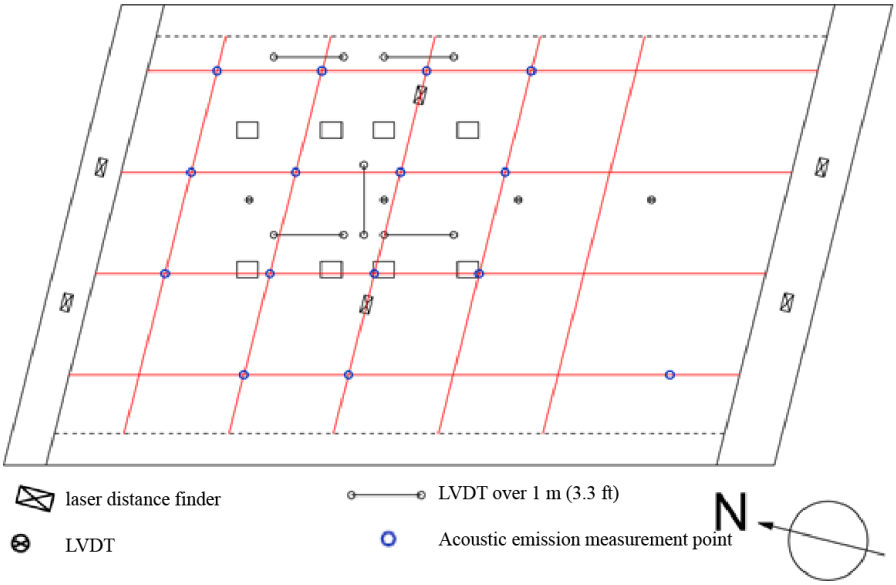

Figure 8 — Overview of resulting sensor plan as used for Viaduct Zijlweg.

For the sensor plan in Figure 8, LVDTs and laser triangulation sensors are used to measure the deflections, and LVDTs are applied over 1 m (3.3 ft) to measure averaged strains on the bottom of the slab. The crack width was measured as well on a longitudinal and transverse crack for the two positions of the proof load tandem that are shown in Figure 8. The positions of the LVDTs measuring crack widths are not shown on the sensor plan as they were drawn on the crack map.

The practical preparations prior to a proof load test focus on ensuring the safety of all parties involved. The safety of all personnel involved with the preparation and execution of the proof load test and its dismantlement is of the utmost importance. The safety of the traveling public and other local parties (press, neighbors …) should be guaranteed, and these parties should receive clear information about the testing and its effect on the local traffic situation. A communications expert of the road authority should prepare this information. As part of the preparation stage, it is required in the Netherlands to deliver a safety report prior to the field test, and to have at least one safety engineer present on site at all times. The safety engineer educates every person entering the test site on the safety policies prior to starting his/her activities on the test site.

Recommendations for the execution of proof load tests

For the execution of proof load tests, two elements are important:

1. the loading protocol and the method of load application, and
2. the interpretation of the measurements and verification of stop criteria in real-time during the proof load test.

Figure 9 — BELFA vehicle on viaduct Vlijmen Oost.

Figure 10 — Use of steel spreader beam, hydraulic jacks, and counterweights in the test on the second span for the Ruytenschildt Bridge.

The first element is the application of the load and the determination of the loading protocol. The pilot proof load tests considered two load application methods: the use of a loading vehicle, see Figure 9, and the use of a steel spreader beam with counterweights and hydraulic jacks, see Figure 10. Both methods are suitable for proof load testing of reinforced concrete slab bridges, and the final choice for a certain proof load test will depend on practical considerations. The general requirements for the loading system are the following:

- the load must be applied in a safe manner, and sudden large deformations should not lead to collapse of the bridge and the loading system,
- the loading system must be suitable for the selected loading protocol and target proof load,
- it must be possible to keep the magnitude of the load constant,
- the loading system must be suitable for applying a cyclic loading protocol,
- the loading system must have the same wheel prints as the proof load tandem assumed to determine the critical position and target proof load.

The experiments on beams cast in the laboratory resulted in the recommend loading protocol. Early on during the pilot proof load tests, a cyclic loading protocol was chosen, to study different load levels, and to check per load level if the structural response remains the same for the repeated load cycles. If this is not the case, nonlinear behavior is taking place, and continuing the proof load test is not allowed. Figure 11 defines the terms load cycle, load level, and load step.

The loading protocol prescribes at least four load levels:

1. A low load level to check the proper functioning of all sensors.
2. A load level that corresponds to the Serviceability Limit State.
3. An intermediate load level, for example the RBK Disapproval level.
4. The target load level, which is the RBK Usage level for the assessment of existing bridges in the Netherlands, plus 5% extra.

The extra 5% on the RBK Usage level covers local variability of the tested span and the chance that another position may be the weakest spot in the slab. Further statistical analyses are necessary to determine the appropriate extra percentage on the target proof load. Note that for the pilot proof load tests the largest load level was the RBK Design level (plus a few percent extra), as the tests covered all load levels of the RBK. However, in general, a load level higher than the RBK Usage level is not necessary. This safety level is required for all existing highway bridges in the Netherlands.

Per load level, at least three cycles are recommended to check the linearity and reproducibility of the measured response. For load levels 3 and 4, after the Serviceability load level, an extra cycle is added in which the load is increased in small steps and kept constant for about two minutes. While the load is constant at these intermediate levels, the engineer checks the measurements to verify if the load can increase further. Unloading in the cycles does not occur to 0 kN (0 kip), but to a small value of the load to make sure that all sensors and jacks remain activated. The loading speed should be a constant value during loading and unloading, and should be a value between 3 kN/s (0.7 kip/s) and 10 kN/s (2.2 kip/s). Considering these recommendations, Figure 12 shows an example loading protocol.

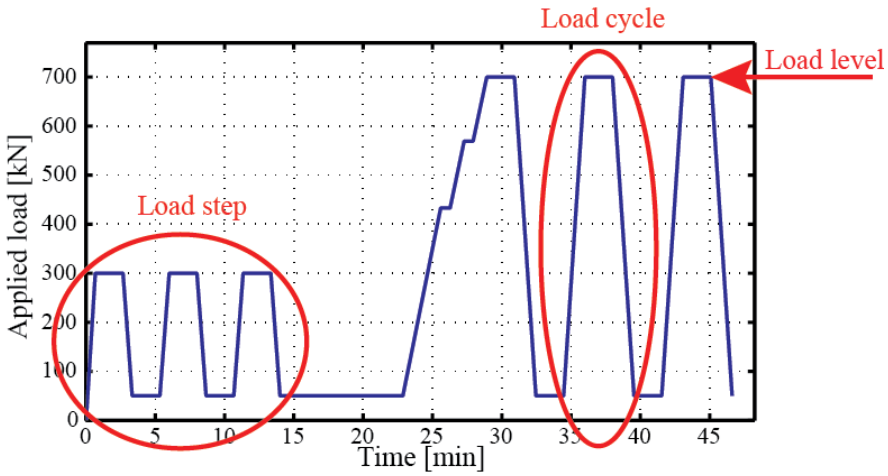

Figure 11 — Definition of load cycle, load level, and load step.

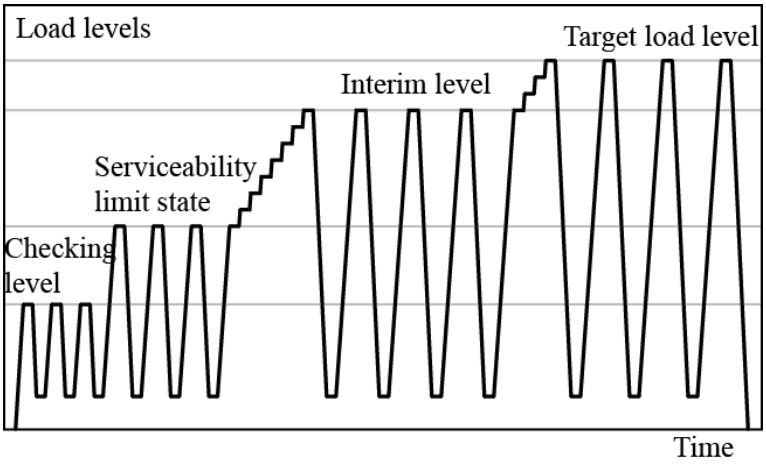

Figure 12 — Resulting recommended loading protocol.

During the proof load test, close monitoring of the structural response is necessary. The measurements should be followed in real-time during the test, and whenever the load is increased, it has to be verified first if no signs of distress are observed. Only after checking all stop criteria and all real-time plots, the engineers following the measurements can communicate to the load operator that they can execute the next load cycle or that they can increase the load. The German guidelines (Deutscher Ausschuss für Stahlbeton, 2000) prescribe stop criteria for proof load testing of plain and reinforced concrete buildings for the failure mode of flexure, and

ACI 437.2M-13 (ACI Committee 437, 2013) prescribes acceptance criteria for proof load testing of concrete buildings for the failure mode of flexure. Based on the pilot proof load tests and lab testing carried out in the Netherlands, a set of stop criteria for flexure and shear are proposed, see Table 2. Further research is necessary on shear-critical elements in the lab to confirm the stop criteria for shear. Moreover, testing of slabs instead of beams in the laboratory is necessary to study the limiting concrete strains and crack widths that can be used for the stop criteria for shear. In the proposal of Table 2, the stop criterion identified with "Concrete strains" is taken from the German guidelines (Deutscher Ausschuss für Stahlbeton, 2000) as:

$$\varepsilon_c < \varepsilon_{c,lim} - \varepsilon_{c0} \tag{1}$$

with ε_c the strain measured in the concrete during proof loading, $\varepsilon_{c,lim}$ a strain of 0.6 ‰ in general, which can be increased to 0.8 ‰ when the concrete compressive strength is larger than 25 MPa (3.6 ksi), and ε_{c0} the analytically determined short-term strain in the concrete caused by the permanent loads that act on the structure before the application of the proof load. At this moment, the stop criterion is the same for the failure mode of shear. However, further research should result in an improved formulation of the strain stop criterion for shear, possibly based on the Critical Shear Displacement Theory (Yang et al., 2016 ; Yang et al., 2017) and more laboratory testing.

Table 2 – Proposed stop criteria, subject to further research, based on Dutch pilot proof load tests and lab testing.

	Previously cracked in bending moment or not?	
Failure mechanism	*Uncracked*	*Cracked*
Flexural failure	Concrete strains $w_{max} \leq 0.5$ mm (0.02 in) $w_{res} < 0.3 w_{max}$ Stiffness reduction ≤ 25 % Deformation profiles Load-deflection graph	Concrete strains $w_{max} \leq 0.3$ mm (0.01 in) $w_{res} < 0.2 w_{max}$ Stiffness reduction ≤ 25 % Deformation profiles Load-deflection graph
Shear failure	Concrete strains $w_{max} \leq 0.4 w_{ai}$ Stiffness reduction ≤ 25 % Deformation profiles Load-deflection graph	Concrete strains $w_{max} \leq 0.75 w_{ai}$ Stiffness reduction ≤ 25 % Deformation profiles Load-deflection graph

The stop criteria for flexure for the maximum and residual crack widths, w_{max} and w_{res} are taken from the German guidelines (Deutscher Ausschuss für Stahlbeton, 2000). For the case of an element previously uncracked in bending, the crack width and residual crack width of a new crack are followed. For the case of an element with existing bending cracks, the increase in crack width of a crack near the load application is measured. For shear, a stop criteria for crack width is derived based on aggregate interlock theory (Lantsoght, 2017b). Further experimental validation of this proposed stop criterion is required. A crack between the load and the support, in the shear span, should be monitored. For a structure with bending cracks, monitoring an existing crack is possible. If no cracks are present at the start of the test, optical measurements are required to follow the development of cracks and the crack width can only be measured when the crack in the shear span has developed. The value of $w_{ai,}$ which is the crack width for which the shear capacity provided by aggregate interlock drops below the inclined cracking load as determined in the RBK, is calculated as:

$$w_{ai} = \frac{0.03 f_c^{0.56} \left(1 + \rho_s n_e - \sqrt{2\rho_s n_e + \left(\rho_s n_e\right)^2}\right)\left(978\Delta_{cr}^2 + 85\Delta_{cr} - 0.27\right) R_{ai}}{v_{RBK}} + 0.01 \tag{2}$$

with

$$\Delta_{cr} = \frac{25 d_l}{30610\phi} + 0.0022 \leq 0.025 mm \tag{3}$$

$$v_{RBK} = \max(1.13 \mathrm{k}_{slab} \mathrm{k} \sqrt{\frac{f_c}{f_y}}; 0.15 k_{slab} k \left(100 \rho_s f_c\right)^{1/3}) \tag{4}$$

$$k = 1 + \sqrt{\frac{200}{d_l}} \leq 2 \tag{5}$$

$$R_{ai} = 0.85\sqrt{\left(\frac{7.2}{f_c - 40} + 1\right)^2} - 1 + 0.34 \text{ if } f_c > 65\text{MPa} \quad (6)$$

with f_c the concrete compressive strength in [MPa], ρ_s the ratio of the longitudinal reinforcement, n_e the ratio of the moduli of elasticity of steel and concrete, Δ_{cr} the critical shear displacement, R_{ai} a correction factor for high-strength concrete with f_c > 65 MPa (9.4 ksi), d_l the effective depth to the longitudinal reinforcement in [mm], ϕ the bar diameter in [mm], v_{RBK} the shear capacity that corresponds to the inclined cracking load, k_{slab} = 1.2 for slabs supported by line supports and 1.0 for all other cases, k the size effect factor, and f_y the yield strength of the steel in [MPa]. In these expressions, units [MPa] and [mm] should be used.

The next stop criterion considers the stiffness reduction. For this evaluation the stiffness observed in the load-deflection diagram is compared for a given load cycle to the first load cycle. If in a given load cycle, the stiffness is less than 75% of the stiffness in the first load cycle, the proof load test should be terminated.

The deformation profiles that are studied as a stop criterion are the profiles of the deflection and/or the horizontal displacement across the different load levels. If the shape of these profiles changes, changes are taking place in the structure and further loading may not be permitted. An example of these profiles is shown in Figure 13, where it can be seen that at 175 kN (39 kip) the repeatability of the results is not obtained across the three load cycles anymore. The stop criterion would thus be exceeded at a load of 175 kN (39 kip), or 42% of the failure load, which allows for a sufficient margin of safety.

The last stop criterion is based on the load-deflection diagram. During the proof load test, the load-deflection diagram of the applied load and the deflection under the load is followed in real-time. When signs of distress, such as nonlinear behavior, are observed in this diagram, the stop criterion is exceeded and further loading is not permitted.

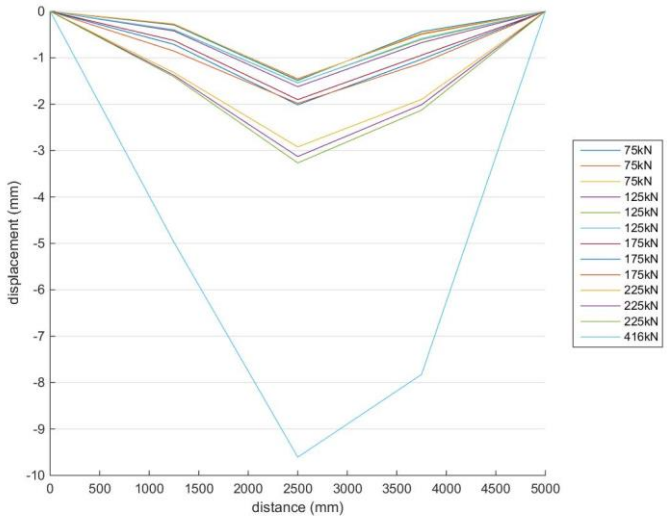

Figure 13 — Deflection profiles measured in RSB02B, a beam sawn from the Ruytenschildt Bridge and tested in the laboratory. Conversion: 1 mm = 0.04 in, 1 kN = 0.225 kip.

Recommendations for the evaluation of proof load tests

A proof load test is successful when the target proof load is applied and no signs for distress are observed during the test and no stop criterion is exceeded. After a successful proof load test, the direct conclusion is that the tested bridge fulfills the code requirements for the factored live loads, provided that the most critical position at the most critical span was tested. In that case, the report about the proof load test contains the post-processed data. In the post-processing stage, the measurements need to be corrected: the deflection measurements of the slab need to be corrected for the deflections of the supports to have the net deflections of the slab, and the strain measurements need to be corrected for the reference strain measurement to exclude the effect of temperature and humidity. Based on these corrected measurements, the verification of the stop criteria is added to the report. The report can include the following graphs:

- The load-deflection diagram showing all cycles, as well as the envelope of the load-deflection diagram. Figure 14 shows an example.
- The measured loading protocol.
- The deflection profiles, also analyzed for the stop criteria, should be plotted for each load cycle.

- The measured crack widths should be plotted as a function of the time and as a function of the applied load.
- The measured strains should be plotted as a function of the time and as a function of the applied load.

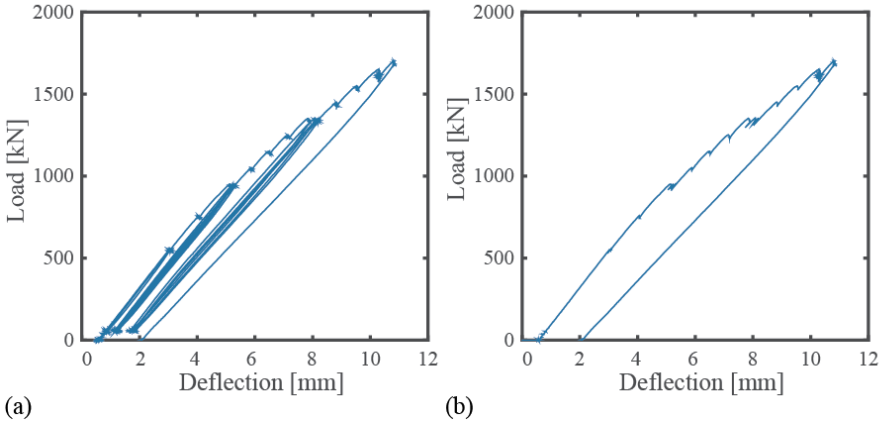

Figure 14 — Load-deflection diagram from Viaduct De Beek (bending moment test), as reported after post-processing: (a) load-deflection diagram showing all cycles; (b) load-deflection envelope. Conversion: 1 mm = 0.04 in, 1 kN = 0.225 kip.

The report should include the total maximum load applied during the proof load test. This value is the measured load on the load cells, plus the weight of the jacks and other elements of the test setup that load the deck directly. A graph showing the measurements of the load at each wheel print (when jacks are used) must show that the load was distributed equally over the wheel prints.

If another span of the bridge can be governing, or if an assessment based on another type of load (for example, a special type of vehicle) is required, then the finite element model that was developed to prepare for the proof load test must be updated with the responses measured during the proof load test. This approach is similar to updating a finite element model after a diagnostic load test (Barker, 2001; Bridge Diagnostics Inc., 2012). The finite element model is altered until the responses in the model correspond reasonably well with the responses measured during the proof load test. This updated model can then be used for the assessment of another span of the bridge, or for applying a different load.

The final report of the proof load test should be submitted to the bridge owner. The owner will make the decisions with regard to the removal of posting or changing of the lane layout based on the recommendations of the report, and takes the full responsibility for these decisions.

DISCUSSION AND FUTURE RESEARCH

Over the past decade, a number of pilot proof load tests have been carried out in the Netherlands, as well as a collapse test. Combined with additional testing of beams in the laboratory, the aim is to develop a guideline for the proof load testing of concrete bridges. At this moment, research resulted in significant steps in this direction, but some uncertainties prevent the publication of such guidelines covering all cases. More research is required before all proof load testing can be transferred to the industry. At this moment, for proof load testing of shear-critical bridges, the involvement of a research-oriented partner that has experience with shear testing is still required. Note that the current recommendations for proof load testing are based on the code requirements for the Netherlands. The application of these recommendations to other countries, such as the USA where AASHTO LRFR governs (AASHTO, 2016), is not straightforward, as the live load model for assessment and the requirements with regard to the target reliability index are different.

For the assessment of reinforced concrete slab bridges, the bridge owner is currently advised to follow the Levels of Assessment. As such, load testing is only considered after rigorous analytical studies based on the available information. Another type of load test that could be interesting, but which is not available yet, is a standard basic test which can be carried out with limited preparation and limited time on-site. In such a test, the application of a certain load and basic measurements should be sufficient to demonstrate that a given bridge can carry the prescribed factored live loads in a safe manner.

A first topic that needs further research and further experiments is the determination of stop criteria for shear. The development of limiting values for the strains and crack widths for the case of an element without flexural cracks and for the case of an element with flexural cracks is necessary. The recommended values should be verified with experimental results. At this moment, only three experiments for shear are available on beams. More experiments, also on slabs, are required to verify the stop criteria for shear.

Another topic that needs further research is the determination of the target proof load based on the concepts of structural reliability (Lantsoght et al., 2017f). It should be studied if the load factors that are used to derive the target proof load can be further reduced. The results of WIM and traffic measurements should be implemented where suitable. For the determination of the probability of failure, it is necessary to describe the probability density functions of the load and resistance. Figure 15 illustrates the effect of proof load testing on the probability density function of the resistance. The description of the probability density function of the load and the resistance requires an estimate of the variability of these properties, for example by defining the coefficient of variation. At this moment, no recommendations for the choice of the coefficient of variation are available. Further statistical analyses are also necessary to determine the extra percentage on the target proof load that corresponds to the RBK Usage level. At this moment, the target proof load plus 5% is applied, to cover local variability of the material properties, but further research should provide statistical support for this practice. Drilling more cores results in a better statistical description of the concrete strength, but statistical analyses are necessary to determine the effect of the distribution of the concrete strength on the proof load test.

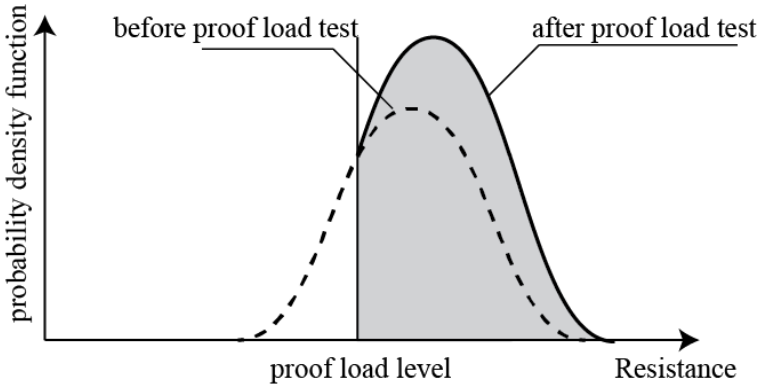

Figure 15 — Effect of proof load testing on probability density function of the resistance.

The calculations that are part of the preparation of a proof load test use the mean material properties. Standard protocols are available in the Netherlands for drilling concrete cores, their transportation, the testing, and the determination of the properties based on statistics (Rijkswaterstaat, 2014). However, for the determination of the properties of steel based on samples taken from an existing bridge, no recommendations are currently available.

The distribution width for the bending moment needs further study. Currently, the industry uses $2d_l$ (based on a rule of thumb). Based on the preparations for proof load testing of Viaduct De Beek, the recommended transverse distribution width for the peak bending moment was determined as 3 m (10 ft). Further research is needed to develop a recommendation for this width.

Currently, the recommendations imply the use of contact sensors. However, when access to the test site makes the application of contact sensors impossible, other measurement techniques become necessary. Additionally, the use of non-contact sensors can speed up the preparations on site, so that the bridge can be closed for a shorter amount of time. Currently, a proof load test takes two days of on-site preparations, one day of testing at two positions, and one day to dismantle all sensors. For this reason, research on the use of digital image correlation and radar interferometry is necessary. The use of a total station may be less suitable for the described proof load tests, since the time required by the total station to measure all points is relatively large. As such, the total station may be too slow to capture the behavior of the structure during the loading branch of a load cycle.

For the extension to wider viaducts, further research is needed. In the pilot proof load tests, only bridges with a width of maximum three lanes were tested. These bridges could be tested with a single proof load tandem. For wider bridges, perhaps more than one proof load tandem should be applied/

At this moment, the assessment of a span that has not been tested is based on updating the finite element model. However, a more direct method is necessary: if the Unity Check in one tested span can be reduced by a certain factor based on the results of the proof load test, what then becomes the reduction of the Unity Check in a span that has not been tested? This reduction should take into account the variability of (material) properties and the uncertainties involved with load testing.

The current research mostly considers reinforced concrete slab bridges. Additional checks and research are necessary to extend these recommendations to other types of reinforced concrete bridges and to prestressed concrete bridges.

SUMMARY AND CONCLUSIONS

A large number of the existing bridges in the Netherlands are approaching the end of their originally devised service life. These bridges require assessment. An initial assessment showed that there are causes for concern with regard to the reinforced concrete slab bridges. Therefore, research was carried out over the past few years to improve the assessment methods for reinforced concrete slabs and slab bridges, especially for shear. When the uncertainties on the capacity are large, analytical methods may not be sufficient, and field testing becomes interesting.

Field testing of bridges contains diagnostic load testing and proof load testing. A diagnostic load test has as its purpose to compare analytical predictions to the structural response in the field, to improve the analytical models and obtain a better assessment. In a proof load test, a load representative of the factored live loads is applied to the bridge. If the bridge can withstand these loads without signs of distress, the bridge fulfills the requirements of the code. Proof load testing can be suitable for reinforced concrete slab bridges when the uncertainties about the effect of material deterioration (such as alkali-silica reaction) on the capacity are large.

Pilot proof load tests since 2007 studied the possibilities for proof load testing on concrete bridges in the Netherlands, with a focus on reinforced concrete slab bridges. Viaduct Heidijk, viaduct Medemblik, viaduct Vlijmen Oost, the Halvemaans Bridge, viaduct Zijlweg, and viaduct De Beek all have been subjected to a proof load test. For the execution of these tests, in some cases a loading vehicle, the BELFA from Germany, was used, and in other cases a system with a steel spreader beam, counterweights, and hydraulic jacks was used. The collapse tests on the Ruytenschildt Bridge add valuable information to the campaign of proof load tests. The loading protocol and the stop criteria were studied in more detail with laboratory testing. Three beams sawn from the Ruytenschildt Bridge and two beams with plain bars cast in the lab were tested to failure, resulting in nine laboratory tests.

With the experience and insights from the pilot proof load tests, the collapse test, and the beam tests in the lab, recommendations have been formulated for the preparation, execution, and evaluation of proof load tests on reinforced concrete slab bridges. For the preparation of proof load testing, it is important to see if a proof load test is the right solution to answer the questions for the bridge under consideration. If this is the case, an inspection of the site and preparatory calculations of the capacity are required. In this stage, a linear finite element model determines the target proof load and its critical position. This information leads to the development of a sensor plan.

The pilot proof load tests and laboratory tests on beams resulted in a recommended loading protocol. During the proof load test, analysis in real time of the measurements and stop criteria is necessary. The currently available stop criteria are based on the information from the pilot proof load tests, the collapse test, and the laboratory testing. However, further experimental evidence is necessary to extend and to validate the proposed stop criteria for shear.

The evaluation stage of the proof load test consists of writing the report that contains the graphs of the most important structural responses measured during the field test. If the bridge can carry the target proof load without signs of distress, the proof load test is successful and the bridge fulfills the code requirements.

At this moment, further research with regard to the target proof load, the stop criteria for shear, the use of non-contact sensors, the transverse distribution width for flexure, the interpretation of material testing for steel samples, the extrapolation of results to other spans, the extension to wider viaducts, and the extrapolation of these recommendations to other reinforced concrete bridge types and prestressed concrete bridges is required before guidelines for proof load testing can be published and used by the industry in the Netherlands.

ACKNOWLEDGEMENTS

The authors wish to express their gratitude and sincere appreciation to the Dutch Ministry of Infrastructure and the Environment (Rijkswaterstaat) for financing this research work. The contributions and help during the pilot proof load tests of our current and former colleagues Albert Bosman, Sebastiaan Ensink, Sonja Fennis, Rutger Koekkoek, Patrick Van Hemert and Yuguang Yang of Delft University of Technology are gratefully acknowledged. The fruitful discussions with Frank Linthorst and Danny den Boef of Witteveen+Bos, responsible for logistics and safety during the pilot proof load tests, and with Otto Illing and the late Chris Huissen of Mammoet, responsible for applying the load during the pilot proof load tests, are also acknowledged.

REFERENCES

AASHTO, 2016, "The manual for bridge evaluation with 2016 interim revisions," 2nd ed. American Association of State Highway and Transportation Officials; Washington, D.C.

ACI Committee 437, 2013, "Code Requirements for Load Testing of Existing Concrete Structures (ACI 437.2M-13) and Commentary ", Farmington Hills, MA, 24 pp.

Aguilar, C. V., Jáuregui, D. V., Newtson, C. M., Weldon, B. D. and Cortez, T. M., 2015, "Load Rating a Prestressed Concrete Double-Tee Beam Bridge without Plans by Proof Testing," *Transportation Research Board Annual Compendium of Papers*, Washington DC, pp. 19.

Anay, R., Cortez, T. M., Jáuregui, D. V., ElBatanouny, M. K. and Ziehl, P., 2016, "On-Site Acoustic-Emission Monitoring for Assessment of a Prestressed Concrete Double-Tee-Beam Bridge without Plans," *Journal of Performance of Constructed Facilities*, V. 30, No. 4.

Arangjelovski, T., Gramatikov, K. and Docevska, M., 2015, "Assessment of damaged timber structures using proof load test – Experience from case studies," *Construction and Building Materials*, V. 101, Part 2, 12/30/, pp. 1271-1277.

Barker, M. G., 2001, "Quantifying Field-Test Behavior for Rating Steel Girder Bridges," *Journal of Bridge Engineering*, V. 6, No. 4, pp. 254-261.

Belletti, B., Hendriks, M. A. N., den Uijl, J. A. and Damoni, C., 2010, "Developing standardized guidelines for safety assessment of shear-critical rc beams based on nonlinear finite element modeling," *3rd fib International Congress*, Washington DC, pp. 13.

Belletti, B., Damoni, c., Hendriks, M. A. N. and Den Uijl, J. A., 2013, "Nonlinear finite element analyses of reinforced concrete slabs: comparison of safety formats," *VIII International Conference on Fracture Mecahnics of concrete and Concrete Structures, FraMCoS-8*, Van Mier, J. G. M., Ruiz, G., Andrade, C., Yu, R. C. and Zhang, X. X., eds., pp. 12.

Belletti, B., Pimentel, M., Scolari, M. and Walraven, J. C., 2015, "Safety assessment of punching shear failure according to the level of approximation approach," *Structural Concrete*, V. 16, No. 3, pp. 366-380.

Bretschneider, N., Fiedler, L., Kapphahn, G. and Slowik, V., 2012, "Technical possibilities for load tests of concrete and masonry bridges," *Bautechnik*, V. 89, No. 2, pp. 102-110 (in German).

Bridge Diagnostics Inc., 2012, "Integrated Approach to Load Testing," 44 pp.

Casas, J. R. and Gómez, J. D., 2013, "Load Rating of Highway Bridges by Proof-loading," *KSCE Journal of Civil Engineering*, V. 17, No. 3, pp. 556-567.

CEN, 2002, "Eurocode – Basis of structural design, NEN-EN 1990:2002 ", Comité Européen de Normalisation, Brussels, Belgium, 103 pp.

CEN, 2003, "Eurocode 1: Actions on structures - Part 2: Traffic loads on bridges, NEN-EN 1991-2:2003," Comité Européen de Normalisation, Brussels, Belgium, 168 pp.

CEN, 2005, "Eurocode 2: Design of Concrete Structures - Part 1-1 General Rules and Rules for Buildings. NEN-EN 1992-1-1:2005," Comité Européen de Normalisation, Brussels, Belgium, 229 pp.

Cochet, D., Corfdir, P., Delfosse, G., Jaffre, Y., Kretz, T., Lacoste, G., Lefaucheur, D., Khac, V. L. and Prat, M., 2004, "Load tests on highway bridges and pedestrian bridges (in French)," Setra - Service d'Etudes techniques des routes et autoroutes, Bagneux-Cedex, France.

Code Committee 351001, 1995, "NEN 6720 Technical Foundations for Building Codes, Concrete provisions TGB 1990 - Structural requirements and calculation methods (VBC 1995) (in Dutch)," Civil engineering center for research and regulation, Dutch Normalization Institute, Delft, The Netherlands, 245 pp.

Cope, R. J., 1985, "Flexural Shear Failure of Reinforced-Concrete Slab Bridges," *Proceedings of the Institution of Civil Engineers Part 2-Research and Theory*, V. 79, No. SEP, pp. 559-583.

den Uijl, J. A. and Kaptijn, N., 2004, "Structural consequences of ASR: an example on shear capacity," *Heron*, V. 47, No. 2, pp. 1-13.

Deutscher Ausschuss für Stahlbeton, 2000, "DAfStb-Guideline: Load tests on concrete structures (in German)," Deutscher Ausschuss fur Stahlbeton, 7 pp.

Dieteren, G. G. A. and den Uijl, J. A., 2009, "Evaluation proof load test Heidijk (in Dutch)," V. 2008-DWARS-MOlO, TNO Bouw en Ondergrond / TU Delft, 70 pp.

Faber, M. H., Val, D. V. and Stewart, M. G., 2000, "Proof load testing for bridge assessment and upgrading," *Engineering Structures*, V. 22, pp. 1677-1689.

Fennis, S. A. A. M. and Hordijk, D. A., 2014, "Proof loading Halvemaans Bridge Alkmaar (in Dutch)," Stevin Report 25.5-14-05, Delft University of Technology, Delft, The Netherlands, 72 pp.

Fennis, S. A. A. M., van Hemert, P., Hordijk, D. and de Boer, A., 2014, "Proof loading Vlijmen-Oost; Research on assessment method for existing structures (in Dutch)," *Cement*, V. 5, pp. 40-45.

fib, 2012, "Model code 2010: final draft," International Federation for Structural Concrete; Lausanne, 676 pp.

Frýba, L. and Pirner, M., 2001, "Load tests and modal analysis of bridges," *Engineering Structures*, V. 23, No. 1, pp. 102-109.

Fu, G., Pezze III, F. P. and Alampalli, S., 1997, "Diagnostic Load Testing for Bridge Load Rating," *Transportation Research Record*, V. 1594, pp. 125-133.

JCSS, 2001, "JCSS Probabilistic Model Code - Part 3: Resistance Models".

Koekkoek, R. T., Lantsoght, E. O. L. and Hordijk, D. A., 2015, "Proof loading of the ASR-affected viaduct Zijlweg over highway A59," Stevin Report nr. 25.5-15-08, Delft University of Technology, Delft, The Netherlands, 180 pp.

Koekkoek, R. T., Lantsoght, E. O. L., Yang, Y. and Hordijk, D. A., 2016, "Analysis report for the assessment of Viaduct De Beek by Proof Loading," Stevin Report 25.5-16-01, Delft University of Technology, Delft, The Netherlands, 125 pp.

Lantsoght, E., 2016, "Literature review on load testing," Stevin Report nr. 25.5-16-07, Delft University of Technology, 102 pp.

Lantsoght, E., van der Veen, C. and de Boer, A., 2016a, "Shear and moment capacity of the Ruytenschildt bridge," *IABMAS 2016*, pp. 8.

Lantsoght, E., Yang, Y., van der Veen, C., de Boer, A. and Hordijk, D., 2016b, "Ruytenschildt Bridge: field and laboratory testing," *Engineering Structures*, V. 128, No. december, pp. 111-123.

Lantsoght, E., 2017a, "Measurements of Ruytenschildt Bridge test and analysis for stop criteria," V. Stevin Report nr. 25.5-17-02, Delft University of Technology, 60 pp.

Lantsoght, E., 2017b, "Development of a stop criterion for shear based on aggergate interlock," V. Stevin Report nr. 25.5-17-09, Delft University of Technology, 33 pp.

Lantsoght, E. O. L., de Boer, A., Van der Veen, C. and Walraven, J. C., 2013a, "Peak shear stress distribution in finite element models of concrete slabs," *Research and Applications in Structural Engineering, Mechanics and Computation*, Zingoni, A., ed. Cape Town, South Africa, pp. 475-480.

Lantsoght, E. O. L., van der Veen, C., de Boer, A. and Walraven, J. C., 2013b, "Recommendations for the Shear Assessment of Reinforced Concrete Slab Bridges from Experiments " *Structural Engineering International*, V. 23, No. 4, pp. 418-426.

Lantsoght, E. O. L., van der Veen, C. and Walraven, J. C., 2013c, "Shear in One-way Slabs under a Concentrated Load close to the support," *ACI Structural Journal*, V. 110, No. 2, pp. 275-284.

Lantsoght, E. O. L., De Boer, A. and van der Veen, C., 2014a, "Determination of distribution width for shear stresses at support in reinforced concrete slab bridges," *EuroC*, St. Anton am Arlberg, Austria, pp. 9

Lantsoght, E. O. L., van der Veen, C., De Boer, A. and Walraven, J., 2014b, "Influence of Width on Shear Capacity of Reinforced Concrete Members," *ACI Structural Journal*, V. 111, No. 6, pp. 1441-1450.

Lantsoght, E. O. L., van der Veen, C., de Boer, A. and Walraven, J., 2015a, "One-way slabs subjected to combination of loads failing in shear," *ACI Structural Journal*, V. 112, No. 4, pp. 417-426.

Lantsoght, E. O. L., Van der Veen, C., de Boer, A. and Walraven, J. C., 2015b, "Proposal for the extension of the Eurocode shear formula for one-way slabs under concentrated loads," *Engineering Structures*, V. 95, pp. 16-24.

Lantsoght, E. O. L., van der Veen, C., Walraven, J. and de Boer, A., 2015c, "Experimental investigation on shear capacity of reinforced concrete slabs with plain bars and slabs on elastomeric bearings," *Engineering Structures*, V. 103, pp. 1-14.

Lantsoght, E. O. L., van der Veen, C. and de Boer, A., 2016c, "Shear capacity of the Rutyenschildt Bridge," *fib Symposium 2016, Performance-based approaches for concrete structures*, Beushausen, H., ed. Cape Town, South Africa, pp. 10.

Lantsoght, E. O. L., van der Veen, C., de Boer, A. and Alexander, S., 2016d, "Bridging the gap between one-way and two-way shear in slabs," *ACI SP International Punching Symposium*, pp. 20.

Lantsoght, E. O. L., van der Veen, C., de Boer, A. and Hordijk, D. A., 2016e, "Probabilistic prediction of the failure mode of the Ruytenschildt Bridge," *Engineering Structures*, V. 127, 11/15/, pp. 549-558.

Lantsoght, E. O. L., van der Veen, C., de Boer, A. and Walraven, J., 2016f, "Using Eurocodes and AASHTO for assessing shear in slab bridges," *Proceedings of the Institution of Civil Engineers – Bridge Engineering*, V. 169, No. BE4, pp. 285-297.

Lantsoght, E. O. L., Yang, Y., Tersteeg, R. H. D., van der Veen, C. and de Boer, A., 2016g, "Development of Stop Criteria for Proof Loading," *IALCCE 2016*, Delft, The Netherlands, pp. 8 pp.

Lantsoght, E. O. L., 2017c, "Beams from Ruytenschildt Bridge: Analysis of stop criteria," Stevin Report 25.5-17-05, Delft University of Technology, 77 pp.

Lantsoght, E. O. L., De Boer, A. and Van der Veen , C., 2017a, "Levels of Approximation for the shear assessment of reinforced concrete slab bridges," *Structural Concrete*, V. 18, pp. 143-152.

Lantsoght, E. O. L., Koekkoek, R. T., Hordijk, D. A. and De Boer, A., 2017b, "Towards standardization of proof load testing: pilot test on viaduct Zijlweg," *Structure and Infrastructure Engineering*.

Lantsoght, E. O. L., van der Veen, C. and de Boer, A., 2017c, "Extended Strip Model for slabs subjected to load combinations," *Engineering Structures*, V. 145, pp. 60-69.

Lantsoght, E. O. L., van der Veen, C., de Boer, A. and Alexander, S. D. B., 2017d, "Extended Strip Model for Slabs under Concentrated Loads," *ACI Structural Journal*, V. 114, No. 2, pp. 565-574.

Lantsoght, E. O. L., Van der Veen , C., De Boer, A. and Hordijk, D. A., 2017e, "Collapse test and moment capacity of the Ruytenschildt Reinforced Concrete Slab Bridge " *Structure and Infrastructure Engineering*, V. 13, No. 9, pp. 1130-1145.

Lantsoght, E. O. L., van der Veen, C., Hordijk, D. A. and de Boer, A., 2017f, "Reliability index after proof load testing: viaduct De Beek," *ESREL 2017*, Protoroz, Slovenia, pp. 8.

Lantsoght, E. O. L., Yang, Y., van der Veen, C., de Boer, A. and Hordijk, D. A., 2017g, "Beam experiments on acceptance criteria for bridge load tests," *ACI Structural Journal*, V. 114, No. 4, pp. 1031-1041.

Lantsoght, E. O. L., van der Veen, C., Hordijk, D. A. and de Boer, A., 2017h, "State-of-the-art on load testing of concrete bridges," *Engineering Structures*, V. 150, pp. 231-241.

Lantsoght, E. O. L., Koekkoek, R. T., van der Veen, C., Hordijk, D. A. and de Boer, A., in press-a, "Case study: Pilot proof load test on viaduct De Beek," *Journal of Bridge Engineering*.

Lantsoght, E. O. L., Van der Veen , C., De Boer, A. and Hordijk, D. A., in press-b, "Proof load testing of reinforced concrete slab bridges in the Netherlands," *Structural Concrete*, pp. 29.

Matta, F., Bastianini, F., Galati, N., Casadei, P. and Nanni, A., 2008, "Distributed Strain Measurement in Steel Bridge with Fiber Optic Sensors: Validation through Diagnostic Load Test," *Journal of Performance of Constructed Facilities*, V. 22, No. 4, pp. 264-273.

Moses, F., Lebet, J. P. and Bez, R., 1994, "Applications of field testing to bridge evaluation," *Journal of Structural Engineering-ASCE*, V. 120, No. 6, Jun, pp. 1745-1762.

Olaszek, P., Świt, G. and Casas, J. R., 2012, "Proof load testing supported by acoustic emission. An example of application," *IABMAS 2012*.

Olaszek, P., Lagoda, M. and Casas, J. R., 2014, "Diagnostic load testing and assessment of existing bridges: examples of application," *Structure and Infrastructure Engineering*, V. 10, No. 6, Jun 3, pp. 834-842.

PN-S-10040/99, 1999, "Bridges. Concrete, reinforced concrete and prestressed structures. Requirements and testing. (in Polish)."

Rijkswaterstaat, 2013, "Guidelines Assessment Bridges - assessment of structural safety of an existing bridge at reconstruction, usage and disapproval (in Dutch), RTD 1006:2013 1.1," 117 pp.

Rijkswaterstaat, 2014, "Guidelines for coring, transporting, and testing of concrete cores and the determination of the compressive and splitting tensile strength (in Dutch)," RTD 1021:2014, Rijkswaterstaat, 29 pp.

Rijkswaterstaat, 2016, "Guidelines for Nonlinear Finite Element Analysis of Concrete Structures," *RTD 1016:2012*, 65 pp.

Russo, F. M., Wipf, T. J. and Klaiber, F. W., 2000, "Diagnostic Load Tests of a Prestressed Concrete Bridge Damaged by Overheight Vehicle Impact," *Transportation Research Record*, V. 1696, pp. 103-110.

Sanayei, M., Reiff, A. J., Brenner, B. R. and Imbaro, G. R., 2016, "Load Rating of a Fully Instrumented Bridge: Comparison of LRFR Approaches," *Journal of Performance of Constructed Facilities*, V. 2016, No. 30, pp. 2.

Saraf, V. K., Nowak, A. S. and Till, R., 1996, "Proof load testing of bridges," *Probabilistic Mechanics & Structural Reliability: Proceedings of the Seventh Specialty Conference*, Frangopol, D. M. and Grigoriu, M. D., eds., Worcester, MA, USA, pp. 526-529.

Stewart, M. G. and Val, D. V., 1999, "Role of load history in reliability-based decision analysis of aging bridges," *Journal of Structural Engineering-ASCE*, V. 125, No. 7, pp. 776-783.

Velázquez, B. M., Yura, J. A., Frank, K. H., Kreger, M. E. and Wood, S. L., 2000, "Diagnostic load tests of a reinforced concrete pan-girder bridge," V. Research Report 7-2986-2, The University of Texas at Austin, Austin, TX, USA, 121 pp.

Vergoossen, R., Naaktgeboren, M., ‘t Hart, M., De Boer, A. and Van Vugt, E., 2013, "Quick Scan on Shear in Existing Slab Type Viaducts," *International IABSE Conference, Assessment, Upgrading and Refurbishment of Infrastructures*, Rotterdam, The Netherlands, pp. 8.

Vrouwenvelder, T., Holicky, M. and Markova, J., 2002, "JCSS Probabilistic Model Code Example Applications," 19 pp.

Yang, Y., 2015, "Experimental Studies on the Structural Behaviours of Beams from Ruytenschildt Bridge," Stevin Report 25.5-15-09, Delft University of Technology, Delft, 76 pp.

Yang, Y., Den Uijl, J. A. and Walraven, J., 2016 "The Critical Shear Displacement theory: on the way to extending the scope of shear design and assessment for members without shear reinforcement," *Structural Concrete*, V. 17, No. 5, pp. 790-798.

Yang, Y., Walraven, J. and den Uijl, J. A., 2017, "Shear Behavior of Reinforced Concrete Beams without Transverse Reinforcement Based on Critical Shear Displacement," *Journal of Structural Engineering*, V. 143, No. 1.

LOAD TESTING OF HIGHLY SKEWED CONCRETE BRIDGES

Mauricio Diaz Arancibia and Pinar Okumus

Abstract: Recurrent service problems and uncertainties in load distribution have been frequently reported by Departments of Transportation for skewed bridges. Service problems, such as deck cracking or excessive bridge racking can lead to bridge deterioration, and indicate the need of a better understanding of the structural response of high skew bridges to service loading. This paper presents the instrumentation and load testing of a three-span, medium span length, prestressed concrete bridge with 64° of skew to understand service, analysis and design problems associated with skew.

The instrumentation plan for the bridge was developed based on service problems observed in concrete bridges with high skew such as deck cracking and displacements, as reported by the literature and by regular bridge inspections. Complete understanding of skew related responses required both short-term testing and long-term load monitoring. Structural responses of the key areas of the bridge to live and temperature loads and shrinkage were measured. The effects of certain bridge details on live load distribution were determined using finite element models validated through short-term load testing data. The evolution and magnitude of bearing movements and deck strains were captured for long periods of opposite thermal tendencies.

Keywords: bearing displacements, deck cracking, load distribution, load testing, shrinkage, skew, temperature

INTRODUCTION

Highly skewed bridges experience several construction and service performance problems. They have regularly been reported by State Departments of Transportation, and have also been described in the published literature[1]. Skew-related problems are observed, even at the component level. For instance, double-tee prestressed concrete bridge girders suffer significant end cracking during prestress release due to torsion and formwork restraint caused by the skewed geometry[2]. At the system level, bridge movements and deck cracking are likely the ones causing the most detrimental effects on the structure. Temperature loads and shrinkage on skewed bridges result in superstructure horizontal movements or a tendency to rotate, which typically leads to premature failure of expansion joints and bearings, and misalignment of parapets between bridge and approach slab. On the other hand, characteristic diagonal acute corner deck cracking observed on skewed bridges may cause corrosion of the deck reinforcement and early deck replacement. In addition to these performance problems, the geometry of skewed bridges yields to modified load paths that can change how superimposed loads are distributed to structural components.

Bridge load testing is an excellent means to evaluate skewed bridge behavior. In general, load testing has been used to rate bridge load carrying capacity under short-term loading (load rating), understand and assess bridge response under long-term loading, or to generate data to validate numerical models that are later employed to study bridge performance. For instance, in 2005, Hag-Elsafi and Kunin[3] developed a live-load testing program for load rating of a single-span, non-skewed, 70-ft long bridge with post-tensioned bulb-T beams built in 1961. A test-based rating was imperative since the bridge had no plans on record, leading to uncertainties on variables that affect load carrying capacity, which in turn prevented an analytical rating. Another example is the investigation on live load shear distribution of prestressed concrete girder bridges performed by French et al.[4] They conducted full-scale laboratory and field bridge live load tests. Laboratory tests on a non-skewed bridge provided insights on shear distribution during the elastic range, and up to ultimate shear failure. Field tests were performed on six prestressed concrete girder bridges to determine shear distribution under service conditions. The effects of skew on shear distribution were also investigated, and tested for a bridge with 30° of skew. Data from load testing were used to validate finite element models for parametric studies on shear distribution. Testing showed that the shear redistributes prior to ultimate failure, and therefore, the use of linear elastic distribution factors is conservative when evaluating the shear ultimate capacity of the bridge. Parametric studies using finite element models, which did not consider the contribution of barriers, diaphragms and skew, showed that girder spacing, deck thickness and span length have the most significant effects on linear elastic shear distribution.

Problems on highly skewed bridges were also investigated using load testing. Fu et al.[5] studied the causes of deck corner cracking on skewed bridges. They instrumented the deck of two girder type bridges. One of the bridges had steel I-beams and 49° of skew, while the other had AASHTO prestressed concrete beams and 46° of skew on the instrumented span. Deck strains and temperature, and ambient temperature and humidity were recorded for short-term loading that consisted of controlled truck loading, and for long-term loading, such as temperature and shrinkage. Using the data together with finite element models, they found that deck corner cracking is caused by thermal loading and shrinkage during concrete hydration, and that fatigue loading caused by traffic may widen the cracks. Huang et al.[6] investigated transverse bending moment distribution on highly skewed steel girder bridges. They instrumented and load tested a two-span, deck-on-steel bridge with a skew angle of 60°. Load distribution was evaluated by comparing load test results with live load distribution factors obtained from AASHTO. The effect of deck stiffness and diaphragms on load distribution was explored using a finite element model validated with test results. Researchers concluded that for bridges similar to the one tested, AASHTO distribution factors are conservative for positive moments and un-conservative for negative moments.

Load testing was employed for this study to understand the behavior of highly skewed medium-span prestressed concrete bridges. The tested bridge was selected due to its high skew and distinctive mixed support fixity arrangement over the piers; a feature designed to minimize horizontal lateral movements. The investigation addressed the most common problems with skewed bridges: load distribution, superstructure horizontal movements and deck corner cracking, using short-term and long-term loading schemes. Short-term loading consisted of truck loading under controlled conditions and was used to generate shear and bending strain data. These data were used to validate finite element models employed for parametric studies dealing with the effects of certain bridge details on shear and bending live load distribution to girders. Long-term loading was composed of temperature loads, shrinkage and traffic load. Under these loads, bearing horizontal movements and deck strains at critical locations were continuously monitored for approximately 5 and 7 months, respectively, to gain a better understanding of how highly skewed bridges move and how deck cracking develops.

BRIDGE DESCRIPTION

The tested structure is identified as bridge B-40-870 in the Highway Structures Information System of Wisconsin Department of Transportation (WisDOT)[7]. It carries the Interstate Highway 94 East-Bound traffic over the Hank Aaron State Trail in Milwaukee County, Wisconsin. All three spans are deck-on-prestressed concrete-girders, continuous for live load and superimposed loads. The bridge has a skew of 64°. General characteristics and geometry of the bridge are presented in Table 1 and Figure 1, respectively.

Table 1—Bridge B-40-870 general features

Skew	Span lengths	Ave. deck width	Girder type	Abutment type	Bearing types	Year built
64°	109.2 ft – 125.4 ft – 85.8 ft [33.3 m – 38.2 m – 26.2 m]	94.9 ft [28.9 m]	54 in. wide flanged prestressed girder	Semi-retaining	Elastomeric (abutments and piers), metallic (piers)	2016

The bridge has fifteen prestressed concrete girders on each span, with varying or flared spacing due to a slight horizontal curvature of 4300 ft [1311 m] of radius. The cast-in-place deck is 8-in [203-mm] thick, fully composite with girders by means of #4 [#13] shear connectors at stirrup spacing. Transversely, girders are connected through steel diaphragms along spans, and through full depth cast-in-place concrete diaphragms over piers. The concrete diaphragms are not in contact with pier caps or girder bearing pads. The specified compressive strength of concrete for deck and substructure is 4000 psi [27.6 MPa]. Pretensioned concrete girders have a specified concrete strength of 8000 psi [55.2 MPa], with 270000 psi [1861.6 MPa] ultimate strength strands. Mild steel reinforcement has a specified yield strength of 60000 psi [413.7 MPa].

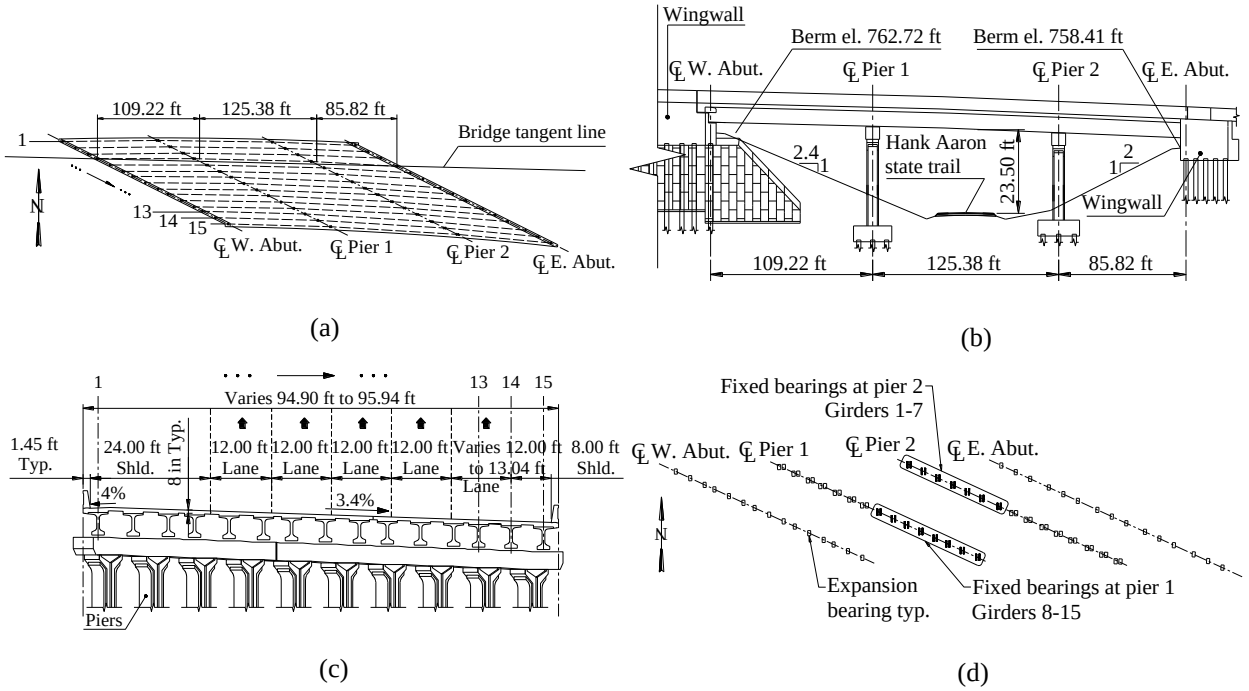

Figure 1—Bridge geometry: (a) plan view; (b) elevation (looking north); (c) cross section (looking east); (d) bearing layout shown on plan view [1 ft = 0.3048 m]

The bridge has a unique configuration of bearing fixity. Bearings over each pier are a mixed arrangement of both expansion and fixed bearings. Bearings over the abutments are expansion bearings only, as shown in Figure 1d. This special bearing arrangement was designed to keep thermal and shrinkage displacements at expansion joints and at parapet expansion joint cover plates under the limits specified on section 28.3.4 of the WisDOT Bridge Manual (BM)[8].

LOAD TEST SET-UP

The load test was conducted to understand the short- and long- term behavior. Short-term results, shear and bending strains on girders, were generated by loading the bridge with trucks moving at crawl speed. These results were used for finite element model validation. Long-term data consist of bearing movements and deck strains at critical locations for a skewed bridge[1]. Long-term loading includes temperature, shrinkage and traffic on the bridge under service.

Short-term loading

Loading to collect short-term data consisted of two dump trucks, positioned in series or parallel, moving at crawl speeds (i.e., less than 5 mph [8 km/h]) to simulate a pseudo-static load. Dimensions and axle weights of the two trucks used are shown on Figure 2. The middle and rear axles were assumed to equally share the measured weight of both axles together.

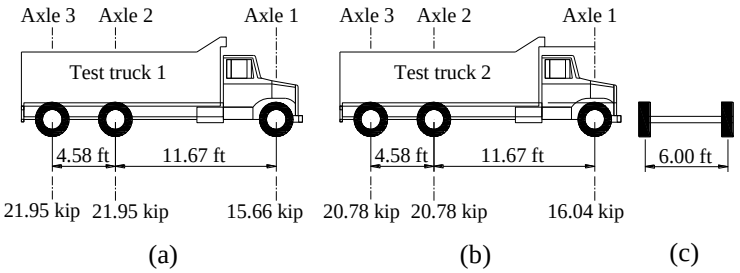

Figure 2—Load test trucks dimensions and axle weights: (a) test truck 1; (b) test truck 2; (c) front view showing axle width [1 ft = 0.3048 m, 1 kip = 4.4482 kN]

The short-term test had four load cases (Figure 3). In all load cases, the trucks moved from west to east. Each load case was run twice to ensure the results were repeatable. During some runs, the trucks came to a full stop at predefined positions to achieve actual static loading by avoiding any dynamic effects coming from motion of the trucks, surface irregularities or bumps on the road. Table 2 presents the details of truck stops.

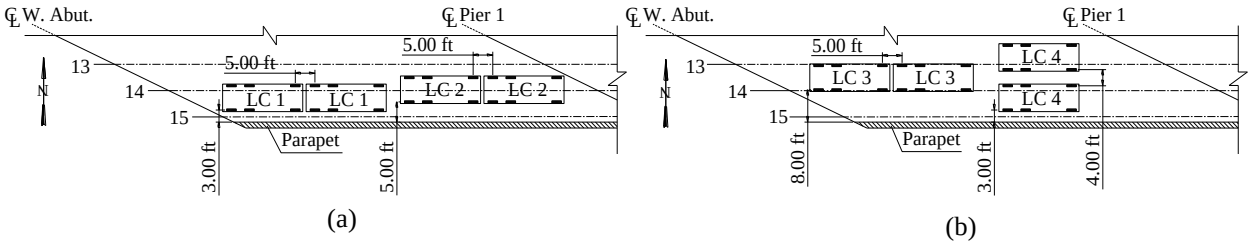

Figure 3—Load test load cases: (a) load cases 1 and 2; (b) load cases 3 and 4 [1 ft = 0.3048 m]

Table 2—Truck stops per load case

Load case	Run	Stops		
		Span 1 at mid-span (west)	Span 2 at mid-span	Span 3 at mid-span (east)
1	1	Yes	Yes	-
	2	-	-	-
2	1	Yes	Yes	-
	2	-	-	-
3	1	-	Yes	-
	2	Yes	Yes	Yes
4	1	Yes	Yes	-
	2	-	-	-

Instrumentation for short-term loading

Sensors for short-term loading consisted of uniaxial resistance strain gages attached on the surface of prestressed concrete girders on the west span (span 1). Strain gages measuring bending strains were installed in pairs on the bottom face of the three girders (girders 13, 14 and 15 in Figures 1a and 4) near the south side, and at three points along their span (at 15ft [4.6 m], 40 ft [12.2 m] and 80 ft [24.4 m] from the west end of girders). Two gages were used at each gage location for redundancy against potentially malfunctioning sensors.

A second set of strain gages was used on the west end of the same girders (girders 13, 14 and 15) to measure shear strains at girder ends. These sensors are located near the obtuse corner where maximum shear response is expected on a skewed bridge. The gages were placed at mid-height of girder webs, where strains reach measurable values (i.e., close to the location of maximum shear strain). For this purpose, three strain gages were arranged in a 45-degree rosette layout, with the central one aligned with the horizontal axis of the girder. This strain gage configuration allows strains in any direction to be determined, in addition to the vertical shear strain determined only from the diagonally-oriented gages. The layout of bending and shear strain gages is presented in Figure 4 shown on plan view.

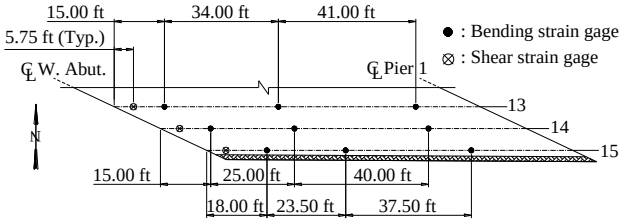

Figure 4—Bending and shear strain gage layout shown on plan view of south-west corner [1 ft = 0.3048 m]

Instrumentation for long-term loading

Long-term monitoring was performed with displacement sensors and vibrating wire embedment strain gages. The displacement sensors were wireless devices that have two components; the displacement sensing element and the wireless transmitter (Figure 5). The displacement sensing element had a mechanical stroke length of 3 in [76.2 mm]. It is connected (i.e., wired) to the wireless transmitter that sends displacement readings, at pre-set time intervals, to a solar powered data collector that allows storage of and remote access to the information. Displacement sensors also measure temperature.

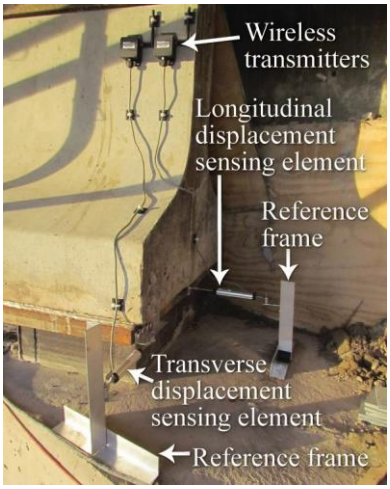

Figure 5—Displacement sensors as installed on the girder bearing at the south-east corner over the abutment

Five displacement sensors were installed on the bridge to understand the global displacement behavior of the bridge in the horizontal space. Girder bearings near the north-west and south-east corners over the abutments had two displacement sensors each (Figure 5). One sensor was placed on the girder near the south-west corner over the abutment. Having two sensors at a particular bearing, one in the longitudinal and the other in the transverse bridge

directions, and under the assumption of small rotations on the horizontal plane enabled the computation of the relative change of bearing position with time. This was not possible with the single sensor near the south-west abutment corner, however, this sensor still provided important bearing transverse displacement measurements. The acute corners of the bridge were chosen to be instrumented for displacements because they may experience significant movements[1]. Figure 6 presents the layout of displacement sensors.

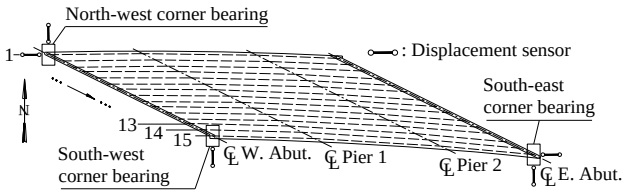

Figure 6—Displacement sensor layout shown on plan view

A total of twelve vibrating wire strain gages were installed in the concrete deck to understand its behavior due to long-term effects. Eleven were embedded in the deck, near the south-east corner of the bridge. The twelfth vibrating gage was used to measure shrinkage and temperature effects. This control gage was installed inside an unloaded, "stress free" concrete cylinder cast with the concrete used in the deck. The cylinder with the gage inside was placed near the bridge so that it is exposed to similar environmental conditions as the deck. Each of the vibrating wire gages was connected to a solar powered data logger that allowed remote access to the information. All vibrating wire gages also measure temperature.

Vibrating wire strain gages in the concrete deck were arranged in two lines: at deck mid-span between girders 14 and 15 (oriented in longitudinal and transverse directions), and along the edge of the top flange of girder 14 (oriented in transverse direction). All gages were attached to the top deck reinforcement, except for two along the latter line which were attached to the bottom reinforcement. Gages on the top layer and bottom layer deck reinforcement were at an average depth of 4 in [10.2 cm] and 6 in [15.2 cm] from the deck top surface, respectively. The layout of vibrating wire strain gages is shown on Figure 7. The acute corner region of the bridge was selected for instrumentation in order to better understand the development and progress of the typical diagonal concrete deck cracks that are regularly reported for skewed bridges.

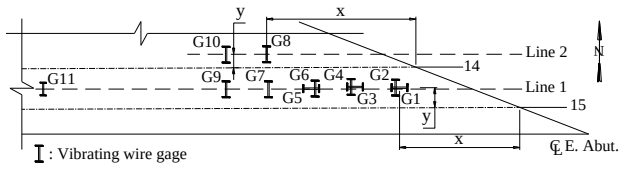

	G1	G2	G3	G4	G5	G6	G7	G8	G9	G10	G11
x [in]	197.10	203.60	271.10	276.60	342.10	335.60	412.10	244.25	481.60	310.75	781.60
y [in]	33.00	33.00	34.00	34.50	31.50	32.00	31.50	22.00	31.50	21.50	33.00

Figure 7—Deck vibrating wire strain gages layout shown on plan view [1 in = 0.0254 m]

LOAD TEST RESULTS

Results for short-term loading and Finite Element Modeling

Since data on the bridge under live load was only collected on three girders out of fifteen, the overall bridge load distribution was evaluated using a finite element model that was created and validated using test data. Finite element models used four-node shell elements for the deck and full depth diaphragms, and used frame elements for girders, parapets, partial depth diaphragms and steel in-span diaphragms. Full composite action was assumed between girders and deck by forcing deck and girder elements to connect at offset coincident nodes. All members were linear elastic.

Validation was achieved by gradually refining the finite element models. Table 3 summarizes changes made to the initial model (model v1). The final model (model v7) includes parapets, end, pier and intermediate diaphragms, stiffnesses of expansion elastomeric bearings, and material properties from cylinder compression tests where they were available. Translational and rotational stiffness of bearings were calculated using expressions on section 14.6.3 of AASHTO LRFD Bridge Design Specifications (BDS)[9] and the upper-bound elastomer shear modulus from section

27.2.1 of the WisDOT BM[8]. The concrete modulus of elasticity for the deck, parapets, pier and end diaphragms was estimated using their 28-day compressive strengths. On other hand, the modulus of elasticity of each prestressed girder was evaluated recognizing the concrete gain of strength with age. In fact, there was an average difference of 203 days between the load test and 28-day cylinder break dates. Projected compressive strengths were calculated using expressions proposed by the ACI Committee 209[10].

Table 3—Refinement steps of the finite element models

Improvements	Models for validation						
	v1	v2	v3	v4	v5	v6	v7 (final)
Parapets	x	✓	✓	✓	✓	✓	✓
End diaphragms	x	x	✓	✓	✓	✓	✓
Pier diaphragms	x	x	x	✓	✓	✓	✓
Intermediate diaphragms	x	x	x	x	✓	✓	✓
Bearing stiffnesses	x	x	x	x	x	✓	✓
Refined material properties	x	x	x	x	x	x	✓

The impact of model refinements on results is presented in Figure 8 as error normalized with respect to the error of the initial model (model v1). Error is assumed as the sum of strain deviations (in absolute value) from load test results at all sensor locations and for all load cases. Figure 8a shows that better estimates of material properties, and inclusion of secondary members such as parapets and end diaphragms play a significant role in bending behavior, and that including estimated bearing stiffnesses had a small contribution to the accuracy of results. In relation to shear behavior, Figure 8b shows a major impact of end diaphragms, followed in importance by bearing stiffnesses. Additional details of the finite element models will be published elsewhere.

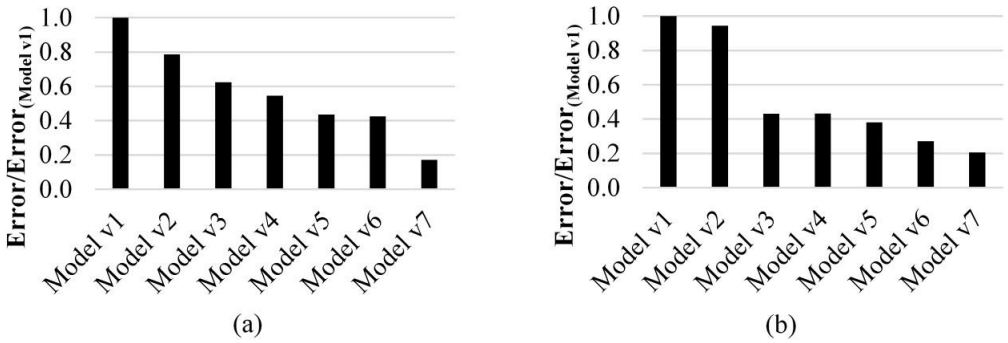

Figure 8—Error from refined models normalized with respect to the initial model: (a) bending; (b) shear

In general, results from truck loading and bridge finite element model (model v7) were in good agreement. Figure 9 compares strains obtained from testing (on the left) to ones obtained from finite element model results (on the right) as a function of approximate position of the front axle of the leading truck. Due to space constraints, in this paper, only results for the second run of the first load case (Figure 3 and Table 2), along the shear and bending strain gage lines at nominal distances of 5 ft [1.5 m], 15 ft [4.6 m], 40 ft [12.2 m] and 80 ft [24.4 m] from the west girder end (Figure 4), are presented as representative examples.

The validated model (model v7) was used to obtain live load distribution and to explore the effect of bridge details on load distribution. The models shown in Table 4 were built. Model 0 is the original bridge with as-built details.

Girder distribution factors for shear and bending moment were computed for all models and compared. These results were also compared with distribution factors obtained with the distribution factor method of AASHTO LRFD BDS[9] with WisDOT BM[8] exceptions, even though these factors do not apply to this bridge as bridge geometry is not regular (e.g., skew beyond 60º). Figure 10 presents the ratio of the AASHTO live load distribution factors to the corresponding factors obtained from the finite element models for shear and moment, on interior and exterior girders. Values of the ratio above 1.0 indicate AASHTO distribution factors are conservative.

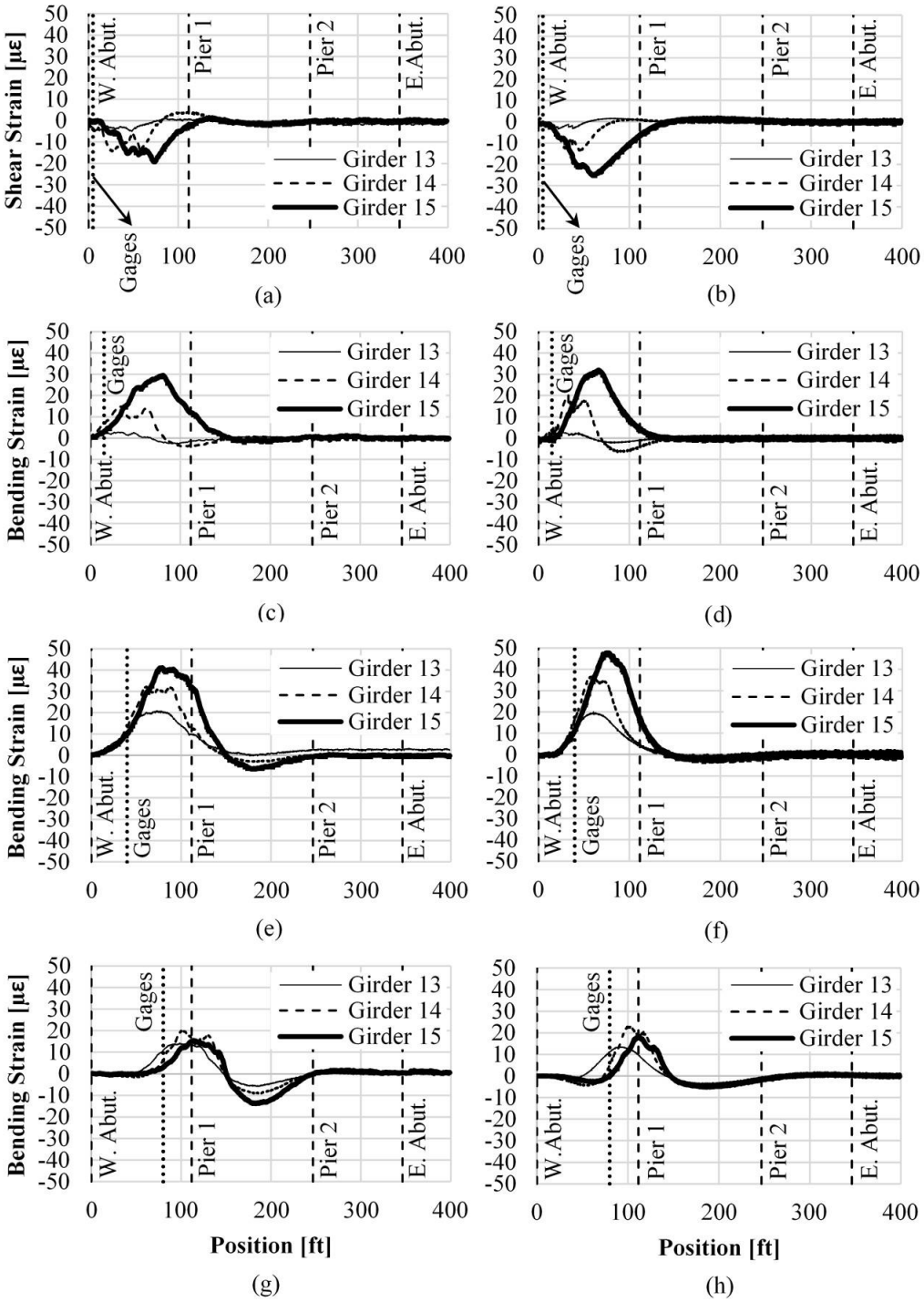

Figure 9—Shear and bending strains under short-term loading as a function of front axle position: from (a) test at 5 ft; (b) model at 5 ft; (c) test at 15 ft; (d) model at 15 ft; (e) test at 40 ft; (f) model at 40 ft; (g) test at 80 ft; (h) model at 80 ft [1 ft = 0.3048 m]

Results on Figure 10 reveal that the bridge details considered in Table 4 have a small influence on load distribution factors for both moment and shear. Changes in abutment diaphragms (Model 1 or 2) have a larger impact on live load distribution than others. For instance, for shear on interior girders of the exterior spans (Figure 10c), and especially on the third span, AASHTO load distribution factor was less conservative, which indicates a reduced ability to

distribute shear forces without an abutment diaphragm. Such results are not evident for shear on exterior girders or for moment. On the other hand, on the exterior spans for positive moment on the interior (Figure 10a) and exterior (Figure 10b) girders, full depth abutment diaphragms (Model 2) caused a more conservative AASHTO distribution factor, which indicates a better distribution of girder bending moments. In the case of shear force distribution, changes caused by full depth abutment diaphragms are negligible.

Table 4—Finite element model parameters

Model	Abutment Diaphragm	Diaphragm along the span	Pier Diaphragm
0	Partial depth concrete	Steel at third points of span	Full depth concrete
1	*None*	Steel at third points of span	Full depth concrete
2	*Full depth without encasing girder bearings*	Steel at third points of span	Full depth concrete
3	Partial depth concrete	*None*	Full depth concrete
4	Partial depth concrete	Steel at third points of span	*None*

Figure 10 also presents how AASHTO distribution factors compare to the ones obtained from finite element models. AASHTO distribution factors for moment are quite conservative for positive moment, and stand close to or at the verge of being un-conservative for negative moment on the interior and exterior girders, respectively. It should be noted that the distribution factors presented do not include moment reduction for skewed bridges following the WisDOT exception to AASHTO LRFD BDS[9]. If reduction factors were included, AASHTO factors will not be able to predict load distribution conservatively. In the case of distribution factors for shear, AASHTO stays moderately conservative for shear on interior girders, and it displays a similar trend for shear on exterior girders, with the exception of the interior span, where it lies on the limit.

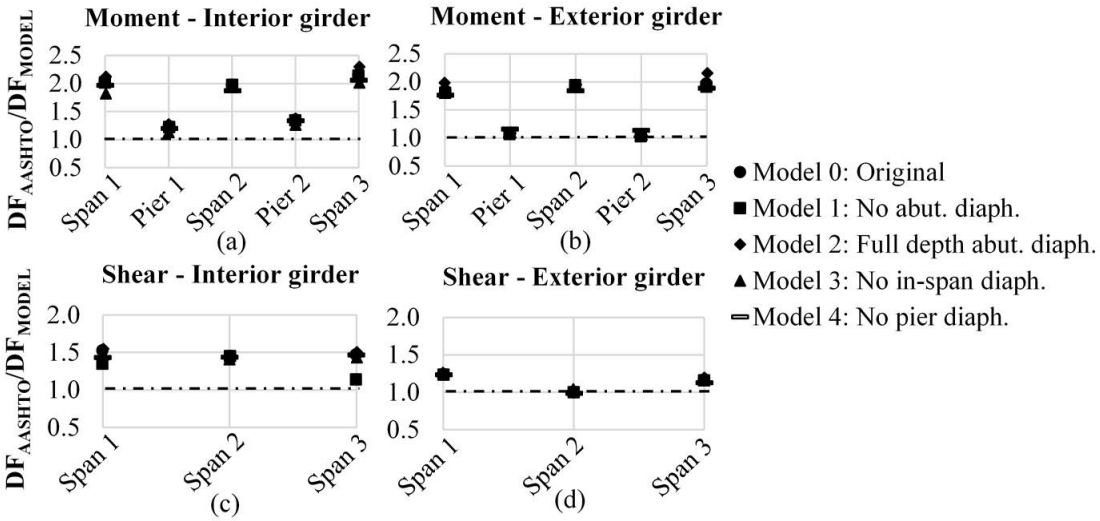

Figure 10—Comparisons of live load distribution factors from AASHTO LFRD BDS and from finite element models for: (a) moment-interior girder; (b) moment-exterior girder; (c) shear-interior girder; (d) shear-exterior girder

Results for long-term loading

Displacement sensors—These sensors measure displacements and temperature from the three corners of the bridge to understand the global displacement behavior of the bridge in the horizontal space under long-term loading. Sensors were attached to the top of the bearings of exterior girders. Data collection from displacement sensors started on November 13, 2016, shortly after construction, and will continue for a year. In this paper, results up to May 16, 2017 are presented on Figures 11-13. Reported displacement values are relative to bearing positions at the beginning of data recording. Since data recording started shortly after construction, displacements at the beginning of recording are expected to be virtually zero. Disturbances to sensors due to continuing construction resulted in loss of data for one month shown as gaps on the figures. The results after the data gap assume that no changes in displacement occurred during the period when no data were recorded. The displacement results are presented in two directions: in transverse (i.e., perpendicular to bridge axis) and longitudinal (i.e., along bridge axis) directions, and in parallel-to-expansion joint (racking) and normal-to-expansion joint directions.

Transverse and longitudinal displacements—Figures 11a-11b display the bearing displacements and the average internal temperature of the corresponding pair of sensors at the bridge acute corners. Figure 11c shows the transverse displacements in the south-west corner bearing and temperature, measured by a single sensor. In Figure 11c, potential impact of longitudinal displacements on transverse displacement measurements, which cannot be captured due to the lack of a second sensor, was neglected.

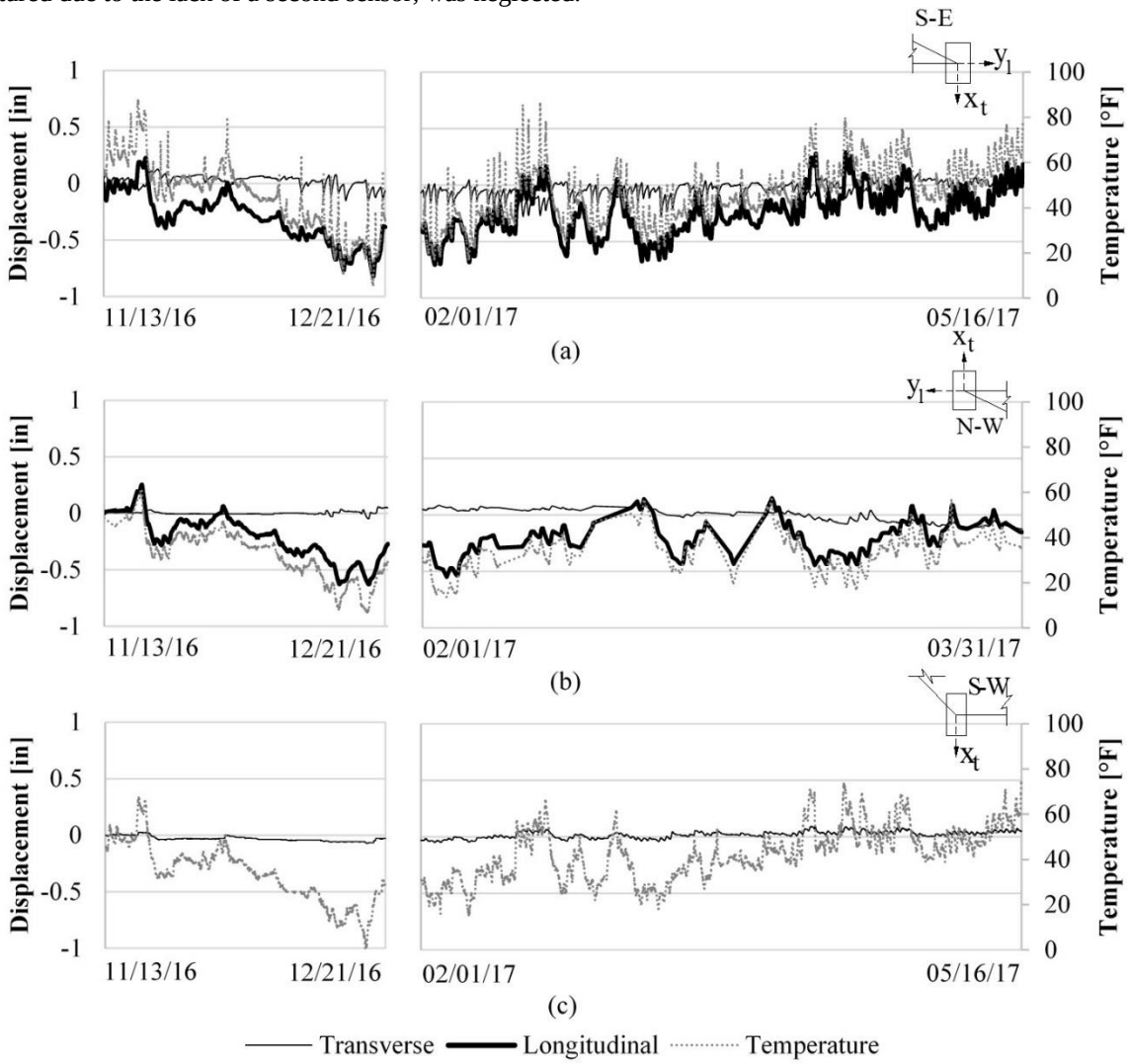

Figure 11—Bearing transverse and longitudinal displacements, and temperature on the: (a) south-east corner; (b) north-west corner; (c) south-west corner [1 in = 25.40 mm]

Results on Figures 11a and 11b show that longitudinal displacements were much larger than transverse displacements (up to 5 times) at both acute corner bearings. In all locations, transverse displacements were smaller than 0.28 in. It is also interesting to note that longitudinal displacements on the south-east bearing are larger than the ones observed on the north-west bearing, even though the expansion length for the latter is longer, as shown on Figure 1a. This can be explained by the horizontal curve of the bridge geometry, which gives rise to an effective expansion length for the south-east bearing more than 10 ft [3.0 m] longer.

Table 5 summarizes maximum values of transverse and longitudinal displacements ($\delta_{max(+)}$ and $\delta_{max(-)}$) since the beginning of data recording (construction), in both positive and negative directions according to the sign conventions shown in Figure 11. Table 5 also presents maximum changes in temperature (ΔT_{max}) between any two dates during data recording, and the corresponding change in transverse and longitudinal displacements ($\Delta\delta$) between those dates.

Table 5—Bearing displacements and temperature in transverse and longitudinal directions

Location	Period	Transverse direction				Longitudinal direction			
		$\delta_{max(+)}$, in [mm]	$\delta_{max(-)}$, in [mm]	ΔT_{max}, °F [°C]	$\Delta\delta$, in [mm]	$\delta_{max(+)}$, in [mm]	$\delta_{max(-)}$, in [mm]	ΔT_{max}, °F [°C]	$\Delta\delta$, in [mm]
S-E corner	1	0.13 [3.28]	-0.15 [-3.87]	-66 [-36]	0.01 [0.35]	0.23 [5.73]	-0.82 [-20.82]	-66 [-36]	-0.98 [-24.80]
	2	0.10 [2.53]	-0.28 [-7.06]	70 [39]	-0.27 [-6.80]	0.29 [7.39]	-0.70 [-17.90]	70 [39]	0.83 [21.20]
N-W corner	1	0.06 [1.47]	-0.05 [-1.24]	-54 [-30]	-0.02 [-0.58]	0.25 [6.46]	-0.63 [-15.93]	-54 [-30]	-0.81 [-20.53]
	2	0.09 [2.25]	-0.13 [-3.19]	44 [24]	0.02 [0.48]	0.15 [3.76]	-0.55 [-13.97]	44 [24]	0.69 [17.55]
S-W corner	1	0.07 [1.83]	-0.02 [-0.61]	-67 [-37]	0.08 [2.09]	N/A	N/A	N/A	N/A
	2	0.05 [1.24]	-0.09 [-2.33]	60 [33]	-0.09 [-2.35]	N/A	N/A	N/A	N/A

Changes in bearing displacements, $\Delta\delta$, caused by maximum temperature changes, ΔT_{max}, as displayed in Table 5 do not correspond to the difference between measured maximum displacements, $\delta_{max(+)}$ and $\delta_{max(-)}$. In other words, maximum displacements do not take place when temperature reaches a maximum or a minimum. The discrepancy is significant for transverse displacements on acute corner bearings, less significant on the obtuse corner bearing, and negligible for displacements in the longitudinal direction. These discrepancies show that transverse displacements are impacted by factors other than temperature.

Figures 11a and 11b show that the longitudinal displacements correlated well with temperature, indicating that temperature change is the main reason for longitudinal bridge displacements. In fact, the Pearson's correlation coefficient, which indicates for a pair of variables how strong their linear association is (i.e., ± 1: perfect linear relationship, 0: no linear correlation)[11], between longitudinal displacements and temperature for both bearings and periods had a strong positive correlation with values above 0.90. On the other hand, correlation coefficients for temperature and transverse displacements on acute corner bearings were below 0.25. Such low coefficients show that transverse displacements and temperature on acute corners did not correlate linearly and that factors other than temperature may have a more important role on transverse displacements. In contrast to this finding, transverse displacements and temperature on the obtuse corner had a strong positive linear association with correlation coefficients of 0.90 for both periods. This may imply that transverse bearing movements also depend on location.

To inspect temperature effects on movement more closely, transverse and longitudinal bearing movements on a single day were investigated and are presented in Figure 12. During a single day, both longitudinal and transverse displacements had a significant linear correlation with temperatures. Pearson coefficient for transverse displacement was -0.90. Figure 12 suggests that temperature could influence transverse bearing movements, but such influence is not obvious when long term displacements are considered (Figure 11).

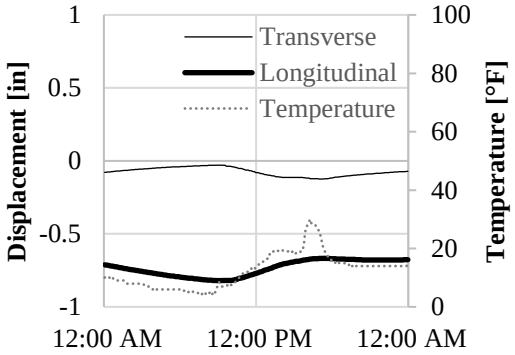

Figure 12—South-east bearing displacements and temperature on December 19, 2016 [1 in = 25.40 mm]

Parallel-to-expansion joint (racking) and normal-to-expansion joint bearing displacements—Results presented in the previous section seem to show that the unique support fixity arrangement (Figure 1d) led to small transverse displacements as intended by design. Figure 13 shows parallel-to-expansion joint and normal-to-expansion joint displacements, calculated from transverse and longitudinal displacements based on bridge geometry. Parallel-to- and normal-to- joint displacements at the south-west corner cannot be calculated since only a single sensor was used at this location.

When Figures 11a and 11b are compared with Figure 13, it can be seen that bearing displacements in parallel-to-joint and normal-to-joint directions are mainly caused by longitudinal movements of the bridge. In fact, given the high skew of the bridge (i.e. 64º), approximately 90% and 40% of the bearing longitudinal displacement translates into the parallel-to-joint displacement, and normal-to-joint displacements, respectively. In general, parallel-to-joint displacements are larger than normal-to-joint displacements.

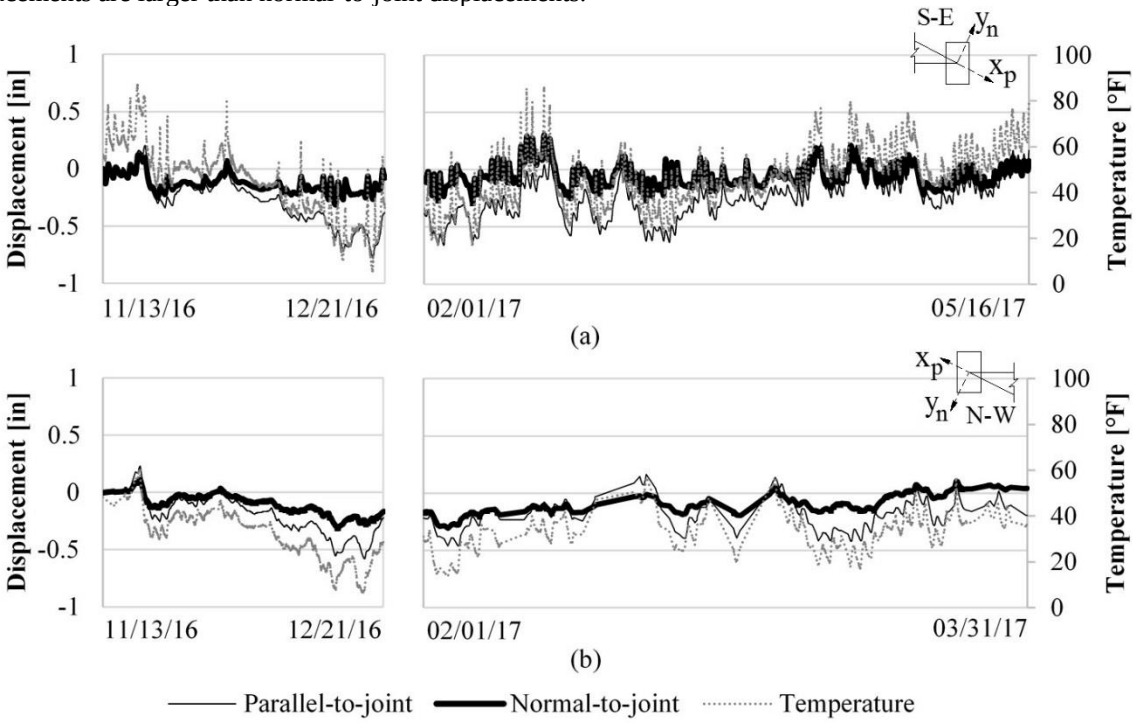

Figure 13—Bearing parallel-to-joint and normal-to-joint displacements, and temperature on the: (a) south-east corner; (b) north-west corner [1 in = 25.40 mm]

Parallel-to-joint displacements at both corners presented a strong positive linear relationship with temperature, with correlation coefficients beyond 0.90. Furthermore, normal-to-joint displacements at both corners exhibited a less strong, still positive, linear correlation, with coefficients between 0.76 and 0.96. As expected, these results confirm the major influence of longitudinal bearing movements on these displacement components. It was also noted that the correlation strength changes from warming to cooling periods. During the seasonal warming period, the linear correlation between displacements (i.e., for all components) and temperature is always less strong, indicating that temperature is more predominant during the cooling period.

Table 6 presents maximum values of parallel-to- and normal-to- expansion joint displacements ($\delta_{max(+)}$ and $\delta_{max(-)}$) recorded since the beginning of data acquisition, in both positive and negative directions according to the sign conventions shown in Figure 13. Table 6 also presents maximum changes in temperature (ΔT_{max}) between any two dates, and the corresponding change in parallel-to- and normal-to- expansion joint displacements ($\Delta\delta$) between those dates. Changes in parallel-to- and normal-to- expansion joint displacements caused by maximum temperature changes as shown in Table 6 are not equal to the difference between measured maximum positive and negative displacement values. For these displacement components, discrepancies are within the range of the ones found for longitudinal displacements, with smaller differences for the parallel-to-joint displacement direction.

Table 6—Bearing displacements and temperature in parallel-to- and normal-to- joint directions

Location	Period	Parallel-to-joint direction				Normal-to-joint direction			
		δ_{max}, in [mm]	δ_{min}, in [mm]	ΔT_{max}, °F [°C]	$\Delta\delta$, in [mm]	δ_{max}, in [mm]	δ_{min}, in [mm]	ΔT_{max}, °F [°C]	$\Delta\delta$, in [mm]
S-E corner	1	0.20 [5.17]	-0.78 [-19.77]	-66 [-36]	-0.91 [-23.03]	0.12 [3.16]	-0.31 [-7.97]	-66 [-36]	-0.36 [-9.22]
	2	0.23 [5.89]	-0.66 [-16.80]	70 [39]	0.68 [17.36]	0.30 [7.73]	-0.29 [-7.30]	70 [39]	0.55 [13.94]
N-W corner	1	0.23 [5.82]	-0.58 [-14.75]	-54 [-30]	-0.73 [-18.56]	0.11 [2.81]	-0.31 [-7.79]	-54 [-30]	-0.35 [-8.80]
	2	0.16 [4.14]	-0.46 [-11.72]	44 [24]	0.62 [15.85]	0.10 [2.66]	-0.31 [-7.79]	44 [24]	0.30 [7.54]

Temperature and transverse displacements seem to have a relationship that is disrupted by other factors, which resulted in a weak correlation between the two measurements. Inclusion of additional variables into analyses (e.g. shrinkage), additional sensors and instrumentation time could help understand global bridge movements. Nevertheless, it is clear from the small lateral bearing displacements that any lateral translation or rotation on the bridge are very small, and that the thermal movements of the bridge are predominantly due to longitudinal expansion or contraction.

Vibrating wire strain gages—Recording of deck strains began on October 18, 2016 (i.e., 85 hours after deck pour), and will be in progress for one year. Figures 14 and 15 present strain and temperature data up to May 13, 2017. Figures 14a, 14c, and 14d display total deck strains along lines 1 and 2. Figure 14b shows transverse deck strains along line 1 after the control gage strains were subtracted (i.e., gage 12 strains). Figure 15 shows temperature on the control gage, and the average of temperature from all deck sensors. Temperatures on deck sensors were similar.

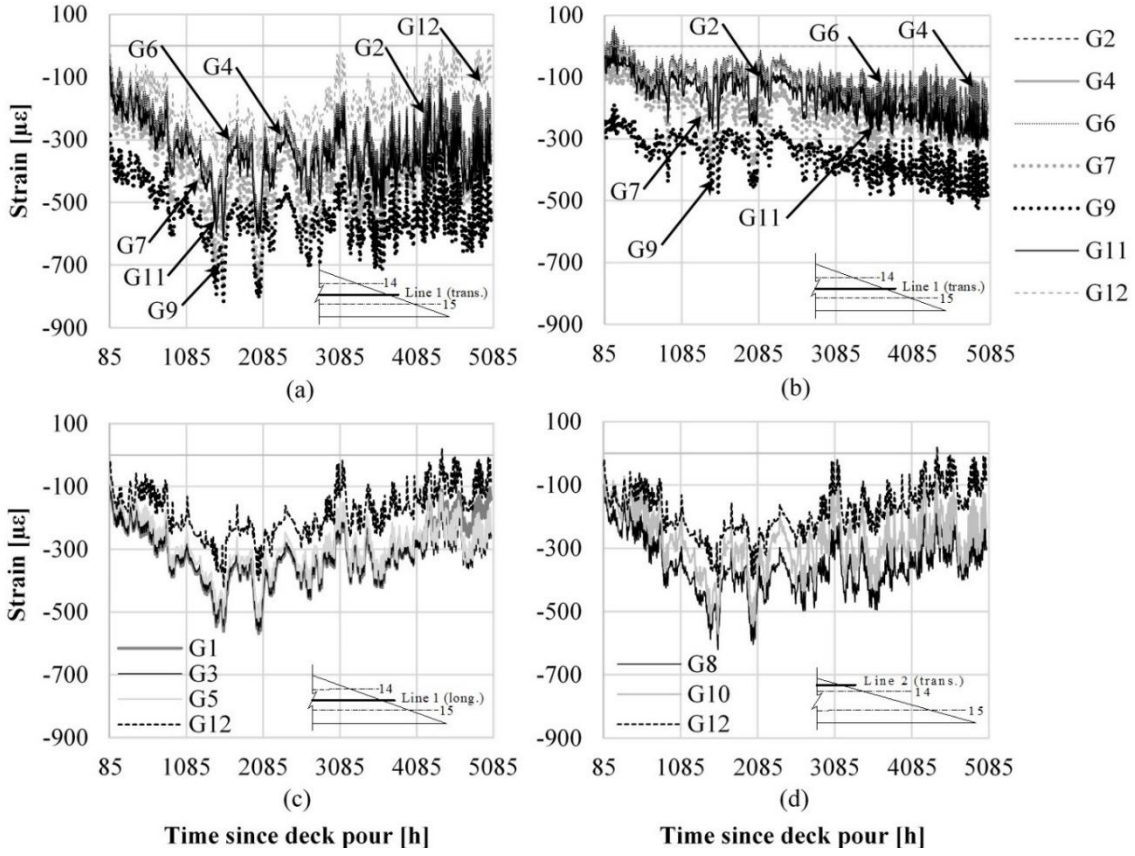

Figure 14—Deck strains: (a) total transverse strains on line 1; (b) transverse strains on line 1 minus strains from gage 12; (c) total longitudinal strains on line 1; (d) total transverse strains on line 2. Tension: (+); compression: (-)

Figure 15 shows that the average lowest temperature registered was of -4 °F (-20 °C) on December 19, 2016, and corresponded to a temperature drop of -77 ºF (-43 ºC) from the beginning of data collection. During this cooling period, the control gage (G12) exhibited a gradual increase in compressive strains (-369 µstrain), typical of negative temperature changes and shrinkage in concrete (Figures 14a, 14c, and 14d). The drop in temperature for the control gage was -61 ºF (-34 ºC). On the other hand, it can be seen on Figure 15 that the average highest temperature was of 81 ºF (27 °C) on April 15, 2017, and was reached after a change in temperature of 85 ºF (47 °C) from the date of the lowest temperature. During the warming period, the control gage presented a gradual increase in tensile strains (361 µstrain), which is expected for positive temperature changes (Figures 14a, 14c, and 14d). The increase in temperature for the control gage was 71 ºF (39 °C).

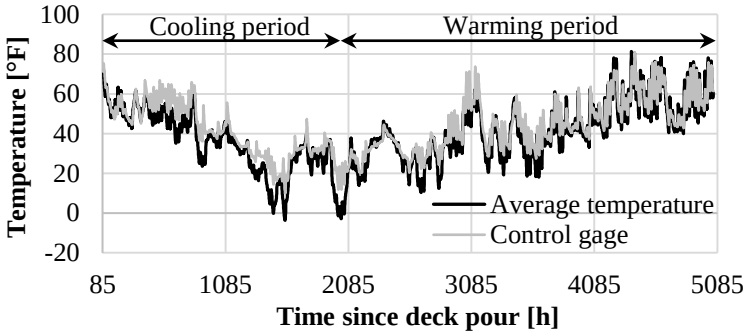

Figure 15—Average temperature of all gages in the deck and temperature in the control gage

Gages on lines 1 and 2 showed a similar behavior when compared to the control gage (Figures 14a, 14c, and 14d). During the cooling period, strains in the instrumented region of the deck dropped significantly. This tendency was more pronounced on transversely oriented gages (Figures 14a and 14d), which exhibited average maximum changes in strain of -556 µstrain and -505 µstrain for gages along lines 1 and 2, respectively. Longitudinal gages on line 1 displayed an average maximum change in strain of -441 µstrain.

During the warming period, strains showed a constant increase in tension. Positive changes in strain (tension) were significant; however, not large enough to take the instrumented region into tension. As in the cooling period, transverse gages registered greater average maximum changes in strain, which were of 482 µstrain and 465 µstrain for gages on lines 1 and 2, respectively. The average maximum change in strain for the longitudinal gages on line 1 was of 411 µstrain.

When strain measurements corresponding to the same temperatures measured at the beginning of the cooling period and at the end of the warming period were compared, the difference was a significant compressive residual strain. Transverse gages along lines 1 and 2 presented average compressive residual strains of 183 µstrain and 154 µstrain, respectively. Similarly, longitudinal gages measured an average compressive residual strain of 109 µstrain. Interestingly, the longitudinal gage 1 on line 1 had almost no residual strain, similar to the control gage, which might be an indicator for tensile strains offsetting the compression strains in this localized region.

Figure 14b shows interesting results for the transversely oriented gages along line 1. It indicates that after the removal of strains captured by the control gage, which are interpreted to be temperature and shrinkage strains, this region of the deck gradually and almost linearly accumulated compressive strains. In effect, almost all gages exhibited the same behavior. Results from other gages are not presented due to space limitations. Longitudinal gage 1 on line 1 was the exception and displayed a rapid increase in tensile strains approximately two months before the end of the warming period. Note that this gage is closer to the end of the bridge, and may be crossed by transverse or diagonal paths of high tensile strains that lead to typical deck acute corner cracking.

The results do not fully explain the accumulation of compressive strains over time. The limited number of monitoring points on the deck made it difficult to visualize global deck deformations. In addition, boundary conditions, exposed surface area of concrete, traffic loading and temperature gradient through the depth of the deck[12] are different for the control gage and gages in the deck. The deck also has mild reinforcement. These may lead to differences in shrinkage

and temperature strains. Therefore, corrections for shrinkage and temperature effects using readings of the control gage should be used with caution.

Figure 16 supplements Figure 14, and presents the total change in strain during the data recording period as a function of gage position along lines 1 and 2. It shows in general that changes in transverse strains along line 1 are significant and beyond -150 μstrain, with a slight tendency to increase towards the pier. A similar trend may exist towards the abutment after gage 4, as suggested by the readings on gage 2. Similar to line 1, changes in transverse strains along line 2 are important. However, with only two gages along this line, it is difficult to distinguish a clear trend. It is only evident that the gage closer to the abutment experienced larger compressive strains. On the other hand, changes in longitudinal strains on line 1 were insignificant at the location of the gage closer to the abutment (gage 1). For locations beyond this gage, changes in longitudinal strains were comparable to changes in strain in the transverse direction, and showed no visible tendency to increase or decrease towards the pier.

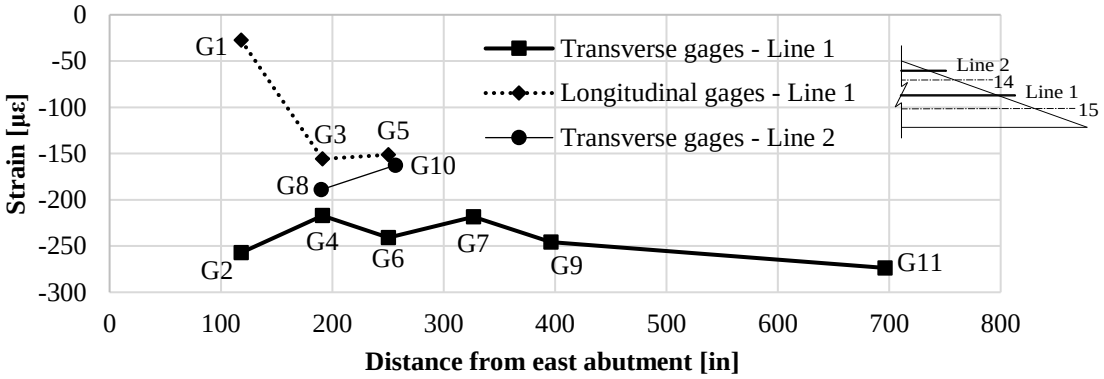

Figure 16—Total change in strain along gage lines 1 and 2 during data recording period. Tension: (+); compression: (-)

CONCLUSIONS

Based on the results presented on this paper, the following conclusions were made:

- Refinements to the bridge finite element model during the validation process revealed that an acceptable representation of the behavior of concrete bridges may require more than the inclusion of only principal structural components. In general, refinement requirements depend on the level of accuracy that is deemed acceptable. It was found that parapets, end and intermediate diaphragms, and enhanced estimates of material properties (modulus of elasticity) are important for predicting girder bending behavior. Girder end shear response is highly influenced by end diaphragms, and to some extent by bearing stiffnesses.

- The validated finite element model showed that the bridge details such as end and intermediate diaphragms have a small influence on girder shear and bending distribution. However, the use of full-depth abutment diaphragms improves girder bending distribution on exterior spans, and that the absence of abutment diaphragms degrades shear distribution on interior girders of exterior spans.

- Evaluations of AASHTO distribution factors for this bridge showed that they are overly conservative for positive moments, even though the factors are not applicable to the bridge due to its high skew. The predictions of negative moments over piers calculated using AASHTO distribution factors essentially match the ones obtained from the finite element model. These distribution factors would be un-conservative if skew correction (reduction) factors for moment were used. Distribution factors for shear are conservative for interior girders, and on exterior girders of exterior spans. Distribution factors for exterior girders of the central span compared well with finite element model estimates.

- Transverse bearing (and therefore girder and superstructure) displacements were small and were below 0.28 in [7.1 mm] during the observation period. Conversely, longitudinal displacements were significant and, on the acute corners, could reach maximum values up to 5 times larger than maximum transverse displacements.

- Even though transverse bearing displacements were minimized, presumably due to the unique support fixity arrangement employed in design, the maximum parallel-to-joint (racking) bearing displacements were only slightly smaller than maximum longitudinal bearing displacements. Similarly, the maximum normal-to-joint bearing displacements were larger than maximum transverse bearing displacements. Parallel-to-joint displacements were consistently larger than normal-to-joint displacements. The high skew of the bridge and the small magnitude of transverse displacements explain such results.

- Longitudinal bearing displacements have a strong positive linear correlation with seasonal and daily changes in temperature. This indicates that longitudinal movements are mainly caused by temperature. On the other hand, transverse bearing displacements do not correlate linearly to seasonal changes in temperature, but they have a linear association with temperature on certain days. This shows that transverse displacements are affected by temperature, but other factors are generally more influential.

- Both parallel-to- and normal-to-expansion joint bearing displacements have strong linear correlations with temperature, with the former having a stronger correlation. This confirms the significant influence of longitudinal movements on these alternative displacement directions.

- Based on the small magnitude of transverse displacements and the evident relationship between significant longitudinal bearing displacements and temperature, movements of the bridge are likely primarily caused by longitudinal thermal contraction and expansion. Any tendency of the bridge to rotate or laterally translate were small.

- Vibrating wire strain gages installed on an acute corner of the deck showed that deck behavior is complex. It seems to be significantly affected by the interaction of the deck with other structural components and by loads other than uniform changes in temperature. This is observed when measurements of strain from the control gage in a stress free concrete cylinder were compared to the ones of gages in the deck. Main observations on the deck behavior are as follows:

  During the cooling period, the concrete deck accumulates significant compressive strains, which is expected for the superposition of shrinkage and negative temperature changes. Negative changes in strain seemed more pronounced in the deck transverse direction.

  During the warming period, significant positive (tensile) changes in strain can develop. Larger changes in strain may be found in the deck transverse direction. In general, changes in strain caused by increasing temperatures were not large enough to create tension in the instrumented region. In fact, compressive strains beyond 150 μstrain could be observed at the end of the observation period at almost all instrumented points.

  The deck behavior can be different in locations close to the abutment and closest to the acute corner of the bridge than other locations near the acute corner. This was suggested by the longitudinal gage 1 on line 1 (closer to the abutment) that presented significantly smaller compressive strains at the end of the warming period. This gage also had a gradual increase in tensile strains when the control gage strains were subtracted.

ACKNOWLEDGEMENTS

This research project was funded through WisDOT and the USDOT. Neither WisDOT nor the USDOT assume any liability for the contents or the use thereof nor does this presentation reflect official views, policies, standard specifications or regulations of either department. The technical support during instrumentation of Michael G. Oliva, professor emeritus, the University of Wisconsin, Madison and staff of the Structural Engineering and Earthquake Simulation Laboratory of the Department of Civil, Structural and Environmental Engineering at the University at Buffalo is particularly acknowledged. Logistic support provided by field engineers, particularly Philip Ciha, Brian Koch of WisDOT; Matt Pokorny, Jason Zembroski of GCG; David Wagner of Collins Engineers, were instrumental in load testing. The opinions and conclusions presented in this paper are of the authors' and do not necessarily reflect the views of the parties acknowledged above.

REFERENCES

1. Diaz Arancibia, M.; Okumus, P.; and Oliva, G. M., "Review of Skew Effects on Prestressed Concrete Girder Bridges: Problems and Current Practices," *Proceedings of the PCI Convention and National Bridge Conference*, Cleveland, OH, February 28-March 4, 2017, 50, p. 18.

2. Diaz Arancibia, M., and Okumus, P., "Causes of Excessive Detensioning Stresses in Northeast Extreme Tee (NEXT) Beams," *PCI Journal*, V. 62, No. 3, 2017, pp. 31-45.

3. Hag-elsafi, O., and Kunin, J., "Load Testing for Bridge Rating: Dean's Mill Road over Hannacrois Creek," *Report* No. 147, Transportation Research and Development Bureau, New York State Department of Transportation, Albany, NY, 2006, p. 60.

4. French, E. W. C.; Dymond, Z. B.; and Shield, K. C., "Investigation of Shear Distribution Factors in Prestressed Concrete Girder Bridges," *Report* No. MN/RC 2016-32, Research Services and Library, Minnesota Department of Transportation, Minneapolis, MN, 2016, p. 595.

5. Fu, G.; Feng, J.; Dimaria, J.; and Zhuang, Y., "Bridge Deck Corner Cracking on Skewed Structures," *Report* No. RC-1490, Construction and Technology Division, Michigan Department of Transportation, Lansing, MI, 2007, p. 153.

6. Huang, H.; Shenton, W. H.; and Chajes, J. M., "Load Distribution for a Highly Skewed Bridge: Testing and Analysis," *Journal of Bridge Engineering*, V. 9, No. 6, 2004, pp. 558-562.

7. Wisconsin Department of Transportation, "Maintenance & Inspection ─ Highway Structures Information System (HSI)," 2017, http://wisconsindot.gov/Pages/doing-bus/eng-consultants/cnslt-rsrces/strct/hsi.aspx.

8. Wisconsin Department of Transportation, "Bridge Manual," 2017, Madison, WI.

9. AASHTO, "LRFD Bridge Design Specifications," Customary U.S. Units, 7th Edition, American Association of State Highway and Transportation Officials, Washington, DC, 2014, p. 1716.

10. ACI Committee 209, "Prediction of Creep, Shrinkage and Temperature Effects in Concrete Structures (ACI 209R-92, Reapproved 1997)," *ACI Manual of Concrete Practice*, American Concrete Institute, Farmington Hills, MI, 1992, p. 47.

11. Walpole, E. R.; Myers, H. R.; Myers, L. S.; and Ye, K., *Probability and Statistics for Engineers and Scientists*, 9th Edition, Prentice Hall, Boston, MA, 2012, p. 812.

12. Phares, M. B.; Greimann, L.; and Liu, Z., "Evaluation of the Need for Longitudinal Median Joints in Bridge Decks on Dual Structures," *Report* No. TR-661, Iowa Highway Research Board, Iowa Department of Transportation, Ames, IA, 2015, p. 97.

ACI student member **Mauricio Diaz Arancibia** is a graduate research assistant in the Department of Civil, Structural and Environmental Engineering at University at Buffalo, the State University of New York, Buffalo, NY.

ACI member **Pinar Okumus** is an Assistant Professor in the Department of Civil, Structural and Environmental Engineering at University at Buffalo, the State University of New York, Buffalo, NY. Her research interests include understanding the fundamental behaviors of reinforced concrete and prestressed concrete highway bridge members, inelastic analytical modeling and experimental verification of shear-dominated zones and extreme response, and accelerated bridge construction.

RATING OF CONCRETE ROAD BRIDGES WITH STATIC PROOF LOAD TESTS

Anna Halicka, Dick A. Hordijk, Eva O.L. Lantsoght

Synopsis: Nowadays, finite element analyses provide information about the performance of a structure, but they are more or less simplified. Therefore, load tests are the only way to find the "real" behavior of an existing bridge subjected to the rating process. In this paper, the *state-of-the-art* concerning load tests of concrete road bridges is presented, and the problems of the execution of such tests are specified. It is pointed out that only load tests accompanied with current finite element analyses may result in a proper assessment of the level of safety of the bridge. The authors' procedure of complex assessment of such bridges combines *in-situ* examination of the structure, load testing, and finite element modeling.

The paper discusses the following topics:

- Aims and fundamentals of static diagnostic and proof load tests,
- The load application method according to different codes and specifications,
- The basis for proper assessment of the target load: reliability index, partial factors approach, global rating factor approach,
- Establishing the load allowable on the bridge, based on the applied proof load,
- The proposed procedure of assessment of existing concrete road bridges by load testing.

Keywords: codes of practice; field testing; finite element modeling; load testing; measurements; proof load testing; reinforced concrete bridges

Anna Halicka is an associate professor and head of Building Structure Unit in Faculty of Civil Engineering and Architecture at Lublin University of Technology, Lublin, Poland. Her research interests include assessment of existing concrete and masonry structures (especially durability and safety aspects), concrete composite structures (interface between two concrete parts and support zones), as well as reinforced and prestressed concrete tanks and silos).

Dick A. Hordijk is a full professor at Delft University of Technology, Delft, the Netherlands. He received his MS and PhD in civil engineering from Delft University of Technology, Delft, the Netherlands, in 1985 and 1990, respectively. His research interests include concrete fracture mechanics, assessment of existing structures, structural application of new concrete types, and forensic engineering.

ACI member **Eva O. L. Lantsoght** is a full professor at Universidad San Francisco de Quito, a structural engineer at Adstren and a researcher at Delft University of Technology. She is a member of ACI 445-0D Shear Databases and of ACI-ASCE 421, Design of Reinforced Concrete Slabs, and an associate member of ACI 342, Evaluation of Concrete Bridges and Bridge Elements, ACI 437, Strength Evaluation of Existing Concrete Structures, and ACI-ASCE 445, Shear and Torsion.

INTRODUCTION

Nowadays, software for structural analysis is widely available and commonly used. Finite element analyses provide insight in the structural performance of the modeled structure, but they are more or less simplified. Therefore, non-destructive load tests are the only way to find the "real" behavior of an existing bridge that needs to be rated. Unfortunately, the high cost of load tests may be the reason why bridge owners are reluctant to use such tests. Another drawback for using load tests is the risk of damage to the structure during the test.

The finite element analysis of a structure needs detailed input values and relationships to simulate the behavior of the structure from initial loading to its ultimate limit state. However, for design, some simplifications are usually introduced:

- Designers often use only two-dimensional schemas in analysis, whereas in reality, the bridge behavior is three-dimensional.
- A simplified static model (e.g. simply or continuously supported beams) is adopted and ideal supports conditions are assumed in the numerical model, which do not always correspond to the actual support stiffness.
- The actual bridge dimensions may differ from the designed ones.
- The location and weight of the non-structural elements (pavements, parapets, railings) are often not the same as in the design drawings, and these elements are sometimes neglected or simplified in the numerical model. However, their effect on the overall structural stiffness can be considerable (Barker, 2001).
- Most often, only a simple elastic-static analysis of the structure is performed using the modulus of elasticity and Poisson's ratio of the designed concrete class. However, the actual concrete might be of a different class than the designed one. Additionally, undetected damage may be present. These differences between designed and actual class may be aggravated by the increase of the concrete strength with age on one hand and concrete deterioration, also connected with age, on the other hand.

These inaccuracies of numerical models result in the risk of an incorrect assessment of the bridge capacity. However, the main goal of design is to ensure that a structure fulfils the requirements of the code concerning the ultimate and serviceability limit states. It is not necessary for the designer to know the residual capacity of the structure at some future time. Anyway, for existing structures subjected to live loads larger than what they were designed for, or whose capacity is subject to discussion due to material degradation, the question about the residual capacity of the structure becomes relevant. Some of the above-mentioned inaccuracies are also characteristic for numerical models used for the assessment of bridges, although the incorrectness can be reduced: the dimensions may be measured, the weight and location of non-structural elements is known, and the concrete strength can be determined based on core samples.

The most important topic for the assessment of an existing bridge is the determination of the actual *load-deflection* relationship. Only load testing allows to verify and determine the generalized actual stiffness of the structure and the (linear) part of the *load-deflection* curve up to the proof load imposed onto the bridge. On that basis it is possible to predict the live load that may be permitted on the bridge. This allowable load usually causes effects in the structure that lie within the linear part of the structural behavior.

The correctness of analyses including load tests results in the safety level of the structure. The required safety level (expressed e.g. by the reliability index) should be determined in relation to bridge importance and

size. For example, a bridge in an important highway connection will require a higher safety level than a bridge in a rural road used by few vehicles. Additionally, the following questions should be answered:

- which level of accuracy of the analysis (especially numerical model) connected with proof loads should be obtained,
- which number of parameters must be measured in the field,
- which target proof load should be applied.

Information about load testing of concrete bridges can be found in the literature. The practical aspects were described (Cai and Shahawy, 2003; Cai et al., 2012; Enochsson et al., 2008; Gutermann et al., 2003; Lagoda and Lagoda, 2014; Lazinski and Salamak, 2010; Myers et al., 2012; Nowak and Saraf, 1996; Olaszek et al., 2012; Olaszek et al., 2014; Puurula et al., 2008; Ransom and Heywood, 1997; Taljsten et al., 2008; Yuefei et al., 2014), and the methods of bridge safety assessment were discussed (Cai and Shahawy, 2003; Casas and Gómez, 2013; Faber et al., 2000; Fu and Tang, 1995; Jeppsson, 2003; Moses et al., 1994; Nowak and Tharmabala, 1988; Stewart et al., 2001; Toprak et al., 2012; Yuefei et al., 2014). Some tests in the past have been continued up to damage of the bridge (Bagge et al., 2015; Haritos et al., 2000; Lantsoght et al., 2016).

In some countries there are codes and requirements dedicated to load tests of bridges: the Manual for Bridge Evaluation (MBE) (AASHTO, 2016), the DAfStb guideline from Germany (Deutscher Ausschuss für Stahlbeton, 2000), and the RIRB requirements from Poland (Research Institute of Roads and Bridges, 2008). In Switzerland codes SIA 505 269:2011 (SIA, 2011a) and SIA 505 269/2 (SIA, 2011b) are dedicated to all structures, not only to bridges.

In this paper, the problems of the execution of static proof load tests of concrete road bridges for bridge assessment and the determination of its load-carrying capacity are discussed on the basis of a *state-of-the-art* analysis and the authors' experience. A detailed assessment procedure for the *in-situ* examination of a structure and steps for load testing is proposed.

RESEARCH SIGNIFICANCE

The presented knowledge may be useful for bridge owners and for experts realizing the rating process. The paper provides guidance for the proof load tests and rating procedure that uses proof load tests. The guidelines for performing proof load tests and determining the target proof load are based both on European and American sources, so they are universal.

TYPES OF BRIDGE LOAD TESTS

The British National Steering Committee for the Load Testing of Bridges (The Institution of Civil Engineers - National Steering Committee for the Load Testing of Bridges, 1998) classifies bridge load tests as *supplementary load tests*, *proof loadings* and *proving load testing* (or *proof load tests* – term used in this paper, and conform the term used in the AASHTO MBE).

The aim of *supplementary load tests* is supplementing analytical methods and providing information of the actual bridge behavior under loading, including the load distribution through the particular structural members. Such load tests are usually complemented with non-destructive testing methods used for finding the concrete and reinforcement characteristics (Varela-Ortiz et al., 2013). The level of load should be sufficient to obtain measurable responses from the structure without causing any permanent structural damage. It is lower than the load applied on the structure under normal traffic. The obtained information is used to verify the initial numerical model. According to Casas et al. (Casas et al. 2009) the structural model is recognized as properly calibrated if the differences between measured and calculated deflections are not larger than 10% in prestressed concrete bridges, and 20% in concrete bridges. In the case of larger differences, the model should be modified.

Proof loadings are undertaken on newly constructed bridges before opening in order to validate the design model and assumptions. These tests are focused on confirming that the bridge satisfies the design requirements and that its capacity is not smaller than the designed one. The level of proof loadings is usually higher than used in supplementary tests and it is close to the serviceability limit state level. Such tests are demanded by codes in some countries e.g. Italy, Poland, Spain, Slovenia (Lagoda and Lagoda, 2014). In Poland, according to PN-S-10040/99 code (PN-S-10040/99, 1999) and RIRB Rules (Research Institute of Roads and Bridges, 2008), all new road bridges of a span length larger than 20 m (66 ft) must be load tested.

Proof load tests are usually undertaken for more realistic assessment of the behavior than that obtained from the theoretical analysis alone and for proving the safety of:

- bridges containing damaged or strengthened elements,
- bridges subjected to larger loads than assumed during design (due to increasing traffic and vehicle weight, or if a special transport is planned e.g. military),
- bridges with durability problems, for which it needs to be certified that the bridge can be used over the next years.

The load is increased in increments to some predetermined maximum (the so-called *target proof load*) or until the structure shows signs of deterioration or distress. The levels of target load are usually higher than used in

other testing and may reach over twice the nominal live load. On the basis of the target proof load, the magnitude of the load allowable on the bridge is deduced. The proof load test results may be also used for updating the numerical model and the verification of the ultimate limit state. The extrapolation to the ultimate limit state is adequate and safe only if the material parameters are determined and some pattern of bridge behavior at advanced levels of loading is known.

The second classification of bridge tests may be made according the manner of load application. The proof load may be:

- static: the load is applied at fixed points (the location and magnitude of the loads are fixed during one test scenario, but they may be changed during the next scenario),
- pseudo-static: trucks move at a low speed,
- dynamic: trucks move at full speed and vibrations are induced. Such proof loading allows to assess the dynamic characteristic of the bridge (frequencies) and as a result establish the critical (safe) velocities. The dynamic characteristics can then also be compared to those assumed during the design stage.

According to (Stewart et al., 2001), even the observation that the bridge has survived the current service load is, in itself, a proof load that provides information about the bridge's safety. Therefore service loads may be treated as a specific type of proof loads with an appropriate uncertainty.

FUNDAMENTALS FOR STATIC PROOF LOAD TESTS

A proof load test proves that the bridge is able to carry its full permanent load and some live load. The aim is to determine the magnitude of live load that can be carried by the bridge safely, or to demonstrate that the bridge fulfils the code requirements at a certain safety level. This target load, lower than the ultimate capacity of the bridge, can be used to evaluate if the bridge fulfils the required level of safety.

Before the proof load is applied, a detailed technical evaluation of the bridge's condition should be made. This inspection should be used for gathering the following information:

- the crack pattern and the size of the cracks,
- the location of weak concrete or losses of concrete,
- the concrete strength, based on core testing,
- carbonation depth, based on chemical tests of the concrete cover,
- presence of corrosion of reinforcement and the extent of section loss.

If rehabilitation measures (e.g. realkalisation, extraction of chloride ions, addition of reinforcement to complement corroded bars, and repair of the destroyed concrete cover) are needed, these should be performed.

The main topics of discussion with regard to static proof load tests are connected with the decisions concerning:

- the load application method and location,
- the target proof load magnitude, which should be based on the specified criteria ensuring no destruction of bridge during tests on the one hand and the demanded level of safety on the other hand,
- the specification of parameters to be measured and the measurement methods.

The load should be placed at a position so that the response in critical bridge members and critical zones in these members can be determined. For instance, to achieve the highest bending moment in simply supported structure, the load should be applied in the middle of the span and close to the support to achieve the highest shear force. It might be required to load the bridge at different load locations along the bridge width in order to show differences in the bridge behavior under load in the middle and edge lanes.

During proof load tests, no irreversible damage should be caused. Increasing the load above the limit of elastic performance is generally forbidden.

The behavior of the bridge is controlled by internal forces, which cannot be measured directly. Only their effects may be measured (e.g. deflection, strain of steel, or deformations and cracks in concrete). The limiting values of these effects, the so-called stop criteria, should be determined prior to the test. The bridge response should be continuously monitored and evaluated in real-time.

The target proof load value L_{targ} is the value of the load intended to be applied to the bridge during proof load tests in the assumed scenario and for the chosen location. It should be larger than the live load expected at future use in order to provide a margin of safety against some uncertainties such as the dynamic action of the load and unexpected overloads. This topic is discussed in a further section of this paper.

The deflection at the middle of the span is the value of primary interest. The resulting load-deflection relationship can be used for the calibration of the numerical model and to determine if the elastic limit was reached. The load-deflection relationship should be monitored continuously during the load test to ensure that the threshold of non-linear behavior is not exceeded. Digital levels, deflection inductive transducers, and surveyor's levelling instruments (optical or laser) may be used for the deflection measurement. The measurement of the support displacements should be carried out as well to find the net deflection of the superstructure (RIRB, 2008).

The appearance of cracking should be monitored, with particular attention given to first cracking. Non-destructive methods (e.g. acoustic emission method (Olaszek et al., 2012) may be used for this purpose.

The DAfStb guideline (DAfStb, 2000) recommends the measurement of the concrete strains at different positions of the height of the considered element at midspan. The strains in the concrete can be measured with electric resistance wire strain gauges, inductive transducers, LVDTs, and laser displacement sensors and the strains in the steel – with electric resistance wire strain gauges. If possible, the strains of stripped reinforcement bars at midspan should be measured.

In cable-stayed bridges the force in cable should be measured. For this purpose the accelerometer/gyroscope sensor (6 degrees of freedom measurements) are attached to the cables (Mariak et al. 2016).

If temperature effects are expected to be important and the influence of temperature on the internal forces is expected to be significant (for example. on sunny days if the proof load test lasts several hours), the temperature of the environment and the temperature of the bridge's upper and bottom surfaces should be measured at midspan. To evaluate the effect of temperature and humidity, a reference strain measurement at a part of the bridge that is not tested may be performed, and the measured strains may be compensated with the reference strain.

The whole process of proof load testing should be documented with photographs and recorded.

For proof load tests, heavy vehicles may be used, and they should be accurately weighed. The incrementally applied proof loads should be moved to different positions to create different load scenarios. The particularities of the proof load application are discussed further in this paper. Before applying the next scenario, all loads corresponding to the previous scenario should be removed from the deck. According to Casas and Gomez (Casas and Gómez, 2013) it is not necessary in the case of simply supported bridges. To apply the large target proof loads, standard vehicles are used (Fig. 1). Sometimes military vehicles (Varela-Ortiz et al., 2013) or even tanks (Nowak and Saraf, 1996) are used. Two test vehicles were built for this purpose in Canada (Ransom and Heywood, 1997), and in Germany, the BELFA load testing vehicle was developed (Steffens et al., 2001).

Figure 1. The application of proof load onto cable-stayed bridge on Wisłok river (phot. K.Wilde).

DETERMINATION OF THE TARGET PROOF LOAD VALUE

Introduction

A bridge assessment is undertaken usually due to changes in use conditions, for example increasing weights and sizes of vehicles on the roads, as well as part of the periodical inspection and evaluation of the existing bridge stock. For this purpose, in this paper the load Q_{cur}, as given by current codes, and Q_{design}, as given by the codes at the time of bridge design, are distinguished. A similar situation takes place if a vehicle of abnormal weight Q_{abn} intends to pass the bridge.

The determination of the target proof load is of great importance. A higher proof load allows to assess bridge safety on a higher level, but the probability of failure during the proof load test increases. Therefore the decision of the target proof load must be premeditated and should be scientifically rational.

Three approaches for determining the target proof load Q_{targ} may be distinguished. The first approach is based on partial safety factors adopting the same reliability level as the design factors. The second method of using a global safety factor gives only rating without precise information of the reliability level. The third is based on the reliability index. These three methods result in a partial factor γ_{test} by which the current live load Q_{cur} should be multiplied in order to ensure safety of the bridge in future:

$$Q_{targ} = \gamma_{test} Q_{cur} . \quad (1)$$

The target proof load Q_{targ} may not be directly related to the nominal code values. The codes give the load scenarios which should be used in design calculations, and for each scenario the nominal load values for particular road types are assigned. It is not always possible to create proof load locations the same as predicted by codes, so the proof load tests scenarios may sometimes differ from code scenarios. This situation takes place if for proof loads only vehicles are available of which the dimensions differ from those assumed in the code scenarios (e.g. military vehicles). Therefore, the loads (proof load and nominal code load) should not be compared directly, but instead only the maximum internal moments and forces (bending moments or shear forces) caused by them.

The following procedure should be used. First, the value of the internal force corresponding to code scenarios should be calculated on the basis of Q_{cur}. Only then the proof load location(s) and the values of the target proof loads Q_{targ} may be assumed. Q_{targ} is the load causing the same internal moments or forces as $\gamma_{test}Q_{cur}$. After proof load testing, the inverse procedure must be undertaken: the load allowed on the bridge corresponding to the code scenarios is calculated by dividing the maximum applied value of the proof load by γ_{test}. This method could also be based on a comparison of stresses instead of internal forces or moments (Chajes et al., 2003).

Partial safety factors approach

A simple method for the calculation of the target load is given in the DAfStb guideline (Deutscher Ausschuss für Stahlbeton, 2000). The same partial safety factors as recommended by Eurocode for design ($\gamma_{Q,1}$, $\gamma_{Q,j}$, $\psi_{Q,i}$) are used (CEN, 2002). The target proof load Q_{targ} is obtained as follows:

$$Q_{targ} = \sum_{j>1} \gamma_{G,j} G_{add,k,j} + \gamma_{Q,1} Q_{k,1} + \sum_{i\geq 1} \gamma_{Q,i} \psi_{0,i} Q_{k,i} \tag{2}$$

and the additional condition should be satisfied:

$$Q_{targ} \geq 0.35 G_{k,1} \tag{3}$$

where $G_{k,1}$ is the characteristic value of the permanent load present during the proof load test, $G_{add,k,j}$ is the characteristic value of permanent load expected to be added onto bridge after proof load, $Q_{k,1}$ and $Q_{k,i}$ are characteristic values of the dominant (due to road traffic) and other live loads, $\gamma_{G,j}$ is the partial safety factor for dead loads, $\gamma_{Q,1}$ and $\gamma_{Q,i}$ are the partial safety factors for the live loads, and $\psi_{0,i}$ is the combination factor for live loads. In Germany, the values of partial factors are given in the DIN codes in accordance with National Annexes for Eurocode EN 1990 (CEN, 2002) and Eurocode EN 1991 (CEN, 2003).

Therefore it can be said that the same level of safety was assumed for newly designed and existing structures. This approach is a simplification of the problem.

Global safety factor approach

The easy manner to show a margin of structural safety is to use a global safety factor, as used in the AASHTO codes:

$$\gamma' = \frac{R}{E_G + E_Q} \tag{4}$$

or

$$\gamma' = \frac{R - E_G}{E_Q} \tag{5}$$

where E is the load effect (bending moment or shear force), with E_G the effect caused by the nominal value of the dead load G, and E_Q the effect caused by the nominal value of live load Q. R is the nominal value of the capacity (bending moment capacity or shear capacity).

The factor γ' follows the philosophy of allowable stress design. The same global safety factor defined in relation to mean values was used by Moses et al. (Moses et al., 1994).

With *in situ* testing of the materials and structure, the capacity and dead load are estimated more precisely ($R_{updated}$, $E_{G,updated}$). If a proof load test with target load Q_{targ} is used, its load effect $E_{Q,targ}$ may be determined based on the measured deflection or strain. The updated global safety factor then becomes:

$$\gamma'' = \frac{R_{updated} - E_{G,updated}}{E_{Q,targ}} \tag{6}$$

If $\gamma'' \geq 1.0$ one can conclude that the capacity is greater than the target proof load. Notwithstanding, such an approach does not provide information about the structural safety margin.

The rating factor *RF* used in North America for assessment (AASHTO, 2016) is calculated based on factored loads and the factored resistance. This approach also considers the impact factor on the live load *I*:

$$RF = \frac{\phi R - E_{\gamma G}}{(1+I)E_{\gamma Q}} \tag{7}$$

where E is the load effect (bending moment or shear force), $E_{\gamma G}$ is the effect caused by the nominal factored dead load G, $E_{\gamma Q}$ is the effect caused by the nominal factored live load Q, and φR is the factored capacity (bending moment capacity or shear capacity).

If the properties of the materials and structure are determined in the field, and if a load with magnitude Q_{test} is applied to the structure, the rating factor can be updated as follows:

$$RF'' = \frac{R_{updated} - E_{G,updated}}{(1+I)E_{Q,targ}} \tag{8}$$

Fu and Tang (Fu and Tang, 1995) calibrated Eq. (8) for RF factors satisfying the AASHTO requirements for assessment and stated that the partial factor for the target load γ_{test} in Eq. (8) should range between 1.35 and 1.90 (depending on the conditions of the traffic and the structure) if the initial rating factor calculated for Q_{cur} is not lower than 0.7. If the rating factor is lower than 0.7, the required factor is higher and ranges between 1.45 and 2.0.

In the Manual for Bridge Rating through Load Testing (NCHRP, 1998), the rating factor after a proof load test is determined as follows:

$$RF'' = \frac{K_o Q_{test}}{(1+I)X_{pa}Q_{cur}}, \tag{9}$$

where Q_{cur} is the maximal legal load, $K_o = 1.0$ if the target load is reached, and $K_o = 0.88$ if a distress level is reached prior to reaching a target load, and $X_{pa} = \gamma_{test}$ is the target live load factor with basic value of $X_{pa} = 1.4$. This factor is altered depending on:

- the number of lanes (15% increase for a bridge with only one lane),
- the condition of the bridge (10% increase if fracture-critical details are present),
- the frequency of inspections (10% increase if inspections are carried out less than once every two years),
- ratability of the structure (5% decrease if the structure is ratable and has no hidden details).

As a result, $1.3 \leq X_{pa} \leq 2.2$. A rating factor RF'' higher than 1.0 proves that the load Q_{cur} fulfils the code requirements and can be safely applied.

Cai and Shahawy (Cai and Shahawy, 2003) calculated the rating factor regarding proof load tests results as:

$$RF'' = \frac{E_{Q,test}}{(1+I)E_{\gamma_{test}Q_{test}}}, \tag{10}$$

with $E_{Q,test}$ the load effect caused by the load applied in the test, I the impact factor, and $E_{\gamma testQtest}$ the factored load effect caused by the target proof load. The recommended value was determined as $\gamma_{test} = 2.17$ in this study. The proof load should be calculated under the assumption that γ_{test} is not lower than values given by AASHTO 1994 ($\gamma_{test} > 1.67$).

Reliability approach

Reliability index - Due to the uncertainty of the future live load and the ongoing process of concrete deterioration, only a time-dependent reliability analysis may form the basis of the assessment of the future safety of the bridge. Therefore, the target proof load must be obtained with a reliability-based approach (Casas and Gómez, 2013; Fu and Tang, 1995; Jeppsson, 2003).

In such an approach, the probability of failure P_f is determined; this is the probability that the effect of the loads is not larger than the capacity of the structure or element under consideration. The probability of failure P_f is expressed as:

$$P_f = P(g \leq 0). \tag{11}$$

The limit state function for structural reliability can be expressed as:

$$g = R - E = R - (E_G + E_Q) = R_Q - E_Q \tag{12}$$

where R is the capacity (bending moment capacity or shear capacity), E is the effect of the load, with E_G the effect of the permanent loads, and E_Q the effect of the live loads. R_Q is the margin of resistance for live load.

The live load and the margin of resistance for live load are the random variables in the limit state function from Eq. 12. On the frequency distribution diagram involving these variables (Figure a), the area can be seen where the two curves overlap. The overlapping area is a qualitative measure of the probability of failure. This area can be decreased by a reduction of the live load or an increase of the capacity e.g. by strengthening of the structure.

The key in the reliability-based approach is the reliability index β. It is defined as the inverse normal distribution of the probability of failure, and can be expressed based on the mean μ and standard deviation σ when the distributions are normally distributed:

$$\beta = \Phi^{-1}(P_f) = \frac{\mu_z}{\sqrt{\sigma_z^2}} = \frac{\mu_R - \mu_E}{\sqrt{\sigma_R^2 + \sigma_R^2}} \tag{13}$$

where μ is the mean value and σ is the standard deviation of Z, R and E, respectively, with Z the limit state function, R the resistance, and E the load effect.

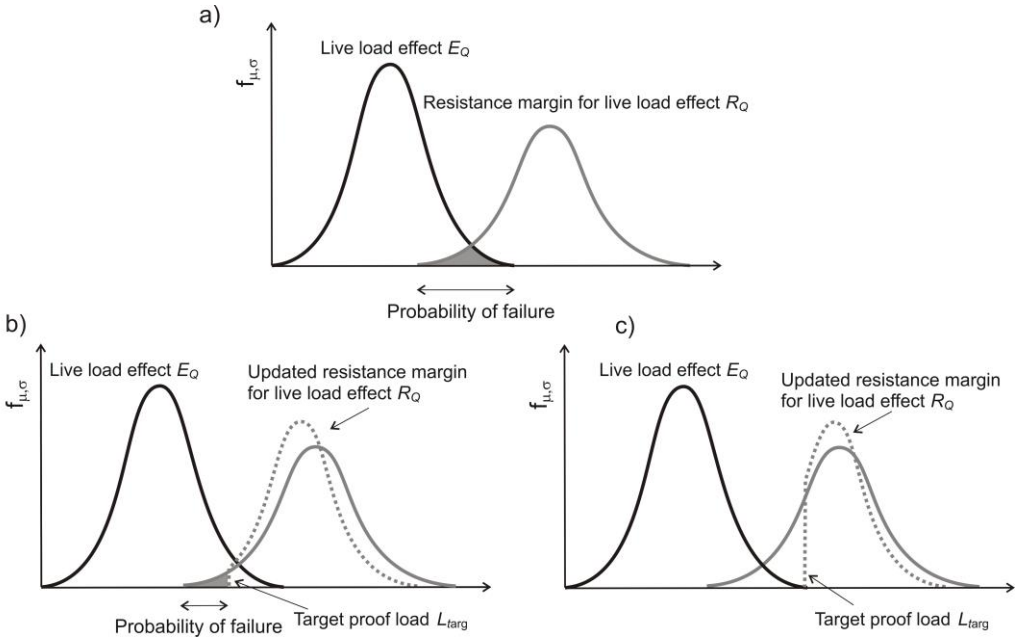

Figure 2. The influence of a proof load test on the probability of failure: a) probability density functions of live load effect and margin of resistance for live load, and the quantification of the probability of failure, b) and c) probability density functions of live load effects and margin of resistance for live load and the quantification of the probability of failure in the case of proof load tests. Note that the target proof load $L_{targ,2}$ in the Fig.2c is higher than $L_{targ,1}$ in Fig. 2b.

The value of the reliability index β depends on the reference period. It may be calculated based on the probabilistic parameters of dead and live load and the material parameters. These parameters can constitute of the mean value, the bias (ratio of mean value to nominal value), the standard deviation, and the coefficient of variation. Normal distributions are usually assumed for the dead load. For the material properties and structural resistance parameters and model uncertainties, lognormal or Weibull distributions are typically assumed. For live load of bridges, lognormal or Gumbel distributions should be used. Analytical methods (such as FORM - First Order Reliability Method, SORM - Second Order Reliability Method, Monte Carlo simulation or numerical integration) are usually applied to solve the convolution integral of the limit state function and determine the reliability index.

The actual reliability index β in existing structures is different from the design value because of a different reference period and the associated changes in probabilistic parameters. What is more, it decreases with time as a result of deterioration. For instance, Jeppsson (Jeppsson, 2003) calculated the reliability index for a bridge erected in 1946 and stated that this value decreased from β = 6.3 in 1946, β = 4.3 in 2001, β = 4.0 in 2007 to β = 3.6 in 2013.

The initial (design) value of the reliability index β lies at the basis for reliability-based design. In EN 1990:2002 (CEN, 2002) one can find the target values, depending on the reliability class (RC) associated with the consequence class (CC), for a reference period of 1 year or 50 years. For example, for the ultimate limit state and a reference period of 50 years, β = 4.3 for the highest RC3 and CC3 classes. Unfortunately, bridges are not mentioned in the tables defining CC classes, although it is generally considered that highway bridges are CC3. Moreover, for bridges, a design working life of 100 years is required. Therefore it may be concluded that the value of the reliability index β should be assessed on an individual basis.

The reliability index should never be lower than a minimum value, determined in relation to the remaining working life. According to ISO/CD 13822 (ISO/CD 13822, 2012) concerning existing structures (not

only bridges), the remaining working life is usually considered as a reference period for a new structure, but a shorter reference period can be reasonable for the ultimate limit state. Adopting the same target reliability index β for existing structures as for new structures is conservative. Reducing the target reliability index with regard to the remaining lifetime will allow owners to spend less funds on bridge strengthening. Koteš and Vican (Koteš and Vican, 2013) calculated and compiled target values for the reliability index β for different values of the remaining lifetime, under the assumption that the bridge has no material degradation and was designed for a lifetime of 100 years. For example: for a 30-year-old bridge, the target reliability index β for a remaining lifetime of 5 years is 3.039 and for a remaining lifetime of 70 years this value is 3.708. For an 80-year-old bridge, the target reliability index β for a remaining lifetime of 5 years equals 3.014 and for a remaining lifetime of 20 years this value equals 3.204.

In the SIA 269 code (SIA, 2011a), which deals with the existing structures, the demands for the target values of the reliability index depend on a cost calculation. Two ratios are introduced:

$$\rho = \frac{C_F}{C_W} \tag{14}$$

$$EF_M = \frac{\Delta R_M}{SC_M} \tag{15}$$

where C_F is the direct cost in the event of failure, C_W is the cost of rehabilitation after failure, ΔR_M is the risk reduction as a result of repairs (expressed by financial worth), and SC_M are all costs of safe exploitation. Assuming a one year reference period, the following target values are given:

- $EF_M < 0.5$ (low EF_M): $\beta = 3.1$ for $\rho < 2$, $\beta = 3.3$ for $2 < \rho < 5$, and $\beta = 3.7$ for $5 < \rho < 10$,
- $0.5 \leq EF_M < 2.0$ (medium EF_M): $\beta = 3.7$ for $\rho < 2$, $\beta = 4.2$ for $2 < \rho < 5$ and $\beta = 4.4$ for $5 < \rho < 10$,
- $EF_M > 2$ (high EF_M): $\beta = 4.2$ for $\rho < 2$, $\beta = 4.4$ for $2 < \rho < 5$ and $\beta = 4.7$ for $5 < \rho < 10$.

Influence of proof loads on the probability of failure - Proof load tests allow to define the input data (concrete strength, dead load value and location and stiffness of the structure) for finite element analyses more precisely. This increase in accuracy of the input can also lead to more precise probabilistic calculations. Very often such data allow to find that the resistance initially calculated in design is lower than the updated one. This can be seen in Fig. 2b and Fig. 2c. The difference between designed and updated resistance may be called "residual resistance" (Walraven, 2012).

Proof load tests, proving the possibility of carrying the real load of target value, are also the way of reducing the probability of failure in the future and increasing the actual reliability index (Bakht and Jaeger, 1990; Faber et al, 2000; Fu, 1995; Moses et al., 1994). The proof load tests demonstrate that the bridge has a minimum capacity. What is more, they truncate the R_Q distribution and reduce the overlapping area of the Q and R_Q distributions and as a result reduce the probability of bridge failure in the future (Figure 2b and c). The higher the value of target load Q_{targ}, the lower the probability of failure in future. Proof load testing allows to adopt a lower reliability level than the levels required at the design stage. Nevertheless, it should be remembered that a higher value of a proof load is associated with a higher probability of failure during the test (Ellingwood, 1996). As a result, the target proof load should be chosen so that the probability of failure in the future is small (high reliability index) and so that the probability of failure during the test is small too.

Moses et al. (Moses et al., 1994) used structural reliability principles to determine the reliability indices β for different target proof load magnitudes and different global safety factors (see Eq. 4). For instance, for a medium span bridge, they found that assuming normal distributions with coefficients of variations for the load COV = 0.2 and for the resistance COV = 0.15, the reliability index β was equal to 1.99, assuming that the global safety factor equaled 1.5. When a proof load was involved with a value equal to the mean live load ($Q_{test} / Q_{cur} = 1$) the reliability index after the successful proof load test β increased to 2.25 (the reliability index during the test was equal to 2.17). When the proof load ratio was increased ($Q_{test} / Q_{cur} = 1.5$), the reliability index after a successful proof load test increased up to $\beta = 3.47$, but the reliability index during the proof load test decreased to 1.08.

Target proof load based on the reliability index. Reliability analyses can be complicated in practice, so, methods have been developed based on structural reliability analyses to determine the target proof load in a more direct way (Casas and Gómez, 2013; Fu and Tang, 1995; Moses et al., 1994).

As mentioned previously, Fu and Tang (Fu and Tang, 1995) calibrated Eq. (8) to determine a partial factor for the target load. They analyzed the requirements of the MBE, which are based on a reliability index of $\beta = 2.3$. For two-span bridges with span lengths between 21 m and 32 m (70 ft – 105 ft), they found that the partial factor γ_{test} should range from 2.80 to 2.91 (for the midspan moment) and from 2.79 to 2.87 (for the support moment).

In another study (Moses et al., 1994), not only the reliability indices β for different values of the target proof load were determined, but also for different rating factors *RF"*. For example, for a medium length span bridge they found, assuming normal distributions, that a target proof load of value $Q_{targ} / Q_{cur} = 1$ results in a

reliability index after a successful proof load test β equal to 2.25, assuming a rating factor RF'' = 1.5. The reliability index β increased to 3.28 when the rating factor increased to RF'' = 2.0.

Casas and Gomez (Casas and Gómez, 2013) reported on the results of the European project "ARCHES" (Assessment and Rehabilitation of Central European Highway Structures). They performed a large reliability analysis. For assessing the live load effects on bridge spans, the method from Ghosn and Moses (Ghosn and Moses, 1986) was used as a starting point. The recordings of Weigh-In-Motion (WIM) systems in five European countries (Slovenia, the Netherlands, Czech Republic, Poland and Slovakia) were used as the input for probabilistic simulations. The analyzed structures were simply supported concrete bridges (precast beams with a deck slab, massive and voided slabs, and box girder cross-sections) with span lengths of 10 m (33 ft), 15 m (50 ft), 20 m (66 ft), 25 m (83 ft), 30 m (99 ft), and 35 m (116 ft). Three target values of the reliability index after a successful proof load test were considered: 2.3 (value assumed by the MBE, taking into account an inspection every two years), 3.6 (similar to the required safety level for a new bridge of CC2 defined in the Eurocode) and 5.0 (the upper bound when a high safety level is required). These analyses resulted in target proof load factors γ_{test}.

The analyses considered two situations: when the design documentation is available, and when the bridge is assessed without this documentation. Below only the second situation will be quoted, because it is the focus of proof load tests described in this paper. The resulting proof load factors based on the WIM measurements of the Netherlands and for the three different reliability indices for one-span highway bridges are shown in Table 1. These values represent the most heavy traffic conditions in the Netherlands. However, they may be excessive when looking at lower road classes. Additionally, atypical bridges (e.g. long-span, historical) require an individual assessment of their reliability.

Table 1. Proof load rating factors γ_{test} for Dutch one-span highway bridges corresponding to three values of the reliability index (Casas and Gómez, 2013). Conversion: 1 m = 3.3 ft.

Span length (m)	β		
	2.3	**3.6**	**5.0**
10	1.18	1.61	2.25
15	1.23	1.67	2.33
20	1.33	1.80	2.51
25	1.40	1.91	2.64
30	1.45	1.95	2.70
35	1.49	1.99	2.75

PROTOCOL FOR PROOF LOAD APPLICATION

The target proof load should be applied in several steps and the response of the structure should be monitored during each step. The load should be applied in steps until the target load or the elastic limit of the measured parameters is reached. If any non-linearity is observed, the loading should be stopped and the bridge should be immediately unloaded (Deutscher Ausschuss für Stahlbeton, 2000; Research Institute of Roads and Bridges, 2008).

The German guideline (Deutscher Ausschuss für Stahlbeton, 2000) requires at least three steps. After each step the structure should be unloaded, and after each loading and unloading cycle, a break should be planned. The first load level should not exceed 25% of the target proof load, and the second load level should not exceed 50% (Casas and Gómez, 2013).

The loading protocol used in Poland (Research Institute of Roads and Bridges, 2008) for a vehicle of abnormal weight Q_{abn} (larger than the nominal design value Q_{design}) is used as shown in Figure . The following load levels are considered:

1. first load level: $L_1 \leq Q_{design}$ - load not higher than the design load,
2. second load level: $L_2 \leq Q_{\text{design}} + ¼ (Q_{abn} - Q_{design})$,
3. third load level: $L_3 \leq Q_{design} + ½ (Q_{abn} - Q_{design})$,
4. fourth load level: $L_4 \leq Q_{design} + ¾ (Q_{abn} - Q_{design})$,
5. fifth load level: $L_5 \leq Q_{abn}$,
6. last load level: $L_6 \leq Q_{design} + 1¼ (Q_{abn} - Q_{design})$.

The same procedure may be applied if the nominal value of the live load in a new code Q_{cur} is larger than the nominal value assumed during design Q_{design}.

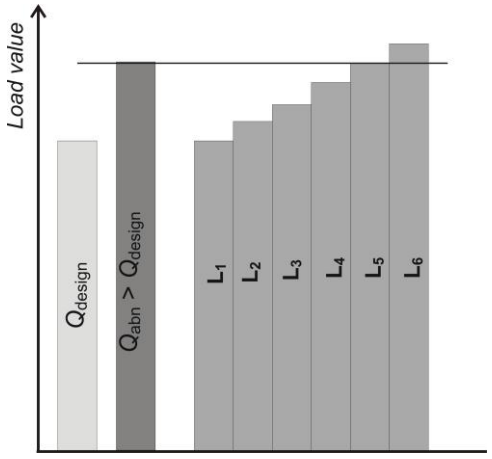

Figure 3. Loading protocol for proof load test for a vehicle of abnormal weight Q_{abn} (Research Institute of Roads and Bridges, 2008)

Each step should last long enough for the structure and the measurements to stabilize. All parameters should be measured during each load step. In accordance with ACI 437.2M-13 (ACI Committee 437, 2013) for buildings, the concrete structure may be considered as stabilized when the difference between successive readings taken not less than 2 minutes apart does not exceed 10% of the initial value recorded for the current step. A different criterion is formulated in the Polish code PN-S-10040/99 (PN-S-10040/99, 1999): the measured value may be considered as stabilized when the difference between successive readings taken no less than 15 minutes apart does not exceed 2% of the previous reading. After stabilization of the readings, the load may be increased to the next load level.

The requirements concerning the last load step also differ in the studied codes and guidelines. The monotonic loading protocol from ACI 437.2M-13 (ACI Committee 437, 2013) requires that the target proof load remains on the structure for 24 hours. The measurements should be recorded at the beginning and at the end of this 24-hour period. After 24 hours the structure should be unloaded and the final readings should be carried out after another 24 hours. In the Polish code PN-S-10040/99 (PN-S-10040/99, 1999), no time duration is given for the last load step, so it can be assumed that it should last as long as the other steps. The Polish code requires that after unloading, the measurements should be recorded at least 3 times every 15 minutes until stabilization of the deflection, where stabilization is defined as a difference smaller than 2% with the previous reading.

According to all consulted guidelines and codes, the proof load test is either terminated when the target proof load Q_{targ} is successfully applied, or when signs of distress or non-linear behavior are observed before the target proof load is achieved.

RATING THROUGH PROOF LOAD TESTING

The main criterion for a bridge to successfully pass a proof load test with a target value Q_{targ} is reaching the target proof load without nonlinear behavior. There are also additional criteria formulated for the deflection remaining after unloading, as well as limiting strains for the concrete and the reinforcement, and limiting crack widths.

A criterion for the deflections after unloading is given by the DAfStb Richtlinie (Deutscher Ausschuss für Stahlbeton, 2000). The residual deflection in reinforced concrete bridges should not exceed 10% of the maximum deflection. In the Polish guidelines (Research Institute of Roads and Bridges, 2008), a residual deflection of 20% of the maximum deflection is allowed in the case of reinforced concrete bridges, and 10% of the maximum deflection for prestressed bridges.

The additional stop criteria that are defined in the German guidelines (Deutscher Ausschuss für Stahlbeton, 2000) are:

- the maximum measured concrete strain ε_c equals:
  $$\varepsilon_c \leq \varepsilon_{c,lim} - \varepsilon_{c0} \quad (16)$$
  where: $\varepsilon_{c,lim}$ = 0.06% for concrete of a class lower than < C20/25 and $\varepsilon_{c,lim}$ = 0.08% for concrete of a class equal to or larger than C20/25 (concrete with a cylinder compressive strength of 20 MPa = 2900 psi), and $\varepsilon_{c,0}$ is the calculated strain caused by the permanent loads,
- the maximal strain in the main reinforcement ε_s equals:

$$\varepsilon_s \le 0.7\frac{f_{ym}}{E_s} - \varepsilon_{s,02} \quad \text{or} \quad \varepsilon_s \le 0.9 f_{y0}\frac{f_{0.01,m}}{E_s} - \varepsilon_{s,02} \text{ when the stress-strain curve of the steel is known,} \tag{17}$$

where: ε_{s02} is the calculated strain caused by the permanent loads, E_s is the steel's elasticity modulus, f_{ym} is the mean value of the steel yield stress, and $f_{0.01m}$ is the stress at a strain of 0.01% determined from the stress-strain diagram of the reinforcement steel.

- the strain in shear zones: the strain in the concrete is limited to 60% of Eq. (16) for the concrete compressive zone, and the strain in the shear reinforcement is limited to 50% of Eq. (17),
- the increase in width of existing cracks in reinforced concrete bridges caused by the proof load should not be larger than 0.3 mm (0.012 in) ($\Delta w \le 0.3$ mm = 0.012 in), and the residual crack width upon unloading and should not exceed 0.2 Δw,
- for new cracks, the width is limited to $w \le 0.5$ mm = 0.020 in and the residual crack width w_{res} for new cracks should fulfil $w_{res} \le 0.3w$.

If all criteria are fulfilled, it can be stated that the bridge successfully passed the test with a target value of the load Q_{targ}. The load Q_{cur} may then be allowed with a reliability index reaching its target value during the assumed reference period.

As mentioned above, if non-linearity is observed or any stop criterion is not fulfilled, the loading should be stopped and the bridge should be immediately unloaded (Deutscher Ausschuss für Stahlbeton, 2000; Research Institute of Roads and Bridges, 2008). It means that the live load of Q_{cur} may not be allowed on the bridge. The value of the load corresponding to the appearance of non-linearity is Q_{max}. The allowable live load resulting from the proof load test $Q_{test,allowed}$ is then determined as:

$$Q_{test,allowed} = \frac{Q_{max}}{\gamma_{test}}, \tag{18}$$

where Q_{max} is the value of the proof load for which loading was stopped or the highest value of the applied load for which all stop criteria are fulfilled. Based on $Q_{test,allowed}$, the value $Q_{allowed}$ in accordance to the current codes, causing the same internal moments or forces as $Q_{test,tallowed}$, should be calculated. $Q_{allowed}$ is then the load permitted on the bridge for the reference period.

PROPOSED PROCEDURE FOR THE ASSESSMENT OF EXISTING CONCRETE ROAD BRIDGES THROUGH PROOF LOAD TESTS

On the basis of the considerations presented previously, a procedure for the assessment of existing concrete road bridges including static proof load tests is formulated and drawn in the flowchart presented in Figue 4. This procedure involves a detailed technical inspection of the bridge's condition before proof loading, three stages of finite element analysis and the assessment of the target value of the proof load based on Table 1.

DISCUSSION OF PRESENTED GUIDELINES

The correctness of the internal forces, calculated even with special software, depends on the accuracy of the input data (dimensions, restraints at the supports, location of reinforcement, material properties). The parameters in the structure often differ from the designed values. Therefore, proof load testing is often a good possibility for demonstrating the safety of a bridge. Especially it may be proven that current live loads may be safely carried by an existing bridge. Nevertheless, proof load tests should to be preceded by detailed inspections and material testing.

A difficulty related to proof load testing is the determination of the target proof load. This value should be determined based on the theory of structural reliability. For practical purposes, the results presented by Casas and Gomez (Casas and Gómez, 2013) may be used.

Regarding the partial safety factor approach to determine the target proof load, in the authors' opinion the level of safety given by a proof load test should be related to a different reference period than for the design of new structures. Additionally, the fact that a proof load test results in more knowledge about the tested structure, and thus less uncertainties, should be factored in.

The German guidelines (Deutscher Ausschuss für Stahlbeton, 2000) recommend the measurements of strains in the concrete and stirrups in the shear zone. But, according to the authors, the determination of stop criteria for shear-critical members is still controversial. Under which angle should the strain gages be applied? Which stirrup should be chosen for the strain measurements, and where exactly should the strain gage be applied on the stirrup? It seems that the only way to assess the behavior of shear zone is control of cracking. Moreover, for bridge types without stirrups, such as concrete slab bridges, this approach will not provide information about the possibility of shear failure during the proof load test.

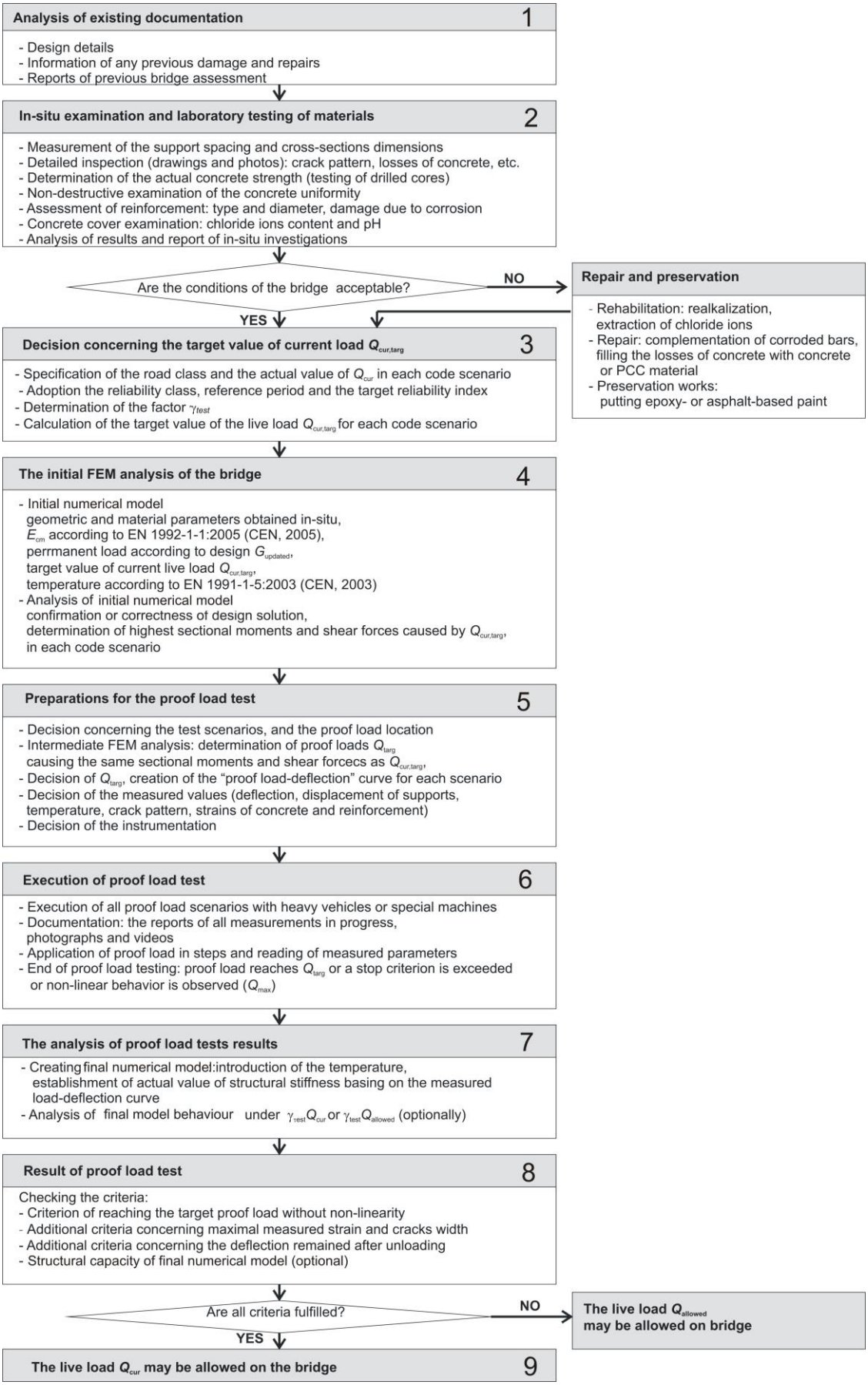

Figure 4. The procedure of the assessment of existing concrete road bridge including static proof loading

SUMMARY AND CONCLUSIONS

This paper considers static proof load tests for the assessment of existing concrete road bridges, and discusses the methods for proof load testing. The different types of load tests are introduced, and then the focus of this paper is on static load tests.

For static load tests, the basic concepts from the Polish and German guidelines are revised. The load is usually applied by using heavy vehicles or special load testing vehicles.

An important research question related to proof load testing is how the target proof load can be determined in such a way that the bridge can be considered safe after it successfully passes a proof load test. Different methods, such as the partial safety factors approach and the global safety factor approach, are revised. For proof load testing of existing bridges, the target proof load should be determined based on the theory of structural reliability. The target reliability index may be different from the requirements of newly designed structures, and the information from Weigh-in-Motion measurements can be factored in to develop target proof load factors.

Once the target proof load is determined, a loading protocol needs to be defined. This paper describes the loading protocols from ACI 437.2M-13, from the German guidelines and from the Polish guidelines. Two scenarios are possible during a proof load test:

1. The target proof load is successfully applied, and the bridge can be assumed safe for the considered live loads;
2. Prior to reaching the target proof load, a stop criterion is exceeded or non-linear behavior occurs. The bridge can then be assessed for a lower load level, but cannot be assumed safe for the considered live loads.

Bringing together the information of the technical inspection of the bridge, the finite element modeling of the structure, and the proof load test is important. For this purpose, a flowchart of practical actions is presented. This method can thus be followed when proof load tests are prepared and executed.

ACKNOWLEDGEMENTS

The authors would like to express their thanks to:

- Polish National Center for Research and Development for funding the research stay of Anna Halicka at Delft University of Technology for the project “Technical University in the future – offer adjusting for the labor market”, supported by the European Social Fund,
- Sonja Fennis from Delft University of Technology – for the fruitful scientific discussions and all help,
- Prof. Krzysztof Wilde from Gdańsk University of Technology for the photographs of his proof load tests of a cable-stayed bridge.

REFERENCES

AASHTO, 2016, "The manual for bridge evaluation with 2016 interim revisions," 2nd ed. American Association of State Highway and Transportation Officials; Washington, D.C.

ACI Committee 437, 2013, "Code Requirements for Load Testing of Existing Concrete Structures (ACI 437.2M-13) and Commentary ", Farmington Hills, MA, 24 pp.

Bagge, N., Sas, G., Nilimaa, J., Blanksvard, T., Elfgren, L., Tu, Y. and Carolin, A., 2015, "Loading to failure of a 55 year old prestressed concrete bridge," *IABSE Workshop*, Helsinki, Finland, pp. 130-137.

Barker, M. G., 2001, "Quantifying Field-Test Behavior for Rating Steel Girder Bridges," *Journal of Bridge Engineering*, V. 6, No. 4, pp. 254-261.

Cai, C. S. and Shahawy, M., 2003, "Understanding Capacity Rating of Bridges from Load Tests", *Practice Periodical on Structural Design and Construction*, V. 8.

Cai, H., Abudayyeh, O., Abdel-Qader, I., Attanayake, U., Barbera, J. and Almaita, E., 2012, "Bridge Deck Load Testing Using Sensors and Optical Survey Equipment," *Advances in Civil Engineering*, pp. 11.

Casas, J. R. and Gómez, J. D., 2013, "Load Rating of Highway Bridges by Proof-loading," *KSCE Journal of Civil Engineering*, V. 17, No. 3, pp. 556-567.

CEN, 2002, "Eurocode – Basis of structural design, NEN-EN 1990:2002", Comité Européen de Normalisation, Brussels, Belgium, 103 pp.

Chajes, M. J., Shenton, H. W., O’Shea, D. and Chaudhri, M., 2003, "Bridge Testing to Enhance Bridge Management in Delaware,"*9th International Bridge Management Conference*, Orlando, FL, USA, pp. 201-204.

Deutscher Ausschuss für Stahlbeton, 2000, "DAfStb-Guideline: Load tests on concrete structures (in German)," Deutscher Ausschuss fur Stahlbeton, 7 pp.

Ellingwood, B., 1996, "Reliability-based condition assessment and LRFD for existing structures," *Structural Safety*, V. 18, No. 2/3, pp. 67-80.

Enochsson, O., Puurula, A., Thun, H., Elfgren, L. and Taljsten, B., 2008, "Test of a concrete bridge in Sweden - III. Ultimate capacity," *IABMAS 2008*, Kohl, M. and Frangopol, D., eds., Seoul, Korea.

Faber, M. H., Val, D. V. and Stewart, M. G., 2000, "Proof load testing for bridge assessment and upgrading," *Engineering Structures*, V. 22, pp. 1677-1689.

Fu, G. and Tang, J., 1995, "Risk-Based Proof-Load Requirements for Bridge Evaluation," *Journal of Structural Engineering*, V. 121, No. 3.

Ghosn, M. and Moses, F., 1986, "Reliability calibration of bridge design code," *Journal of Structural Engineering-ASCE*, V. 112, No. 4, Apr, pp. 745-763.

Gutermann, M., Slowik, V. and Steffens, K., 2003, "Experimental safety evaluation of concrete and masonry bridges," *Non-Destructive Testing and Condition Monitoring*, V. 45, No. 12, pp. 805-808.

Haritos, N., Hira, A., Mendis, P., Heywood, R. and Giufre, A., 2000, "Load testing to collapse limit state of Barr Creek Bridge," *Fifth International Bridge Engineering Conference, Vols 1 and 2: Bridges, Other Structures, and Hydraulics and Hydrology*,pp. A92-A102.

ISO/CD 13822, 2012, "Bases for design of structures – Assessment of existing structures,"

Jeppsson, J., 2003, "Reliability-based assessment procedures for existing concrete structures," Ph.D. Thesis, Lund University, Lund, Sweden, pp. 198.

Koteš, P. and Vican, J., 2013, "Recommended Reliability Levels for the Evaluation of Existing Bridges According to Eurocodes," *Structural Engineering International*, V. 23, No. 4, pp. 411-417.

Lagoda, G. and Lagoda, M., 2014, "The problem of proof loading in the bridges diagnostic (in Polish)," *Inzynieria I Budownictwo* V. 7, pp. 368-371.

Lantsoght, E., Yang, Y., van der Veen, C., de Boer, A. and Hordijk, D., 2016, "Ruytenschildt Bridge: field and laboratory testing," *Engineering Structures*, V. 128, pp. 111-123.

Lazinski, P. and Salamak, M., 2010, "The activity of Roads and Bridges Department concerning proof loadings of bridges (in Polish)," *Inzynieria i Budownictwo* V. 5, No. 6, pp. 300-303.

Moses, F., Lebet, J. P. and Bez, R., 1994, "Applications of Field Testing to Bridge Evaluation," *Journal of Structural Engineering*, V. 120, No. 6.

Myers, J. J., Holdener, D. and Merkle, W., 2012, "Load Testing and Load Distribution of Fiber Reinforced, Polymer Strengthened Bridges: Multi-year, Post Construction/Post Retrofit Performance Evaluation," *FRP Composites and Sustainability: Focusing on Innovation, Technology Implementation and Sustainability*, New York, NY, pp. 163-191.

NCHRP, 1998, "Manual for Bridge Rating through Load Testing," NCHRP Project 12-28(13)A, Washington, DC, 152 pp.

Nowak, A. S. and Tharmabala, T., 1988, "Bridge reliability evaluation using load tests," *Journal of Structural Engineering-ASCE*, V. 114, No. 10, Oct, pp. 2268-2279.

Nowak, A. S. and Saraf, V. K., 1996, "Load testing of bridges," Research Report UMCEE 96-10 University of Michigan, Department of Civil and Environmental Engineering, Construction and Technology Division.

Olaszek, P., Świt, G. and Casas, J. R., 2012, "Proof load testing supported by acoustic emission. An example of application," *IABMAS 2012*.

Olaszek, P., Łagoda, M. and Casas, J. R., 2014, "Diagnostic load testing and assessment of existing bridges: examples of application," *Structure and Infrastructure Engineering*, V. 10, No. 6, pp. 834-842.

PN-S-10040/99, 1999, "Bridges. Concrete, reinforced concrete and prestressed structures. Requirements and testing. (in Polish),"

Puurula, A., Enochsson, O., Thun, H., Taljsten, B. and Elfgren, L., 2008, "Test of a concrete bridge in Sweden - I. Assessment Methods," *IABMAS 2008*, Kohl, M. and Frangopol, D., eds., Seoul, Korea.

Ransom, A. L. and Heywood, R. J., 1997, "Recommendations for Proof Load Testing in Australia," *Proceedings of the Autostrads 1997 Bridge Conference "Bridging the Millennia"*, Sydney, Australia.

Research Institute of Roads and Bridges, 2008, "The rules for road bridges proof loadings (in Polish)," Warsaw, Poland.

SIA, 2011a, "Existing structures – Bases for examination and interventions SIA 505 269:2011," 26 pp.

SIA, 2011b, "Existing structures – Concrete Structures SIA 505 269/2:2011," 44 pp.

Steffens, K., Opitz, H., Quade, J. and Schwesinger, P., 2001, "The loading truck BELFA for loading tests on concrete bridges and sewers (in German)," *Bautechnik*, V. 78, No. 6, pp. 391-397.

Stewart, M. G., Rosowsky, D. V. and Val, D. V., 2001, "Reliability-based bridge assessment using risk-ranking decision analysis," *Structural Safety*, V. 23, No. 4, 10//, pp. 397-405.

Taljsten, B., Bergstrom, M., Nordin, H., Enochsson, O. and Elfgren, L., 2008, "Test of a concrete bridge in Sweden - II. CFRP Strengthening and Structural Health Monitoring," *IABMAS 2008*, Kohl, M. and Frangopol, D., eds., Seoul, Korea.

The Institution of Civil Engineers - National Steering Committee for the Load Testing of Bridges, 1998, "Guidelines for the Supplementary Load Testing of Bridges," London, UK, 44 pp.

Toprak, S., Inel, M., Senel, S. M., Lara, C. and Tanner, P., 2012, "Proof loading," *Innovative methods for the assessment of existing structures*, Diamantidis, D. and Holicky, M., eds., Prague.

Varela-Ortiz, W., Cintrón, C. Y. L., Velázquez, G. I. and Stanton, T. R., 2013, "Load testing and GPR assessment for concrete bridges on military installations," *Construction and Building Materials*, V. 38, pp. 1255-1269.

Yuefei, L., Dagang, L. and Xueping, F., 2014, "Reliability updating and prediction of bridge structures based on proof loads and monitored data," *Construction and Building Materials*, V. 66, pp. 795-804.

Bridge Load Testing and Monitoring for Super-Heavy Permit Loads

Brett Commander P.E. and Jesse Sipple PhD, P.E.

Synopsis: Load testing and structural monitoring facilitated the passage of several super-heavy permit loads at the Burns Harbor access bridge near Portage, IN. Twenty super-heavy permit loads, with gross vehicle weights reaching 848 kips (3770 kN), were required to cross the bridge, which was the only feasible route out of the port. Preliminary load ratings were acceptable due to three factors; the specialized transport's large footprint effectively distributed load, the bridge was designed for Michigan Truck Trains, and the bridge was assumed to be in good condition. The last condition came into question due to significant cracks throughout the prestressed concrete girders caused by delayed ettringite formation (DEF). While DEF cracks were a function of improper curing and not related to live-load effects, the Indiana Department of Transportation (INDOT) was concerned that repeated heavy loads would negatively influence cracks and the bridge's overall long-term performance. Due to the cargo's importance to the local community and lack of an alternate route, INDOT allowed use of the bridge after load tests proved that the transports would not cause damage or reduce the bridge's service life. Structural monitoring performed during the entire transport period verified structural performance was not diminished during the numerous crossings.

Key Words: delayed ettringite formation (DEF), load rate, load test, permit load, prestressed concrete (PS/C), structural monitoring, super-heavy transport, strain transducer, crack gage.

ACI member Brett Commander is a co-founder of Bridge Diagnostics, Inc. (BDI) where he is the Vice President of Engineering. His primary contribution to the field of structural engineering has been to transform instrumentation as a research activity to a practical tool for structural evaluation. Mr. Commander is a licensed Professional Engineer in in fourteen states and one Canadian Province.

ACI member Jesse Sipple is the Engineering Division Manager at Bridge Diagnostics, Inc. (BDI). In addition to division oversight and management, Dr. Sipple also serves as a Senior Analysis Engineering for both field testing and analysis of complex projects at BDI. Dr. Sipple is a licensed Professional Engineer in Colorado, New York, and Louisiana.

INTRODUCTION

A combination of load testing and structural monitoring was implemented for the crossing of several super-heavy permit loads on a port access bridge to verify safety and examine effects on long-term performance. Bridge Diagnostics, Inc. (BDI) was initially contracted by Barnhart Crane & Rigging (BCR) to perform load ratings for a series of super-heavy permit loads scheduled to cross the Burns Harbor Bridge in Portage, IN. As this bridge was the only route out of the port, a total of 20 super-heavy transports, with gross vehicle weights ranging from 595 to 848 kips (2650 to 3770 kN), were required to cross the structure. Despite the large load magnitudes, preliminary load ratings based on finite element analysis resulted in acceptable rating factors based on AASHTO Load and Resistance Rating (LRFR) criteria[1-2]. The favorable load ratings were a result of three primary factors; a) the load was highly distributed due to the large footprint of the specialized transport, b) the bridge was designed for Michigan Truck Trains which are significantly heavier than standard design vehicles, and c) it was assumed that the bridge was in good condition. The last condition came into question as the prestressed concrete (PS/C) Bulb-T girders had significant cracks throughout the girders due to delayed ettringite formation (DEF). While the DEF cracks were a function of improper curing and not related to live-load effects, the Indiana Department of Transportation (INDOT) was concerned that repeated heavy loads would negatively influence the cracks and diminish the bridge's overall long-term performance.

Due to the lack of a reasonable route alternative combined with the importance of the cargo, INDOT agreed that further investigation could be performed to determine if the bridge could serve as a viable route without experiencing any significant loss of serviceability. BCR and BDI performed a series of diagnostic load tests to examine how the DEF cracks and existing substructure cracks were influenced by heavy truck loads. In addition, load test data was used to generate field verified load ratings for the heavy permit vehicles and thereby reduced any uncertainty in the current structural performance.

Diagnostic load test procedures were chosen over proof load tests for a variety of reasons. The primary issue was that the bridge provided the only truck route out of the port. Therefore, any disruptions to traffic were not allowed and any methods that could potentially be destructive or diminish the remaining serviceability were unacceptable. Furthermore, the bridge crossed several railroad tracks carrying highspeed passenger trains and freight lines so access to the underside of the bridge was limited to brief work windows, which would not be conducive to incremental proof loading. While it was assumed that the proposed super-heavy transports would produce the greatest response conditions ever experienced by the bridge, calculated responses were still within design serviceability limits; the controlling limit corresponding to total midspan tensile stress being less than allowable tensile stress values. Therefore, there was no concern of non-linear behavior resulting from the proposed load crossing making diagnostic load tests the preferred choice.

As is often the case, results from the diagnostic load tests showed secondary stiffening effects were present that reduced live-load stress values compared to initial analytical predictions. These conditions were beneficial from both load rating and long-term performance perspectives as they effectively reduced midspan stresses and improved the already acceptable serviceability load ratings. Increased load ratings essentially corresponded to an increased factor of safety for not exceeding any allowable stress limits. Direct observation of crack movement showed that DEF cracks were not adversely influenced by heavy live-load application; crack movement corresponded with normal Poisson strain behavior and there was no indication that de-bonding of prestress tendons would occur or be accelerated.

Load test results and revised load ratings provided INDOT with an additional level of confidence to issue permits for the super-heavy hauls. Due to a lack of available information regarding long-term performance of PS/C girders with DEF cracks, a stipulation to the permits was to monitor the bridge before, during, and after each permit load crossing. Monitoring goals were to examine peak responses and verify allowable limits were not exceeded, make sure all strains and crack movements returned to the original condition after each heavy load event, and examine response trends over the duration of the 20 super-heavy crossings. This was accomplished with installation of a structural health monitoring (SHM) system that continuously recorded all live-load events. Instrumentation was installed to capture midspan strain and crack movement during every heavy vehicle crossing. Data was captured automatically by triggered events and observed remotely in real-time during every scheduled permit crossing. The transport schedule and monitoring period covered approximately one month. While the largest measured responses were in fact induced by the heaviest (848 kip / 3770 kN) permit loads, several other vehicle or combined vehicle crossings induced response magnitudes in the same range as the scheduled permit loads. Based on all captured truck crossings, it was verified that no damage was induced by the permit loads; measured responses were always at or below expected values and always returned to

previous state. Since all the permit configurations had an identical footprint and there were four identical sets of five modules, follow up analysis was done to verify all responses remained linear with respect to transport weight.

The following sections describe the processes applied to verify safety and serviceability of a bridge in questionable condition for use with super-heavy permit loads. Procedures discussed include the initial load rating, load testing and refined rating, monitoring, and final performance verification. The primary goal of this paper is to illustrate how instrumentation and field verified structural performance can be used to make important transportation and asset management decisions.

INITIAL LOAD RATINGS

During the early stages of the route selection process, preliminary load ratings were performed on numerous bridges to define viable routes. Bridge crossings were only one of several issues that had to be addressed prior to transporting vehicles of this size and weight. For example, overhead clearances with powerlines and signs as well as turn radii also had to be examined for the entire route, but bridges had to be dealt with early because they can often be "deal breakers" and define whether a route is a "go" or "no-go" situation. The route with the shortest haul on land was based on the heavy cargo being shipped from South Korea through the Arctic shipping routes, into the Great Lakes, and delivered to the Port of Indiana at the southern tip of Lake Michigan.

The first and nearly only major land obstacle was the Burns Harbor Bridge, immediately out of the gate. This bridge consisted of ten continuous spans, each composed of four prestressed concrete (PS/C) girders and a reinforced concrete (RC) deck. Span lengths range from 80ft (24.6m) to 115ft (35m) and were continuous for live-load. There were also relatively large concrete parapets running along each side of the bridge deck that are continuous over the length of the bridge. As shown in Figure 1, the bridge crossed four lanes of US-12, several active railroad tracks, and a service road.

Finite Element Analysis

Preliminary analyses and load ratings were performed on the Burns Harbor Bridge using a planar finite element model of the structure and a two-dimensional footprint of the transport wheel configuration. All structural analyses were based on linear-elastic behavior, but refined geometry of the load configuration and structure was required to simulate realistic load distribution of the bridge deck and the transport itself. The transport consisted of a dual-lane, 14-line, EasTrac Goldhofer trailer with 80 kip (356 kN) prime movers in front and back of the trailer. An illustration of the heaviest transport with a GVW of 848 kips (3770 kN) is shown in Figure 2. An image of the entire bridge model along with a section containing the longest span and the footprint of the permit vehicle is shown in Figure 3. All 20 proposed transports had identical wheel configurations and geometry, the only variations were the trailer weights. Each wheel-line of the trailer consisted of 8 tires with a total width of 18ft (5.5m). Because of the wheel configuration, beam-line analysis methods based on standard distribution factors would not be applicable.

The structure model was designed to provide realistic planar geometry with correct beam spacing as well as beam and bent widths. All nodal points resided in a single plane, however Quasi-3D modeling was performed through geometric transformations providing out-of-plane offsets between beamlines, bearing locations, and deck components. The PS/C bulb-T girders and RC diaphragms were modeled as frame elements with appropriate stiffness properties based on member cross-sectional geometries. An eccentricity term was applied to the frame elements to provide the distance between the centroid of the girders relative to the nodal points, which were located at the center of the deck slab. The deck was represented by a mesh of quadrilateral shell elements capable of resisting flexural moment about both horizontal axes, vertical shear, and in-plane membrane forces. Girders were supported by large hammerhead piers with solid integral diaphragms connecting the girders, deck, and pier into a solid system. The girder bearings were initially simulated as simple pin supports however, it was known that this would be a conservative modeling technique. Additional conservatism was built into the model as the large continuous RC parapets were assumed to not provide additional stiffness and were treated as additional dead-load only. The primary goal of this model was to provide realistic load path geometry and eliminate the need of distribution factor.

The second step toward achieving realistic load distribution was correct representation of the transport itself. The entire transport, including prime movers, was simulated by a grid of point loads with individual tire weights and correct relative planar locations. The array of wheel loads was then moved incrementally across the bridge model to generate a series of individual load cases making up an entire load cycle. Being a special permit condition, where the transport would be completely escorted, the travel path was centered along the roadway, maximizing the load distribution throughout the entire bridge cross-section. Variability of +/- 2 feet (0.6m) was considered within the

analysis to ensure worst case conditions were captured. Analysis results from the truck path were enveloped to provide extreme member response values for every member over the entire load cycle (vehicle crossing). These enveloped responses were then factored and compared with calculated member capacities to compute load rating factors for the individual structural members. The permit vehicle Load Rating Factor was then defined by the lowest component rating factor.

Load Rating

AASHTO LRFR procedures were implemented for the entire process with respect to computation of member capacities and implementation of appropriate resistance factors and load factors. For the special hauling permit vehicle live-load factors were reduced to lower level of 1.3 because the load application was well defined. The load configuration and wheel weights were precisely known and the vehicle would be completely escorted so no other traffic or live-loads would be on the bridge during the crossing and the path of the vehicle could be specified. In addition, the speed of the transport would be controlled and limited to crawl speed to eliminate dynamic or impact amplification. The special permit nature of the project greatly benefitted the transport load rating due to the reduction of live-load amplification compared to standard design or load ratings.

Another important aspect of the bridge load rating was the bridge's original design load. Being a port access structure, heavy vehicles were considered in the design. The bridge was designed for HS20-44, which was standard for the year of construction (1999), but the design also considered much heavier Michigan Train Trucks (shown in Figure 4) consisting of 11 axles and a GVW of 134 kips (596 kN). While the special permit vehicles were still significantly heavier than the Michigan Train Trucks, the design was based on the vehicles being in both lanes simultaneously, crossing the bridge frequently, and traveling at normal highway speeds with full dynamic/impact effects applied. Therefore, along with side-by-side loading, the load factors associated with the design vehicles were significantly greater than required for fully escorted permit vehicles.

The result of the preliminary load rating process was that the heaviest special permit vehicle had satisfactory load rating factors of 1.01 for Serviceability limits and 1.34 for Strength limit states. The caveats to these load ratings were that the super-heavy transport had to be the only live-load on the structure, the transport had to travel down the roadway centerline, and the vehicle had to cross at crawl speed so that all dynamic behavior was eliminated. In summary, the favorable load ratings were attributed to the following factors:

- The super-heavy permit vehicle had an extremely large footprint that occupied both traffic lanes and extended beyond the length of the longest span.
- The Burns Harbor Bridge was designed for Michigan Train Trucks which were considerably heavier than the standard highway design load and the design accounted for the Train Trucks being applied to both lanes simultaneously.
- Being a special permit, uncertainty of the load application was greatly reduced and therefore the load factors were also reduced. The wheel configuration and weight were precisely known, the path of the vehicle could be precisely defined, and the speed of the vehicle could be controlled so that dynamic effects were eliminated from the applied live load response calculations.
- No reduction in Serviceability or Strength flexural moment capacities were applied to account for the presence of the DEF crack formations.

The last factor concerning the serviceability capacity was still a concern for INDOT, because while there was no research indicating the DEF cracks would reduce load capacity, there was equally little information regarding long-term effects of DEF cracks with repeated heavy loads. INDOT engineers agreed that the proposed permit loads could safely cross the structure, but they needed further assurance that allowing the permit vehicles to cross would not have a detrimental impact on the structure's service life.

Crack due to Delayed Ettringite Formation (DEF)

While this enterprise was entirely commercial and not intended to be a research project, some research into DEF was required due to the extensive quantity of DEF cracks in the bulb-T girders. To define realistic vehicle load ratings, it was necessary to understand how and why cracks formed in the PS/C girders and if they would influence girder load capacity and/or serviceability.

DEF cracks were present on nearly all girders on nearly all spans. Based on inspection reports and conversations with INDOT officials, the cracks began forming within a year of the bridge construction and have progressively increased

in length and quantity at a slow but steady rate. Once the cracks began to form, they were identified as DEF which was due to improper curing temperatures during casting. DEF cracking is caused by a delayed formation of the mineral ettringite in the early stages of cement hydration. This delayed formation causes expansion and therefore cracking of the concrete[3]. The time in which this bridge was construction, 1990s, aligns with information in the literature for when there were several similar cases[4].

Production of defective girders caused the prestressing plant to go out of business but the fact remained that numerous bridges were built with girders effected by DEF and many are still in service. There was not a lot of research available on the long-term effects of DEF on girder performance. INDOTs approach has been to keep track of the crack formation and growth during inspections and paint over cracks in an attempt to seal them and protect the prestressing steel from moisture ingression.

The existing research shows that the actual mechanism that causes the cracking, and therefore effect on the concrete itself, is still being researched[4]. So, while the load rating analyses indicated that the permit loads could safely cross the bridge, INDOT had valid concern that repeated heavy loads could potentially cause de-bonding of concrete and prestress steel and thereby increase the deterioration rate. There was no research indicating serviceability would be at risk, but there was also no research indicating serviceability wouldn't be affected.

Due to the importance of the cargo to the neighboring community, INDOT was willing to move forward with the permitting process as long as it could be demonstrated that no measurable damage or deterioration would be caused by the permit loads. The proposed path was to perform load tests and examine the performance of the girders and the influence of heavy loads on the DEF cracks. Providing that the load tests showed there would likely be no acceleration of DEF deterioration, the bridge would then be monitored for the duration of the permit load crossings to verify no measurable change occurred during that period. Methods, procedures, and results from testing and monitoring efforts are presented in the following sections.

LOAD TEST PROGRAM

Test Procedures and Observations

The primary goals of the load test were to verify the load ratings and to examine the effects of heavy loads on the existing DEF cracks. Load tests were performed on two adjacent interior spans as these spans exhibited relatively extensive DEF cracks in the girders and instrumentation could be performed with minimal impact on railway or roadway traffic below.

For the load test, the structure was instrumented with 56 reusable surface-mounted strain transducers and 6 tiltmeter rotation sensors. Strain transducers were attached to each beam line at several cross-sections to measure flexural bending and the rotation sensors were attached to the beams near the piers to provide a global measurement of continuity between spans. The general instrumentation layout is shown in Figure 5 and photographs of the various sensor installations are provided in Figure 6 through Figure 8.

The controlled load was applied by a 226-kip (1005 kN) GVW test vehicle provided by BCR. The transport consisted of a single prime mover tractor pulling a 12-line, single wide, 156-kip (694 kN) Goldhofer trailer shown in Figure 9. This truck was lighter than the permit loads but had a much smaller foot-print. The goal was to apply a similar load to the most significant design load (Michigan Truck Train #8) so as not to overload the bridge in any way but generate structural responses greater than typically experienced by the bridge. Additional restrictions to the test vehicle were that it had to be a single wide and only occupy a single lane as one lane had to remain open for traffic entering and leaving the port. Weights of the transport were obtained by the trailer hydraulic pressure gages and verified in portions by the port scale. While the gross weight was greater than the scale load limit, the portion that could fit on the scale was within the limits. The selection of this vehicle was primarily based on availability.

Once the instrumentation was installed, a series of controlled load tests was completed with the test vehicle traveling at crawl speed (3 to 5 mph). During testing, data was recorded on all channels at sample rate of 50 Hz as the test vehicle crossed the structure in the westbound direction. Three different lateral positions were implemented for the truck paths to establish lateral distribution characteristics. The truck's longitudinal position was wirelessly tracked so that the response data could later be viewed as both a function of time and vehicle position. During the test procedures, traffic was periodically stopped so that the test vehicle was the only live-load applied to the structure.

Responses from the load test were examined visually to provide a qualitative review of the structural performance. Through this process data was examined in the form of response influence graphs and comparison plots for discrete load conditions. The goal of this process was to evaluate the quality of the load test data and obtain insight on the interaction of the various structural components. A series of qualitative review procedures performed on the load test data are outlined below:

- Reproducibility of duplicated truck passes provided a high level of consistency as shown in Figure 10. In addition, symmetry of responses from symmetrical load conditions provided evidence that all responses were linear and elastic. There was no evidence of any permanent displacement, non-linear behavior, or distress resulting from the load tests.
- By examining responses from each girder for a specific instance in time or load position, the effective lateral load distribution could be observed (Figure 11). Similar procedures were performed for instrumentation locations along a girder line to quantify the level of flexural continuity across the piers.
- Strain measurements recorded at the top and bottom of the girders were used to calculate the location of the neutral axis, which verified composite behavior and provided information on how best to analyze the deck and girder interaction. Figure 12 provides an illustration of the neutral axis measurement for an interior girder.
- Neutral axis measurements from the exterior girders were significantly higher than the observed at the interior girders as shown in Figure 13. This result combined with strain responses on upper and lower portions of the parapets showed that the continuous parapets were composite with the deck-slab and the exterior girders. Therefore, the effective stiffness of the exterior girders was significantly greater than the interior girders, which would greatly influence the structure's overall lateral distribution of load.
- The movement of several DEF cracks were examined with respect to the passage of the heavy test load. The instrumented cracks were typically on the bottom flange portion of the girders near midspan. Observed crack movement was extremely small and tended to close when the girders experienced positive flexure (bottom flange went into tension). In general, the crack movement was inversely proportional to the flexural tension stress and the magnitude was consistent with normal Poisson strain. Therefore, there did appear to be any adverse behavior of the cracks associated with the heavy live-load activity. Furthermore, all crack movement appeared to be completely elastic as all measurements returned to the original state after each load cycle as shown in Figure 14.

Modeling, Analysis, and Data Correlation

Insight gained from the data review provided the basis for any required modifications to make the bridge model more representative of the actual structure. For example, it was apparent that the parapets were continuous and composite with the deck and exterior beams. The frame elements representing the parapets should therefore have a positive eccentricity relative to the deck/node plane. The observed negative moment values near the piers and degree of continuity across the piers suggested relatively complex bearing conditions existed that would not be well represented by a simple pin type support. Therefore, modeling elements were required to simulate the width of the pier as well as the interaction between the pier and superstructure. Beyond recognizing required model changes, the next step was to quantify the actual behavior and performance of the structure. This was done through a structural identification process based on direct comparison between the measured load test results and analysis results. There are four general procedures to obtain a field verified model and include:

- **Simulate:** The entire load test was simulated so that a set of analysis results could be directly compared with the load test data. This included installation of virtual sensors on the model at the same locations applied during the load test. To assist data management, the virtual sensors had the same name and sensor type information. The test vehicle was also modelled and applied to the model in a series of load cases that represented each test run across the bridge. Figure 3 provides an illustration of the bridge model with the test truck traveling down the centerline of the roadway.
- **Compare:** Direct comparison between measured and theoretical results was performed to establish an error vector. This error vector contained the response difference for every sensor and every truck position (load case) and generally consisted of several thousand comparison points. Establishing the error vector was extremely important because it provided statistical measures accuracy and provided a basis for quantifying change in accuracy with any changes in model parameters.
- **Optimize:** Numeric optimization techniques based on Least Squares were implemented to minimize the error at each comparison point and overall system error. Model parameters including rotational resistance at girder bearings, effective girder stiffness, effective RC deck stiffness, and parapet contribution were incrementally modified. Effects of the changes to the error vector were examined with each increment so that new stiffness

parameters could be estimated. This process was done in an automated fashion until a best fit condition was achieved. While the computer code to perform this task was proprietary, general concepts and methodology were developed by Goble, Commander, Schulz at the University of Colorado[5,6].

- **Reality check:** As with any computer process, results can only be as good as the simulation, input data, and limits. Therefore, all results had to be examined and checked for reasonableness.

Following the calibration process, a model closely representing the actual structure was obtained. This was determined through statistical validation as well as graphical comparisons as shown in Figure 15 through Figure 17. Numerous response history plots were examined throughout the optimization process to provide the rating engineer a means to observe model improvement. Once model had the correct response shapes at all sensor locations and error values were minimized to acceptable levels, the model was considered a valid representation of the real structure. In this case, the goal was to obtain realistic lateral load distribution including the contribution of the parapets and correct longitudinal flexure characteristics for all vehicle positions. With regards to response history shapes, it was important that the model not only matched well at peak values but also minimum values when a span or girder was not directly loaded. Obtaining a good match at all locations for all vehicle positions was the criteria for model accuracy.

Field Verified Load Rating

The same load rating procedures that were performed during the preliminary load rating were repeated on the field verified model. The primary difference between the two models was that field verified model realistically represented the interaction of the superstructure and large hammerhead piers, the continuity of the spans across the piers, and the effective contribution of the parapets to the overall structural stiffness and load distribution. The end result was that the controlling load rating for the heaviest permit vehicle increased by more than 40 percent. Table 1 provides a summary of the load factors applied during the load rating and the resulting rating factors for serviceability and strength limit states before and after the model calibration process. An increase in load rating was expected because there were numerous conservative assumptions in the preliminary load rating due to uncertainties in actual behavior. The initial model did not account for contribution of the parapets and the pier supports were assumed to be simple pins. Operational stipulations of the ratings were that the transports be fully escorted so that no other vehicles would be on the bridge during crossing, travel across the bridge had to be centered on the roadway, and maximum speed of 5 mph (8 kph) was required to eliminate dynamic effects.

Table 1 Load Rating Results for 848-kip (3770 kN) Permit Load Configuration.

Model	Limit State	Applied Load Factors			Rating Factor
		Dead Load	Live Load	Dynamic	Escorted Permit
Initial Model	Service	1.00	1.00	0.0	1.01
	Strength I	1.25	1.30	0.0	1.34
Field Verified Model	Service	1.00	1.00	0.0	1.56
	Strength I	1.25	1.30	0.0	2.56

As with the initial load rating, no reduction in girder capacity was applied to account for the presence and concern for the DEF cracks. This was done to be consistent with the previous load rating and because the load test showed that there were no ill effects on the cracks due to heavy vehicle applications. However, the increased load rating provided by the field verified model did provide a greater margin of safety, so there was room to account for a condition factor on the girder capacity computations and the load rating would still be acceptable. After the load test and load rating results provided to INDOT, the transport permits were approved with the condition that the structure be monitored during all heavy transport crossings.

STRUCTURAL MONITORING

INDOT accepted the load test and load rating results but still had concerns regarding potential reduction of long-term performance due to the weight of the permit vehicles and the number of required vehicle crossings. Therefore, permits for the transports were approved with the provision that the structure be monitored continuously over the period between the first and last permit vehicle crossing. This was achieved by installing a monitoring system on the same spans instrumented during the load test with a similar sensor configuration. The system's purpose was to monitor structural responses due to permit modules as they crossed the structure leaving Burns Harbor. A combination of strain transducers, resistive displacement sensors (crack-meters), and thermistors at four super-structure cross sections were installed to monitor the structure's live-load and thermal movement. Instruments were intended to continuously

capture flexural responses, check for any changes in cross-sectional behavior, lateral load distribution, continuity between spans, and inelastic deformations. Immediate goals were to verify that stress induced by the permit loads did not exceed allowable concrete tensile stress limits (AASHTO 5.9.4.2.2), verify that all measured responses returned to their original state, and identify any trends indicating non-linear behavior or a reduction in stiffness.

The monitoring system continually measured responses at 20 Hz for from a total of 48 sensors. The monitoring system was mounted to one of the piers and was powered by a diesel generator with 48 hours of battery backup. Communication to the system was provided by an IP addressable modem so that event data could be downloaded on a regular basis and measured responses could be remotely viewed in real-time during actual transport crossings. Installation of the SHM system took place October 19th and 21st and the monitoring duration spanned approximately 4 weeks - October 25th to November 20th, 2016. Data collection was programmed to record hourly statistical data (maximum, minimum, and average) and contiguous data records during triggered live-load events. Real-time monitoring was performed for each of the 20 scheduled permit crossings so that any significant variation in response could be detected and reported immediately. Figure 19 provides an example data capture that was recorded during one of the heaviest permit load crossings; bottom flange strains from midspan of Spans F & G are shown for all girders. The maximum measured midspan strain during the entire monitoring period was 116με. Whereas the approximate strain value corresponding to the allowable midspan tensile stress, available for live-load, was 244με. Therefore, the midspan stresses were well below the AASHTO serviceability limit.

Real-time examination of the data was performed during all but one of the permit load crossings. Measured responses were immediately compared with expected strains and it was verified that no responses exceeded allowable limits and that no residual effects occurred after any vehicle crossing. Since the load geometry was the same for all transports, expected strains were computed from previous crossings and proportionality of the trailer weights. Throughout the monitoring duration, all responses were observed to be linear with respect to load magnitude. Also contained in Table 2 are the peak midspan strain values recorded during each permit transport crossing. Figure 20 shows maximum midspan strain magnitudes measured at each girder plotted with respect to trailer gross weight. Variations of 5 to 10 percent deviation from linear were apparent but these were primarily a function of vehicle lateral position or slight variations in the lateral center-of-gravity. Figure 21 shows cross-sectional strain distributions for midspan at Span F and the influence of lateral load position was apparent. In general, there were minor variations in load distribution among the interior girders with larger variations at the exterior girders.

In general, responses captured during the permit load crossings were smaller in magnitude than predicted from the field verified model. This was partially due to the model being intentionally conservative by not accounting for secondary stiffening conditions, but it was also likely that the cargo being transported was stiffer than the bridge itself which altered the applied load distribution. Of the 20 permit loads, there were 5 different load configurations, with 4 of each type. Therefore, it was a simple process to verify that peak responses from each truck pass were proportional to the gross trailer weight. While there was some variation in strain magnitude among supposedly identical transports, there was no apparent trend between magnitude and time. For example, later vehicle crossings did not produce greater responses than the earlier crossings. The variations appeared to be primarily due to small differences in lateral position, but could have been slightly different weights or variations in hydraulic suspension. In theory, the linked hydraulic suspension should have maintained equal axle and tire weights on the trailer as it traveled along the roadway, however friction in the cylinders would cause minor deviations associated with bridge deflections and changes in super-elevation. From a practical view point, the responses were very consistent among the different transport crossings. Variations were measurable at the micro-strain level but the differences were very small compared to the available factor of safety.

After the first few days of monitoring normal traffic and permit vehicles, the event trigger limit was defined as 60με for the midspan gages. The events were defined to capture 90 seconds of data before the trigger condition and 240 seconds of data after the event trigger. The goal was to capture heavy vehicles but not every truck crossing; the lightest permit truck induced a peak midspan strain of 67με, while there were numerous load conditions that produced strains in excess of 50με. With the applied trigger settings, the data logger successfully captured all permit vehicle crossings along with several additional vehicle crossings. Peak strains associated with the BCR permit vehicles are provided for each girder in Table 2 whereas Table 3 provides a list of triggered events unrelated to the BCR project. While no random vehicle crossings produced midspan responses as large as the heavier permit loads, there were several occurrences in the range of the lighter permit configurations. Many of those occurrences were likely multiple presence

conditions with legal weight vehicles. One crossing was a known permit load unrelated to this project. Three events were due to single heavy vehicles traveling in and out of the port.

Table 2 Maximum Midspan Strains Measured During Permit Load Crossings (10/25/2016 – 11/22/2016)

Transport	Date	Time	Module	GVW	Trailer Wgt	Midspan Peak strains (με)				
				kips (kN)	kips (kN)	G1	G2	G3	G4	Max
Transport 1	10/25/2016	8:52	1	595 (2647)	435 (1935)	47	67	63	48	67
Transport 2	10/25/2016	9:25	1	595 (2647)	435 (1935)	50	68	63	48	68
Transport 3	10/27/2016	8:36	2	848 (3772)	688 (3060)	88	112	99	68	112
Transport 4	10/27/2016	9:13	2	848 (3772)	688 (3060)	78	108	101	74	108
Transport 5	10/31/2016	9:11	3	831 (3696)	671 (2985)	85	110	101	67	110
Transport 6	10/31/2016	9:38	3	831 (3696)	671 (2985)	69	105	108	82	108
Transport 7	11/2/2016	13:02	4	794 (3532)	634 (2820)	78	109	105	74	109
Transport 8	11/2/2016	13:28	4	794 (3532)	634 (2820)	73	106	105	75	106
Transport 9	11/7/2016		5	798 (3550)	638 (2838)	-	-	-	-	-
Transport 10	11/7/2016	9:28	5	798 (3550)	638 (2838)	70	101	100	71	101
Transport 11	11/9/2016	9:29	1	595 (2647)	435 (1935)	50	71	71	53	71
Transport 12	11/9/2016	9:34	1	595 (2647)	435 (1935)	46	68	70	55	70
Transport 13	11/11/2016	8:38	2	848 (3772)	688 (3060)	82	116	112	78	116
Transport 14	11/11/2016	9:16	2	848 (3772)	688 (3060)	74	112	114	85	114
Transport 15	11/14/2016	8:55	3	831 (3696)	671 (2985)	79	110	107	76	110
Transport 16	11/14/2016	9:26	3	831 (3696)	671 (2985)	78	107	102	72	107
Transport 17	11/16/2016	9:09	4	794 (3532)	634 (2820)	70	98	97	72	98
Transport 18	11/18/2016	8:49	4	794 (3532)	634 (2820)	74	105	103	74	105
Transport 19	11/18/2016	9:10	5	798 (3550)	638 (2838)	72	103	100	71	103
Transport 20	11/20/2016	9:59	5	798 (3550)	638 (2838)	66	95	95	71	95

Table 3 Maximum Midspan Strains Measured from Random Vehicles (11/2/2016 – 11/22/2016)

Date	Time	Description	Peak Midspan Strain
11/2/2106	10:22	Other special permit vehicle (escorted)	71
11/8/2016	7:10	Random double crossing	73
11/8/2016	12:09	Random double crossing	73
11/9/2016	23:08	Random double crossing	71
11/11/2016	8:04	Random double crossing	73
11/14/2016	14:28	Random multiple crossing	62
11/18/2016	8:00	Random multiple crossing	63
11/18/2016	18:15	Single heavy vehicle exiting port	73
11/21/2016	23:35	Single heavy vehicle entering port	67
11/22/2016	0:33	Single heavy vehicle entering port	84

CONCLUSIONS

The Burns Harbor load test and monitoring program is an example of how field instrumentation can be an integral part of a major transportation project. Due to the lack of information on DEF cracks and how they influence strength and serviceability performance, INDOT had no basis to provide permits allowing the heavy equipment to leave the port. The transport foot-print had already been maximized to the point of diminishing returns so there was no benefit in load reconfiguration. Shoring the bridge was not a viable option either due to the number of spans and impact on

traffic under the bridge. Re-routing the cargo to another port, would have been extremely expensive and may not have provided viable solutions either; with a longer land route, the number of bridge encounters would have increased. Therefore, due to the importance of the cargo and the lack of alternatives, there was a significant incentive by the hauler and INDOT to investigate the feasibility of utilizing the bridge. By physically measuring the performance of the DEF impacted girders under heavy loads, INDOT had confidence that allowing the heavy transports to cross would not reduce the service life of a critical structure. Monitoring during the actual transports provided additional assurance to both INDOT and BCR that no damage was done during the project.

As is typical with diagnostic load tests, estimated bridge performance was based on a field verified model calibrated with load conditions significantly less than the heavy permit loads. A frequent question regarding this procedure is if the "extrapolation" to heavier loads is valid. As illustrated by this project, the process is valid for applications resulting in acceptable Serviceability Load Ratings because results are based on a full structural model. The process is not simply and extrapolation of test data or peak responses. The primary requirement is that all responses throughout the model remain in the linear response range. This conclusion was further verified by the recorded measurements obtained during the monitoring of the actual permit vehicles. Linear behavior was observed during all transport crossings proving the validity of the linear-elastic model. The extension of this process to produce Strength Load Ratings is not as applicable, however results are generally conservative for primary structural elements such as girders because load distribution to the damaged components remains constant. Non-linear behavior associated with ultimate load scenarios generally results in load being shed away from components as they become more flexible. Nearly all bridge serviceability and strength load ratings performed throughout all state DOTs are based on linear-elastic models.

Beyond the technical aspects providing the required data, the greatest contributor to the project success was the teamwork between the various stakeholders and consultants. INDOT and the Port of Indiana were willing to provide access to the bridge and participate in the investigation including onsite inspection and bringing in technical reviewers from their bridge consultants and Purdue University. The cargo owner and the hauler (BCR) provided the resources and technical consultants (BDI) to perform a thorough investigation and performance verification program. While all direct costs were covered by the cargo owner, all stakeholders shared risk and invested time and effort towards completion of the project.

REFERENCES

[1] AASHTO, (2014). "AASHTO LRFD Bridge Design Specifications, Seventh Edition." Washington, D.C.

[2] AASHTO, (2013). "The Manual for Bridge Evaluation, Second Edition, with 2015 Interim Revisions." Washington, D.C.

[3] The Concrete Society. (2017, June). Delayed ettringite formation (DEF). Retrieved from http://www.concrete.org.uk/fingertips-nuggets.asp?cmd=display&id=932

[4] Portland Cement Association, 2001, Godart & Loic, 2013, Larson, Bayrak, & Jirsa, 2012

[5] "SIMPLE LOAD CPACITY TESTS FOR BRIDGES TO DETEREMINE SAFE POSTING LIMITS", Goble, G., Commander, B., Schulz, J., Submitted to Pennsylvania Department of Transportation by University of Colorado, Boulder, Sept. 1992

[6] "LOAD PREDICTION AND STRUCTURAL RESPONSE", Goble, G., Commander, B., Schulz, J., Submitted to Federal Highway Administration by University of Colorado, Boulder, Nov. 1990

FIGURES

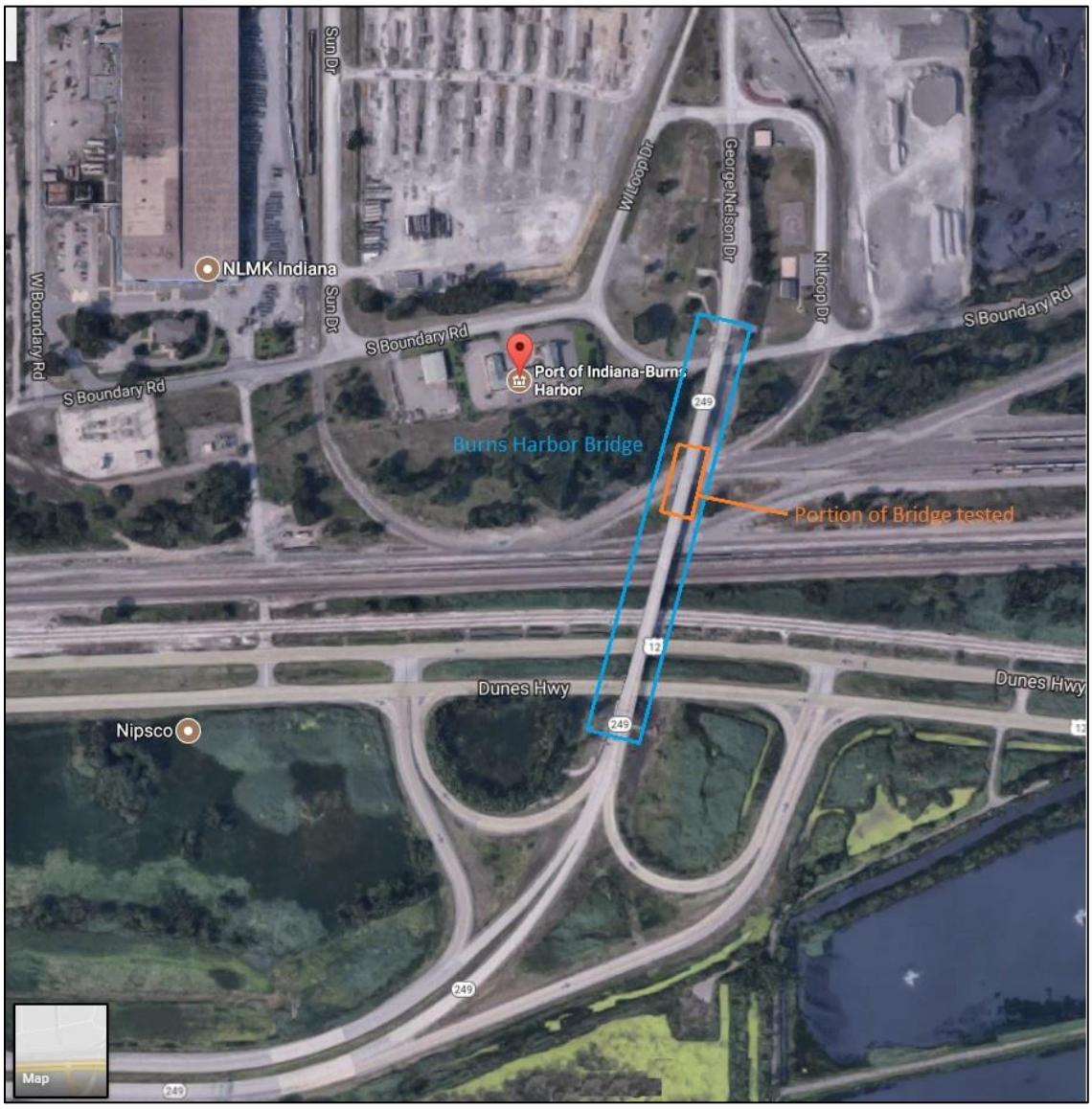

Figure 1 **Bridge location and portion of structure instrumented and tested.**

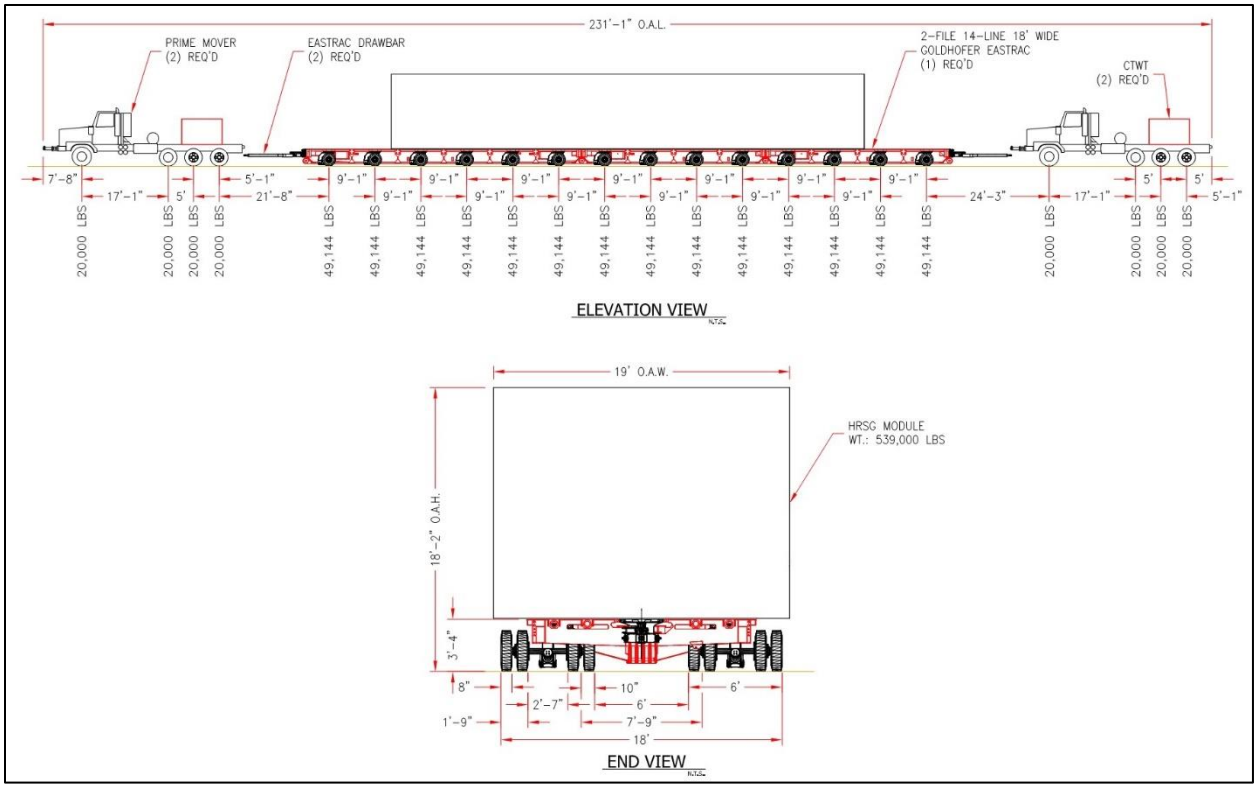

Figure 2 Axle and weight configuration of heaviest proposed permit load.

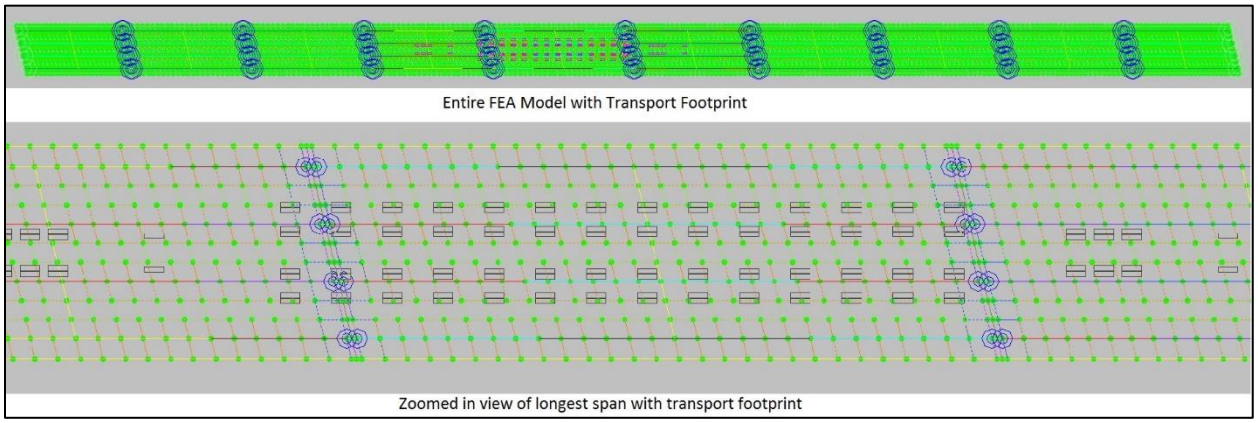

Figure 3 FEA Model with section showing longest span and permit transport footprint.

Figure 4 Michigan Truck Train #8 – 134-kip (596 kN) supplementary design load

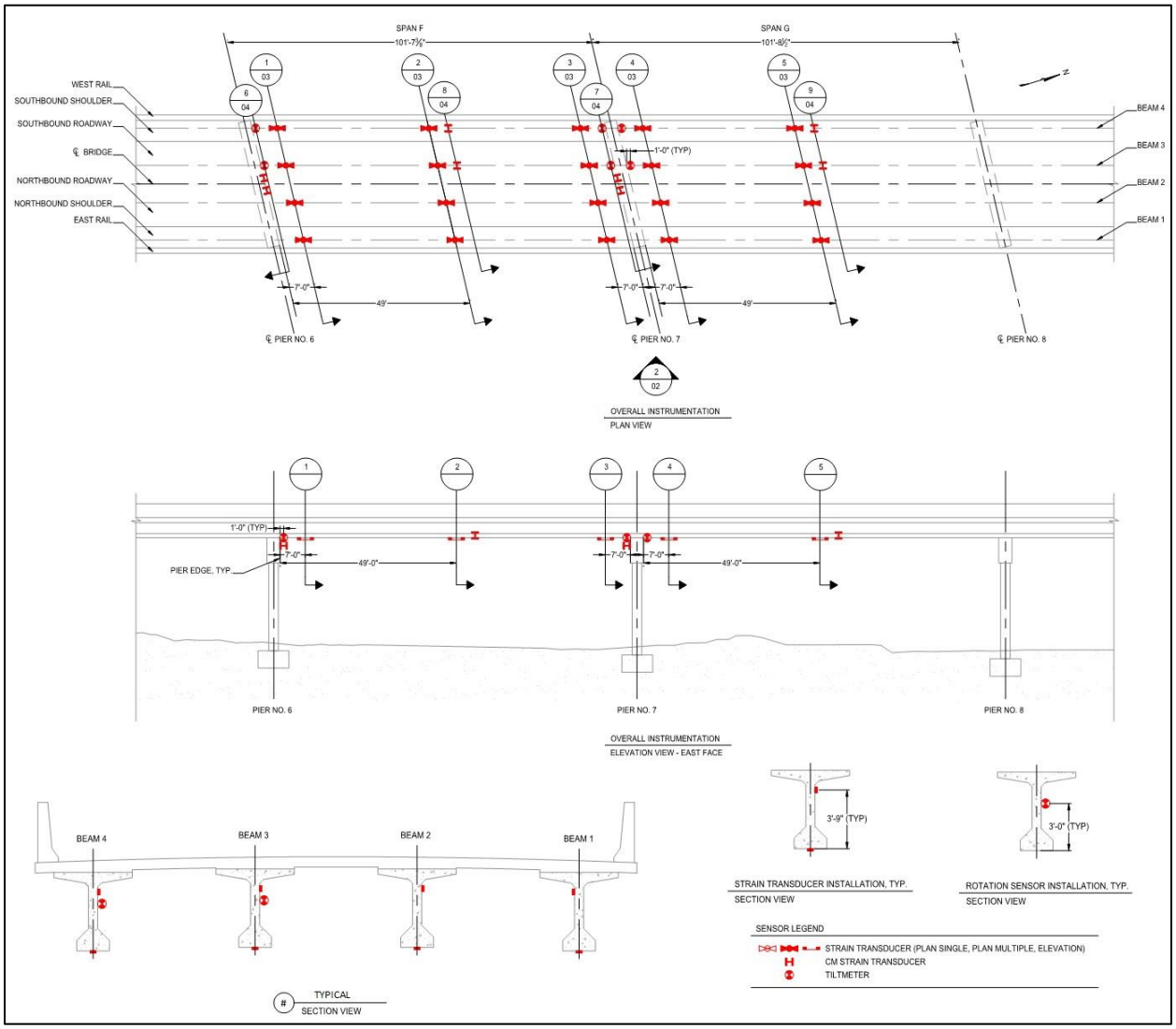

Figure 5 Load Test Instrumentation Layout.

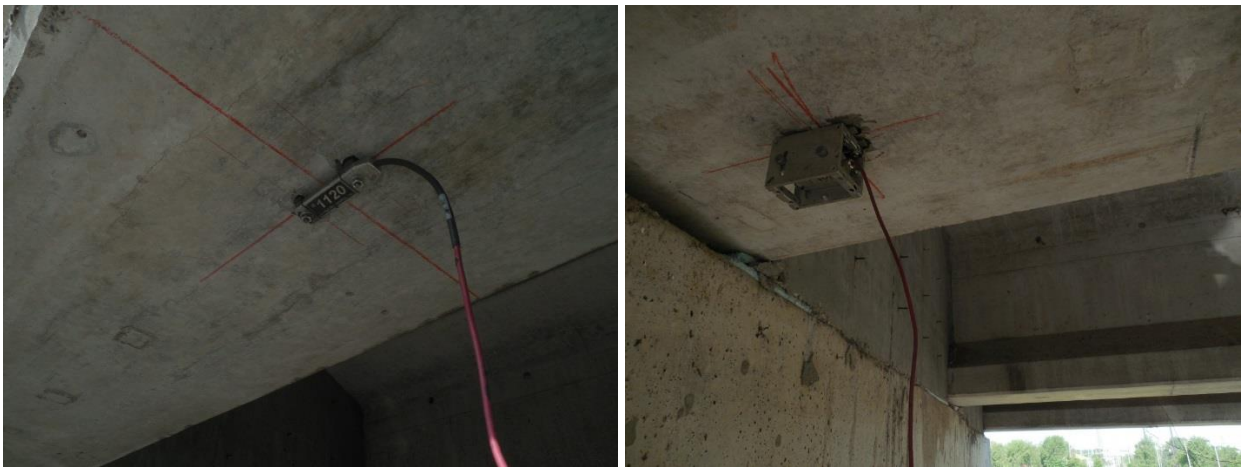

Figure 6 Surface mounted strain transducer and rotation sensor attached to PS/C girders (typical).

Figure 7 Top and Bottom strain transducers on parapet (typical).

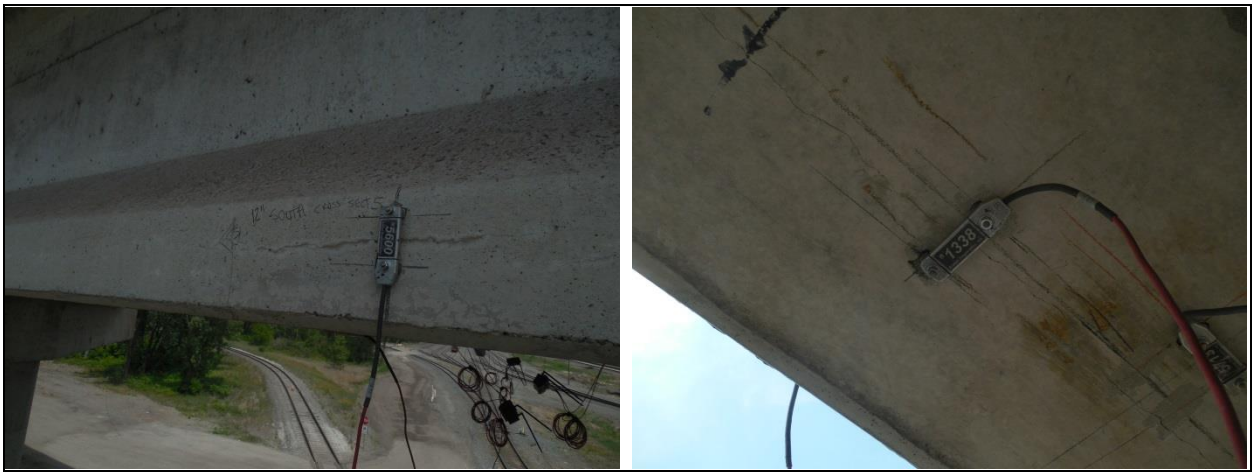

Figure 8 Strain transducers mounted across girder DEF cracks to measure crack movement (typical).

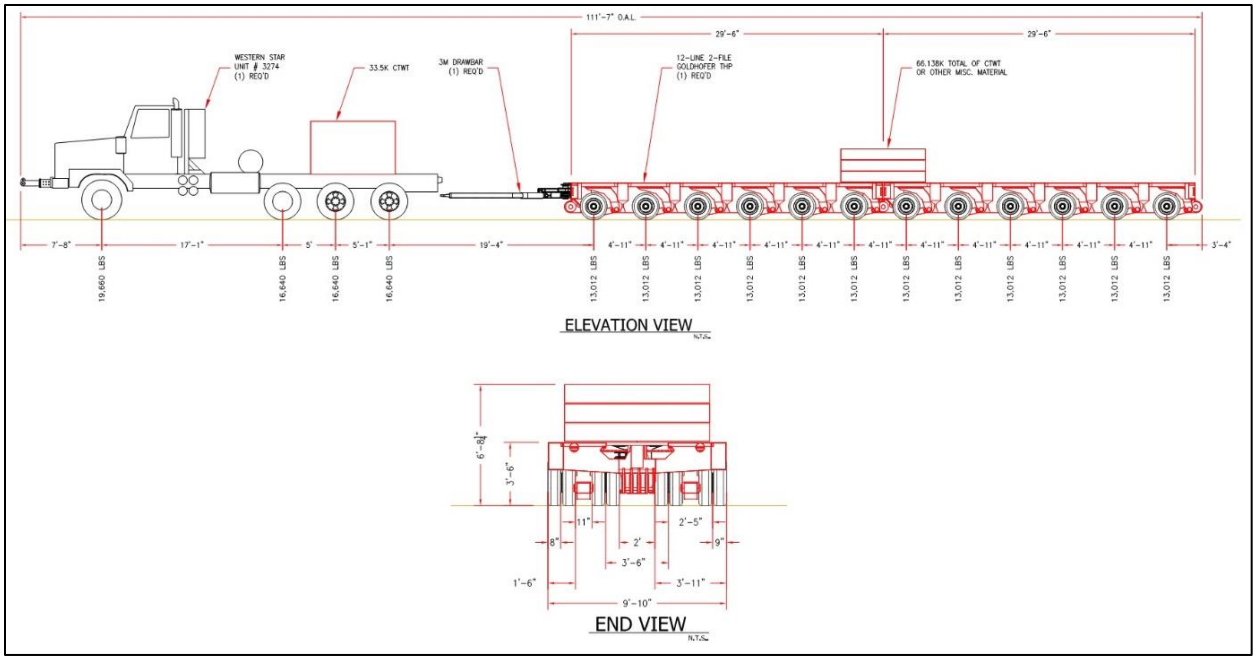

Figure 9 Axle and weight configuration for load test vehicle.

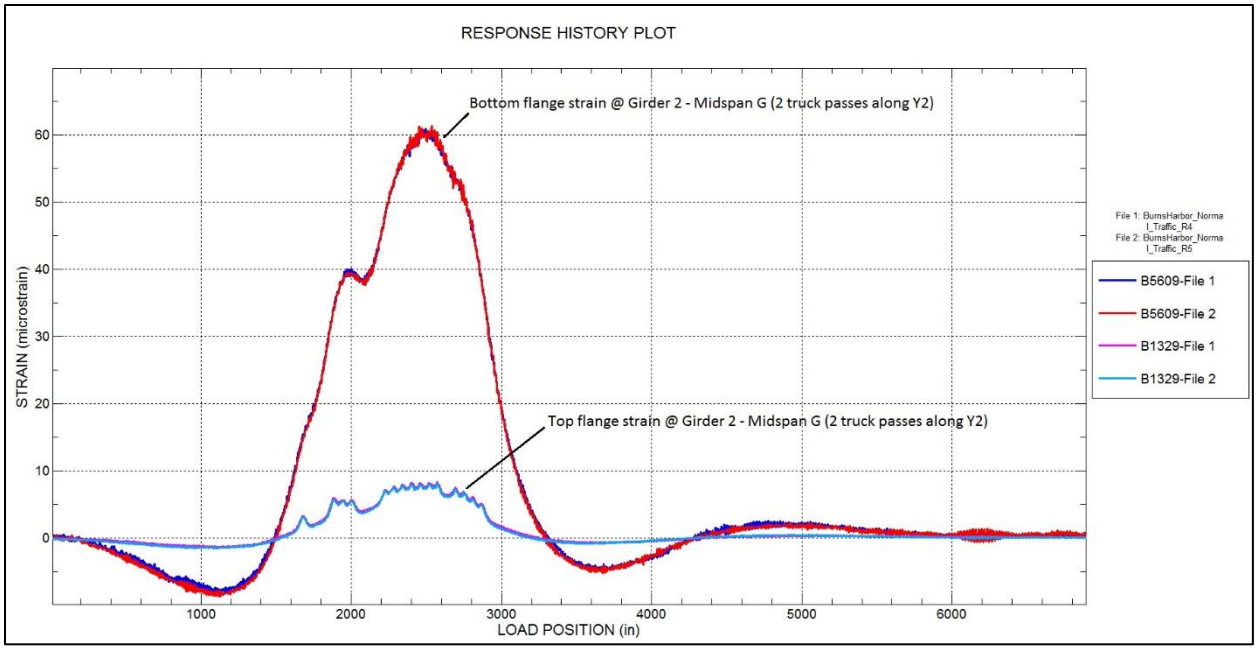

Figure 10 Reproducibility of strain response history at midspan of Girder 2 for two identical truck paths.

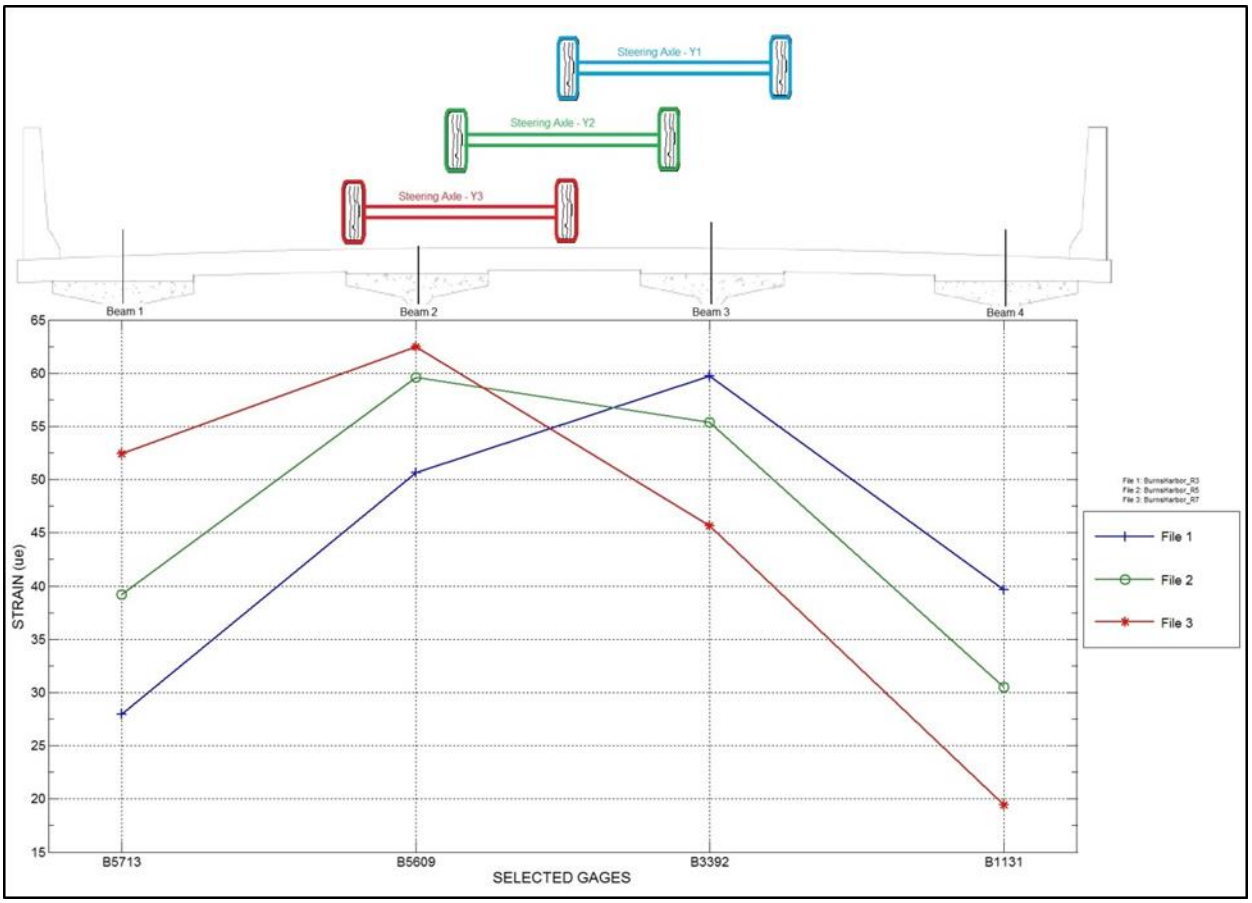

Figure 11 Lateral strain distribution at midspan from three different truck paths.

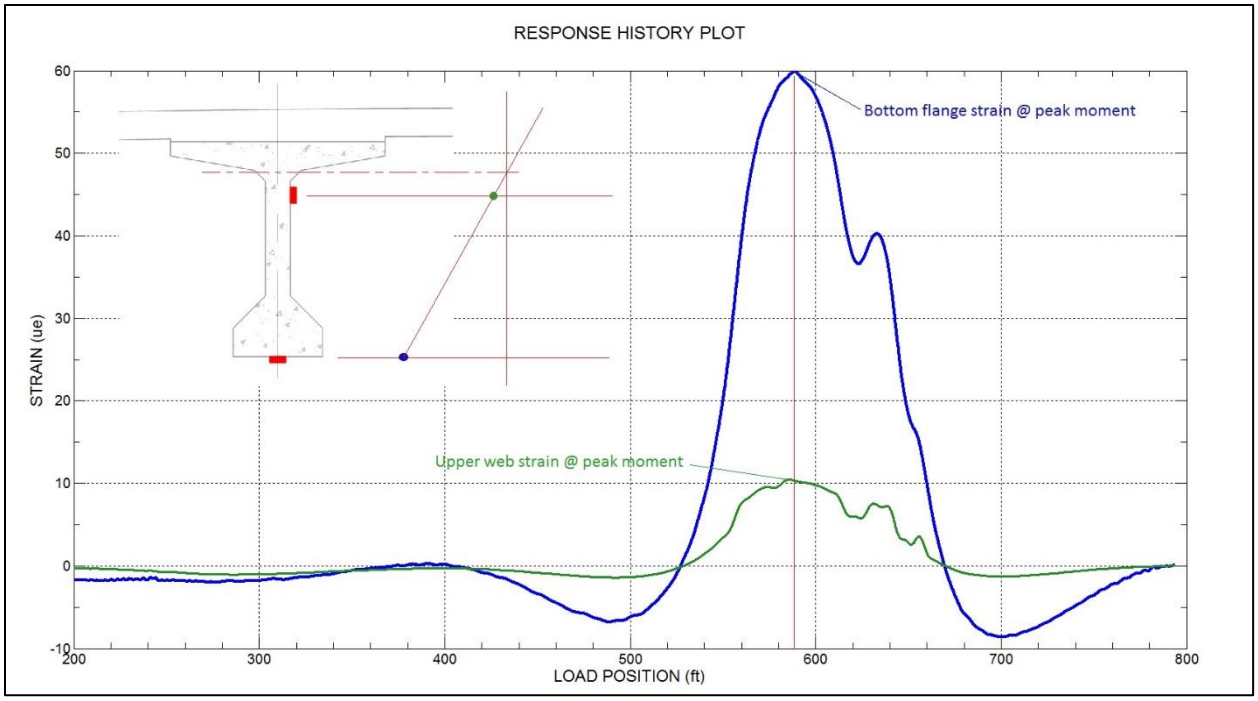

Figure 12 Measured location of neutral axis verifying girder-to-deck composite behavior

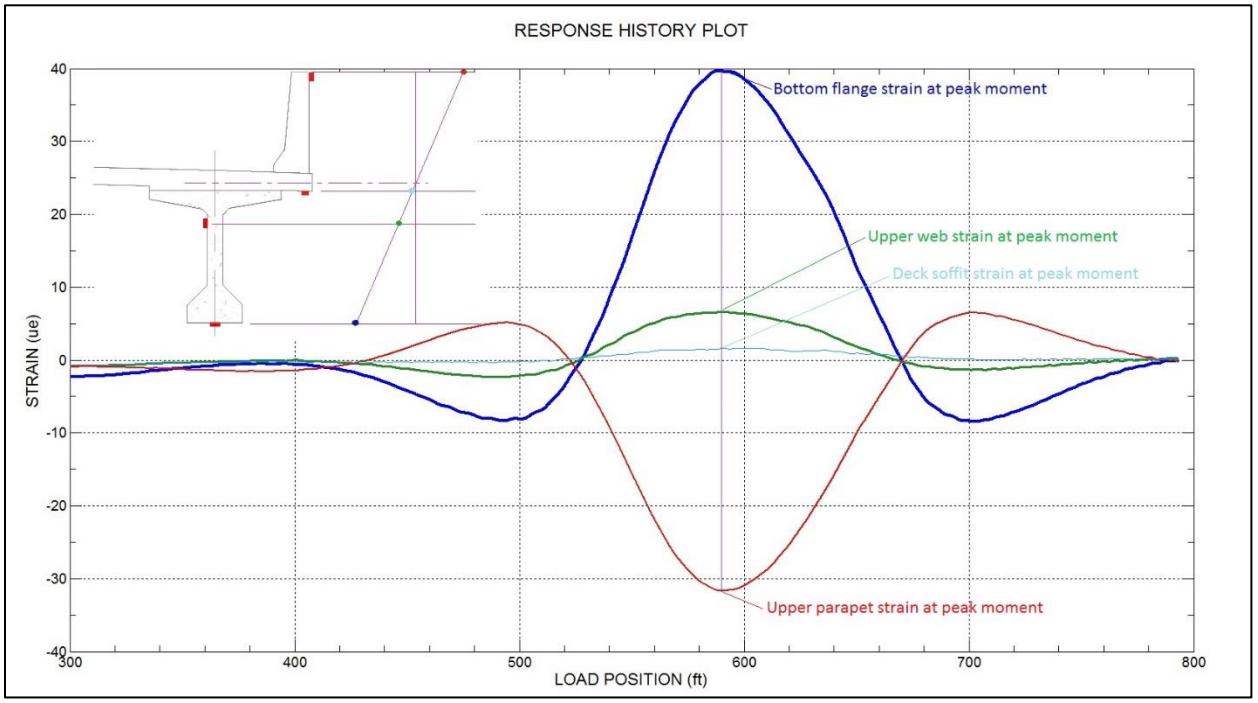

Figure 13 Measured location of neutral axis verifying composite behavior of girder, deck, and RC parapet

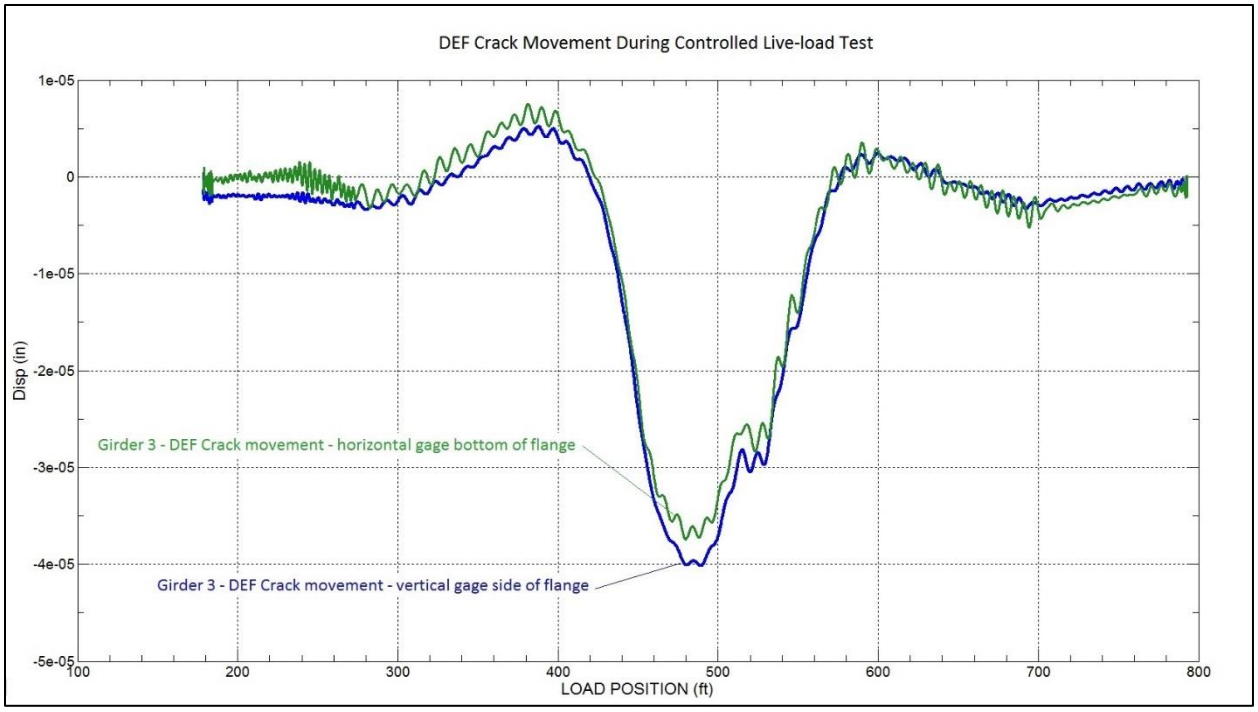

Figure 14 Measured crack movement during load test – two DEF cracks on bottom flange of girder

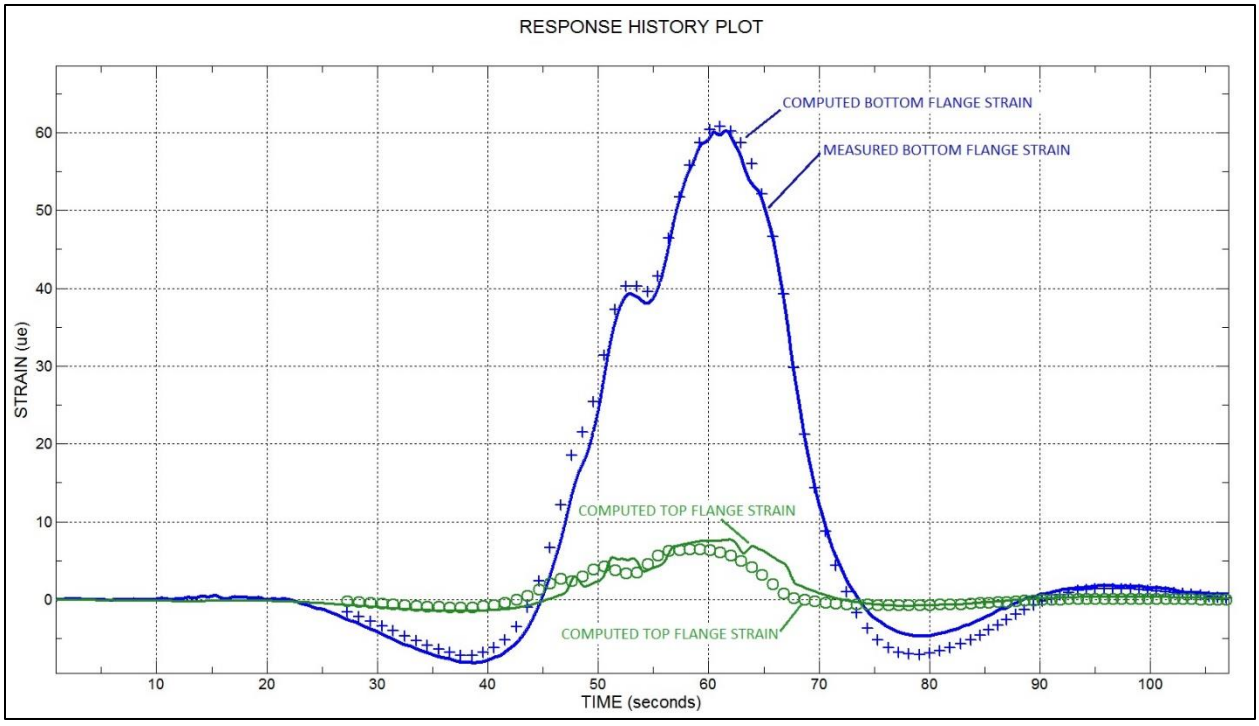

Figure 15 Measured and computed bottom flange and upper web strains of interior Girder 2 @ midspan

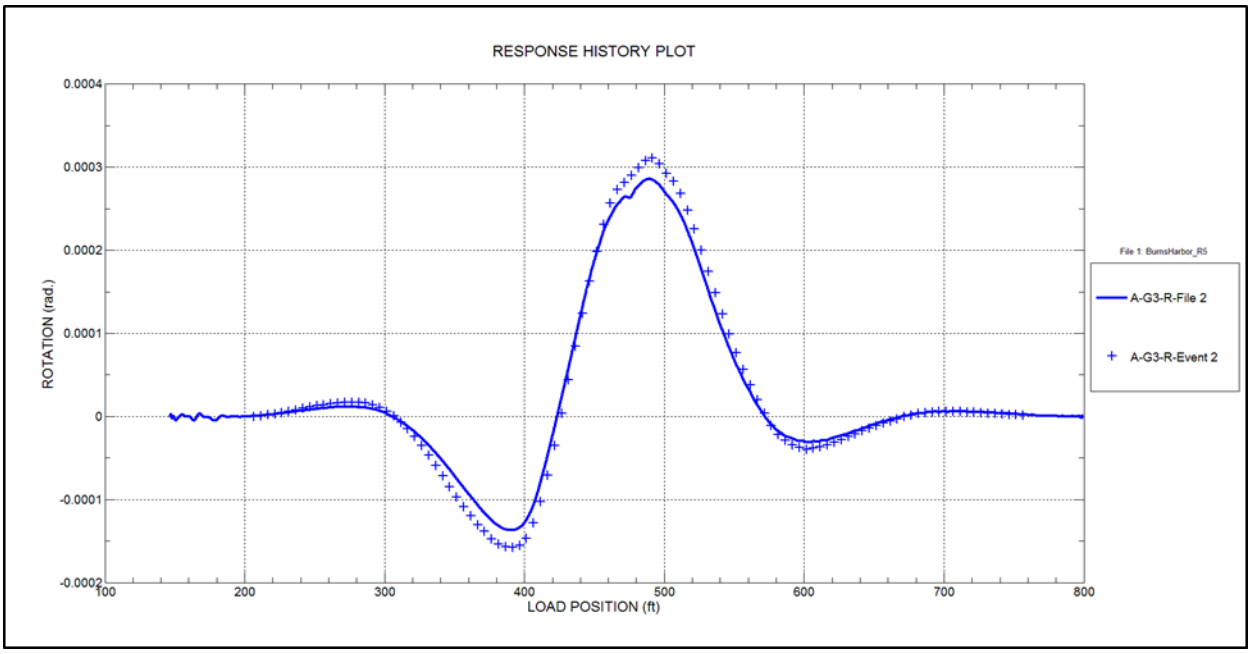

Figure 16 Measured and computed beam-end rotation of interior girder G3 @ Pier 6 – Span F

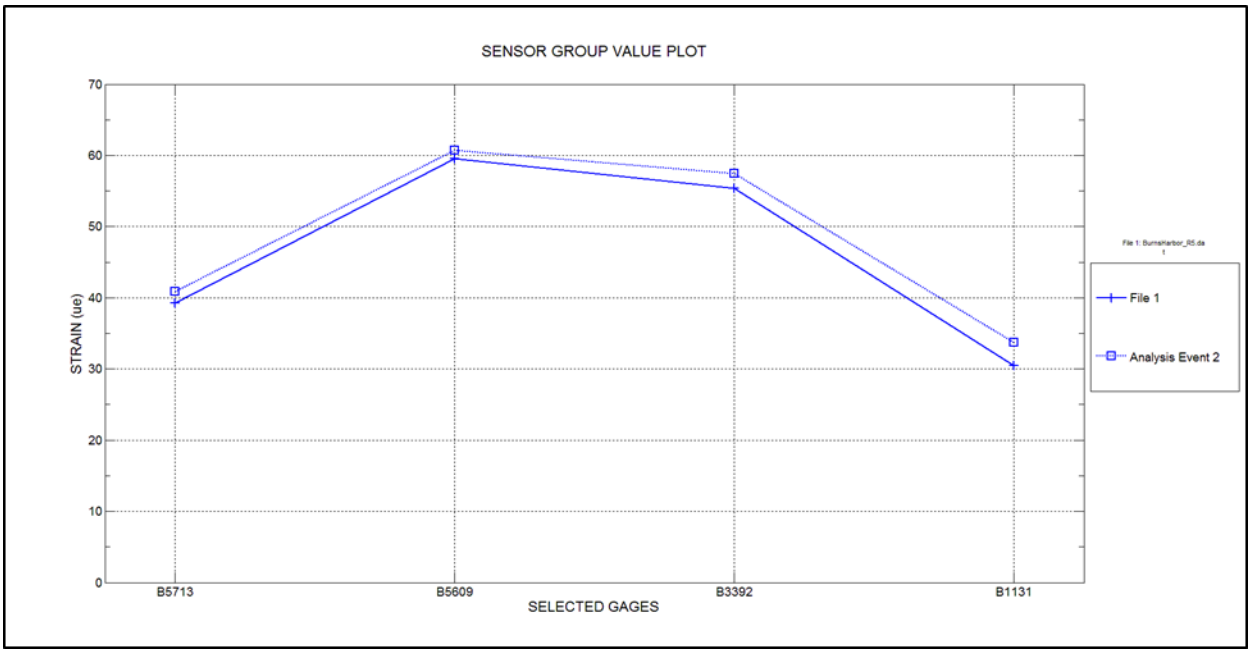

Figure 17 Measured and computed midspan lateral strain distribution - Girders 1 - 4 @ maximum moment

Figure 18 Super-heavy permit vehicle crossing Burns Harbor Bridge -Module A 848-kip (3770 kN)

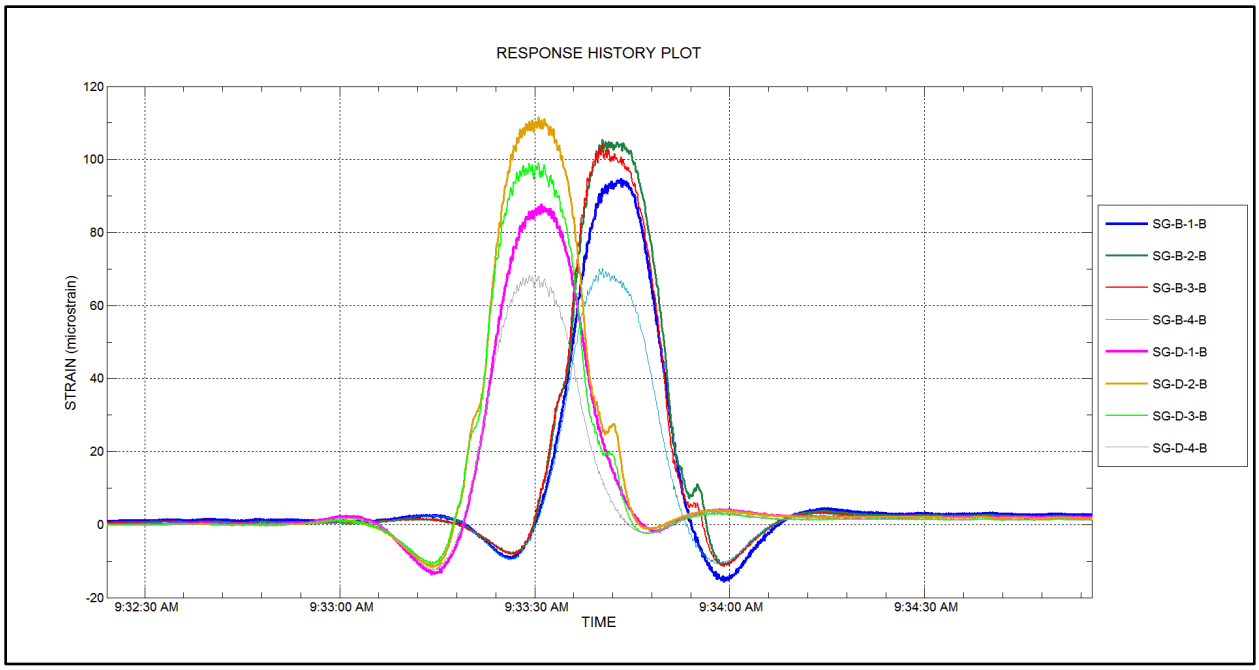

Figure 19 Mid-span strain responses due to Module 2 – 848-kip (3770 kN) GVW.

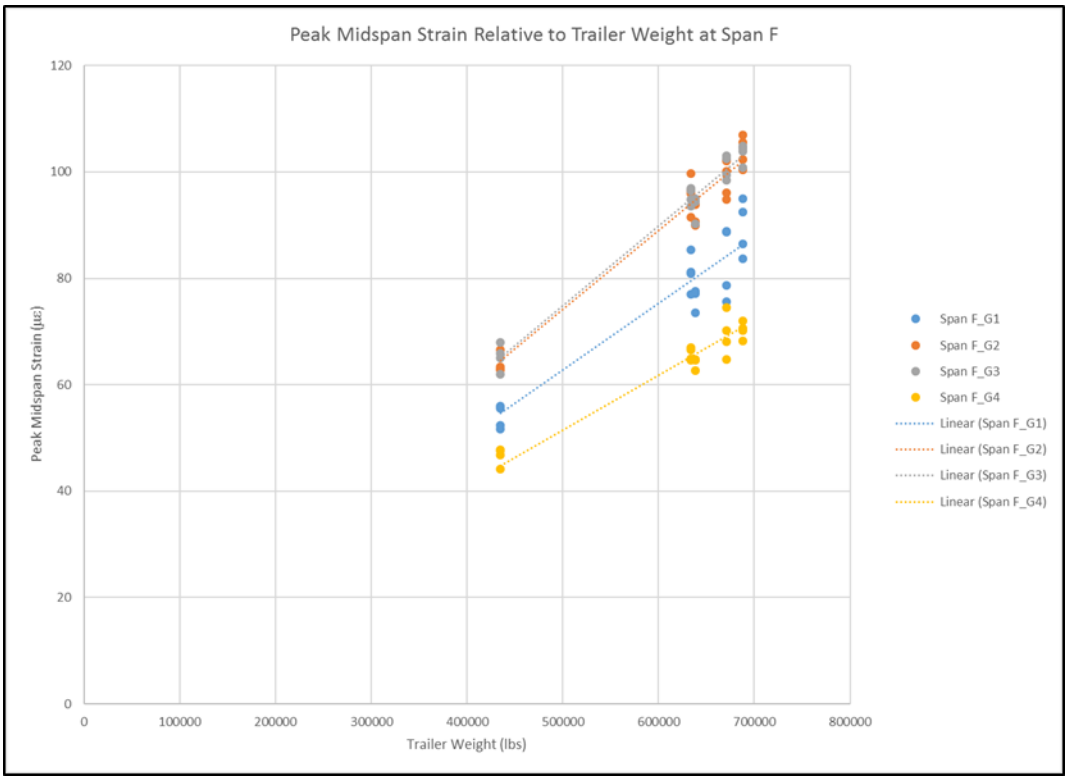

Figure 20 Mid-span F - Peak Girder Strain as a Function of Trailer Weight

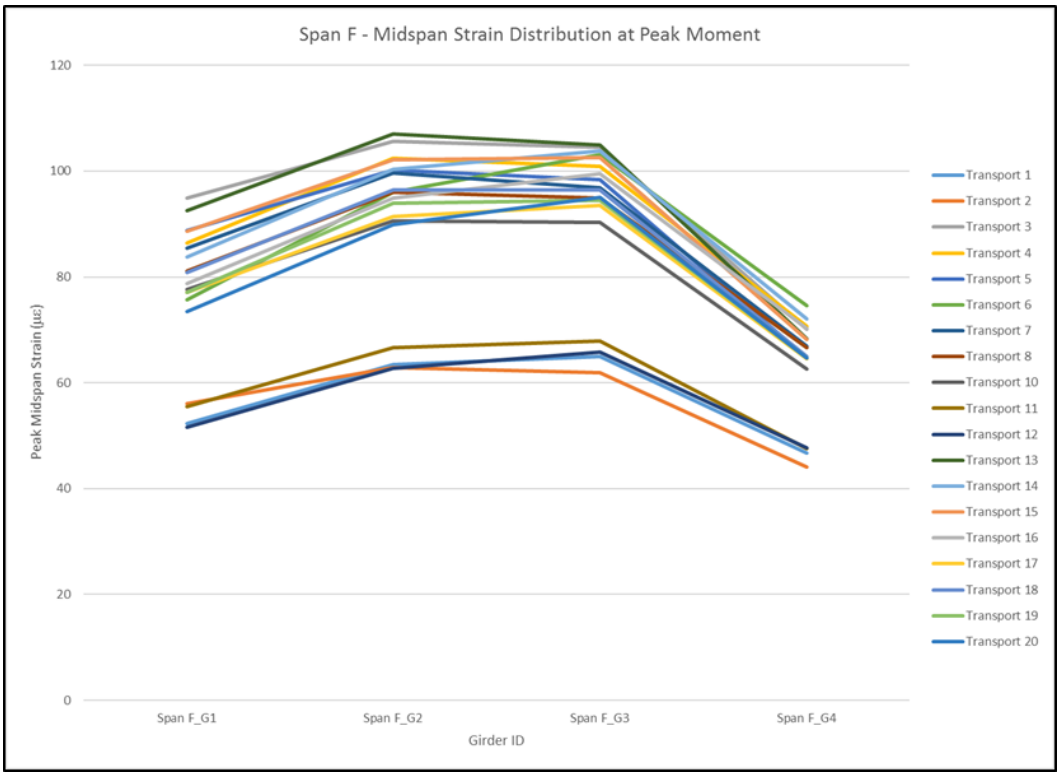

Figure 21 Mid-span F - Peak Girder Strain Distribution for all Transport Crossings

Rating of Prestressed Concrete Adjacent Beam Bridges without Plans

Carlos V. Aguilar, David V. Jáuregui, Brad D. Weldon and Craig M. Newtson

Synopsis: Off-system concrete bridges with no design plans are currently a concern in New Mexico as many exist throughout the State. Load rating these bridges is problematic since the design documentation is limited or missing, thus creating uncertainties regarding the safe load limits. Two prestressed concrete bridges, a double T-beam and box beam bridge, were evaluated using advanced analyses and experimental methods (including load testing and rebar scanning). Both bridges have damaged and/or missing shear keys between the adjacent beams and thus, the load distribution path was uncertain. The bridges were evaluated based on the following procedures: estimating the material properties from past specifications and amount of prestressing steel via Magnel diagrams; verifying the steel estimate with a rebar scanner; load testing based on strain measurements; and rating the bridges using the load test results. Rating factors were determined for legal loads based on serviceability (i.e., concrete cracking) and strength (i.e., shear or flexural capacity). The serviceability ratings from load testing and strength ratings from analytical software were compared to determine the final load ratings and need for posting the bridges.

Keywords: concrete cracking, diagnostic testing, load rating, Magnel diagram, prestressed concrete bridge, proof testing, rebar scanner, shear key, strain measurement

Carlos V. Aguilar is a Structural Engineer in Training (EIT) at HDR in Albuquerque, New Mexico. He has experience in bridge load testing and rating as well as bridge inspection, analysis, and design. He received both his Bachelor of Science and Master of Science degrees in Civil Engineering from New Mexico State University.

Dr. David V. Jáuregui is the Foreman Professor and Department Head of Civil Engineering at New Mexico State University (NMSU) and Director of the NMSU Bridge Inspection Program. He is a registered Professional Engineer in New Mexico and his research focuses on the inspection and evaluation of bridges using finite element analysis, virtual reality, close-range photogrammetry, and diagnostic / proof load testing.

Dr. Brad D. Weldon is an Associate Professor in the Department of Civil Engineering at New Mexico State University. He is active in research in bridge design and behavior, structural engineering, earthquake engineering, and innovative, sustainable structural materials. He has significant experience in large scale testing and evaluation of structural systems under various loading scenarios and in the inspection, evaluation, and testing of bridges.

Dr. Craig Newtson is a Professor and Structures Coordinator in the Civil Engineering Department at New Mexico State University. He is an active researcher with interests in concrete behavior, durability, and sustainability as well as nondestructive testing of concrete materials and structures. He has published several papers related to these topics and currently serves on ACI committee 306, Cold Weather Concreting.

INTRODUCTION

In the United States, the load rating methods and procedures are specified by the American Association of State Highway and Transportation Officials (AASHTO) in the AASHTO *Manual for Bridge Evaluation*[1]. As in other states, the majority of bridges in New Mexico have design plans and thus, can readily be load rated using analytical software. However, a considerable number of New Mexico bridges do not have design plans (mainly off-system concrete bridges) and are difficult to evaluate. A major challenge in evaluating concrete bridges without plans is obtaining the location and size of steel reinforcement inside the main concrete members, which is essential for the load rating analysis. Without design plans, conservative assumptions may be made to define the reinforcement configuration and concrete properties for use in the analysis. Alternatively, load ratings may be determined based solely on engineering judgement without an actual structural analysis. Ratings determined in this manner may be unreliable. Consequently, a project was conducted for the New Mexico Department of Transportation (NMDOT) to develop a procedure to better determine load ratings for concrete bridges without plans. In New Mexico, most bridges without plans are locally owned by a city or county. These bridges tend to have adjacent members with shear keys and no deck. As a result, this paper will focus on two superstructure types: a prestressed concrete double T-beam bridge and a prestressed concrete box beam bridge. Both bridges are owned by Dona Ana County, New Mexico.

A literature review was conducted focusing on work related to load testing and load rating concrete bridges without plans. Prior to the year 2000, several state DOTs employed load testing to determine capacity ratings, including the states of Alabama[2], Florida[3,4], Michigan[5], and New York[6]. More recently, the states of Georgia[7,8], Iowa[9], Delaware[10], and Vermont[11] sponsored research within the last 10 years to develop bridge testing capabilities for load rating purposes. It was found that the majority of proof tests conducted in prior research was performed on reinforced concrete and steel bridges. For prestressed concrete bridges, diagnostic testing was preferred. Apart from the U.S., a major project was conducted in Europe entitled Assessment and Rehabilitation of Central European Highway Structures (ARCHES) that focused on the use of soft, diagnostic and proof testing for bridge evaluation[12]. Outside of ARCHES, few studies were found related to proof testing of prestressed concrete bridges without plans.

BRIDGE DESCRIPTIONS

Bridge 7701, double T-beam

Bridge 7701 was constructed in 1974 and is a single-span, prestressed concrete bridge with a 31 foot (ft) [9.45 m] span and nine adjacent double T-beams, each of which is 33 inches (in.) [838 mm] wide and 19.5 in. [495 mm] deep. The bridge beams are connected by intermittent shear keys and the beam flanges act as the deck. There is no wearing surface and the overall bridge width is 24 ft 9 in. [7.54 m], while the roadway width is 23 ft 5 in. [7.14 m] from curb to curb. The bridge carries County Road B-31 over an irrigation canal near NM-478. See pictures given in Figure 1. At the time of this investigation, the most current inspection report indicated a condition rating of 6 for the deck, superstructure, and substructure. Overall, the beams were in satisfactory condition and no flexural cracks were found. Each beam has seven shear keys spaced 4 ft 3 in. [1.30 m] apart and each shear key consists of two 1 ft [305 mm] long

steel angles welded together with a short piece of rebar. The shear keys connecting the beam top flanges varied in condition. All the exterior keys between beams 1 and 2 (north side), and beams 8 and 9 (south side) were filled with grout and functioning properly. However, the majority of the interior keys between beams 4 and 5, and beams 6 and 7 were damaged (i.e., broken weld between rebar and one of the two angles).

Bridge 7722, box beam

Bridge 7722 was constructed in 1966 and is a 44.4 ft [13.53 m] simple-span bridge with a 16-degree skew and 21 ft [6.40 m] wide roadway. The bridge has seven adjacent box beams (PCI-AASHTO section type BI-36) that are 36 in. [914 mm] wide and 27 in. [686 mm] deep; the exterior beams support two gas utility pipelines. The wearing surface is a 4 in. [102 mm] asphalt overlay and the bridge carries County Road B-108 near NM-185. See pictures given in Figure 2. In the pertinent inspection report, the deck, superstructure, and substructure were all rated a 6. Asphalt material was falling through the joints between all beams and the gap was 2 1/8 in. [54.0 mm] between beams 1 and 2 (north side) and 1 1/4 in. [31.8 mm] between beams 6 and 7 (south side). The gaps observed on the bridge soffit between the exterior beams and the adjacent interior beams suggest that the bridge was widened. In addition, there were large openings in the asphalt overlay at the exterior-interior beam joints and concrete work was also done on the abutments which provided further evidence of the widening.

GENERAL PROCEDURE

A basic procedure for field testing of prestressed concrete bridges without plans was developed in this project. First, the total number and eccentricity of the prestressing strands in the bridge beams are estimated using Magnel diagrams[13]. Second, a rebar scanner is used to detect the prestressing steel to verify the strand estimate and also determine the shear reinforcement layout. Third, a diagnostic load test is performed to determine the critical transverse truck paths (i.e., ones producing the largest measured strains at midspan of the bridge) and to compare the measurements with analytical predictions. Fourth, a proof load test is conducted under increasing truck loading until the allowable tensile stress or the target proof load is reached.

Proof testing procedures in the AASHTO *Manual*[1] were developed primarily for reinforced concrete and steel bridges whereas guidance for testing of prestressed concrete bridges is lacking. Due to the likelihood of exceeding the cracking moment under the target proof load specified in the AASHTO *Manual*[1], the load testing of prestressed concrete bridges in this study was planned and conducted based on serviceability (i.e., concrete cracking) rather than strength. This approach is practical and conservative since a much smaller target proof load is required which limits the amount of damage imposed on the bridge during testing. The AASHTO *Manual*[1] allows the optional serviceability check to be considered for the legal load rating.

ESTIMATE OF PRESTRESSING STRANDS

The amount of prestressing steel was estimated using Magnel diagrams for HS-20, H-20, and H-15 truck loadings based on the serviceability criteria (i.e., allowable stresses) for compression and tension at transfer and service. The Magnel equations written in terms of the inverse of the initial prestressing force ($1/P_i$) are[14]:

$$P1(e) = \frac{1}{P_i} \geq \frac{1}{A*\left(f_{bi}+\frac{M_{DL}}{S_b}\right)} + \frac{e}{S_b*\left(f_{bi}+\frac{M_{DL}}{S_b}\right)} \quad \text{(Eq. 1)}$$

$$P2(e) = \frac{1}{P_i} \leq \frac{-1}{A*\left(f_{ti}+\frac{M_{DL}}{S_t}\right)} + \frac{e}{S_t*\left(f_{ti}+\frac{M_{DL}}{S_t}\right)} \quad \text{(Eq. 2)}$$

$$P3(e) = \frac{1}{P_i} \leq k * \left(\frac{1}{A*\left(-f_{bf}+\frac{M_{Tot}}{S_b}\right)} + \frac{e}{S_b*\left(-f_{bf}+\frac{M_{Tot}}{S_b}\right)}\right) \quad \text{(Eq. 3)}$$

$$P4(e) = \frac{1}{P_i} \geq k * \left(\frac{-1}{A*\left(-f_{tf}+\frac{M_{Tot}}{S_t}\right)} + \frac{e}{S_t*\left(-f_{tf}+\frac{M_{Tot}}{S_t}\right)}\right) \quad \text{(Eq. 4)}$$

where *P1*, *P2*, *P3* and *P4* are the range of solutions that satisfy the serviceability criteria at the beam midspan based on the bottom compressive stress at transfer (f_{bi}), top tensile stress at transfer (f_{ti}), bottom tensile stress at service (f_{bf}), and top compressive stress at service (f_{tf}), respectively. In addition, e is the prestressing steel eccentricity; S_b and S_t are

the beam section moduli at the bottom and top; A is the beam cross-sectional area; k is the prestress loss factor; and M_{DL} and M_{Tot} are the dead load moment and total moment (i.e., dead load plus live load moments), respectively, at midspan. The Magnel diagram is constructed by plotting the P1 through P4 lines resulting from Eqs. (1) through (4) that satisfy the serviceability criteria. The P1 and P2 lines correspond to the beam stresses at transfer and are thus, not affected by the truck loading. The area enclosed by the four lines represents the possible combinations of the initial prestressing force (P_i) and eccentricity (e) satisfying the allowable stresses at transfer and service. Any combination of P_i and e within this bounded area can then be used to estimate the number of strands and spacings.

Bridge 7701, double T-beam

Bridge 7701 was constructed in 1974 when the 11th Edition of the AASHO Standard Specifications for Highway Bridges[15] and 1970 NMSHD State Specifications[16] were in effect. Based on these specifications, the concrete strengths were assumed to be 4500 psi [31.0 MPa] at release (f_{ci}'), which is slightly greater than the 4000 psi [27.6 MPa] minimum for pretensioned members, and 5000 psi [34.5 MPa] at 28 days (f_c'). The prestressing steel was assumed to be 0.5-in. [12.7 mm] diameter, Grade 270, seven-wire, stress-relieved strands and the prestress losses were estimated as 25%. The allowable stresses were taken from the AASHO specifications and equal:

$$f_{bi} = 0.6f_{ci}' = 2700 \text{ psi} \quad [18.6 \text{ MPa}]$$

$$f_{ti} = 3\sqrt{f_{ci}'} = 201.2 \text{ psi} \quad [1.39 \text{ MPa}]$$

$$f_{bf} = 6\sqrt{f_c'} = 424.3 \text{ psi} \quad [2.93 \text{ MPa}]$$

$$f_{tf} = 0.4f_c' = 2000 \text{ psi} \quad [13.8 \text{ MPa}]$$

The dead load moment was computed from the beam self-weight since there is no wearing surface or deck and the live load impact and wheel distribution factors were computed as 1.3 and 0.458, respectively.

Figure 3 shows the Magnel diagram for the H-20 design truck and Table 1 summarizes the high prestress / low eccentricity (i.e., intersection of lines P3 and P4) and low prestress / high eccentricity (i.e., intersection of lines P2 and P3) combinations for all three design trucks. The effective prestressing force (P_e) was computed as kP_i with k equal to 0.75. To determine the area of the prestressing strand (A_s), P_i was divided by the initial strand stress at transfer (f_{pi}) which was assumed to be 70% of the ultimate strand stress (f_{pu}) as specified in the AASHO specifications. The number of strands was then computed by dividing A_s by the single strand area (equal to 0.153 in^2 [98.7 mm^2]).

Figure 4 shows the standard beam section for Bridge 7701. Assuming a 3 in. [76.2 mm] cover to the strand center and a strand spacing of 1 in. [25.4 mm], the eccentricities were 10.28 in. [261.1 mm] for two strands, 9.78 in. [248.4 mm] for four strands, and 9.28 in. [235.7 mm] for six strands. Based on Table 1, the beam section is best suited for the H-20 design truck since the 10.2 in. [259.1 mm] eccentricity agrees well with the possible strand patterns.

Bridge 7722, box beam

Bridge 7722 was built in 1966 at which time the provisions of the AASHO 8th Edition[17] were in effect. Accordingly, the concrete strengths were taken as f_{ci}' = 4000 psi [27.6 MPa] and f_c' = 4500 psi [31.0 MPa]. Based on the construction year, a tensile strength of f_{pu} = 250 ksi [1724 MPa] was assumed for the prestressing strands per the AASHTO *Manual*[1]. The initial prestressing stress, f_{pi}, was taken as 70% of the ultimate tensile strength, f_{pi} = 175 ksi [1207 MPa], and 20% total losses were assumed resulting in an effective prestress of f_{pe} = 140 ksi [965 MPa]. Note that AASHO[17] stated that prestress losses of 35 ksi [241 MPa] may be used for pre-tensioned members which agrees with the 20% assumption discussed earlier. The prestressing steel was assumed to be Grade 250, seven-wire, low-relaxation strands with diameters of 0.375 in. [9.53 mm] and 0.4375 in. [11.1 mm] for the interior and exterior beams, respectively. Allowable stresses were taken from AASHO[17] and are equal to the following values:

$$f_{bi} = 0.6f_{ci}' = 2400 \text{ psi} \quad [16.5 \text{ MPa}]$$

$$f_{ti} = 3\sqrt{f_{ci}'} = 189.7 \text{ psi} \quad [1.31 \text{ MPa}]$$

$f_{bf} = 0$ psi [0 MPa]

$f_{tf} = 0.4f_c' = 1800$ psi [12.4 MPa]

The AASHO dynamic impact allowance, *IM*, is given as:

$$IM = \frac{50}{L+125} \quad \text{(Eq. 5)}$$

where L = span length in feet which resulted in an impact factor of 0.295. The AASHO lateral distribution factors for interior concrete box beams are $S/8$ (one lane) and $S/7$ (two or more lanes) where S is the average beam spacing in feet. For an exterior box beam, the distribution factor is $w_e/8$ where w_e is the beam width in feet.

Bridge 7722 consists of seven adjacent PCI-AASHTO BI-36 beams with a width (*W*) of 36 in. [914 mm] and height (*H*) of 27 in. [686 mm] as shown in Figure 5. The distribution factors are 0.375 and 0.429 for one traffic lane and two or more traffic lanes, respectively. Reconstruction marks on the abutments and wing walls, and longitudinal gaps between the exterior and interior beams indicated that the bridge was widened. Consequently, it was assumed that the bridge was only one lane wide for the original construction and two lanes after widening. Hence, the distribution factors were taken as 0.375 and 0.429 for the interior and exterior beams, respectively, to estimate the prestressing strand. The dead load moment was computed based on the beam self-weight and a 4.0-in. thick asphalt wearing surface. An additional dead load of 100 lb/ft [689 kPa] was applied to the exterior beam for the utility pipeline and guardrail.

Figure 6 shows the Magnel diagram for an exterior beam, under H-20 loading. Due to the geometry of the box beams, lines P1 through P4 intersected only at two points, contrary to the four points for Bridge 7701 (see Figure 3). The prestressing force may be computed from these two points; however, the estimate corresponds to the highest level of prestressing and thus, the steel area will be unconservative. Alternatively, the two intersection points were vertically projected onto line P3 to obtain the smallest prestressing force and a conservative estimate of the number of strands. Lines PP1 and PP2 shown in Figure 6 are the projected lines. The high and low initial prestressing forces were then computed from the P3 expression at the points of intersection with lines PP1 and PP2. Table 2 summarizes the exterior beam Magnel diagram results for the three design trucks. The maximum eccentricity (assuming 2 in. [51 mm] cover to the center of the strand) is 11.6 in. [295 mm] and the strand areas are 0.080 in^2 [51.6 mm^2] and 0.108 in^2 [69.7 mm^2] for 0.375 in. [9.53 mm] and 0.4375 in. [11.1 mm] diameters, respectively. The prestressing steel was based on the H-20 truck due to the design year and amounted to 14 strands for the exterior beam and 16 strands for the interior beam.

DETECTION OF STEEL REINFORCEMENT

A rebar scanner was used to scan the location, size, and cover of the steel reinforcement (including the longitudinal strands and transverse bars) in the prestressed concrete beams of Bridges 7701 and 7722. The scanner provides the most accurate results for the first layer of reinforcement and a minimum ratio of 2:1 is required for the rebar spacing to concrete cover. The accuracy of the rebar size estimate is ±1 standard bar diameter and the reinforcement must be within 2.4 in. [61.0 mm] from the concrete surface. In general, the scanner is best suited for detecting mild steel reinforcing bars and not as accurate for prestressed concrete bridges due to the seven-wire strand arrangement. The scanner generates imagescans of a 2 ft by 2 ft [0.61 m by 0.61 m] area which can be connected to produce blockscans of a larger area.

Bridge 7701, double T-beam

The rebar scanner was used to generate blockscans of the north exterior beam and the center beam (i.e., beams 1 and 5) of Bridge 7701. Several other 2 ft by 2 ft [0.61 m by 0.61 m] areas on the remaining seven beams were also scanned to check the blockscans of beams 1 and 5. Figure 7 shows the east half of the exterior beam. The blockscan of beam 1 showed three longitudinal strands running along the beam length that are harped at approximately 0.4L. In the middle 20% of the beam, the prestressing strands are tightly spaced and due to the seven-wire strand arrangement, the bar size measurement varied widely from a #11 [#36] to a #3 [#10]. The imagescans showed a 2 in. [51 mm] and 4 in. [102 mm] strand spacing near the abutments and a 1 in. [25.4 mm] spacing at the center of the beam which agreed with the strand estimate from the Magnel diagram. The interior beams of Bridge 7701 have the same geometry as the exterior beams and there was no indication that the bridge had been widened in the past.

Bridge 7722, box beam

A standard AASHTO BI-36 box beam of Bridge 7722 is shown in Figure 5 along with the available prestressing strand positions. The figure shows two available rows of prestressing strands in the bottom flange for up to 34 strands at 2-in. [51 mm] center-to-center spacing. Additional strands may be placed in the webs and/or the top flange. Due to the close strand spacing and possibility of multiple strand layers, the scans obtained for Bridge 7722 were difficult to interpret. Imagescans were taken on the bottom sides of several beams. Figure 8 shows a blockscan for an interior beam displayed at different depth ranges. As shown in Figure 8(a), there are numerous wide, dark strips in the vertical direction representing the longitudinal prestressing strands. What is not clear is whether the strips represent closely spaced strands or multiple layers of strands, or both. The depth range feature in the scanner software was used to pan in and out of the flange depth. As shown in Figure 8(b), the thin gray lines in the images begin to blur and disappear from view at shallower depths which is a clear indication that those strands are in the first layer and there are no multiple layers of strands at those locations. On the other hand, the thick gray lines begin to separate into two or more bars, thus confirming the presence of multiple strands in more than one layer.

Based on this interpretation, it was concluded that the interior beam has a maximum of 18 and a minimum of 14 strands in the bottom flange. Figure 9(a) shows the measured strand arrangement in the interior beam; strands marked with a red dot were identified with more certainty than those marked with a blue dot. Similarly, a maximum of 16 and a minimum of 12 strands were measured in the exterior beam (see Figure 9(b)). Recall that the amount of steel estimated using the Magnel diagrams was 16 and 14 strands for the interior and exterior beams, respectively, which are the average quantities measured with the scanner.

DIAGNOSTIC LOAD TESTS

Diagnostic load tests were performed on Bridges 7701 and 7722 before the proof tests to study the actual bridge behavior and determine the critical truck paths (i.e., those that produce the largest measured strains). Dump trucks weighing much less than the target proof load were applied along different transverse positions over the bridge width. The critical paths were later used to develop the loading procedure for the proof tests.

Bridge 7701, double T-beam

Due to the condition of the shear keys, the live load distribution between the beams of Bridge 7701 was uncertain and thus, caution needed to be taken to avoid overloading the bridge. Using the prestressing strand estimate discussed earlier, calculations were performed to determine the cracking moment, available moment, target moment, and test truck moment for an interior beam. In addition, the available strain and test truck strain were computed to monitor the bridge beams during the load test. The cracking moment was determined using the following equation:

$$M_{cracking} = S_b * \left[P_e * \left(\frac{1}{A} + \frac{e}{S_b}\right) + f_{cr}\right] \quad \text{(Eq. 6)}$$

where f_{cr} is the modulus of rupture (equal to 7.5 times the square root of f_c' according to the AASHO specifications). For f_c' equal to 5000 psi [34.5 MPa], f_{cr} equals 530 psi [3.65 MPa] and the cracking moment equals 148.4 kip-ft [201.2 kN-m]. The available moment was the cracking moment minus the dead load moment which amounted to 112.6 kip-ft [152.7 kN-m]. For the diagnostic load test, dump trucks with a tandem axle weight of 27.8 kips [123.7 kN] were used which provided a test truck moment of 92.5 kip-ft [125.4 kN-m]. Using a factor of 0.458 from the AASHO specifications, the test truck moment reduced to 42.4 kip-ft [57.5 kN-m]. Due to the shear key damage, the actual test truck moment was expected to fall somewhere between 42.4 kip-ft [57.5 kN-m] and 92.5 kip-ft [125.4 kN-m]. Hence, the test truck moment was less than or equal to the available moment suggesting that the bridge should remain uncracked.

The cracking strain and the expected test truck strains were calculated at the location 1 in. [25.4 mm] from the bottom of the beam stem (i.e., the transducer location). These values were then compared to the strains measured during the load testing to monitor the bridge behavior for cracking and also to check the actual live load distribution. The following equation was used to determine the strain values:

$$\varepsilon = \frac{M}{S_b * E_{design}} \quad \text{(Eq. 7)}$$

where M is the available or test truck moment, S_b is the section modulus of the beam at the transducer location, and E_{design} is the modulus of elasticity of the beam. The available strain was calculated to be 532 με and the test truck strain (determined using the distribution factor of 0.458) amounted to 200 με. The available strain amounted to 532 με and the test truck strains were expected to range between 200 and 436 με computed based on the design distribution factor of 0.458 and a maximum distribution factor of 1.0.

The diagnostic load test consisted of two phases. In the first phase, the front axle of the dump truck was positioned along seven transverse paths to maximize the load on each beam. For paths 1 and 7, the truck was positioned approximately 2 ft [0.61 m] from the curb and for paths 2 through 6, the truck was centered about beams 3 through 7, respectively. In each transverse path, the truck's font axle (weighing 14.72 kips [65.5 kN]) was moved along the bridge length incrementally until it was 1 ft [0.31 m] from midspan. Strain transducers with a full Wheatstone bridge and a precision of ±2 με were placed on all nine beams at midspan at a distance of 1 in. [25.4 mm] from the bottom of the stem (a total of 18 strain transducers) and the BDI (Bridge Diagnostics, Inc.) structural testing system was used to measure the beam strains under truck loading. The largest measured strains were 202 με and 152 με for transverse paths 5 and 7, respectively. Consequently, in the second phase of testing, two dump trucks were placed side-by-side with the first truck positioned in path 5 or path 7 and the second truck placed approximately 2 ft [0.61 m] from the first truck. As shown in Figure 10, the dump trucks were positioned in paths 1 and 5 for the first run, and then in paths 3 and 7 for the second run. In these two runs, the trucks were backed up onto the bridge and the load was applied by the tandem axle. Side-by-side trucks in paths 3 and 7 was the most critical pattern as this loading arrangement resulted in measured strains as large as 312 με (approximately 1.6 times the expected test truck strain of 200 με). The maximum strain measured with the trucks in paths 1 and 5 was 265 με. This was a clear indication that the shear keys were not functioning as intended, which was a concern before the test due to the visible damage.

Bridge 7722, box beam

Similar to Bridge 7701, a diagnostic load test was performed on Bridge 7722 to assist in planning the proof test. The bridge was instrumented with strain gages on the bottom flanges of all beams. Based on the number of prestressing strands determined previously, the cracking, available, target, and test truck moments for the exterior and interior beams were computed. The cracking moment was determined using Eq. (6) given earlier assuming a prestress loss of 30% (and f_{cr} equal to 6 times the square root of f_c') which resulted in available moments of 223.3 kip-ft [302.8 kN-m] and 190.9 kip-ft [258.8 kN-m] for the exterior and interior beam, respectively. Live load moments were calculated under a 40-kip [178 kN] test truck (assuming a 31.1-kip [138.3 kN] back axle and 8.9-kip [39.6 kN] front axle). Due to the poor condition of the shear connection, the live load distribution was uncertain and thus, caution needed to be taken to avoid overloading the beams. Available strains of 177 με and 151 με were calculated using Eq. (7) for an exterior and interior beam, respectively, which exceeded the estimated test truck strain of 59.1 με.

The diagnostic load test of Bridge 7722 included three patterns of loading: single dump truck; two dump trucks side-by-side; and two dump trucks back-to-back. Each dump truck weighed roughly 42.7 kips [189.9 kN] with front and rear axle weights of 12.7 kips [56.5 kN] and 30.0 kips [133.4 kN], respectively. For the single truck loading, the truck was centered along five transverse paths (labeled path 1 through path 5) and stopped at several longitudinal locations per path. The largest measured strains under a single dump truck were 46 με and 49 με at the exterior beams 1 and 7, respectively, for transverse paths 1 and 5. Consequently, in the second phase of loading, two dump trucks were placed side-by-side with the first truck positioned in path 1 or path 5 and the second truck placed adjacent to the first truck. As shown in Figure 11, the dump trucks were positioned in paths 1 and 4 and paths 2 and 5.

Comparison of the measured strains for paths 1 and 4 with paths 2 and 5 showed a strong correlation, indicating that the bridge behavior was symmetrical. The maximum strains for the different paths were 55 με (beam 1) and 51 με (beam 7) which are close to the estimated strain of 59 με reported earlier. Based on these results, the two trucks were placed back-to-back in the third phase of testing in paths 1, 3, and 5 to maximize the strains in the two exterior beams and the middle interior beam. Strains as high as 78 με and 77 με at beam 1 and beam 7, respectively, were recorded. However, a much smaller strain of 43 με was recorded at beam 3 which was a clear indication that the shear keys between the interior beams were functioning well compared to the shear keys between the exterior and interior beams.

PROOF LOAD TESTS

For the proof tests, the dump trucks were loaded much heavier and were applied along the critical transverse paths determined from the diagnostic tests. The goal of the proof test was to maximize the midspan moment applied to the bridge without exceeding the cracking moment. Strain gauges were installed solely to monitor the flexural response

of the bridge beams at midspan, however, analytical shear checks were also made to ensure the beams would not crack near the supports due to diagonal tension. The proof tests were executed in multiple phases, with each phase using a single truck or multiple truck combination to maximize the bending moment. The final truck positions and corresponding midspan moments were used for load rating the bridges based on the serviceability limit state (i.e., concrete cracking). The serviceability-based ratings were calculated in accordance with the AASHTO *Manual*[1].

Bridge 7701, double T-beam

The proof load test of Bridge 7701 consisted of four phases. For the first phase, the tandem back axle of a single truck weighing roughly 42 kips [186.8 kN] was applied. The truck was centered in paths 5 and 7, and backed up the same way as during the diagnostic test. The more critical of the two paths was then used in phase three, where two trucks were placed back-to-back to simulate single lane loading. For the second phase, two trucks were placed side-by-side, first in paths 1 and 5 and then in paths 3 and 7. The more critical loading configuration was then used in phase four, where four trucks were placed side-by-side and back-to-back on the bridge. Strain transducers were placed at the bottom of each stem, similar to the diagnostic test. The diagnostic test results showed the largest strains at beams 4 through 7; therefore, these four beams were instrumented with more transducers at midspan.

To check that the bridge beams would not crack due to shear, a thorough shear capacity evaluation was performed. Assuming a shear distribution factor of one, the maximum shear for a single beam caused by 42-kip [186.8 kN] tandem axles placed back-to-back amounted to 21.0 kips [93.4 kN]. The web-shear cracking force, V_{cw}, was estimated using the following formula[18]:

$$V_{cw} = f_t\sqrt{1 + \frac{f_{pc}}{f_t}}b_w d + V_p \qquad \text{(Eq. 8)}$$

where f_t is the concrete tensile strength; f_{pc} is the compressive concrete stress after all losses at the beam centroid; b_w is the beam web width; d is the distance from the compression face to the centroid of the tension reinforcement (not less than 80% of overall beam depth); and V_p is the vertical component of the effective prestressing force. The concrete tensile strength varies between 2 and 4 times the square root of f_c' (equal to 5 ksi [34.5 MPa]); the former value applies to reinforced concrete members or prestressed concrete members with a low level of prestressing while the latter value applies to end regions of fully prestressed members[18]. Employing Eq. (8) with these two values, V_{cw} ranged between 27.2 kips [121.0 kN] and 41.9 kips [186.4 kN], which exceeded the sum of the live load shear of 21.0 kips [93.4 kN] and dead load shear of 5.0 kips [22.2 kN]. Thus, concrete cracking due to shear was not expected.

In phase one, the truck was able to reach the final position with the front of the rear axle located 14 ft [4.3 m] from the support as shown in Figure 12(a) without exceeding the available strain of 532 με. Table 3 lists the measured strains in all phases of the proof test. The beams and stems are numbered from north to south and are labeled B#S# (e.g., B3S1 corresponds to beam 3, stem 1). The table shows that path 5, centered along beam 6, produced the largest strain of 508 με. In phase two, the test was stopped once the rear axles reached 10 ft [3.0 m] (see Figure 12(b)) since the measured strains was close to the available strain. Paths 3 and 7 produced a larger strain than paths 1 and 5 (528 με compared with 474 με, respectively). In phase three, two trucks were placed back-to-back along the critical path 5, to simulate the most critical single lane loaded condition. In phase four, the four trucks were placed side-by-side and back-to-back in paths 3 and 7 to simulate the most critical multiple lanes loaded condition. The trucks were stopped when the rear axles were at 6.5 ft [2.0 m] in phase three (see Figure 12(c)) and 5.0 ft [1.5 m] in phase four (see Figure 12(d)) since the maximum measured strain was close to the available strain. Table 3 shows the measured strains for these test phases which provided strong evidence that the shear keys were not functioning properly, particularly between beams 4 and 5. A large difference in strain was measured between beams in the single lane loaded configurations. When a single truck was placed in path 5 for phase one, a difference of 508 με can be observed between beams 4 and 5. Similarly, in phase three when two trucks were placed back-to-back along path 5, a strain difference of 414 με was measured. Pictures of the instrumentation and proof test for Bridge 7701 are given in Figure 13.

Load transfer between beams 4 and 5 for Bridge 7701 was poor, even at low load levels, as evident from the measured strains. This was expected based on the initial bridge inspections that showed the shear keys were damaged (i.e., exposed steel, broken welds, etc.) between several beams, mainly beams 4 and 5. As shown in Figure 10, for example, beams 4 and 5 are directly loaded by a wheel line for truck paths 1 and 5. For this load configuration, it was observed that Bridge 7701 essentially responded as two separate structures with little to no transfer between beams 4 and 5 as the measured strains were large for both beams with similar values. The strain measurements showed much better

load distribution between other beams with undamaged shear keys. The results of the proof test of Bridge 7701 illustrate the influence of the shear key conditions for bridges with no deck. If shear keys are exposed (due to omission or loss of grout), the redundancy and ductility of a bridge can certainly be affected if enough connections are damaged. In the case of Bridge 7701, beams 4 and 5 could be compromised if loaded directly under legal load levels. Similar load transfer issues were found at Bridge 7722 due to reflective asphalt cracking and large gaps in the connections between the interior and exterior beams (discussed in the next section). Note that the type of shear keys used in Bridge 7701 and Bridge 7722 were used by local owners over 40 years ago and new bridges require an engineered connection design approved by the NMDOT.

Bridge 7722, box beam

The proof test for Bridge 7722 included four phases of loading: single dump truck; two dump trucks side-by-side; two dump trucks back-to-back; and four dump trucks (side-by-side and back-to-back). Each truck weighed approximately 60 kips [267 kN]; the front and rear axle weights averaged 15 kips [67 kN] and 45 kips [200 kN], respectively. The same instrumentation plan was used in the diagnostic and proof tests of Bridge 7722.

The first phase of loading consisted of a single truck centered along three transverse paths. Recall that maximum strains of 46 με and 49 με were measured at the exterior beams 1 and 7, respectively, for paths 1 and 5 in the diagnostic test. Also, path 3 resulted in a maximum strain of 31 με for the interior beams. The second phase of loading was two trucks side-by-side. The third and fourth phases of loading consisted of two trucks back-to-back and four trucks (side-by-side and back-to-back). The trucks were placed in the same paths in both the diagnostic and proof tests of the bridge. Similar to Bridge 7701, a shear evaluation was done prior to testing. Assuming a shear distribution factor of one, the maximum shear for a single beam caused by 48.2-kip [214.4 kN] tandem axles (i.e., the largest truck axle load) placed back-to-back was 24.1 kips [107.2 kN]. The web-shear cracking force, V_{cw}, ranged between 50.4 kips [224.2 kN] and 86.0 kips [382.5 kN], which significantly exceeded the sum of the ultimate live load shear of 24.1 kips [107.2 kN] and dead load shear of 17.0 kips [75.6 kN]. Thus, concrete cracking due to shear was not expected.

Table 4 shows the measured beam strains for all phases of loading. The beams and gauges are numbered from north to south and are labeled B#G# (e.g., B3G1 corresponds to beam 3, gauge 1). The values represent the maximum strains recorded at the gauges installed at the bottom of the beams at midspan. From Table 4, the largest measured strains were 78 με, 46 με, and 84 με at beams 1, 4 and 7, respectively, for paths 1, 3 and 5 in phase 1. Note that the reported maximum strains are substantially less than the available strains for the interior (151 με) and exterior (177 με) beams. Furthermore, the exterior beam strains exceeded the estimated strain of 69 με (based on linear extrapolation from the diagnostic test results) which indicates that the load distribution factor was larger for the proof test compared to the diagnostic test due to the poor shear key connection. At the interior beam, the measured strain agreed with the estimated strain of 44 με since the shear keys were in better condition. Note that the ±2 με precision of the strain transducer equates to an error less than 5% of the smallest strain which was considered satisfactory for the proof test.

In the second phase of loading, two dump trucks were placed side-by-side in paths 1-4 and paths 2-5. The maximum strains were 81 με (beam 1) and 90 με (beam 7) which are only 6% larger than the recorded strains for single truck loading meaning that the second truck had minimal effect on the exterior beams due to the poor shear connection. In addition, the maximum strains for side-by-side loading remained significantly less than the available strains. Two trucks back-to-back and four trucks (side-by-side and back-to-back) were placed in the third and fourth phases, respectively, to reach the target moments. The trucks were placed along the same paths as phases one and two. Strains as large as 126 με and 136 με at beams 1 and 7, respectively, were measured for phase three and a maximum of 132 με was measured for phase four, also at the exterior beams. The maximum strains for the interior beams were 67 με and 116 με for phases three and four, respectively. Note that these maximum strains were 23% less than the available strains for the exterior and interior beams, which showed that the bridge was able to easily carry the largest test truck loading without cracking. Instrumentation and proof test pictures for Bridge 7722 are given in Figure 14.

Similar to Bridge 7701, strains measured during the proof test gave evidence that the shear connections between beams were poor. For Bridge 7722, this behavior was most obvious between beams 1 and 2 and beams 6 and 7. Large strain differences were observed between the two beams, particularly under single lane loading (i.e., phases 1 and 3). Recall that the test strains were approaching the available strain for Bridge 7701 before the trucks reached the maximum moment positions in phases two through four, and the tests were stopped early. For Bridge 7722, the trucks reached their final positions and the bending moments were maximized in all phases. A possible explanation for this behavior is the increase in beam stiffness due to the 4 in. asphalt wearing surface for Bridge 7722. This stiffness increase may

have allowed the bridge to carry a greater load although the shear keys were not functioning at the exterior beams. During the proof test of Bridge 7722, the average ambient temperature was approximately 75 degrees Fahrenheit [24 degrees Celsius] and the load duration per test phase ranged between 15 to 30 minutes.

LEGAL LOAD RATINGS

The AASHTO *Manual*[1] provides guidance for load rating bridges using proof testing at the strength limit state. Since the proof tests performed in this study were based on concrete cracking, necessary adjustments were made to the AASHTO *Manual*[1] procedure for the service limit state. The final truck positions were used to calculate the maximum midspan moments applied during the proof tests and corresponding legal load moments were determined by structural analysis. The experimental (i.e., proof test) and analytical (i.e., structural analysis) moments were then used in the equations given in Section 8.8.3.3 of the AASHTO *Manual*[1] to load rate each bridge.

The strength limit state was also checked using a bridge load rating software program. Models were created using material property estimates determined from the applicable AASHTO specifications, the AASHTO *Manual*[1], and State provisions. In addition, the amount of reinforcement (i.e., bar size and spacing) and the concrete cover were estimated using the Magnel diagrams and/or the results from the rebar scanner. Member dimensions were determined from field measurements. Two sets of ratings (proof test ratings based on service and analytical ratings based on strength) were computed and the final ratings were established using engineering judgement.

Bridge 7701, double T-beam

Based on the measured strains given in Table 3 and corresponding truck positions given in Figure 12, load rating factors were determined from the proof load test. For all four test phases, the test truck moments were used to compute the final load ratings for AASHTO and New Mexico legal loads. Recall that the available strain of 532 με used to monitor the beams during the proof test was based on $7.5(f_c')^{1/2}$. To determine the final load ratings, however, the test truck moments associated with an available strain of 507 με based on an allowable concrete stress of $6(f_c')^{1/2}$, were used. From Section 8.8.3.3 of the AASHTO *Manual*[1], the adjusted target live-load factor (X_{pA}) and the target proof load (L_T) were first determined using the following equations:

$$X_{pA} = X_p\left(1 + \frac{\Sigma\%}{100}\right) \quad \text{(Eq. 9)}$$

$$L_T = X_{pA}L_R(1 + IM) \quad \text{(Eq. 10)}$$

where X_p is the initial target load factor, Σ% is the sum of the X_p adjustment factors given in Table 8.8.3.3.1-1 of the AASHTO *Manual*[1], L_R is the unfactored live load due to the rating vehicle, and IM is the impact factor (equal to 1.33). The recommended minimum value for X_p is 1.4, however, since the proof test was executed based on serviceability (limiting concrete tensile stress at service load) rather than strength, a factor of 1.0 was used which is permitted for legal load rating. Also note that L_T and L_R were determined in terms of the maximum midspan moment rather than load since the rating vehicles and proof test trucks do not have the same axle configuration. The applicable adjustment factors from the AASHTO *Manual*[1] included one-lane loading (+15%), non-redundant load path (+10%), in-depth inspection performed (-5%), and ADTT less than 1000 (-10%) which resulted in an X_{pA} equal to 1.1 for one lane loaded and 0.95 for multiple lanes loaded (Eq. 9). Target proof moments were then computed using Eq. (10) for the AASHTO legal loads (Type 3, Type 3-3, and Type 3S2) and the New Mexico legal loads (NM 2, NM 3A, and NM 5A) which are listed in Table 5 along with the vehicle weight, *W*.

The target proof moments were then compared to the moments applied by the dump trucks during the actual proof test. For phases one and three (single lane loaded), the test truck moments were 279 kip-ft [378 kN-m] and 368 kip-ft [499 kN-m], respectively, while for phases two and four (multiple lanes loaded), the test truck moments were 256 kip-ft [347 kN-m] and 300 kip-ft [407 kN-m], respectively. The operating level (*OP*) capacity was computed using the following equation from the AASHTO *Manual*[1]:

$$OP = \frac{k_0 L_P}{X_{pA}} \quad \text{(Eq. 11)}$$

where k_0 is a factor that depends on how the proof test was terminated (1.0 if the target proof moment is reached and 0.88 if the test is stopped due to signs of distress) and L_P is the applied moment. Although the proof test was ended before the truck axles reached the final position, k_0 was taken as 1.0 since the concrete design strength was used rather

than the actual strength to determine the available strain and prevent cracking. Consequently, the *OP* moments equaled 253 kip-ft [343 kN-m] for phase one, 270 kip-ft [366 kN-m] for phase two, 335 kip-ft [481 kN-m] for phase three, and 316 kip-ft [428 kN-m] for phase four. The final load ratings were computed based on phase one which had the smallest moment. Recall that the truck was stopped in this phase when the back axle reached 14 ft [4.3 m] resulting in a measured strain of 508 με which equaled the available strain. The rating factors, RF_O, for the legal load were computed using the following equation:

$$RF_O = \frac{OP}{L_R(1+IM)} \quad \text{(Eq. 12)}$$

The safe posting loads were then determined based on Section 6A.8.3 of the AASHTO *Manual*[1] as follows:

$$Safe\ Posting\ Load = \frac{W}{0.7}[(RF_O) - 0.3] \quad \text{(Eq. 13)}$$

Table 5 lists the rating factors and safe posting loads for each legal load. The table shows that Bridge 7701 needs to be posted for all legal loads excluding the Type 3-3 and NM 2. For legal load rating, strength is the primary limit state for prestressed concrete bridges specified in the AASHTO *Manual*[1]. Consequently, a legal load rating analysis of Bridge 7701 was performed based on the bridge geometry, material properties, and steel reinforcement discussed earlier. Using a load rating software program, rating factors were computed according to the Load Factor Rating (LFR) and Load and Resistance Factor Rating (LRFR) methods for the strength limit state. Note that the difference between the two methods is that the LFR method is consistent with the design philosophy of the AASHTO *Standard Specifications for Highway Bridges* while the LRFR method conforms with the AASHTO *LRFD Bridge Design Specifications*. Due to the poor condition of the shear keys, the rating analysis was also performed assuming a wheel distribution factor of 1.0 for LFR and axle distribution factor of 0.5 for LRFR. These values signify complete breakdown of the shear keys and thus, is a worst case scenario. The analytical rating factors for strength (controlled by ultimate flexure) all exceeded the values for service (based on concrete cracking) determined from the proof test. This comparison confirmed that the load carrying capacity of the bridge was controlled by the optional check at the service limit state.

Bridge 7722, box beam

Legal load rating factors for Bridge 7722 were determined from the proof test similar to Bridge 7701. The applicable adjustment factors to the initial target load factor (X_p) for Bridge 7722 included one-lane loading (+15%), in-depth inspection performed (-5%), and ADTT less than 1000 (-10%). Accordingly, X_{pA} was 1.0 for one lane loaded and 0.85 for multiple lanes loaded. Target proof loads were then computed using Eq. (10) for the legal loads which are listed in Table 6 along with the vehicle weight, *W*. For the different test phases, the maximum midspan moments were 535 kip-ft [725 kN-m] (phase one), 517 kip-ft [701 kN-m] (phase two), and 753 kip-ft [1021 kN-m] (phases three and four). Based on the target moments and the applied proof test moments, the operating level capacity (*OP*) was calculated using Eq. (11). Since the proof test was not terminated due to distress levels, k_o was taken as 1.0 for Bridge 7722. Using Eq. (12), the legal load rating factors for each loading scenario of the proof test were calculated.

All the operating rating factors exceeded one. For single truck loading (phase one) and two trucks side-by-side loading (phase two), the rating factors were close to 1.0 for certain legal loads. Although the computed rating factors were near 1.0, the corresponding maximum strains measured under the single truck and two trucks side-by-side loads were significantly smaller than the available strains. This indicates that there is unused capacity. Consequently, the final operating ratings were based on single lane, back-to-back truck loading (i.e., phase three) due to the poor condition of the shear keys between the exterior and interior beams. Analytical rating factors for the strength limit state were different for the interior and exterior beams due to differences in the amount of prestressing steel and mild shear reinforcement, and also load distribution. The ratings were controlled by flexural strength for LFR and shear strength for LRFR. The service-based rating factors determined from the proof test were smaller than the strength-based rating factors from the software program with the exception of the LRFR shear ratings for the exterior beam. Consequently, since the service-based rating factors were similar in magnitude to the LRFR ratings for the exterior beam and smaller than the LFR ratings, the bridge capacity for legal loads were set based on the service limit state.

CONCLUSIONS

Based on the experience gained in this study, a multiple-step load rating procedure was developed for simple-span prestressed concrete bridges without plans in New Mexico. The implementation of this procedure yielded the following conclusions:

- Conducting load tests of prestressed concrete bridges based on serviceability (concrete cracking), was adopted to ensure the bridges remained uncracked. Diagnostic load tests were helpful in planning the proof tests of prestressed concrete bridges in cases where the live load path was uncertain due to missing or damaged shear keys. These tests provided useful information on the actual bridge behavior under truck loading below the estimated cracking load.
- The monitoring of strain was effective in performing the diagnostic and proof tests to avoid overloading the prestressed concrete bridges. Preparatory calculations were required to determine the available strains that the bridges could endure without cracking, and the load tests were monitored by ensuring that the measured beam strains did not exceed the available strains.
- Based on the final dump truck positions in the proof tests, the applied moments were computed and compared to the target moments for the AASHTO and New Mexico legal loads. These comparisons were then used in accordance with the AASHTO *Manual*[1] to develop rating factors and safe posting loads for prestressed concrete bridges. Proof testing showed that the load ratings determined assuming complete shear transfer between beams may overestimate the capacity of damaged bridges.
- A software based load rating analysis should be performed for prestressed concrete bridges to check the strength limit state (i.e., flexural and shear capacity) for comparison with the ratings determined based on the proof test results for serviceability. In addition, the software analysis should be performed using the LFR and LRFR methods to select the most appropriate load ratings using engineering judgement.

It is important to note that even though the AASHTO *Manual*[1] was generally used in this study, there are no specific guidelines in the manual that address the load rating of prestressed concrete bridges through proof load testing. The manual provides guidance for proof testing based on strength but not serviceability. Although common testing procedures were employed herein, the procedures were adapted to the service limit state for concrete tension, which required a unique approach not provided by the AASHTO *Manual*[1].

REFERENCES

[1] American Association of State Highway and Transportation Officials (AASHTO). (2011). *Manual for Bridge Evaluation*, 2nd Edition, Washington, D.C.

[2] Conner, G. H., Stallings, J. M., McDuffie, T. L., Campbell, J. R., Fulton, R. Y., Shelton, B. A., and Mullins, R. B. (1997). "Bridge Load Testing in Alabama." Transportation Research Board.

[3] Shahawy, M. E. and Garcia, A. M. (1990). "Structural Research and Testing in Florida." *Transportation Research Record*, No. 1275, pp. 76-80.

[4] Shahawy, M. A. (1995). "Nondestructive Strength Evaluation of Florida Bridges." Proceedings of SPIE – The International Society of Optical Engineering (Nondestructive Evaluation of Aging Bridges and Highways), Society of Photo-Optical Instrumentation Engineers, Vol. 2456, pp. 101-123.

[5] Saraf, V., Sokolik, A. F., and Nowak, A. S. (1996). "Proof Load Testing of Highway Bridges." *Transportation Research Record*, No. 1541, pp. 51-57.

[6] Kissane, R. J., Beal, D. B., and Sanford, J. A. (1980). "Load Rating Of Short-Span Highway Bridges." *Interim Report on Research Project 156-1*, Research Report 79 (US DOT/FHWA), Engineering Research and Development Bureau, New York State Department of Transportation.

[7] Ellingwood, B. R., Zureick, A.-H., Wang, N., and O'Malley, C. (2009). "Condition Assessment of Existing Bridge Structures: Report of Task 4 – Development of Guidelines for Condition Assessment, Evaluation and Rating of Bridges in Georgia." *Report of GTRC Project No. E-20-K90 and GDOT Project No. RP05-01*, Georgia Department of Transportation and Georgia Institute of Technology, Atlanta, GA.

[8] Wang, N., Ellingwood, B. R., and Zureick, A.-H. (2011b). "Bridge Rating Using System Reliability Assessment. II: Improvements to Bridge Rating Practices." *ASCE Journal of Bridge Engineering*, Vol. 16, No. 6, pp. 863-871.

[9] Wipf, T. J., Phares, B. M., Klaiber, F. W., Wood, D. L., Mellingen, E., and Samuelson, A. (2003). "Development of Bridge Load Testing Process for Load Evaluation." *Final Report on Iowa DOT Project TR-445 / CTRE Project 00-65*, Research Report TR-445, Iowa Highway Research Board, Iowa Department of Transportation.

[10] Chajes, M.J., and Shenton, H.W. (2006). "Using Diagnostic Load Tests for Accurate Load Rating of Typical Bridges," *Journal of Bridge Structures*, Vol. 2, No. 1, pp. 13-23.

[11] Jeffrey, A., Breña, S. F., and Civjan, S. A. (2009). "Evaluation of Bridge Performance and Rating through Non-destructive Load Testing." *Final Report*, Research Report 2009-1, Vermont Agency of Transportation.

[12] Casas, J. R., Olaszek, P., Sajna, A., Znidarie, A., and Lavric, I. (2009). "Sustainable Development, Global Change and Ecosystems (Sustainable Surface Transport): Deliverable D16: Recommendations on the Use of Soft, Diagnostic, and Proof Load Testing." *Document No. ARCHES-02-DE16*, Assessment and Rehabilitation of Central European Highway Structures (ARCHES) Management Group.

[13] Krishnamurthy, N. (1983). "Magnel Diagrams for Prestressed Concrete Beams." *ASCE Journal of Structural Engineering*, Vol. 109, No. 12, pp. 2761-2769.

[14] Hag-Elsafi, O. and Kunin, J. (2006). "Load Testing for Bridge Rating: Dean's Mill over Hannacrois Creek." *Report FHWA/NY/SR-06/147*, Transportation Research and Development Bureau, New York State Department of Transportation.

[15] American Association of State Highway Officials (AASHO). (1973). *Standard Specifications for Highway Bridges*, 11th Edition, Washington, D.C.

[16] New Mexico State Highway Department (NMSHD). (1970). *Standard Specifications for Road and Bridge Construction*, Santa Fe, NM.

[17] American Association of State Highway Officials (AASHO). (1961). *Standard Specifications for Highway Bridges*, 8th Edition, Washington, D.C.

[18] Hawkins, N. M., Kuchma, D. A., Mast, R. F., Marsh, M. L., and Reineck, K.-H. (2005). "Simplified Shear Design of Structural Concrete Members." *Final Report*, NCHRP Report 549, National Cooperative Highway Research Program, Washington, D.C.

Table 1 – Estimate of prestressing strands for Bridge 7701

Variable	HS-20		H-20		H-15	
	High P/S	Low P/S	High P/S	Low P/S	High P/S	Low P/S
$1/P_i$ x 10^{-3} (1/kip)	2.14	6.60	2.14	8.56	2.14	14.5
P_i (kip)	468.4	151.5	468.4	116.8	468.4	69.1
e (in.)	1.48	8.84	1.01	10.2	1.87	14.0
P_e (kip)	351.3	113.6	351.3	87.6	351.3	51.8
A_s (in^2)	2.48	0.801	2.48	0.618	2.48	0.366
No. of strands	16.2	5.24	16.2	4.04	16.2	2.39

[1 kip = 4.45 kN; 1 in = 25.4 mm; 1 in^2 = 645.2 mm^2]

Table 2 – Estimate of prestressing strands for Bridge 7722 (exterior beam)

Variable	HS-20		H-20		H-15	
	High P/S	Low P/S	High P/S	Low P/S	High P/S	Low P/S
$1/P_i$ x 10^{-4} (1/kip)	20.4	36.7	22.2	41.3	26.0	50.9
P_i (kip)	489.5	272.6	449.8	241.9	384.9	196.4
e (in.)	3.60	11.9	3.20	11.9	2.70	11.9
P_e (kip)	391.6	218.0	359.9	193.5	307.9	157.1
A_s (in^2)	2.80	1.56	2.60	1.38	2.20	1.12
No. of strands	25.9	14.4	23.8	12.8	20.4	10.4

[1 kip = 4.45 kN; 1 in = 25.4 mm; 1 in^2 = 645.2 mm^2]

Table 3 – Maximum measured strains from proof load test (Bridge 7701)

Transducer Location	Strain (με)					
	Phase One		Phase Two		Phase Three	Phase Four
	Path 5	Path 7	Paths 1 & 5	Paths 3 & 7	Path 5	Paths 3 & 7
B1S1	0	-2	149	62	18	84
B1S2	1	-6	235	80	11	115
B2S1	4	2	228	83	17	111
B2S2	6	-3	255	224	28	195
B3S1	3	10	248	191	24	161
B3S2	21	9	341	197	55	203
B4S1	21	21	363	182	63	196
B4S2	38	33	**474**	158	82	205
B5S1	**508**	94	448	**528**	**496**	**494**
B5S2	372	157	391	470	407	456
B6S1	339	172	367	455	432	450
B6S2	279	269	239	316	348	344
B7S1	275	**348**	245	443	360	471
B7S2	213	189	233	227	242	289
B8S1	223	186	247	220	280	279
B8S2	87	277	105	266	146	288
B9S1	79	243	99	250	151	258
B9S2	56	175	68	140	93	228

Table 4 – Maximum measured strains from proof load test (Bridge 7722)

Transducer Location	Strain (με)						
	Phase One			Phase Two		Phase Three	Phase Four
	Path 1	Path 3	Path 5	Paths 1 & 4	Paths 2 & 5	Path 5	Paths 2 & 5
B1G2	**78**	---	---	**81**	---	---	---
B2G2	24	30	---	47	---	---	---
B3G1	38	43	15	60	54	30	85
B3G3	36	44	16	63	52	23	75
B4G2	32	**46**	31	71	80	47	116
B5G1	16	44	42	46	74	62	104
B5G3	18	44	43	49	70	67	102
B6G2	---	32	29	---	38	27	54
B7G2	---	---	**84**	---	**90**	**136**	**132**

Table 5 – Target proof moments, rating factors, and posting loads for Bridge 7701

Legal Load	W (kips)	L_R (kip-ft)	L_T (kip-ft)		RF_o	*Safe Posting Load* (tons)
			One Lane	Multiple Lanes		
HS-20	72.0	284	416	359	0.67	19.1
Type 3	50.0	235	344	297	0.81	18.2
Type 3S2	80.0	231	338	292	0.83	30.0
Type 3-3	72.0	190	278	240	1.00	N/A
NM 2	33.6	179	262	226	1.06	N/A
NM 3A	46.3	235	344	297	0.81	16.9
NM 5A	80.6	247	361	311	0.77	27.3

[1 kip = 4.45 kN; 1 kip-ft = 1.357 kN-m; 1 ton = 8.90 kN]

Table 6 – Target proof moments and rating factors for Bridge 7722

Legal Load	W (kips)	L_R (kip-ft)	L_T (kip-ft)		RF_o
			One Lane	Multiple Lanes	
HS-20	72.0	518	689	586	1.09
Type 3	50.0	400	532	452	1.41
Type 3S2	80.0	368	489	416	1.54
Type 3-3	72.0	332	442	375	1.70
NM 2	33.6	289	384	326	1.96
NM 3A	46.3	388	516	439	1.46
NM 5A	80.6	400	532	452	1.41

[1 kip = 4.45 kN; 1 kip-ft = 1.357 kN-m; 1 ton = 8.90 kN]

Figure 1 – Bridge No. 7701 (prestressed concrete double T-beam)

Figure 2 – Bridge No. 7722 (prestressed concrete box beam)

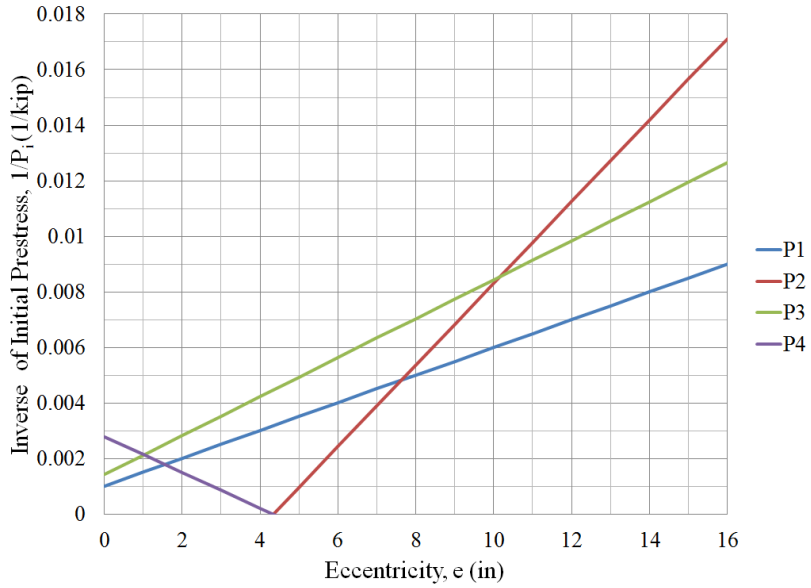

[1 kip = 4.45 kN; 1 in = 25.4 mm]

Figure 3 – Magnel diagram for H-20 design truck (Bridge 7701)

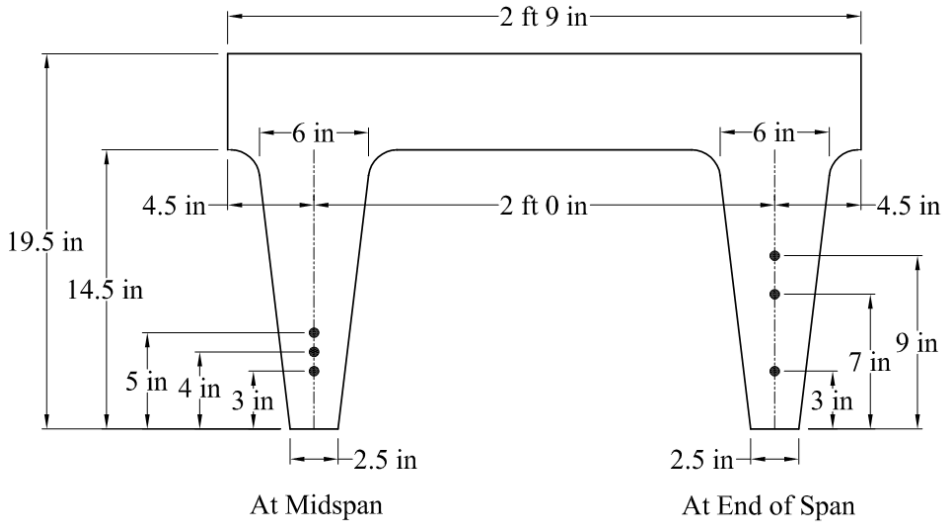

[1 in = 25.4 mm]

Figure 4 – Standard beam section of Bridge 7701

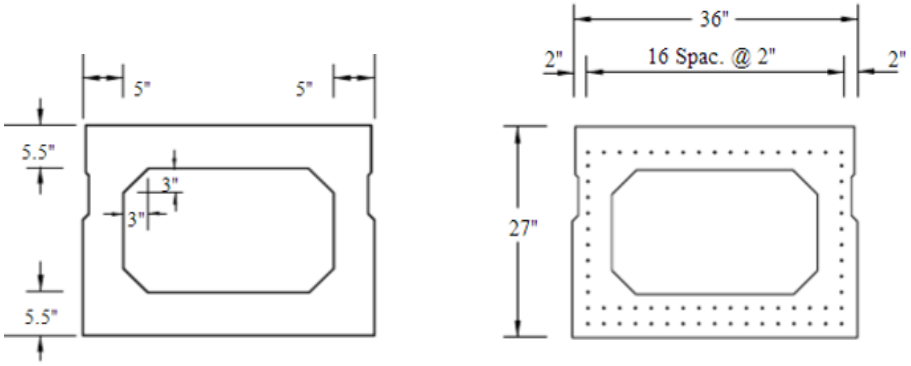

[1 in = 25.4 mm]

Figure 5 – Standard AASHTO Type BI-36 box beam of Bridge 7722

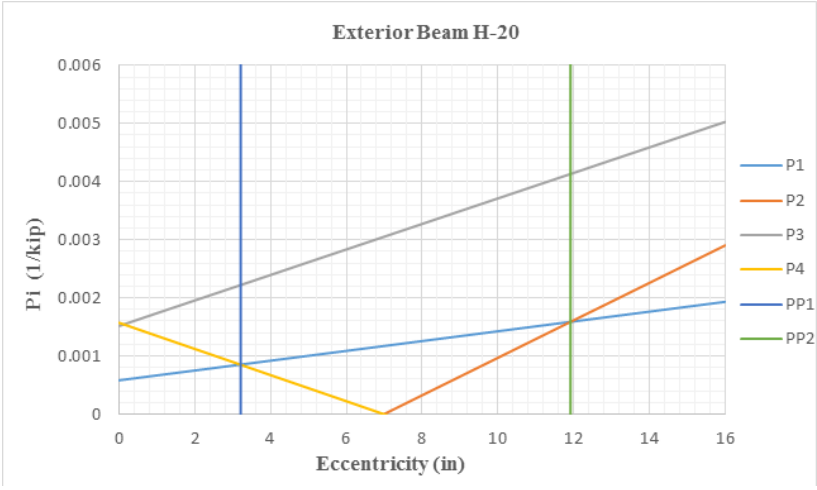

[1 kip = 4.45 kN; 1 in = 25.4 mm]

Figure 6 – Magnel diagram for exterior beam under H-20 design truck (Bridge 7722)

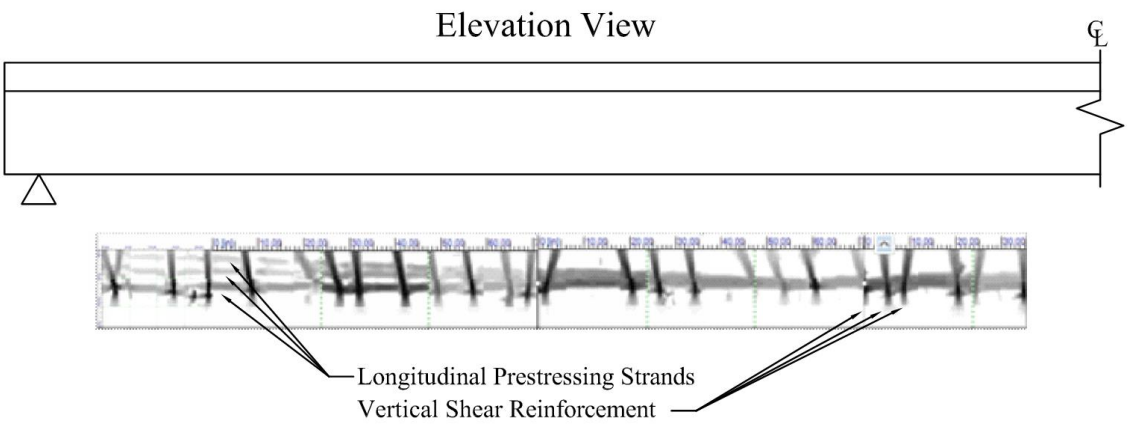

Figure 7 – Blockscan of north exterior beam from east abutment to center line (Bridge 7701)

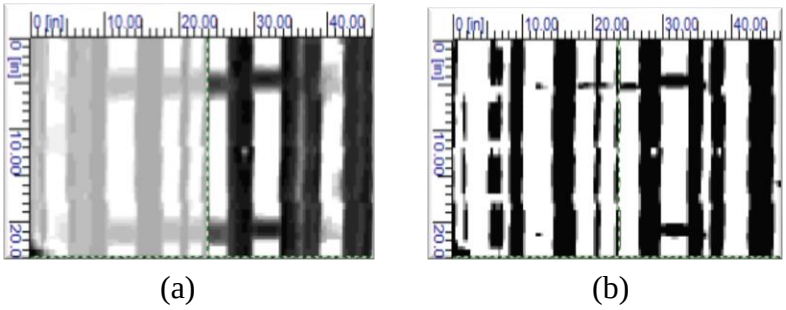

Figure 8 – Blockscans between two interior beams of Bridge 7722 at depth ranges of (a) 5 inches [127 mm] and (b) 2 inches [51 mm]

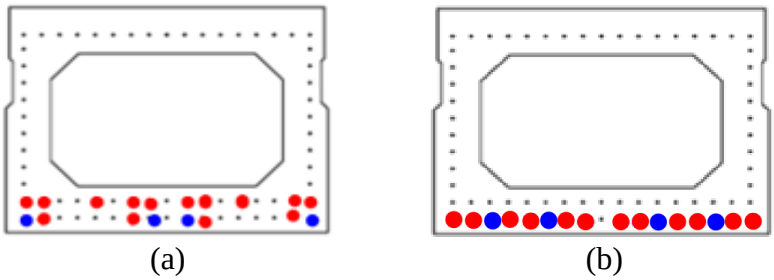

Figure 9 – Strand configuration in (a) interior and (b) exterior box beam of Bridge 7722 determined with rebar scanner

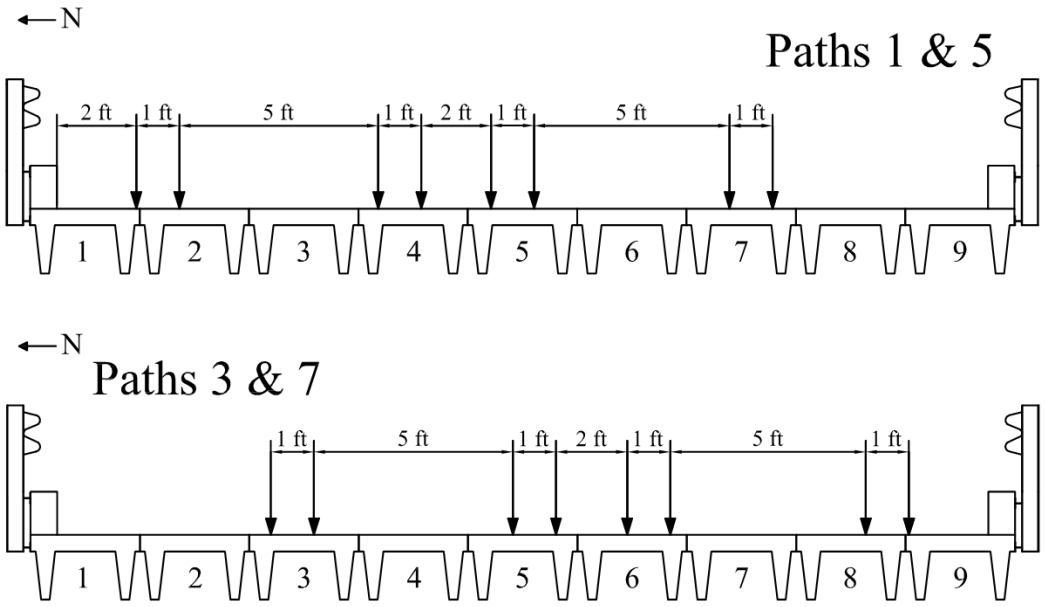

[1 ft = 305 mm]

Figure 10 – Transverse truck paths 1 & 5 and 3 & 7 for second phase of diagnostic testing (Bridge 7701)

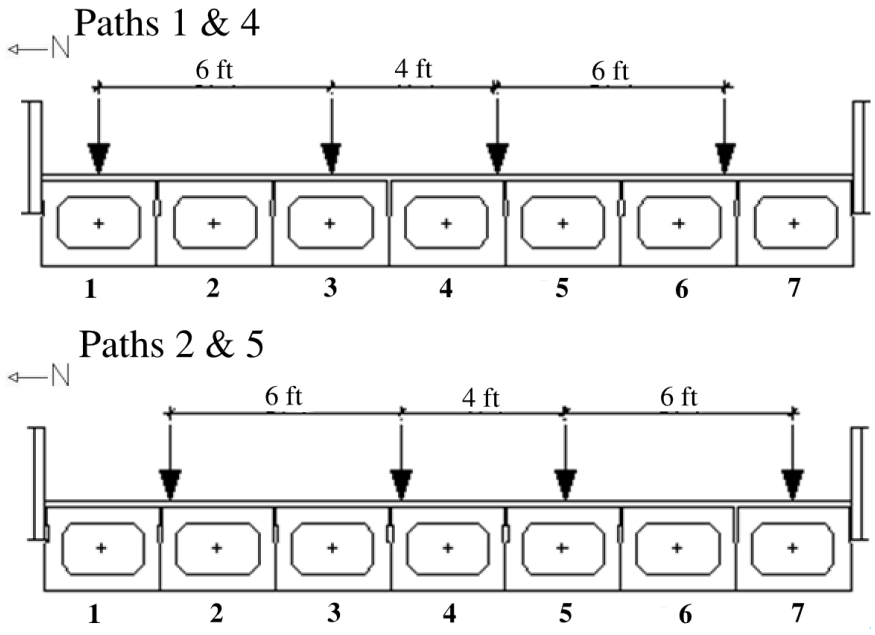

[1 ft = 305 mm]

Figure 11 – Transverse truck paths 1 & 4 and 2 & 5 for second phase of diagnostic testing (Bridge 7722)

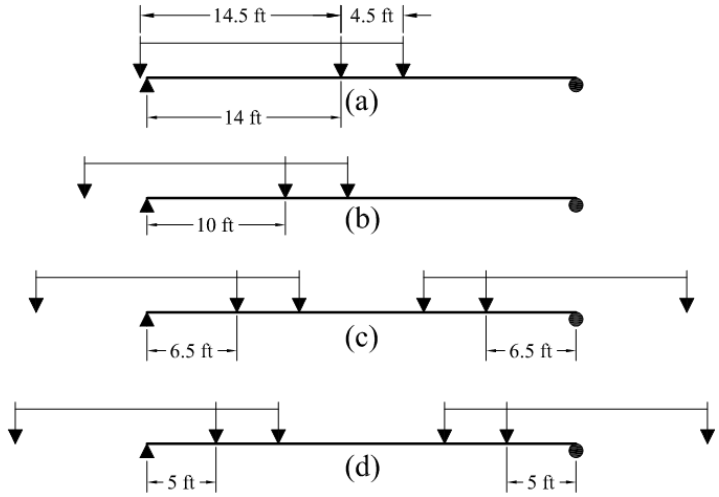

[1 ft = 305 mm]

Figure 12 – Final longitudinal truck positions for (a) first, (b) second, (c) third, and (d) fourth phase of proof testing (Bridge 7701)

Figure 13 – Instrumentation and proof testing of Bridge No. 7701

Figure 14 – Instrumentation and proof testing of Bridge No. 7722

BRIDGE LOAD TESTING IN GERMANY

Gregor Schacht, Frederik Wedel, Steffen Marx

Synopsis: This paper presents the current practice of bridge load testing in Germany. At first a brief summary of the historical value and meaning of load testing bridges at commissioning is given and also accidental over-load tests are described. While load testing of brides as part of the commissioning is common in many European countries today, in Germany load testing is only permitted in exceptional cases and to evaluate damage or questioned existing bridges. While proof loading is rare, short and long time test under serviceability loads are a common engineering task in Germany. Especially the calibration and verification of numerical models by load testing shows a high potential for the future. As the infrastructure gets older and the traffic loads increase a high demand for experimental evaluation methods becomes more important and request further research work to answer open questions. The four given examples of load tests demonstrate possible applications and different tasks for load testing of concrete bridges.

Keywords: load testing, bridges, diagnostic load test, proof load test, Monitoring, Railway bridges

Dr.-Ing. Gregor Schacht is a practical engineer at the Marx Krontal GmbH and a Lecturer at the Leibniz Universität Hannover. He is Vice-Chair of the DAfStb (German Association of Reinforced Concrete) Committee, Load Testing and Monitoring. His research interest are the theoretical and experimental evaluation of the load bearing behavior of existing concrete structures.

Frederik Wedel, M. Sc. is a PhD student in structural engineering at Leibniz Universität Hannover, Institute of Concrete Construction and also working as a practical engineer at the Marx Krontal GmbH. His research interests include the monitoring and analysis of the structural behavior of reinforced and pre-stressed concrete bridges.

Prof. Dr.-Ing. Steffen Marx is a professor of civil engineering at the Leibniz Universität Hannover and the Head of the Institute of Concrete Construction. He is Chair of the DAfStb (German Association of Reinforced Concrete) Committee, Load Testing and Monitoring. His research interests include the fatigue behavior of Concrete Structures, Integral Bridges and High Speed Railway Bridges

INTRODUCTION

People have been striving to be as safe as possible in all areas of their lives since prehistoric times. Safety is especially important in the construction industry, because the failure of built structures is much less accepted in society than, for example, failures of motor vehicles or electronic devices. We feel particularly secure if we really know, or are able to witness, that structural components can withstand the acting loads. Safety can be defined mathematically but is mainly empirical in nature, chiefly because its assessment is always based on subjective judgements. Providing confidence in the load-bearing capacity of structures is the goal of all load tests. They confirm the safety of a structure in a way that can be understood by anybody. New construction methods or novel structural elements always have to earn this confidence by passing at least one load test. In the 19th and 20th centuries, load tests were always used to prove sufficient load-bearing capacity of bridge structures[1]. And even today they have their place in the assessment of the load-bearing behaviour of new and old bridge constructions. The paper gives an overview about the practise of load testing of concrete bridges in Germany and describes the existing rules for the performance and evaluation of proof load test on concrete structures.

HISTORICAL DEVELOPMENT

Load tests as part of the commissioning of a new bridge have a long tradition. On the one hand this is due to the capability of load tests to confirm the required load-bearing capacity in a way that even laymen can understand. It was also used to compensate for the deficits in the existing, still not very sophisticated, calculation methods and to dispel all remaining doubts with respect to the structural capacity of the finished structure. Also, material defects could often be detected only during a load test.

To produce the sometimes very heavy loads required for the load tests, ballast masses were placed directly on the structures. Depending on the location and function of the bridge and the availability of the required materials, different types of ballast were used. Depending on the individual circumstances of every bridge water tanks, sandbags, steamrollers or heavy trucks were used to produce the loads[1]. Only the deflections were generally measured, as they were considered the most important effect in the structure due to the load. If they were sufficiently small or close to the calculated deflections, proof of sufficient load-bearing capacity was considered to have been provided.

That small deflections during load testing were no sign of a capable and secure structure was demonstrated in several failures of tested bridges. The road bridge near Salez (in the canton of St. Gallen, Switzerland) collapsed during a load test in 1884, at a measured elastic deformation of only 10 mm (3/8 in.). Failure was caused by buckling of the top chords of the steel trusses due to a missing bracing and poor construction of the junction plates. The bridge collapsed abruptly, even though the theoretical permitted maximum deflection had been determined to be 17.5 mm (2/3 in.)[2]. Other sudden failures occurred because of imprudence or gross negligence during testing. The Rhône bridge near Peney (Switzerland), having a span of 100 m (328 ft), passed a load test in which sandbags were used as ballast. After the test, however, heavy rain started and the sandbags absorbed so much water that the anchorages failed and the bridge collapsed. In 1873, the bridge over the Broye near Payerne also passed a load test, but it collapsed when workers

carelessly began throwing the used water tanks off the bridge, because he wanted to get to the bridge opening party quickly, and damaged a main girder[3].

Because of some spectacular bridge collapses, such as the collapse of the Münchensteiner bridge (Switzerland) in 1891, the Swiss railway department demanded regular inspections of all railway bridges[4]. During these inspections simple load tests had to be carried out in which the bridge was loaded according to the load assumptions of the previously performed structural analysis. Thus, load tests became standard procedure, with the consequence that the results of the tests were often not even analysed. The bridge was considered to have sufficient load-bearing capacity if it did not collapse during the load test and if some further easily confirmed criteria were fulfilled. These limit criteria had been derived from long experience, and personal assessments, and affected mainly the serviceability of the construction, i.e. deflections and vibrations. Other countries in Europe and the Western World followed the Swiss railway and defined similar regulation for the load testing of bridges at the end of the 19th century[1].

As an extreme and unique example for the enormous efforts which were undertaken to proof structural safety the load test of the Sydney Harbour Bridge shall be described. After the first test train, a steam locomotive, had safely crossed the bridge on 19 January, 1932, a full load test with 96 steam locomotives arranged on all four rail tracks was carried out in February 1932 (Fig. 1). The load test was carried out over three weeks, and subsequently the bridge was declared safe and ready to be opened[5].

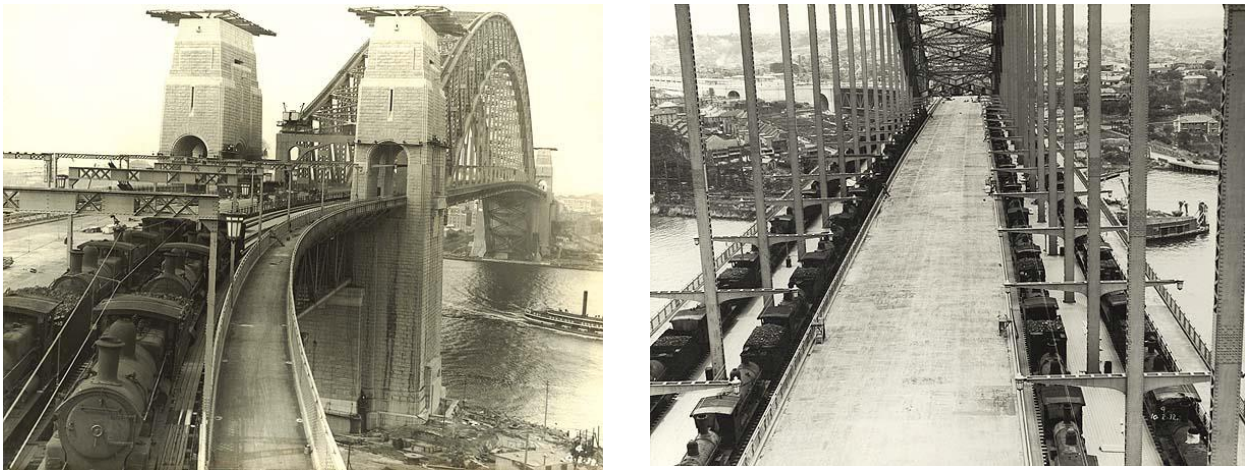

Fig. 1 —Load test of the Sydney Harbour Bridge in 1932[6]

LOAD TESTING OF BRIDGES IN GERMANY

The German Guideline for Load Testing of Concrete Structures

In the 1950s intense development of calculation methods began, primarily due to the increased use of computer technologies. Professionals and laymen became confident that it was possible to calculate the load-bearing capacity of structural elements with sufficient accuracy. As a result of this development and the discussion about the usefulness of load tests, no rules for load tests have been included in design standards since DIN 1045:1972[7] was issued. For the design of new structures, structural analysis is usually considered as the more suitable approach. During the last few decades, when it became necessary for engineers to assess and evaluate an increasing number of existing constructions and especially existing concrete structures, it became clear that rules for load tests for the assessment of existing structures needed to be included in the standards. However, it was also clear that load tests had to be updated in line with the state of the art technically as well as theoretically.

The necessary work to include rules for load tests in the design standards took place almost simultaneously in East and West Germany, but the actual work done headed in quite different directions. In the former GDR, Schmidt and Opitz[8] developed the theoretical basis for the planning and assessment of load tests which is still used today. They developed a safety concept which is still applicable today, and used partial safety factors. This concept ensures a safety level similar to that of computational analysis, which is also tailored to the specific constraints of load tests. Furthermore they defined specific assessment criteria for the possible failure modes, which allow an assessment of the load-bearing behaviour during the test. The developed rules were included in TGL 33407/04[9], which allowed the execution of load tests in the GDR according to standardised rules from 1986 onwards.

In former West Germany, the testing technology underwent significant developments under the supervision of Steffens[10]. He developed a mobile loading device of steel elements which, together with a hydraulic system, precluded the need for ballast masses. When this loading device is used, the produced hydraulic test loads are anchored close to the tested structure. The structure is therefore restrained, and if the loading device is sufficiently stiff and the structure is sufficiently ductile, an automatic self-securing effect is achieved. If the structure deforms, the hydraulic pressure is automatically reduced and the overall system is put into a secure state of equilibrium. Thus, failure can be avoided for a sufficiently ductile construction. The rapidly developing computer technology combined with electronic measuring technology allows online detection and analysis of the measured data and thus a detailed assessment of the load-bearing behaviour during load tests.

A considerable leap forward in load test technology occurred when the two streams of development were combined after the reunification of Germany. Within some cooperative research programs the theoretical basis and functional loading and measuring technologies were developed further and brought into practice. As a result of this development, the Deutscher Ausschuss für Stahlbetonbau published the guideline “Belastungsversuche an Betonbauwerken”[11] in 2000. This guideline outlines the fundamentals for the planning, execution and evaluation of load tests in Germany. The guideline defines minimum requirements for the magnitude of the applied test load, the kind of loading that has to be used, loading and unloading cycles and safe stop criteria which allow the detection of critical structural states before damage to the structure occurs. Figure 2 shows the recommended loading regime for proof-load testing.

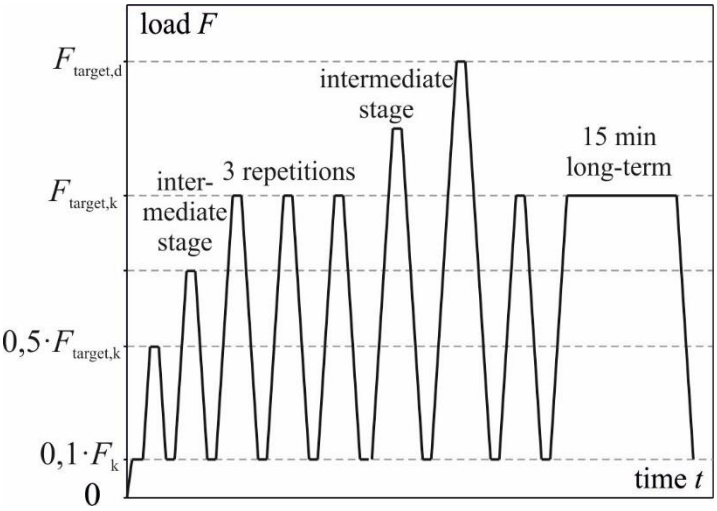

Fig. 2 — Loading regime for load testing of concrete structures[12]

In load tests the properties of the tested structure and its self-weight are considered deterministic values and no safety factors have to be used for calculating the target test load. Only the superimposed dead and live loads have to be multiplied by the appropriate safety factors. The externally applied part of the required test load (ext$F$target) is determined with Equation (1). The applied load must represent the worst-case scenario and produce maximum stresses in the construction. The target test load is determined on the basis of the theoretical loads and has always to be smaller than the ultimate test load ext$F$ult. The ultimate test load is the load at which first structural changes in the load bearing

behaviour are detected by the measurements taken. The allowable deformations which announce beginning structural damage are limited by stop criteria, which are defined very conservatively and secure a safe usage of the structure after testing. The stop criteria given in the German Guideline are explained below.

$$\mathrm{ext}F_{\mathrm{target}} = \sum_{j>1} \gamma_{\mathrm{G,j}} \cdot G_{\mathrm{k,j}} + \gamma_{\mathrm{Q,1}} \cdot Q_{\mathrm{k,1}} + \sum_{i>1} \gamma_{\mathrm{Q,i}} \cdot \Psi_{0,\mathrm{i}} \cdot Q_{\mathrm{k,i}} \leq \mathrm{ext}F_{\mathrm{ult}} \qquad (1)$$

$\mathrm{ext}F_{\mathrm{target}}$	External part of the target test load (excluding existing self weight)
$\mathrm{ext}F_{\mathrm{ult}}$	External part of the ultimate test load (excluding existing self weight)
$\gamma_{\mathrm{G,j}}$	Partial safety factor for dead load (for existing dead loads: $\gamma_{\mathrm{G}} = 1.0$, for additions dead load $\gamma_{\mathrm{G}} = 1.35$)
$G_{\mathrm{k,j}}$	Characteristic value of dead loads
$\gamma_{\mathrm{Q,1}}$	Partial safety factor for the dominant live load $\gamma_Q = 1.50$
$Q_{\mathrm{k,1}}$	Characteristic value of the dominant live load
$\gamma_{\mathrm{Q,i}}$	Partial safety factor for additional live loads $\gamma_Q = 1.50$
$\Psi_{0,\mathrm{i}}$	Combination factor for additional live loads $\Psi_{0,\mathrm{i}}$= 0.4 …0.8 according to [13]
$Q_{\mathrm{k,i}}$	Characteristic value of additional live loads

Because the resistance of the tested structure is also deterministic, no additional safety factors have to be used to account for the scatter of the structural capacity. This makes it possible to use hidden reserves for future additional live loads. The relation between calculation and load test as well as the connection between target and ultimate test load are shown in Fig. 3.

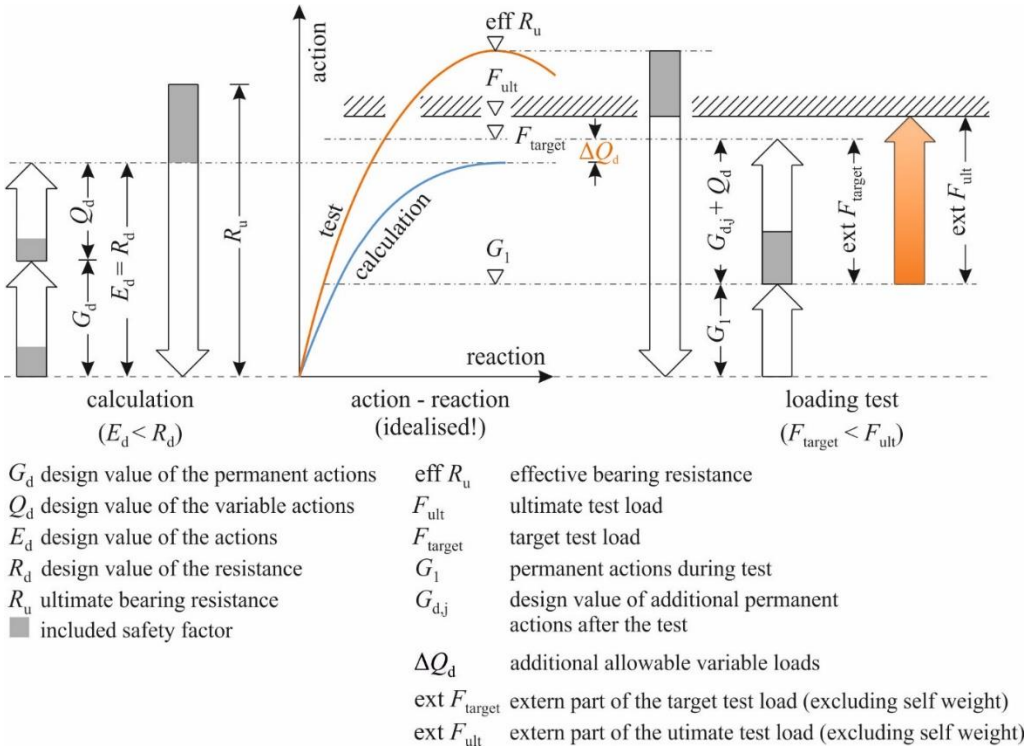

Fig. 3 —Concept of proof load testing compared to calculation, after[13]

Using ballast masses to prove that a structure has sufficient load-bearing capacity (proof load test) is very dangerous, both for the people involved in the testing and the structure itself, because the applied load level is significantly above that of the serviceability limit state (SLS). In a self-securing system with a loading frame the applied loads are generated by hydraulic jacks and anchored close to the tested structure so that neighbouring elements are not loaded unintentionally (Fig. 4). Provided that the loading frame is sufficiently stiff and the behaviour of the tested element is ductile, the load test is self-secured, because the hydraulic pressure is automatically reduced with increasing deformation[14].

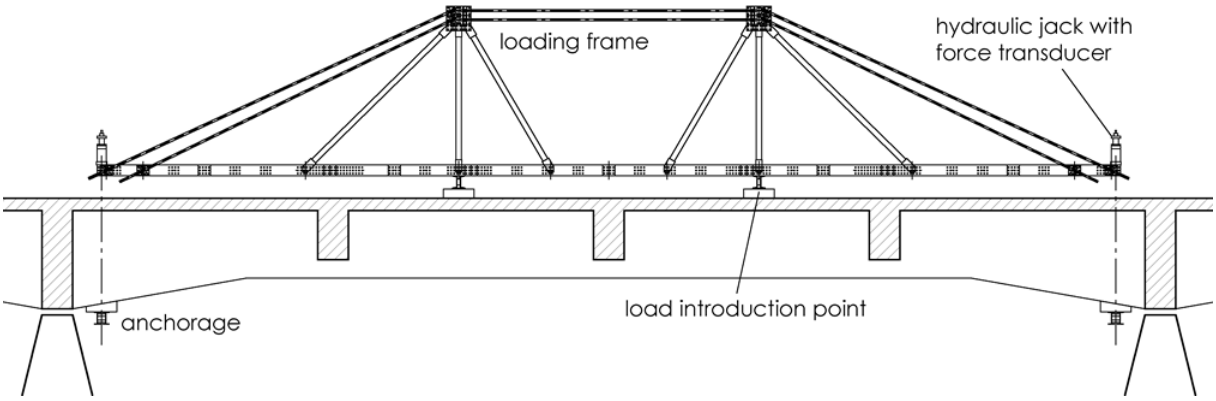

Fig. 4 — Example for the application of a loading frame for proof load tests

To be able to carry out online evaluations of the load-bearing behaviour of the tested structure during the load test, the relevant reactions have to be measured electronically and visualised on a computer. This is essential for early detection of beginning nonlinear structural changes. Depending on the structural defects which are to be evaluated the structural

deformations which have to be monitored, have to be chosen. The following deformation limits and stop criteria are listed in the German guideline for load tests[15]:

- Limitation of the concrete strain to a level where stable microcracking occurs
- Limitation of the reinforcement strain to within the elastic range
- Limitation of the crack widths and the rate of change of the crack widths during loading
- Limitation of nonlinear and residual deflections
- Limitation of deformations in the shear area (concrete strain in the compression struts and tensile strain in the web reinforcement)
- Critical values of the measured load–deformation relationship or of acoustic emissions
- Critical bearing displacements

Deformation criteria based on concrete or reinforcement strain are difficult to evaluate because the magnitude of the elastic strain caused by self-weight has to be known ahead of time and the exact location of maximum strain is unknown prior to cracking. For evaluations of structures subjected to bending stresses, load–deformation curves are generally used. Conventional measuring techniques allow reliable detection of any decrease in bending stiffness caused by cracking of the concrete. The information gathered during unloading cycles adds valuable information to the understanding of the load-bearing behaviour, and beginning nonlinear deformation can be detected early. The criteria listed above allow determination of the load-bearing capacity without any damage to the construction. In special cases, specialised measuring technologies, such as acoustic emission analysis or photogrammetry, are used to reliably determine crack initiation in the concrete. The state of the art of the rules for load testing is given in[12]. The authors are revising the German Guideline for load testing and the stop criteria are improved based on new experimental findings[16].

Load testing of bridges

Besides the development of a guideline for load tests in 2000, research projects for the development of mobile bridge load-testing equipment were carried out. BELFA (for road bridges)[17] and BELFA DB (for railway bridges) mobile loading trucks were developed. These trucks are equipped with a complete servo-hydraulic system and were developed for load testing of bridges having short and medium spans (Fig. 5).

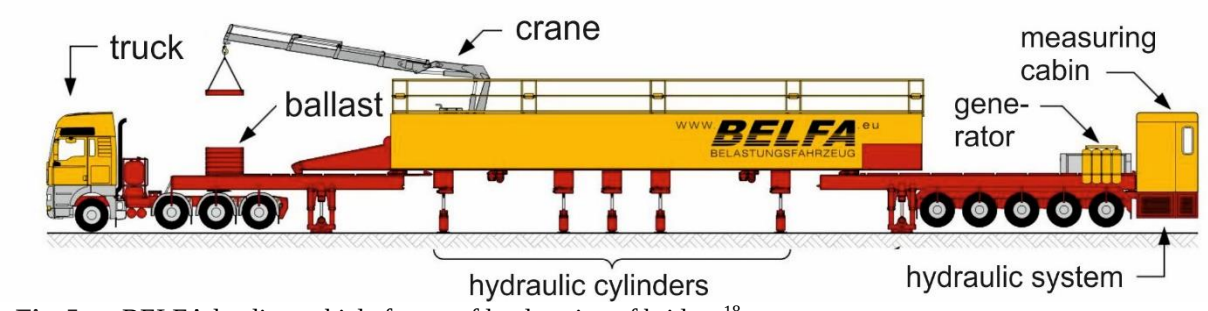

Fig. 5 —BELFA loading vehicle for proof load testing of bridges[18]

So far, over 42 bridges have been load-tested using the BELFA and have demonstrated the considerable advantages of this technology: short track possession times, moderate costs and an increase in the allowable live loads[18].

The reason why the BELFA did not become a standard method for the evaluation of existing bridges was a statement by the German Ministry of Transport in the 1990s, which said that load testing of bridges must not be performed under any circumstances. The same recommendation was given to local road administrations. The misunderstandings that led to these recommendatioins were resolved during the following years and the German Ministry of Transportation and Construction (Bundesministerium für Verkehr, Bau und Stadtentwicklung) now permits load testing of bridges in special cases. However, because a special guideline for bridge load testing is not yet available, specific conditions are formulated for each test, which is why load tests are still very rare[18].

But times are changing. Load testing has been reintroduced into European standards. According to Eurocode 2[13] structural design may be complemented by load testing in the following cases:

- If no adequate structural models are available
- For the design of serially produced structural elements
- To check assumptions made in the structural analysis of constructions

The need for reliable methods for the assessment of the structural safety of the ageing European infrastructure led to the creation of a new initiative responsible for developing regulations for bridge load tests and their evaluation. Load testing for the evaluation of bridges is included as Level 3 of the assessment process proposed in the German Guideline for the evaluation of existing bridges (Nachrechnungsrichtlinie)[20]. Level 3 of the assessment process in the Guideline takes measured bridge deformations into account. During load testing of bridges, deformation measurements are generally taken at critical sections, and strain measurements at selected cross sections. These measurements reflect the load-bearing behaviour under service loads and allow a realistic description of the state of the structure. Level 3 is used for validation of the chosen structural model. Load testing is restricted to special cases and the permission of the German Federal Road Administration is required[20].

For Bridges owned by local bridge authorities load test are easier to accomplish. For railway bridges the German railway (DB AG) is even requesting load testing for new construction methods or special bridge structures as a common way for commissioning. The international state of the art of bridge load testing is given in[21].

Classification of bridge load testing

For the evaluation of Bridges by load testing different task can be distinguished. Load tests can be used to validate structural calculations and designs or to calibrate numerical models, to proof a sufficient structural safety or to determine the bearing strength by failure tests[22]. In Tab. 1 the various tasks of load tests of bridges are summarised and the various types are classified.

Tab. 1—Classification of the different possibilities of bridge load testing

Type of load test		Aim of load test	Comments
diagnostic load testing (characteristic service loads)	Short term F_k	Determination of deformations and strains as well as the structural behaviour under service loads; calibration of numerical models; verification of the assumptions of structural analyses	No temperature influence; numerical models can be improved; difficult extrapolation of the load-bearing capacity; dynamic effects
	Monitoring F_k	Determination of time-dependent deformations and strains; verification of the assumptions of structural analyses; assessment of damage development, durability	Long-term deformation behaviour (creep; temperature effects) stable measuring equipment; big data
Proof load test (factored design loads)	F_{aim}	Proof of sufficient structural safety under a defined test load without the occurrence of critical deformations	Standard test situation for evaluation of the load-bearing reserve of existing structures
	F_{lim}	Determination of the maximum load under which no critical deformations and strains are detected	Increased measurement efforts; danger of irreversible damage to the structure
Failure load test	F_{ult}	Proof of the structural capacity	Very helpful for the evaluation of the structural safety

Depending on the goals of a load test and the required loads, different methods of load generation can be distinguished:

- with ballast masses (trucks, trains, mass loads)
- using hydraulic loading systems: loading frames, loading vehicles (BELFA), pile foundations, special constructions for activation of dead load[21, 23]

For diagnostic load tests the applied loads are on the level of characteristic load (serviceability limit state). For proof load tests the applied loads contain the required load factors (ultimate limit state). The use of mass loads is only allowed for generation of loads below the serviceability limit load because a safe structural state above these loads cannot be guaranteed. Therefore, loading with mass loads is limited to system calibrations. An extrapolation from the results gained from a test under serviceability loads is dangerous because a linear behaviour on higher load levels is not guaranteed.

Hydraulic loading systems have the advantage that self-secured loading is possible, i.e. that the pressure of the jacks – and hence the load on the structure – automatically decreases with increasing deformations. A disadvantage is that for larger structures the anchoring of loads is usually difficult and very time- and resource-intensive. The BELFA has a hydraulic loading system but does not need additional anchorage constructions. Therefore, only a short track possession time is needed for the test. The BELFA is limited to medium-span bridges (up to a span of 20 m (66 ft) and maximum load of 1580 kN (355.3 kips))[19]. For larger bridges a proof load test with hydraulic loading systems is extreme expansive and complicated.

EXAMPLES OF BRIDGE LOAD TESTS

Masonry arch bridge over the Aller near Verden (Germany)

After 150 years in operation the historic masonry arch bridge over the Aller near Verden (Germany) was taken out of service in October 2015. The damage caused by moisture and age had increased disproportionately during the last years of operation so it was decided to build a new bridge, which was opened to railway traffic in 2015. Before the demolition of the old bridge there was an opportunity to perform a load test, subjecting it to a load level far beyond service loads and thereby gain experience in the evaluation of the nonlinear load-bearing behaviour of real masonry arch bridges and to identify possible stop criteria which can be used for the early detection of beginning structural damage[24]. The load test was a scientific investigation and represents a test to failure according to table 1.

Preliminary finite element calculations showed that most critical load-bearing states (compressive and tensile strains) occurred under asymmetric loading (when the load was applied from the end to mid-span of the bridge) of more than 5 MN (1124 kips). Therefore, it was decided to apply a test load of 5.6 MN (1259 kips), which is more than five times the service load of the train load model with four axle loads stipulated in current design codes (LM 71). The load was applied by four 2 MN (449.6) hydraulic jacks arranged at the same distance apart as train axles. The bars via which the hydraulic loads were introduced were anchored 18 m (59 ft) into the soil by micropiles (see Fig. 6).

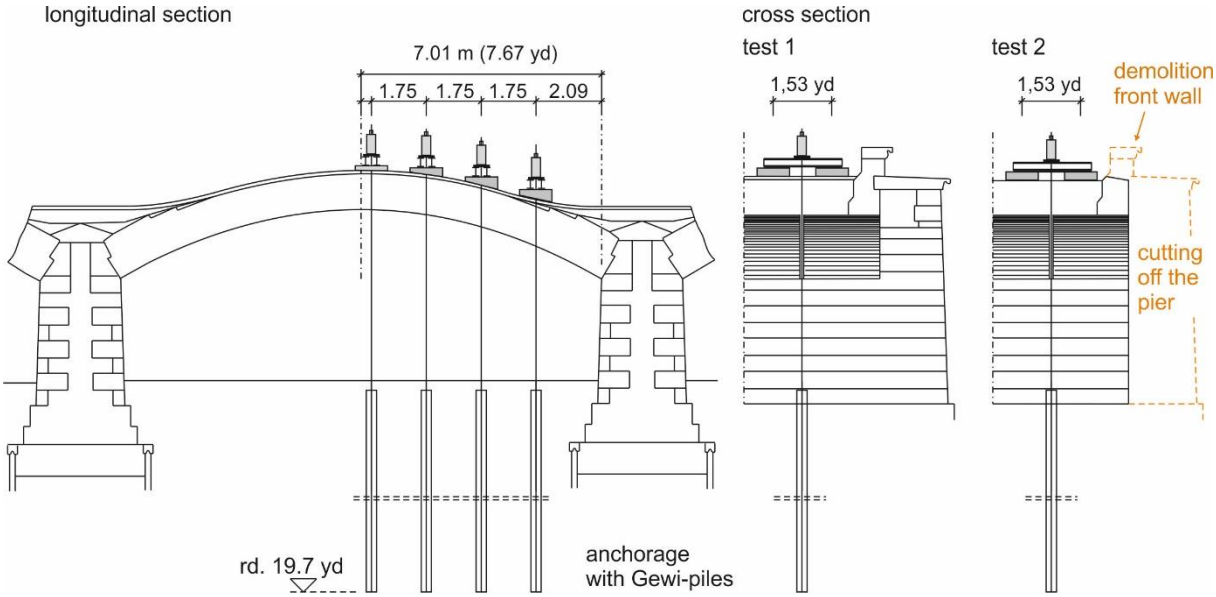

Fig. 6 —Load and testing arrangement for the masonry arch bridge over the Aller

The two tests, which were carried out in March and June 2016, took place at different stages of the demolition process (before and after demolition of the front wall and the concrete filling on top of the arch). To monitor the load bearing behaviour several measurements were done (Fig. 7).

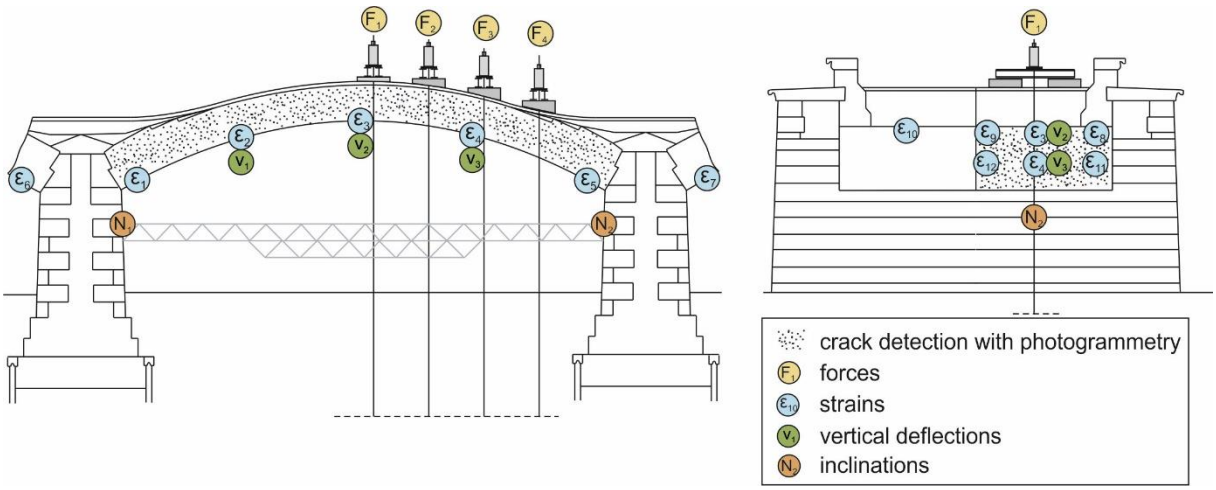

Fig. 7 —Arrangement of measuring techniques

The results of both load tests yielded detailed information of the load-deformation characteristics of masonry arch bridges under very high loads. The measured deformations agreed well with the results of theoretical models used to simulate the load-bearing behaviour of this bridge. Critical structural states were not detected, even when the bridge was loaded with six times the service load[25]. The influence of the front wall and the concrete filling could be quantified (Fig. 8). The gained information is used for the further development of calculation models for concrete and masonry arch bridges.

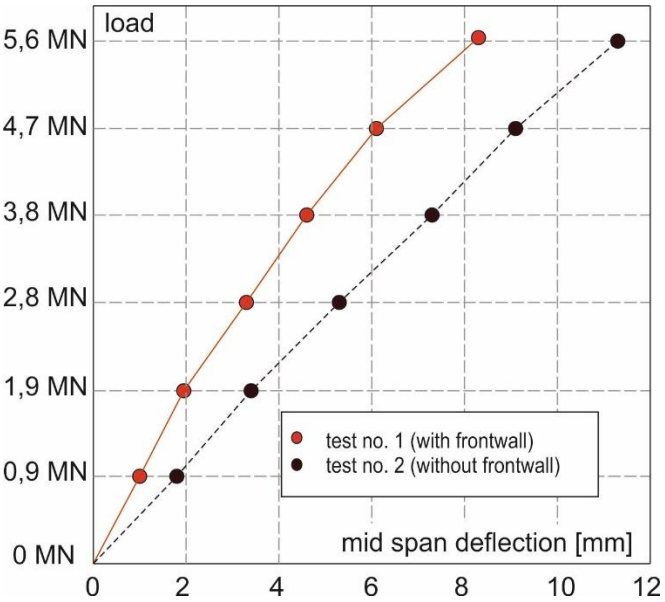

Fig. 8 —Influence of the front wall on the stiffness and deformation behaviour

Scherkondetalbrücke (railway bridge)

On the new high-speed railway line between Erfurt and Leipzig/Halle in eastern Germany, Deutsche Bahn AG built Germany's first semi-integral railway bridge (Scherkondetalbrücke). Its 577 m (631 yd) prestressed superstructure consists of a very slender T-beam. The height of the beam is 2 m (2.2 yd) at the centre of each span and increases towards the pillars (see Fig. 9)[26].

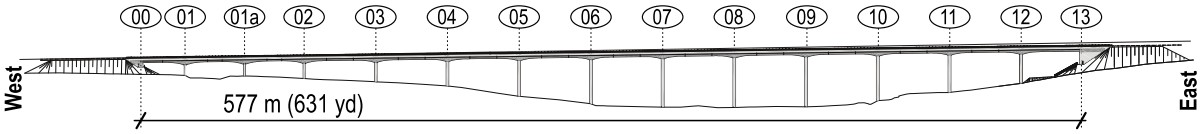

Fig. 9—Profile of Scherkondetalbrücke[27]

From axis 0 to axis 10, the superstructure is monolithically connected to the substructure. At the other axes, spherical bearings connect the pillars to the superstructure. For further information on dimensions and a detailed construction drawing see[28,29]. Not only was this type of static system used for the first time for a railway bridge in Germany, the track was also built as nonballasted track, which had not been used before on long semi-integral bridges. Because of the lack of experience with this unusual construction method (semi-integral) in combination with nonballasted track on the bridge, the load-bearing behaviour under high vertical loads needed to be investigated. The aim of the performed tests was to obtain results that could be compared with those from the structural analysis in order to verify the predicted structural performance of the semi-integral bridge (diagnostic load test – short term and Monitoring, see Table 1).

In the performed test two heavy loaded freight trains with a length of 145 m (159 yd.) each and a total weight of 960 t (1058 US) per train were used (Fig. 10). The trains drove over the bridge either one by one or simultaneously with a maximum speed of 20 km/h (12.4 mph). Additionally, the trains stopped at specific positions on the bridge in order to cause maximum deflections and rotation of the superstructure at axis 13 because theoretical calculations indicated

maximum deformations at this axis. A high-precision measuring system recorded these deformations: stresses in the reinforcing steel in the pier heads (strain gauges installed when building the piers), the inclination of superstructure (inclination sensor) and the deformation of the bridge joint in longitudinal direction (distance sensors). In addition, geodetic measurements were taken to record the deflections of the superstructure.

Fig. 10—Freight trains on the Scherkondetalbrücke

From the analysis of the measured data, which required complex data preparation, it was possible to identify various influencing factors. The results include influence lines showing the curvature of the pier heads, the rotation of the superstructure and the deflection of the superstructure as a function of the position of the trains.

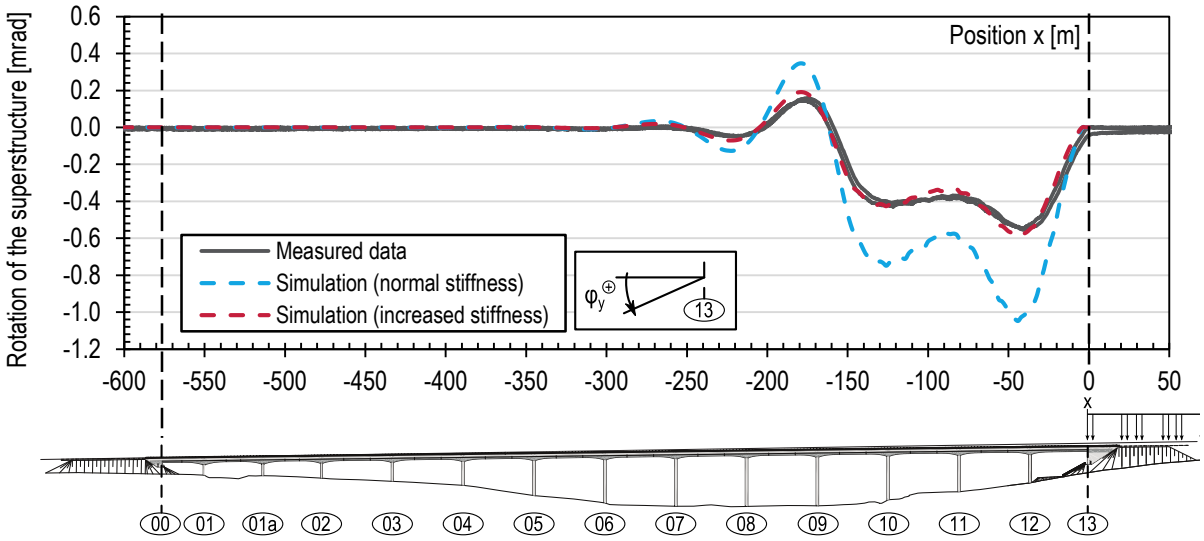

Fig. 11—Influence lines for the measured and calculated rotation (φ_y) of the superstructure at axis 13

Fig. 11 shows the influence lines for the rotation of the superstructure at axis 13 (φ_y) determined from the measured data and from a numerical model. This rotation is an integral measure for the global deformation characteristic of the semi-integral bridge and allows a good evaluation of the bearing behaviour. Because the bridge behaved more stiffly than expected in the preliminary design calculations, the stiffness of the superstructure in the model was increased by

a factor of 1.8. The results of the numerical simulations with the higher stiffness agree very well with the experimental results. Not only had the rotation of the superstructure agreed very well between measuring and calculation, also the comparison between the measured and calculated data of the curvature of the pear heads and the deflection of the superstructure were delivered good results. The assumption of a greater stiffness of the superstructure is justified because the nonballasted track participates in the load transfer of the applied vertical loads.

The test and the way it was performed provided insights into the load-bearing behaviour of Germany's first semi-integral concrete railway bridge and added to the knowledge about this construction method for future railway bridge construction[27]. The system calibration test took place in the serviceability limit state. Therefore, the test does not provide direct information about the ultimate limit state. Nevertheless, the desired goal of a system calibration could be reached with this kind of test and the way of measuring. For future load tests, it could be learned that the measured rotation of the superstructure and the deflection of the superstructure is a good indicator for the global structural deformation behaviour.

Saale-Elster-Valley bridge (railway bridge)

The Saale-Elster-Valley bridge is also located on the new high-speed railway line between Erfurt and Leipzig/Halle. With a total length of 8,577 m (9,380 yd) the bridge is the longest railway bridge in Germany and is special because the track and the bridge split up and continue as two separate structures. Fig. 12 gives an overview of the bridge and Fig. 13 gives a closer look of the construction itself.

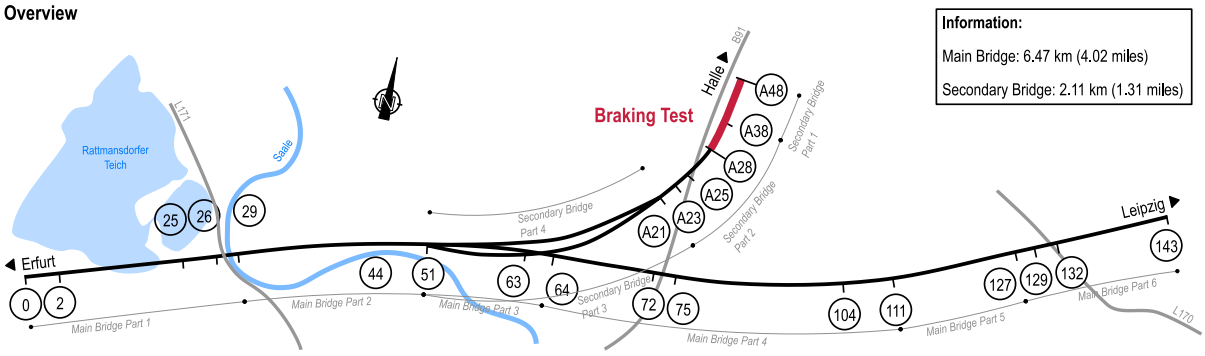

Fig. 12 —Overview of the whole Saale-Elster-Valley bridge

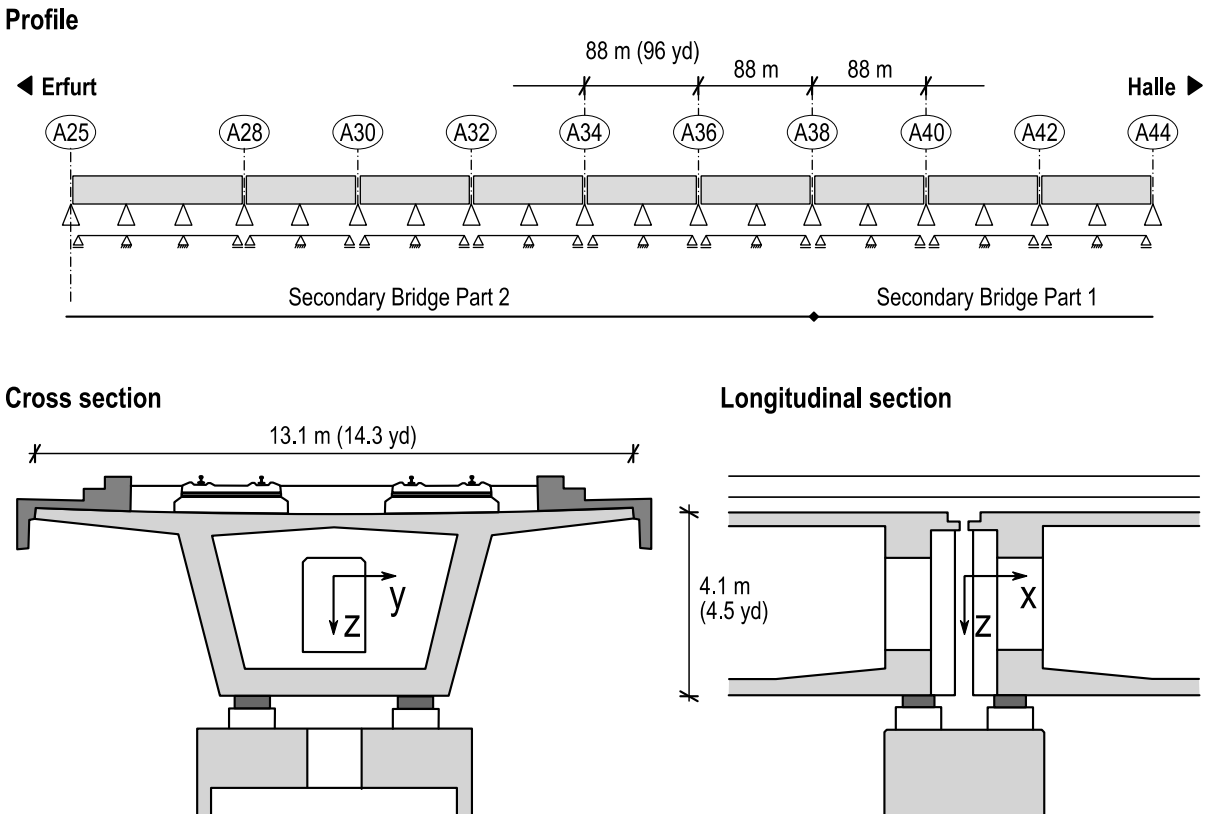

Fig. 13 —Profile of a part of the secondary bridge, cross section and longitudinal section

Generally the bridge's pre-stressed concrete superstructure is continuous over two spans, with only few exceptions (for example a tied arch bridge around axis 64 where the split up tracks cross). The middle pier of the two-span beams is built as a fixed point.

To verify the assumptions made in the design of the bridge, braking tests were performed between axis A28 to A48[30,31]. These test were diagnostic load test according to table 1. The main goal of the braking tests was to gain information about the actual stiffness of the piers and about the global load-bearing behaviour. The stiffness of the piers was a doubtful size during the design process but it has a main influence on the overall deformation behaviour. Because the stiffness is defined as the quotient of force and displacement, it was necessary to measure the (horizontal) displacement of the piers and the (horizontal) force that is transferred by the piers. The displacement of the piers was measured geodetically, the stresses in the rail were measured with strain gauges on the rails, the deformation of the bridge joints in longitudinal direction with distance sensors and the bearing displacement at the fixed points was monitored with longitudinal displacement transducers. Two heavy loaded freight trains with a length of 80 m (87.5 yd) each and a total weight of 488 t (538 US) per train were used for the braking tests. With slow train passages (maximum speed of 20 km/h (12.4 mph) the numerical model was calibrated and the measuring systems could be checked for plausibility.

Fig. 14 —Manual signaling to start the braking process with a flag

The evaluation of the braking test showed that the calculated dynamic stiffness of the piers is about 3 to 6 times higher than the static ones from the soil expertise. With these experimentally determined values for the pier stiffness the numerical model was updated. The numerical model contains the part of the secondary bridge between axis A23 and A48. Both, the superstructure and the rails are designed as beam-elements and the piers are either modelled as fixed bearings (fixed points) or as floating bearings (piers at the bridge joints). The results of the comparison between the test and the numerical simulation are presented in Fig. 15. Both results are compared by showing the occurring forces in the rails and the displacements of the bridge joints at the time of braking as a function of the bridge's length.

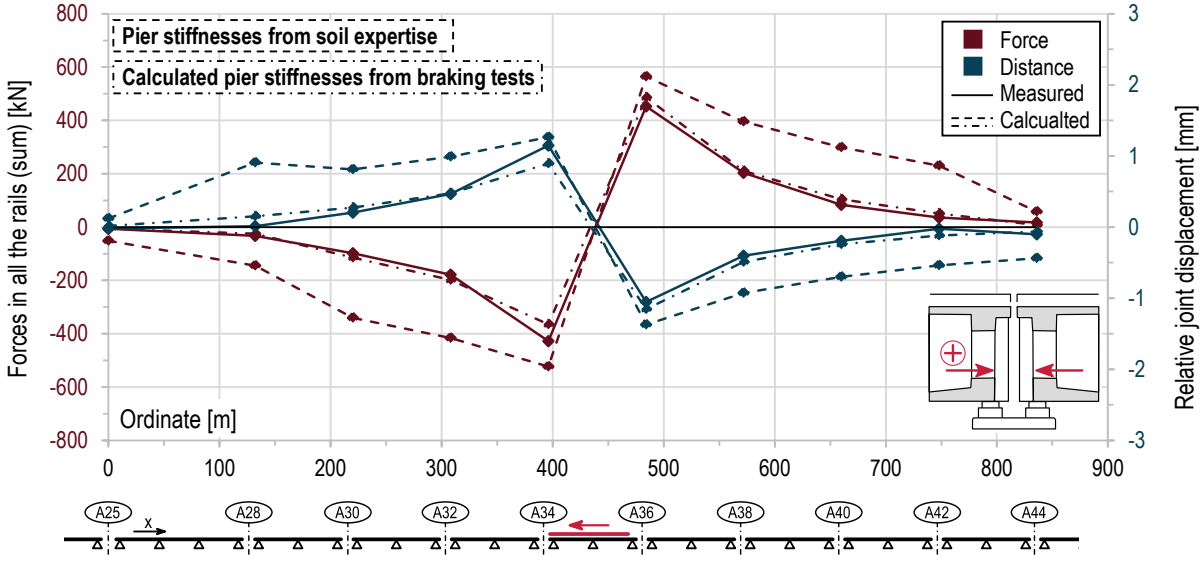

Fig. 15 —Results of the braking test and numerical calculation before and after calibration of the model

Fig. 15 compares the relative joint displacement measured during the test with the results of the numerical simulation without and with updated values for the pier stiffness. The model prior to the calibration contained the (static) stiffnesses from the soil expertise which were much lower (1/6 to 1/3) than the calculated (dynamic) stiffnesses from the braking tests. The displacement calculated with the calibrated model fits the measured ones very well. In addition, the effective load-bearing length of the bridge can be seen from the evaluation and is is about 350 m (383 yd) in each direction (700 m (766 yd) in total) from the braking position.

With the performed braking test on the Saale-Elster-Valley bridge, the open questions concerning the real stiffness of the piers and global load-bearing behaviour could be answered. The load test successfully supported the numerical simulations for the determination of the load bearing behaviour and demonstrates the potential of experimental assistance in design.

Measurements at the coupling joints of a road bridge

In a 130 m (142 yd) prestressed concrete road bridge the fatigue check for the tendons at the coupling joints could not be satisfied. Therefore, a diagnostic load test (table 1) was performed, as recommended in the guideline Nachrechnungsrichtlinie[20]. They consisted of long-term measurements to obtain information on the temperature behaviour, and short-term measurements which included a load test.

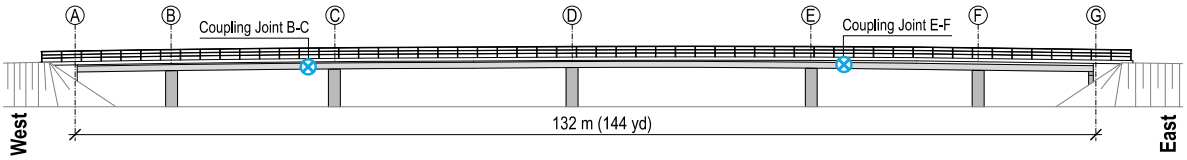

Fig. 16 —Profile of the bridge, showing the coupling joints

The bridge has two coupling joints, where all tendons running in the longitudinal direction are coupled. Fig. 16 shows the bridge with its seven axes and two coupling joints. The coupling joints are located in the spans between axes B and C, and axes E and F.

The aim of the performed tests was to obtain strain measurements at the – possibly cracked – coupling joints in order to compare them with the measurements taken at various reference measurement locations with uncracked concrete. Such a comparison yields information about the condition of the coupling joints and indicates whether critical cracks exist at the joints. Therefore, the results measured on the coupling joints are compared to measurements on a (uncracked) reference point which is located on a position were similar bending moments to the ones in the coupling joints occur when the trucks are passing.

Strain measurements of the superstructures concrete in the longitudinal direction of the bridge were taken by distance sensors as seen in Fig. 17. The sensors were located in different sections of the bridge as seen in Fig. 19. Several sensors were installed at the two coupling joints and the various reference measurement points. Furthermore, laser measurements of the deflection of the span between axes B and C were performed. The lasers were located on the ground underneath the bridge facing upwards to the superstructure and measuring the deflections of the superstructure as the trucks were passing.

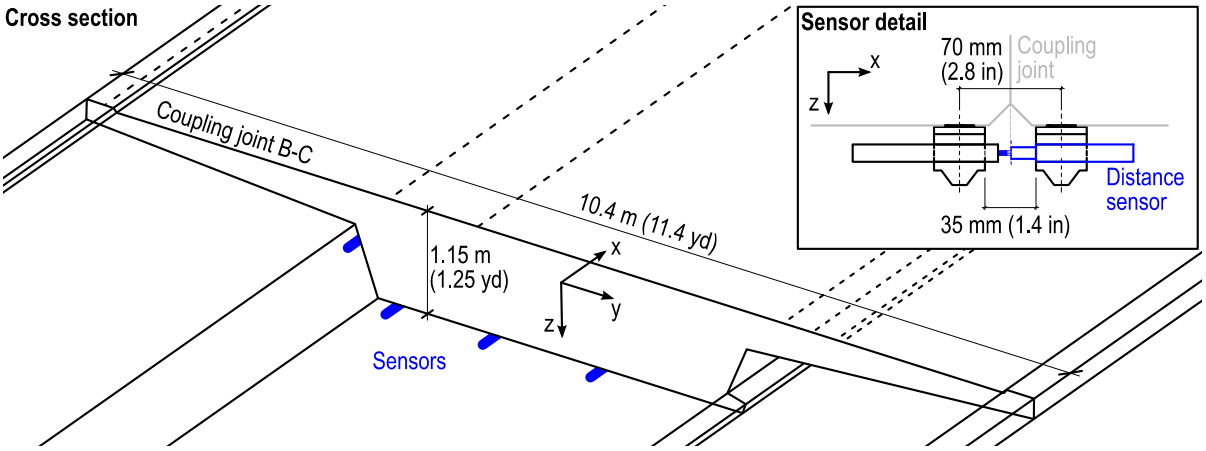

Fig. 17 —Cross section of coupling joint B-C with sensors and a detail of the application of the sensors

In the performed tests, two 26 t (26.7 US) trucks drove over the bridge one after the other or simultaneously on parallel lanes. The trucks also stopped at specific positions that had been determined beforehand from a numerical model. The stopping positions were chosen to maximise the relevant actions that were to be measured.

Fig. 18 —Two trucks driving over the bridge simultaneously

The measurement results of the performed test provide insight into the state of the coupling joints. The strains measured at the two coupling joints were much higher than those measured at reference point 2 where the bending moment is similar to that at the coupling joints. Fig. 19 shows a comparison of the results.

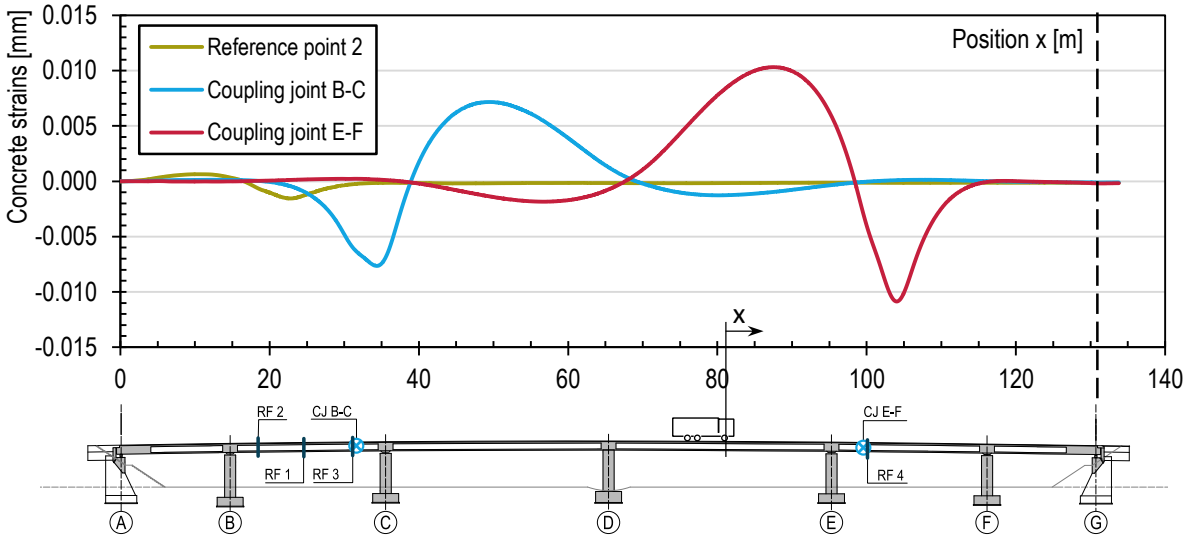

Fig. 19 — Concrete strains in the coupling in reference point 2 vs the position of the trucks

This indicates the presence of cracks in both coupling joints, which was expected. Because the coupling joints are also construction joints, no tensile stresses can be transferred across the joint via the concrete. A numerical model containing the whole superstructure was created to recalculate the test. In this model the superstructure was defined as beam-elements. Using this numerical model calibrated with the measured data (using mainly the deflections but also the strain-measurements), conclusions were drawn about crack depths and the stresses occurring in the tendons.

SUMMARY AND CONCLUDING REMARKS

This paper describes the current practice of load testing of existing and new built concrete bridges in Germany. Since 2000 a guideline is regulating loading tests, but this guideline is preferably applicated for load test of existing building structures. Despite the very good experiences in a very large number of load tests on building structures, load testing of bridges is still an exception. However time and opinions are changing since there are strong demands for extending the life time of existing concrete bridges. The German Guideline is a valuable basis for engineers to plan, execute and evaluate load tests, but no specific rules for load testing of bridges are yet defined. Therefor further research is necessary to define basic regulations for load tests of concrete bridges. The high value of load testing for the overall evaluation of the bearing characteristics of concrete bridges is demonstrated in the described examples.

REFERENCES

[1] Schacht, G.; Bolle, G.; Marx, S.: Loading Tests of Existing Concrete Structures – Historical Development and Present Practise. 4th International fib Congress, Prague, June 1 – June 4 2011, DVD.

[2] Zimmermann, H.: Einsturz einer Straßenbrücke bei Salez in der Schweiz, Centralblatt der Bauverwaltung (1884), S. 548–549.

[3] Stamm: Brückeneinstürze und ihre Lehren, Mitteilungen aus dem Institut für Baustatik, ETH Zürich, Zürich, Verlag Leeman (1952).

[4] Waldner, A.: Das Eisenbahnunglück bei Mönchenstein, Schweizerische Bauzeitung, Vol.17, Nr. 25, 26 und Vol.18, Nr. 1, 2, 3 (1891).

[5] https://en.wikipedia.org/wiki/Sydney_Harbour_Bridge: checked: 05/17/2017

[6] www.pictureaustralia.org

[7] DIN 1045 – Beton und Stahlbetonbau, Bemessung und Ausführung (Ausgabe 01.1972)

[8] Schmidt, H., Opitz, H.: Experimentelle Erprobung von Stahlbetonbauwerken in situ, 13. Kongress des IVBH in Helsinki, 6.–10.6.1988.

[9] TGL 33407/04 – Nachweis der Trag- und Nutzungsfähigkeit aufgrund experimenteller Erprobung, Fachbereichsstandard, November 1986.

[10] Steffens, K.: Experimentelle Traglastermittlung an Bauwerken – Grundlagen, Technik, Anwendungen; Schriftenreihe des Fachbereiches Bauingenieurwesen der Hochschule Bremen (1988), Heft 1.

[11] DAfStb-Richtlinie Belastungsversuche an Betonbauwerken, Ausgabe September 2000, Beuth Verlag GmbH, Berlin und Köln.

[12] Schacht, G.; Bolle, G.; Marx, S.: Belastungsversuche – Internationaler Stand des Wissens. Bautechnik 93 (2016) 2, S.85-97. DOI: 10.1002/bate.201500097

[13] DIN EN 1992. Design of concrete structures. 2012

[14] Marx, S.; Bolle, G.; Schacht, G.: Kapitel 3.2 – Bestandsaufnahme und Bestandsbewertung und Kapitel 7 – Bewertung der Tragfähigkeit auf Grundlage von Belastungsversuchen. In: Fingerloos, F.; Schnell, J.; Marx, S. (Hrsg.): Tragwerksplanung im Bestand, Betonkalender 2015.

[15] Schacht, G.; Bolle, G.; Marx, S.: Load Testing of Concrete Structures in Germany – General practice and recent developments. fib symposium 2017, Maastricht, 12-14 Juni 2017.

[16] Schacht, G.; Bolle, G.; Curbach, M.; Marx, S.: Experimentelle Bewertung der Schubtragsicherheit von Stahlbetonbauteilen. Beton- und Stahlbetonbau 111 (2016) 6, S. 343-354. DOI:10.1002/best.201600006

[17] Steffens, K.; Gutermann, M.: Entwicklung, Bau und Erprobung eines Belastungsfahrzeuges. Abschlussbericht, Hochschule Bremen, 2002.

[18] Gutermann, M.; Schröder, C.: 10 Jahre Belastungsfahrzeug BELFA. Bautechnik, 88 (2011) p. 199–204. doi:10.1002/bate.201110020

[19] Bretschneider, N.; Fiedler, L.; Kapphahn, G.; Slowik, V.; Technische Möglichkeiten der Probebelastung von Massivbrücken. Bautechnik, 89 (2012) p.102–110. doi:10.1002/bate.201100010

[20] Richtlinie für die Nachrechnung von Straßenbrücken im Bestand. BMVI. 2011

[21] Lantsoght, E.; van der Ven, C.; de Boer, A.; Hordijk, D.: Proof load testing of reinforced concrete slab bridges in the Netherlands, Structural Concrete, 2017. https://doi.org/10.1002/suco.201600171

[22] Lantsoght, E.; Yang, Y.; van der Ven, C.; de Boer, A.; Hordijk, D.: Ruytenschildt Bridge: Field and laboratory testing. Engineering Structures 128 (2016), p. 111-123.

[23] Busch, E.; Ehmann, R.; Steffens, K.: Spannbetonbrücke Baiersdorf über den Main-Donau-Kanal - Hybride Standsicherheits- und Gebrauchstauglichkeitsbewertung. Bautechnik 72 (1995) 3, S. 152-162.

[24] Schacht, G.; Piehler, J.; Müller, J.Z.A.; Marx, S.: Belastungsversuche an der historischen Gewölbebrücke über die Aller bei Verden. Bautechnik 94 (2017) 2, S.125-130 DOI: 10.1002 / bate.201600084

[25] Schacht, G.; Schwinge, E.; Krontal, L.; Hahn, O.; Marx, S.: Die Allerbrücke in Verden. In Jäger, W. (Hrsg.): Mauerwerkskalender, Ernst & Sohn, 2018.

[26] Marx, S.; Herrmann, R.; Wenner, M.; Schenkel, M.; Curbach, M. (Hrsg.): Monitoring an Talbrücken im Eisenbahnhochgeschwindigkeitsverkehr, Tagungsband des 23. Dresdner Brückenbausymposiums. Planung, Bauausführung, Instandsetzung und Ertüchtigung von Brücken. Dresden, 12. März 2013. Technische Universität Dresden, S. 131-152.

[27] Marx, S.; Beltran, R.; Wenner, M.: Long-term behaviour of integral concrete constructions subjected to axial internal forces induced by constraint, Fischer. O.; (Hrsg.) Proceedings of the 10th Japanese - German Bridge Symposium, Munich, Germany 16.-19 September 2014

[28] Wenner, M.; Marx, S.: Concrete slab track - bridge interaction and its impact on bridge design, Avraham N. Dancygier (Hg.): Proceedings of the fib Symposium. Engineering a concrete future: Technology, Modeling & Construction. Tel Aviv, Israel, 22-24 April 2013, p. 403-406.

[29] Marx, S.; Wenner, M.: Structural Health Monitoring (SHM) an der Scherkondetalbrücke: eine semi-integrale Eisenbahn-Betonbrücke, Beton- und Stahlbetonbau Spezial (2015), p. 2-8, Ernst & Sohn, 2015

[30] Wenner, M.; Lippert, P.; Plica, S.; Marx, S.: Längskraftabtragung auf Eisenbahnbrücken Teil 1: Geschichtliche Entwicklung und Modellbildung. Bautechnik 93 (2016) 2, p. 59-67. DOI: 10.1002/bate.201500107

[31] Wenner, M.; Lippert, P.; Plica, S.; Marx, S.: Längskraftabtragung auf Eisenbahnbrücken Teil 2: Hintergründe des Nachweises, Bautechnik 93 (2016) 7, p. 470-481. DOI: 10.1002/bate.201600034

DIAGNOSTIC LOAD TESTING OF CONCRETE BRIDGES, PRINCIPLES AND EXAMPLE

Joan Ramon Casas, Piotr Olaszek, Juliusz Ciesla, Krzysztof Germaniuk

Synopsis: The paper presents principles of diagnostic load tests of concrete bridges performed in Europe and one example of application from Poland. The common basis of the load testing techniques and methods were developed within the European Research Project ARCHES (Assessment and Rehabilitation of Central European Highway Infrastructure) and the main objectives and results of the project will be presented herein. Based on that, an example of application will follow.

The presented example of load tests is an evaluation of newly built reinforced concrete slab bridge. The bridge is a seven-span continuous structure with spans length of 14.05+18.03+15.31+15.63+18.97+18.60+14.34 m [553+710+603+615+747+732+567 in]. After construction, during cleaning the bottom surface of the structure many cracks were noticed in the tension zone. The process of bridge load testing was concentrated on the analysis of the cause of cracks appearing and estimation of the load carrying capacity of the bridge. The investigation range contained the following: tests of material properties, analytical calculations, visual examination of the bottom surface of the structure before, during and after load testing; measurements under test loading: deflection, selected cracks width and supports displacement. The final conclusions included the causes of crack appearing and recommendations for the future bridge service.

Keywords: diagnostic load testing, concrete bridges, cracks

INTRODUCTION

The Specific Targeted Research European Project ARCHES (Assessment and Rehabilitation of Central European Highway Infrastructure) was planned in response to an European Commission's call for proposals addressing the topic 'Design and manufacture of new construction concepts' of objective 'Sustainable Surface Transport' under the Thematic priority 'Sustainable Development, Global Change and Ecosystems' of the GROWTH part of the Sixth Framework Program of the European Union.

The increasing volume of European transport urgently required an effective road and rail system in New Member States (NMS) of the European Union (EU) and Central and Eastern European countries (CEEC). To bring this transport infrastructure up to modern European standards requires an immense investment – and therefore difficult to achieve in the medium term. New motorways will be required with many new bridges. Numerous existing bridges will need to be assessed, and a large portion of them improved or replaced.

The overall goal of Project ARCHES was to develop ways to raise the standard of the highway structures of NMS and CEEC to the level necessary for their full economic integration into the EU and for the future development of the Union. The works focused on the development of technologies and procedures for optimized conservation of highway structures, taking into account issues particular to the NMS. This was achieved by a global conceptual approach that can be summarized as Avoid, Prevent and Harden. Rehabilitation and replacement had to be as far as possible avoided by developing better safety assessment methods. Several assessment methods of existing bridges were analyzed within the Project, always on a wide European perspective, looking to the different methodologies and techniques used in the different European countries. Among others, load testing was one of the assessment methods investigated. One deliverable (Casas et al. 2009) reports on the work carried out in the task "*Load carrying capacity based on load testing results"* which main objective was to optimize bridge assessment by using load tests and/or computational analysis to find reserves in load carrying capacity of existing bridges. The report presents the proposed recommendations concerning the load testing possibilities in bridges with the objective of their safety assessment. The types of tests considered are: soft, diagnostic and proof load test. The recommendations are divided into two parts: 1) recommendations on the most appropriate type of load test according to the proposed objectives of the assessment and 2) recommendations on the use of test results for bridge assessment depending on the type of load test executed. As mentioned, according to the European background, 3 types of load testing were identified and categorized as follows:

1. The soft load test uses the actual traffic in the bridge as the loading source. Using a Weigh-In-Motion (WIM) system not only the main characteristics of exciting traffic are obtained, but also information about the structural behaviour of the bridge, through the calculation of experimental influence lines, dynamic amplification factors and load distribution to different structural members. In this way, the test is aimed to supplement and check the assumptions and simplifications made in the theoretical assessment. Therefore, the main objective is to optimise the structural model used for safety assessment. The execution of the test does not require the closure of the bridge to normal traffic. It is also shown in the report (Casas et al. 2009) how soft load test can be used to evaluate the characteristic total load effect of traffic action in a quite simple way, provided sufficient time data of traffic records are available.
2. Similar to soft load test, diagnostic tests serve to verify and adjust the predictions of an analytical model. However, in this case the level of load in the bridge is higher and introduced by different devices (trucks, water tanks, ballast…) with accurately measured weight. Normally the bridge is closed to traffic during the execution of the test to better control the relationship between the load level and the bridge response. The loading source may be static or dynamic. The following information can be obtained: experimental influence lines, dynamic amplification factors, load distribution, dynamic parameters (natural frequencies, mode shapes, damping)
3. In the case of proof load test, the aim is not to supplement and check assumptions and simplifications of the theoretical model (as in the case of soft and diagnostic tests), but to provide a complementary assessment methodology to the theoretical one. The aim of the test is not to up-date the parameters of an existing theoretical model, but to discover hidden mechanisms of response that cannot appear under "normal" levels of load, but that develop at higher ratios of load and may increase the bridge load capacity. For this reason, in such test, the load introduced in the bridge is relatively high and due to the risks of damaging the structure, this type of tests is restricted to bridges that have failed to pass the most advanced theoretical assessment or when such theoretical assessment is not possible due to the lack of bridge documentation. The objective of this test is to directly obtain the maximum allowable load in the bridge with a required safety level.

Based on the main characteristics of the different test types and the resulting data provided by them, the following recommendations were derived:

1) Due to its ease of application, the soft load test is particularly useful for:

1. Old bridges, with no drawings and no information about the design and construction details and about behaviour under loading. Longitudinal and transverse influence lines (distribution factors) can be obtained for normal traffic load.
2. Posted bridges, to check if the posting (limiting of the traffic loading) is justifiable or it can be released or removed.
3. Providing input data for efficient management of heavy vehicles with special permits.
4. To obtain experimental dynamic amplification factors to be used for the assessment of existing bridges under normal traffic
5. To the assessment of site-specific bridge characteristic total load (including dynamic effects) caused by traffic

2) Due to its test execution characteristics and the load level attained, the diagnostic load testing is particularly useful for:

1. Bridges where there are doubts on the analytical load rating model and where the model can or should be developed to be useful in the process of bridge load carrying capacity assessment
2. Bridges with sufficient data and information on as-built bridge details, dimensions and materials or, alternatively, sufficient data obtained through inspections and material testing. In this case, the test can confirm the obtained data.
3. Bridges with no limits concerning span length and deck width and static configuration, where there may be some troubles when applying soft load testing.
4. Bridges with some doubts about unintended composite action of bridge main or even secondary member, which could appear during testing with low load level (for example soft load testing), but can disappear at higher load ratios.
5. Bridges that should be assessed versus dynamic forces (earthquake, wind, vehicle collision, mining damage)

3) Proof load tests may be performed if documentation is not available and the effects of deterioration and/or damage cannot be evaluated in alternative ways. The use of such tests, due to the risks of collapse or of damaging essential elements of the structure, must be restricted to bridges that have failed to pass the most advanced theoretical assessment and are therefore condemned to be posted, closed to traffic or demolished. Therefore, the application of this type of test is quite exceptional, being the main candidates, old bridges with lack of documentation and bridges with high level of redundancy (robustness). Bridges that fall into those two categories are masonry arch bridges. If according to the bridge response and material, the failure could be sudden, without warning, proof load testing should not be used.

PRINCIPLE OF DIAGNOSTIC LOAD TESTS

Based on a survey carried out within the ARCHES Project, it was realized that many countries in Europe perform diagnostic load tests on new and rehabilitated bridges. The Deliverable D07 of ARCHES (Internet Database of Load Test Results and Analytical Calculations) contain information on the correlation between the real structure behaviour (load testing results) with corresponding results of analytical calculation of different types of bridges from different countries (available data from national resources and from other projects, including tests of bridges before putting them into service, assessment of load carrying capacity of existing bridges and load tests done for research purposes). The database of load testing results makes possible to correlate data on load testing with corresponding results of analytical calculation of different types of bridges. The database allows the end users, to judge quickly the behavior of the structure under the loading and suggest the structural assessment method to be used – computation analysis or load testing.

A diagnostic load test is also aimed to supplement and check the assumptions and simplifications made in the theoretical assessment. This type of test is looking for a better structural idealisation and appraisal of material properties and structural behaviour. Diagnostic tests serve to verify and adjust the predictions of an analytical model. Contrary to the soft load test, the bridge is closed to normal traffic and the applied load is at a level similar to the serviceability conditions or normal use of the bridge. As a consequence, extrapolation of the analytical models up-dated via diagnostic test to the assessment of bridge performance at the ultimate limit states is not feasible at all. There is no safe basis to extrapolate the results of tests carried out with fairly low levels of loading, unless the materials and their interconnections can be determined with a degree of certainty and some pattern of load carrying behaviour at advanced levels of loading has been established. As an example, several tests have

shown how the unintended composite action in slab on steel beams bridges gets lost when the level of load reaches the ultimate capacity of the bridge. Similar behaviour on the continuity through upper slab of simply supported spans made of precast concrete girders has been also detected (Casas et al. 2009).

Normally, diagnostic tests are classified according to the variation with position/time of the load applied to the bridge. Therefore, they are divided into: static (the load, a vehicle or a weight, is applied in fixed points), pseudo-static (a vehicle moves across the bridge at a crawl speed) and dynamic (the vehicle moves at full speed).

One of the main objectives of this type of test is the correct estimation of the traffic load distribution between the main carrying members. The tests provide useful information when structural models including grillage or finite element methods can not accurately predict behaviour due to uncertainties in member properties, boundary conditions and influence of secondary members. In the design of the test, it is important to assure the placement of the test load at various positions to determine the response in all critical bridge members.

The load level achieved in the test must be representative of serviceability conditions. It is recommended to achieve a load level corresponding to a 5-year return period. In practice, this means to raise the test load up to approximately 60 % of the characteristic live load present in the design code. It is recommended to never go beyond the 70 % of the design load or 100 % of the un-factored traffic load.

Two types of diagnostic load tests are possible: static and dynamic. Static tests are the main form of diagnostic load testing. The test load consists of stationery weights or loaded vehicles with known weight and axle configuration, which are placed at pre-selected locations to obtain the maximum load effect. In the case of road bridges, the natural way of loading is using vehicles. In the most cases of pedestrian bridges it is necessary to use weights. The most popular are concrete pavement slabs and bags or containers filled with water. The variation of static tests is pseudo-static. Loaded vehicle or set of vehicles (with known weight and axle configuration) move across the bridge at a crawl speed to produce the maximum load effect at each measurement point. Dynamic tests are an additional form of diagnostic load testing which is a supplement to static load tests. During dynamic tests the forced or free vibration are used to evaluate the performance of a structure. In the case of road bridges, the natural way of loading is using vehicles which move at different speeds (from minimal – usually 10 km/h [6.21 mph] to maximal which is possible to obtain or permitted). For the purpose of getting considerable free vibration the vehicle crossing of artificial surface irregularities or sudden stopping by braking are often used. In the case of pedestrian bridges dynamic tests consist of different behaviour of single or set of people: (jumping, running, rhythmical march, etc.)

According to the results of ARCHES, there are two ways to incorporate the results of the diagnostic static tests in the assessment process:

1.- By up-dating the structural model and calculation of the new bridge capacity (reliability index, load factor) based on the new model. The idea is to change the bridge properties (area, inertia, modulus of elasticity) in the way that the theoretical model matches as better as possible the results of the load test.
To this end, an acceptable match is considered to have been reached when the differences between the site-measured maximum deflections and the analytical values are within the following limits:

- +/- 10% for prestressed concrete and metallic bridges
- +/- 15 % for reinforced concrete and composite bridges

Once the model is up-dated, the assessment calculations are carried out using the revised model and they can be used in the recalculation of the bridge safety (reliability index, load factor)

2.- By direct calculation of the load capacity from the test results. In this case, it is assumed that the bridge assessment is carried out using the partial safety factor format and the load capacity is the value for which the rating live load should be multiplied to reach the failure limit state.

In the case of a diagnostic dynamic test, the results are usually a measure of stiffness rather than strength. The results may be used to validate the prediction of calculations. The structural model updating and calculation of the new bridge dynamic properties should be done together with the up-dating of the structural model in the static tests range. The other application of dynamic testing is a comparison of results over time that may be used to monitor any deterioration or serious damage to the structure. However, it should be noted that the modification of dynamic parameters may be not sufficient to detect damages. Variations of these parameters may be caused by changes of environmental conditions such as temperature or humidity. This effect has to be deeply considered when evaluating the results of a dynamic test. The importance of dynamic tests is caused by several additional reasons. For instance, earthquake response is dependent on bridge frequency and damping. Dynamic behaviour

and repeated stress oscillations may have big influence on fatigue assessment. The assessment of the bridge safety under these dynamic effects requires in many cases the execution of a dynamic test.

As an example of the European background regarding diagnostic load testing, the case of Poland is presented.

Diagnostic load testing in Poland

The origin of test loading comes from the necessity of investigating the ability of the bridge structure to carry the designed loads before starting operation. Load testing has been performed in Poland for a long time and relates to the tradition that obliged the designer to stand underneath the structure while the test was being carried out.
In case of reinforced and prestressed concrete bridges the Polish Norm (PN 1999) has been in force since 1999. And the Recommendations of General Director for National Roads and Motorways (GDDKiA 2008) were introduced in case of road structures. The Recommendations are aimed to determine the requirements, possibilities, conditions and results of carrying out test loads of bridge structures. They refer both to accepting new bridges before entering into service and assessing the load capacity of old existing structures that have been in service for a long time. The Recommendations refer to static and dynamic load tests, to all types of structures. In case of reinforced and prestressed concrete bridges a level of static load was recommended to be applied during carrying out acceptance tests so that they achieve a load level from 75% to up to 100 % of the characteristic live load present in the design code. Positive results of an acceptance static load test carried out on such structures should guarantee that the measured values of the elastic deflection are lower or equal to the calculated values. In Poland, the load levels of the diagnostic load tests are high (close to design loads) and the significant values of permanent deflection often appear during the first loading of the bridge (during the acceptance test). For this reason, according to the Polish regulations, the permanent deflection (after the load testing) in relation to total deflection value should not exceed 20% in reinforced concrete structures and 10% in prestressed concrete structures.

Presently (in 2017) the works on introducing document DAB-15 2017 are being finalized by the Polish Centre for Accreditation. Document DAB-15 has been drawn up in order to harmonize the approach to the accreditations of laboratories which carry out test loads on road and railway bridges in the context of the requirements defined in the standard PN-EN (2005). This document harmonizes the scope and method of acceptance of static and dynamic load tests carried out after completion or alteration of a structure. The document appendices determine models of the scope of accreditation as well as the minimum scope of tests programs for various types of bridge structures: railway bridges, road bridges and footbridges.

EXAMPLE OF TESTS – INTRODUCTION

The example presented herein refers to the estimation of the load carrying capacity of a newly built reinforced concrete slab bridge. At the last stage of construction, during cleaning the bottom surface of the load-carrying structure slab, before applying anti-corrosion protection, many cracks were noticed which were concentrated at the 1/3 length of each mid-span. The distance between the cracks was approximately 0.20 m [8 in]. Besides the crack concentration areas, single cracks were also noticed on the slab and the cantilevers from below. The majority of the cracks go across the whole width of the slab. They are perpendicular to the structure's length. The load tests and additional examinations were aimed to verify the load capacity and serviceability of the cracked bridge. Other examples where the execution of a diagnostic load test allowed to identify serviceability and safety concerns in 3 Polish bridges can be found in (Olaszek et al. 2013). Contrary to the majority of cases of diagnostic load tests presented in literature, where the experimental results (deflections, strains) are very close or lower than the predicted ones and for this reason such tests are expected to validate the existing structure, in the cases presented there, it is shown how the experimental results differ considerably from the expected ones and this allowed to obtain the causes of the bridge malfunction.

STRUCTURE DESCRIPTION

The structure under examination is a 7-span continuous reinforced concrete bridge curved in plan. Its total length is 114.93 m [4 525 in] and the span lengths are 14.05+18.03+15.31+15.63+18.97+18.60+14.34 m [553+710+603+615+747+732+567 in]. The total width is 10.64 m [419 in]. The load bearing structure of the bridge is made from a reinforced concrete slab of 0.90 m [35.4 in] in thickness. The slab is 5.93 m [233.5 in] wide and it has cantilevers of 2.30 m [90.6 in] width on each of both sides. There is a carriage road of 6.00 m [236.2 in] in width and a walkway of 3.28 m [129.1 in] in width designed on the structure. The external supports are made as bridge abutments, while the intermediate supports as double columns of circular cross-section of 1.00 m [39.4 in] in diameter. Figure 1 presents a general view of the bridge.

Figure 1 – Bridge views after applying anti-corrosion protection and putting into service: *on top*: from the support side No 1; *bottom*: from the support side No 8 (support numbering is also presented at Figure 3).

At the last stage of construction the cracks were noticed on the lower slab surface of the all spans of the bridge. The cracks on the lower bottom of the slab became clearly visible after it was mechanically cleaned before applying anti-corrosion protection. During the cleaning the crack edges were exposed and the measured on the concrete surface (with broken off edges) were approx. 2.0 mm [0.079 in]. On spans: 1-2, 2-3, 4-5, 5-6 and 6-7 the most cracked areas are in about 1/3 length in the middle of each span. On spans: 3-4 and 7-8 the length of the most cracked areas is smaller. The average crack spacing in the most cracked areas is approximately 0.20 m [8 in]. In less cracked areas the average crack spacing is approx. 1.5 m [59.1 in]. On the upper surface of the slab single cracks were noticed over pillars 5, 6 and 7. Figure 2 presents photos of the cracked surface and Table 1 shows selected results of the crack width measurements. The crack widths measured on spans 7-8, 6-7 and over pillar 7 exceed the permissible crack width which is 0.3 mm [0.012 in] (according to the relevant standard (PN-EN 2008).

Figure 2 – Views of the cracks on the bottom surface of the slab perpendicular to the span 6-7; *right*: close-up view of an open crack – crack edge damage is visible.

Table 1 – Results of cracks width in-site measurements on most cracked bridge elements

Bridge element	Crack width		
	Min value (mm)	Max value (mm)	Average value (mm)
Span 7-8	0.3	0.5	0.37
Span 6-7	0.3	0.5	0.44
Span 5-6	0.1	0.5	0.29
Cantilever over support 5 (bottom surface)	0.2	0.2	0.20
Slab over support 7 (top surface)	0.3	0.4	0.37
Span 1-2	0.1	0.3	0.20

[1 mm = 0.0394 in]

THE INVESTIGATION RANGE

Because of the observed cracks, the investigation was aimed to determine the reasons of their appearance and to verify the load capacity and serviceability of the cracked bridge. The carried out tests, included:

- laboratory test,
- load testing:
  - analytical calculations,
  - visual examination of the surface of structure before, during and after load testing,
  - deflection measurements of all spans,
  - measurements of selected cracks width openings,
  - measurements of supports displacement,
- estimation of the load carrying capacity of the bridge.

Figure 3 presents the scheme of the bridge and deflection measurement points location.

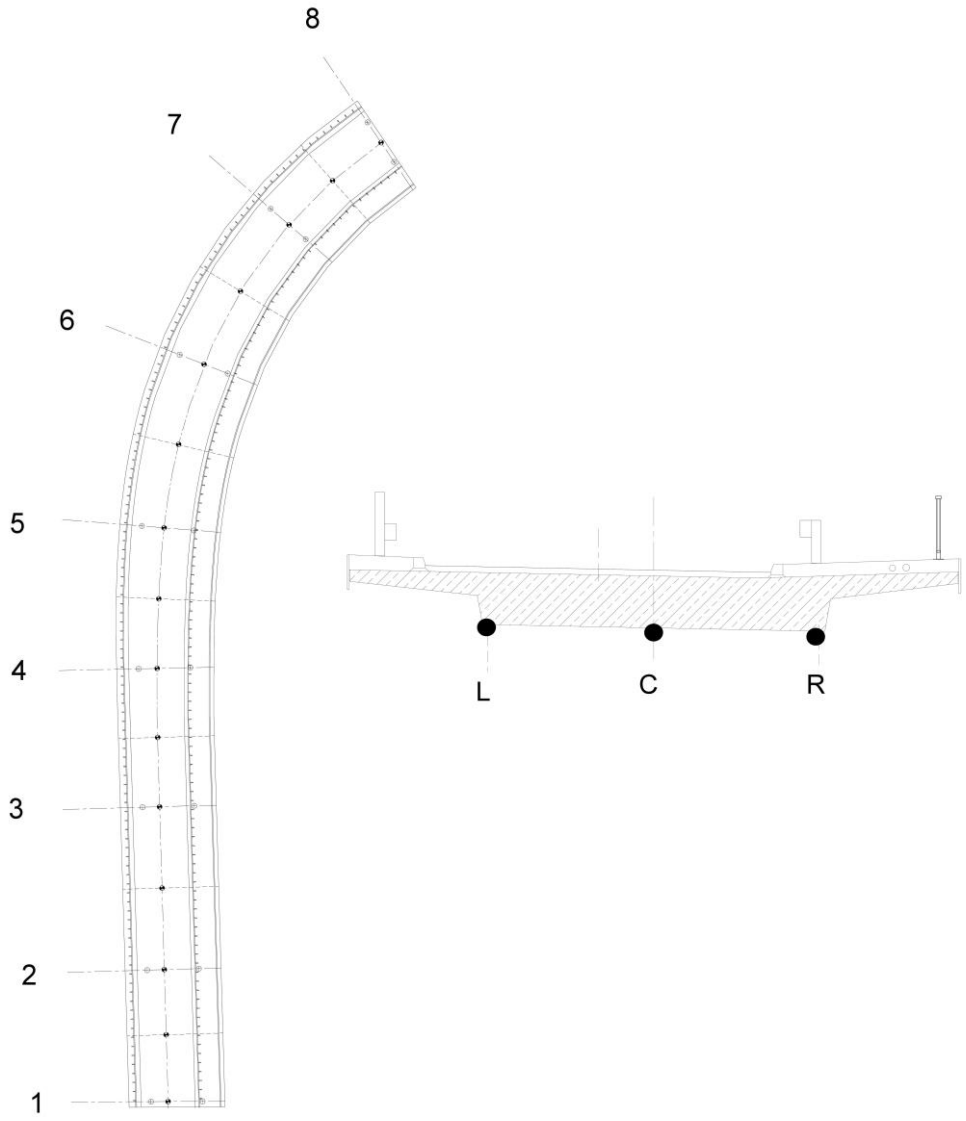

Figure 3 - The scheme of the bridge and deflection measurement points location: *left*: top view; *right*: cross-section view with measurement points location: L - left, C - centre and R - right.

Laboratory tests

The laboratory tests were carried out on concrete boreholes of Ø 100 mm [3.937 in] and Ø 150 mm [5.906 in] in diameter taken in selected spans. The boreholes were perpendicularly to the slab side surface, of the half thickness of the load-bearing slab (Figure 4). Depth of all cracks noticed in the boreholes are as high as 0.40 m [15.8 in] from the lower slab surface. In case of some boreholes it was observed that the cracks go as far as the whole length of a borehole (about 0.45 m [17.7 in]), which means that the concrete in the slab has cracked in the whole tension zone, probably almost up to the neutral axis of the cross-section. The cracks widths were measured in places where the edges were not damaged. The results of the crack width measurements at different depths are presented in Table 2. The crack widths do not exceed the permissible crack width which is 0.3 mm [0.012 in] according to the norm (PN-EN 2008).

On the basis of the concrete boreholes tests, the following concrete examination results were obtained:

- compressive strength of concrete f_{cm} = 58.0 MPa [8412 psi]
- modulus of elasticity of concrete E_c = 39.6 GPa [5743 ksi]

Figure 4 – Cracks width laboratory measurements at concrete borehole: *left:* crack at drilling place; *right:* crack at borehole.

Table 2 – Results of crack width laboratory measurements on the concrete specimen

Place of concrete specimen	Crack width		
	Min value (mm)	Max value (mm)	Average value (mm)
Face surface	0.1	0.3	0.19
Reinforcement cover	0.1	0.2	0.13
In the depths of the specimen under the reinforcement	< 0.05	0.2	0.12

[1 mm = 0.0394 in]

Load testing

Load tests were preceded by a numerical analysis. Calculation of the deflection values were made in two variants: for the structure with un-cracked and cracked elements. In the first stage, the structure was divided in un-cracked finite elements with their corresponding geometrical and boundary conditions. For this stage, calculations were performed in the linear-elastic range. A numerical model of the structure was made using its real shape and dimensions and using concrete parameters obtained in laboratory tests. In the second stage, the calculations were executed, using the method taken from the Polish standard (PN 1992). In this method, the stiffness of the cracked element is calculated based on its shape and the percentage of existing reinforcement. The method has been confirmed by numerous experimental tests. In both cases, the secondary stiffening elements as parapets and sidewalks were taken into account

Static and dynamic load tests were carried out. The static load testing was carried out with the anticipation of the load for all the spans for the maximum span moment and on the supports No. 3 and 7 for the maximum support moment.

A set of four-axle trucks of an average total weight of 39,370 kg [86,796 lb] each was used in the load testing. The maximum level of load test ranged from 70 % for spans No 3-4 and 4-5 to 90 % for span No 5-6 in proportion to the effect of the standard characteristic load. The level of load test for the support cross-sections ranged from 84 % over the support No. 7 to 92 % over the support No.7 in proportion to the effect of the standard characteristic load.

During the static load tests of the superstructure, the vertical displacements and support settlement were measured. In case of the most cracked spans 2-3, 5-6 and 6-7 a detailed inventory of the cracks was made and detectors to measure the selected cracks width were installed (Figure 5). They were measured with inductive transducers with a computer registration system. It was applied continuous monitoring of deflection with the sampling rate of 5 Hz.

The displacements of supports were measured by using the digital level. Thanks to the continuous monitoring of the displacements it was possible to monitor the process of stabilization of the test results during and after applying a load to the bridge. Thus, in this way it is possible to minimize the error of obtaining the elastic and permanent values of the measured quantities, according to the methodology presented in (Olaszek et al. 2016). During the dynamic load tests only the vertical displacements of spans were measured. The same set of inductive transducers with a computer acquisition system was used with the sampling rate of 200 Hz.

The static load tests started from the most cracked spans. In this way the first span to be examined was the span 5-6. It was planned that, if the effect of the loads on the first or second span had been negative because of excessive displacements or cracks, the load would have been stopped and no other span would have been loaded. In the case of those spans, the trucks were placed on the spans one after another. In this way, once a vehicle was placed on the span, the measured quantities were analyzed and next the decision of placing or not another vehicle could be taken.

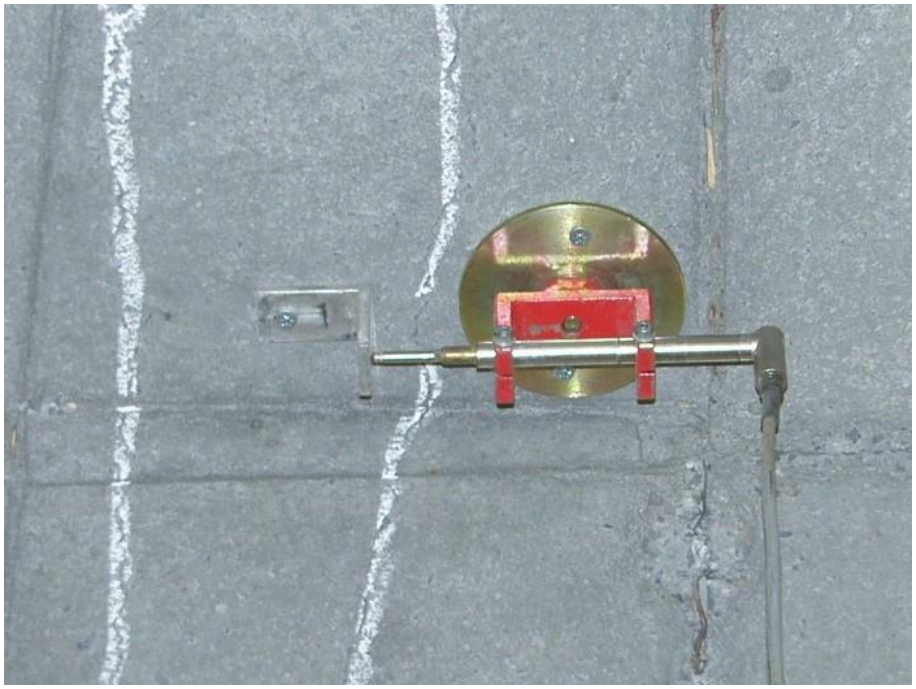

Figure 5 – Preparation of the bridge for the tests: *on top*: span 2-3 visible inductive sensors to measure the vertical displacements and cracks marked on the structure; *bottom*: close-up view of inductive sensor to measure the crack width (cracks are marked on the structure).

During the load testing of the first most cracked spans no abnormal behaviour of the structure was observed. In each stage of the load the displacement quantities stabilized relatively fast, and after removing the load no excessive permanent values were registered. Figure 6 presents time-history of displacement during loading of span 5-6, and Table 3 presents the values of registered total deflections and the values of permanent deflections.

The observations made during the load testing as well as successive visual examination did not show any other damage in the tested structure which might result from the load tests. No increase in the length, width or number of the cracks was observed. We should realize that the measurements of the cracks width with the use of inductive

gauges contain two components: the change in crack width and the strain of the concrete within the measuring basis. After taking into account the strain of the measurement basis the change of crack width during the load test was not higher than 0.013 mm [0.0005 in]. The permanent values of the width change after the load tests were below 0.005 mm [0.0002 in], which is close to the value of the measurement precision. Figure 7 presents the time-history of the crack width evolution in span 5-6 during the tests.

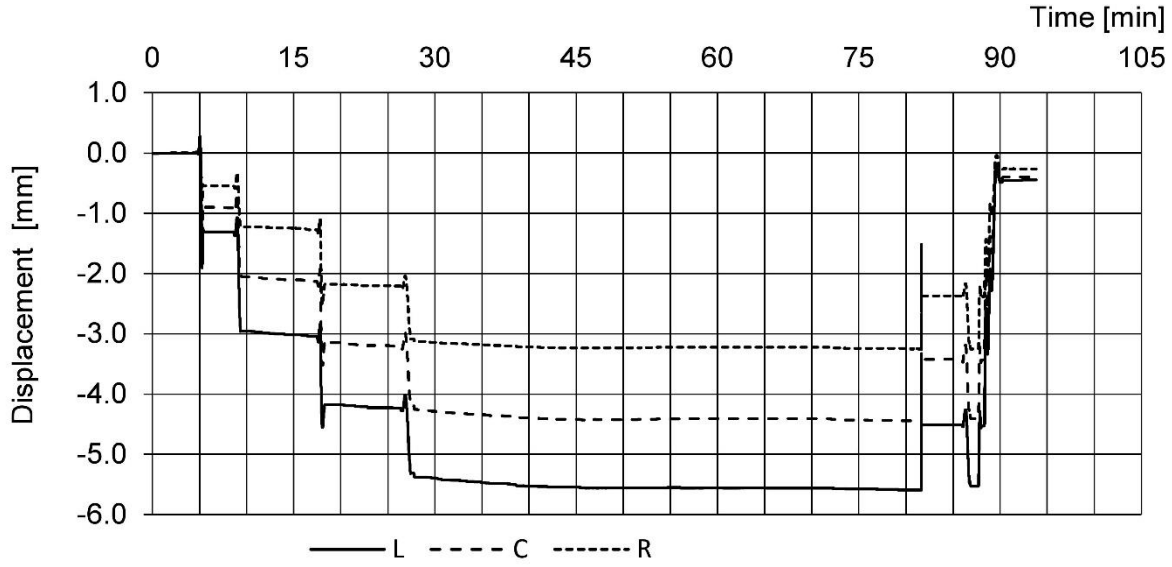

Figure 6 - Time-history displacements during load testing at span 5-6 in three lateral locations: L - left, C - centre and R - right (see Figure 3) [1 mm = 0.0394 in].

Table 3 - Values of recorded total and permanent deflections in percentage of total deflections during load testing of individual spans.

Span	Total deflection [mm]		Permanent deflection relative to total value [%]	
	Max	Min	Max	Min
5-6	-5.40	-3.14	7	8
6-7	-4.55	-2.61	6	5
2-3	-4.59	-3.61	4	5
7-8	-2.37	-1.18	6	4
1-2	-2.28	-1.54	7	5
3-4	-2.51	-1.82	4	3
4-5	-2.86	-1.95	5	5

[1 mm = 0.0394 in]

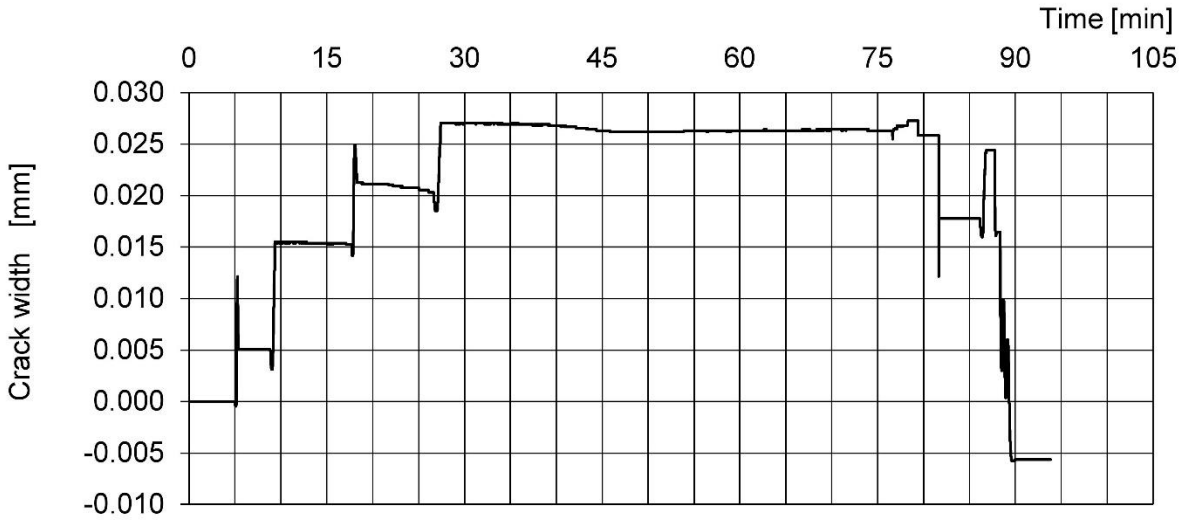

Figure 7 - Time-history of crack width increase during load testing at span 5-6 [1 mm = 0.0394 in].

During the dynamic load test the span deflections were measured. An example of the time-history of the measured span deflections is presented in Figure 8. The structure is characterized by a low vibration level and substantial vibration damping. No other adverse effects, such as fluttering or resonance, were observed).

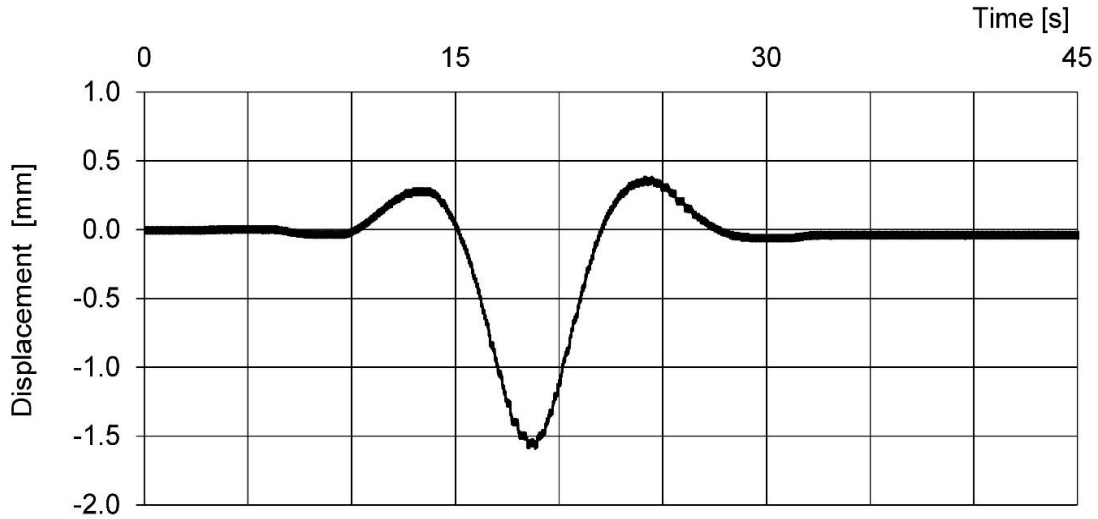

Figure 8 - Time-history displacement of span 5-6 during dynamic load testing – truck passage with 30 km/h [18.64 mph] speed [1 mm = 0.0394 in].

Estimation of the load carrying capacity of the bridge

The experimental elastic deflections were compared to the calculated deflections of the two assumed models: with and without cracks on the concrete taken into consideration. The results of the analysis of each span at various points of most loaded cross-sections are presented in Table 4.

The measured elastic deflections ranged from 50 % to 84 % of the deflections calculated for the model with cracked cross-section. Additionally, in case of the external spans 1-2 and 7-8, the measured elastic deflections did not exceed 99 % in comparison with calculated values using the model with un-cracked cross-sections.

In case of the loads over the supports the measured elastic deflections did not exceed 109% of the values calculated using the model with non-cracked cross-section and 69% using the model with cracked cross-section.

This means that values of measured deflections are much closer to the values calculated for the model with un-cracked elements than to the cracked model. As a result, we can draw the following general conclusions from the comparison between measured and calculated values:

- influence of cracks on the stiffness of the tested structure seems not to be very significant,
- calculated values by the method taken from the Polish standard (PN 1992) for the structure in cracked stage seem to be overestimated,
- On the basis of the permanent deflections, one can conclude that the structure worked within the elastic range.

Table 4 - Comparison of experimental and theoretical deflections calculated with the two assumed behavior models: with and without cracks on the concrete taken into consideration. The results are presented together for spans with similar behaviour.

Span	Measured elastic deflection/ calculated deflection [%]			
	No cracks in the model		Cracks in the concrete	
	Min	Max	Min	Max
2-3	108	112	70	73
3-4	100	111	60	66
4-5	112	115	61	62
5-6	95	119	66	84
6-7	88	107	62	75
1-2	86	99	53	61
7-8	77	98	50	64

Additional shrinkage tests were performed in the concrete mix used in the bridge. Four samples were tested, two of them were properly stocked, and the other two were unprotected before drying. The first change in sample lengths occurred after 3 hours for the unprotected concrete and after 7 hours for protected concrete. It was found that unprotected concrete after 12 hours of concrete pouring had more than 3 times the plastic shrinkage of the protected concrete. The final value of shrinkage of concrete after 90 days was pointed out to 0.57 mm/m [$0.57*10^{-3}$ in/in] for the protected concrete and 0.91 mm/m [$0.91*10^{-3}$ in/in] for unprotected one. These tests have confirmed the importance of concrete pouring, including the avoidance of early evaporation of water and shrinkage development. Minor mistakes made in the care of concrete in the initial period of hardening may result in early cracking of concrete

Therefore, the origin of the observed cracking can be due to the following facts:

1.- Incorrect application of measures to avoid early evaporation and shrinkage after concrete pouring
2.- The use of large diameters (∅ 28 mm [1.102 in]) for the reinforcing bars placed to resist the bending moments, jointly with the important concrete cover (56 mm [2.205 in]) and the absence of additional reinforcement to control crack width

These 2 facts were the origin that total cracking in reinforced concrete due to the shrinkage and the bending moment due to permanent loads after formwork removal, was not spread along the bridge causing many cracks of very small size, but a reduced number of very large cracks.

According to the design, calculated maximum values of the elongation ε_s of steel and concrete cover under dead load in the most loaded spans are:

- span 2-3 $\varepsilon_s = 0.54$ ‰
- span 5-6 $\varepsilon_s = 0.66$ ‰
- span 6-7 $\varepsilon_s = 0.55$ ‰
- span 7-8 $\varepsilon_s = 0.71$ ‰

These values of ε_s together with shrinkage of concrete show a possible cause of cracking after removing the formwork, because of the interaction of shrinkage and flexural work of the structure. Additionally, it was investigated whether they had occurred formwork settlement after concreting of the bridge, or extremely heavy

trucks crossed the bridge before the tests. In both cases, the answer was negative, and these events cannot be the cause of observed cracks.

It seems, then, that the origin of the observed damage was in the design stage, as the reinforcement had to be designed in order to have a crack width within the allowable limits. The serviceability limit state of cracking was not properly checked. However, the load test demonstrated that the bridge response is stil valid for operational loads and strengthening is not necessary. The only action to be undertaken in the bridge is to fill and seal the cracks in order to avoid durability problems in the future and propose a surveillance programme during the first years of the bridge operation.

CONCLUSIONS

The presented herein load test is an example of examination which made it possible to approve the structure to be put in service without limitations despite numerous doubts concerning the important cracking. At first suspicion, the location of the cracks, corresponding to locations of high flexural effects, would point to gravity loads (permanent loads plus live load) as the main cause of damage rather than shrinkage. The load test was carried out just after the finishing the bridge and before the opening to traffic. An exceptionally heavy load crossing the bridge before the tests was excluded, because after completion of the construction works practically there was no access to the bridge. The execution of a diagnostic load testing supported with additional material tests allowed to validate the constructed bridge without initial repair or strengthening and only some special short-term actions were foreseen. It was identified the high value of the concrete shrinkage, jointly with and incorrect checking of the serviceability limit state of cracking and the bending moments due to the permanent loads as the three effects provoking the observed damage. Because of the considerable area affected by cracking in the tested structure, a special maintenance programme was recommended. It was advised to monitor vertical displacements in half of span and support cross-sections of the structure using precise leveling. Benchmarks should be made on the slab. In the first year, measurements should be carried out every 3 months, in the next years the period is extended to 6 months. So far, results of the vertical displacements monitoring show that the existing cracks did not affect the serviceability and safety of the bridge. After one year, the measured vertical mid-span deflections did not exceed the monitoring accuracy value (1-2 mm [0.039-0.079 in]. However, after three years of the bridge exploitation, in case of any doubts concerning the proper behaviour of the structure, it is recommended to examine the elastic range of the structural behaviour under a new load test.

ACKNOWLEDGMENTS

Special thanks are due to all colleagues from Bridge Structure Research Laboratory for their active participation in the presented load test. The authors extend their thanks to colleagues from Concrete Division for their support in Laboratory tests and from Bridge Research Center, Branch "Kielce" for their support in analytical calculations.

REFERENCES

Casas JR, Znidaric A, Olaszek P (2009) Recommendation on the use of soft, diagnostic and proof load testing. Deliverable D16. EU project ARCHES. Brussels. (available on line at http://arches.fehrl.org).

DAB15 (2017) Accreditation of laboratories performing load testing of bridges. Polish Centre for Accreditation

GDDKiA (2008) Recommendations for the load testing of road bridges. General Directorate for National Roads and Motorways (in Polish)

Olaszek, P., Casas, J. R., & Swit, G. (2016) Some relevant experiences from proof load testing of concrete bridges. In Fifth International Symposium on Life-Cycle Civil Engineering (IALCCE 2016), pp. 1092-1099.

Olaszek, P., Lagoda, M., Casas, J.R. (2014) Diagnostic load testing and assessment of existing bridges. Examples of application". Structure and Infrastructure Engineering, Vol. 10, N.6, pp. 834-842.

PN-91/S-10042 (1992) Bridges - Concrete, reinforced concrete and prestressed concrete structures - Design (in Polish)

PN PN-/S-10040 (1999) Reinforced, prestressed and concrete bridges. Specifications and technical testing (in Polish)

PN-EN ISO/IEC 17025 (2005) General requirements for the competence of testing and calibration laboratories

PN-EN 1992-1-1 (2008) Eurocode 2: Design of concrete structures - Part 1-1: General rules and rules for buildings (in Polish)

Joan Ramon Casas is a Professor of Bridge Engineering at the Technical University of Catalonia (UPC-BarcelonaTech). He is the Secretary General of IABMAS (International Association for Bridge Maintenance and Safety). His research interests include bridge safety and assessment, bridge management and quality control of existing bridges, structural health monitoring of bridges and static and dynamic testing.

Piotr Olaszek is an Associate Professor at Road and Bridge Research Institute in Warsaw - Poland. He is a Head of Bridge Structures Research Laboratory at Bridge Division. He graduated from Fine Mechanics Faculty of Warsaw University of Technology and was awarded with PhD in mechanical engineering. He was awarded with Habilitation in Civil Engineering. His research interests include load testing and monitoring of bridges, measurements techniques and dynamics.

Juliusz Ciesla is an Associate Professor at Road and Bridge Research Institute in Warsaw – Poland. He is a Head of Structures Team at Concrete Division. He was awarded with PhD in Civil Engineering. His research interests include concrete and prestressed concrete structures, strengthening of existing structures by external cables, testing of bridges.

Krzysztof Germaniuk is an Assistant Professor at Road and Bridge Research Institute in Warsaw – Poland. He is working in Bridge Diagnostics & Repairs Unit at Bridge Division. He was awarded with PhD in in Civil Engineering. His research interests include concrete structures, testing of concrete structures.

Assessment and Loading to Failure of Three Swedish RC Bridges

Jonny Nilimaa, Cristian Sabau, Niklas Bagge, Arto Puurula, Gabriel Sas, Thomas Blanksvärd, Björn Täljsten, Anders Carolin, Björn Paulsson, and Lennart Elfgren

Synopsis: Current codes often underestimate the capacity of existing bridges. The purpose of the tests presented here has been to assess the real behaviour and capacity of three types of bridges in order to be able to utilize them in a more efficient way.

The three studied bridges are: (1) Lautajokk – A one-span trough bridge tested in fatigue to check the shear capacity of the section between the slab and the girders; (2) Övik – A two span trough bridge strengthened with Near Surface Mounted Reinforcement (NSMR) of Carbon Fibre Reinforced Polymers (CFRP) tested in bending, shear and torsion; and (3) Kiruna – A five-span prestressed three girder bridge tested to shear-bending failures in the girders and in the slab.

The failure capacities were considerably higher than what the code methods indicated. With calibrated and stepwise refined finite element models, it was possible to capture the real behaviour of the bridges. The experiences and methods may be useful in assessment and better use of other bridges.

Keywords: Ultimate load carrying capacity, bridges, full scale testing to failure, shear, bending, torsion, bond, assessment, strengthening, reinforced and prestressed concrete

INTRODUCTION

Assessment of the load-carrying capacity of existing bridges is an important task. It can be used to check if a bridge is still fit for fight or if the allowable loads must be reduced or if they may even be increased. Three bridges in Sweden are presented here. They have been tested to failure and assessed using standard code models and advanced numerical methods.

The starting point was the desire in the 1990ies of the Swedish railway authorities to increase the allowable axle load from 25 ton (57 kips) to 30 ton (68 kips) on the 500 km (310 miles) long iron ore line in northern Sweden. The goal was to be able to carry heavier wagons with more iron ore and thus reducing transportation costs. Preliminary assessments showed that the concrete fatigue capacity of many of the bridges would be jeopardized. However, the senior authors of this paper were convinced that the codes were conservative in this respect, so they organized the testing of a decommissioned bridge, see further below. The results were very positive and the allowable axle load could be raised after minor improvements (Paulsson et al.1996, 1997). The experience initiated a European Research Project "Sustainable Bridges" 2003 –2007 (Olofsson et al. 2005, Sustainable Bridges 2007). In the project another bridge was tested, see below.

The results from the tests may help to make more accurate assessments of similar existing bridges. Full scale tests may bring up necessary information on the real structural behaviour, detect weak points in the structure and provide knowledge on how to model the bridge in a correct way. A survey of 30 concrete bridges tested to failure worldwide, (Bagge et al. 2017b), come to the conclusion that the final failure often was hard to predict; it was due to shear instead of flexure in ¼ of the cases; boundary conditions were not always understood correctly; and bridges usually had a higher capacity than what was predicted, (Plos et al. 1990, 1995, Täljsten, 1994).

The assessment procedure of a bridge can effectively be carried out in three levels according to Figure. 1. The procedure is based on (Schneider 1964, 2017, Sustainable Bridges 2007, UIC Code 778-4 2009, ISO 16311-2 2014 and Paulsson et al. 2016). Further refinements in Phase 3 have been proposed by (Plos et al. 2016) and (Bagge 2017) and examples are given in e.g. (Wang et al. 2016).

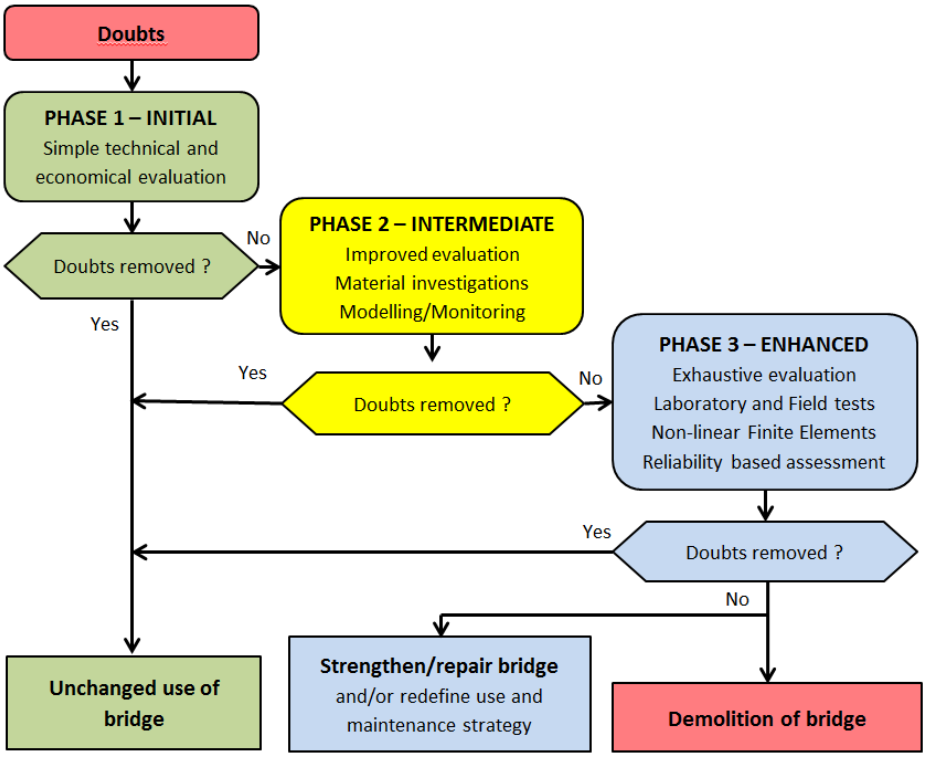

Figure 1 - Flow chart for the assessment procedure of a bridge with three phases. Based on (Schneider 1994, 2017, Sustainable Bridges 2007, UIC Code 778-4, 2009, ISO 16311-2,2014 and Paulsson et al.2016).

LAUTAJOKK TROUGH BRIDGE – FATIGUE 1996

Background

The railway line between Luleå and Narvik in northern Sweden and Norway was built 1884-1902 to transport iron ore from the mines in Kiruna and Gällivare to the harbours in the Baltic Sea and the Atlantic Ocean. Originally, the line was designed for an axle load of 14 ton (≈ 140 kN = 32 kips). In 1960 it was raised to 25 ton (≈ 250 kN = 57 kips) and in the 1990ies there was a wish to increase it to 30 tons (≈ 300 kN = 68 kips). An investigation was carried out regarding the capacity of the bridges along the line and as part of that, a decommissioned bridge from Lautajokk was transported to Luleå University of Technology and tested for fatigue; see Figures 2 and 3. According to the codes, the fatigue capacity of the slab was too low in many of the bridges (Paulsson et al 1996, 1997, Thun et al. 2000). The tested bridge was rather small and had a length of 7 m (23 ft) and a height of 1 m (3.2 ft).

Figure 2 - Full scale fatigue test of a 29 year old railway trough bridge at Luleå University of Technology (Paulsson et al. 1996, Thun et al. 2000).

Experimental Program

The bridge was loaded with 6 million cycles with an axle load of 1.2×300 = 360 kN (82 kips) (including a code dynamic load factor of 20%). The mid-point deflection is given in Figure 4. Its increase with time is mostly due to creep in the concrete. No notable damages were observed and only hair line cracks appeared in the bottom of the slab. Finally, the bridge was loaded to the maximum capacity of the jacks, 875 kN (1,995 kips), see Figure 4b. A beginning of yielding in the reinforcement can be seen but the ultimate load capacity was probably slightly higher taking some strain hardening in the reinforcement into consideration.

The design concrete compressive strength was 40 MPa (5.8 ksi). However, due to coarse grinding of the cement the strength increased over time. After testing, 16 concrete cores were drilled, tested and found to have a compressive strength f_{cc} = 72.6 MPa (10.5 ksi) (mean of 6 tests) in the slab and f_{cc} = 81.2 MPa (11.8 ksi) (2 tests) in the beams and

a tensile splitting strength (4 cylinders) f_{cspl} = 4.4 MPa (638 psi) and a uniaxial tension strength (4 cylinders) f_{ct} = 2.9 MPa (421 psi).

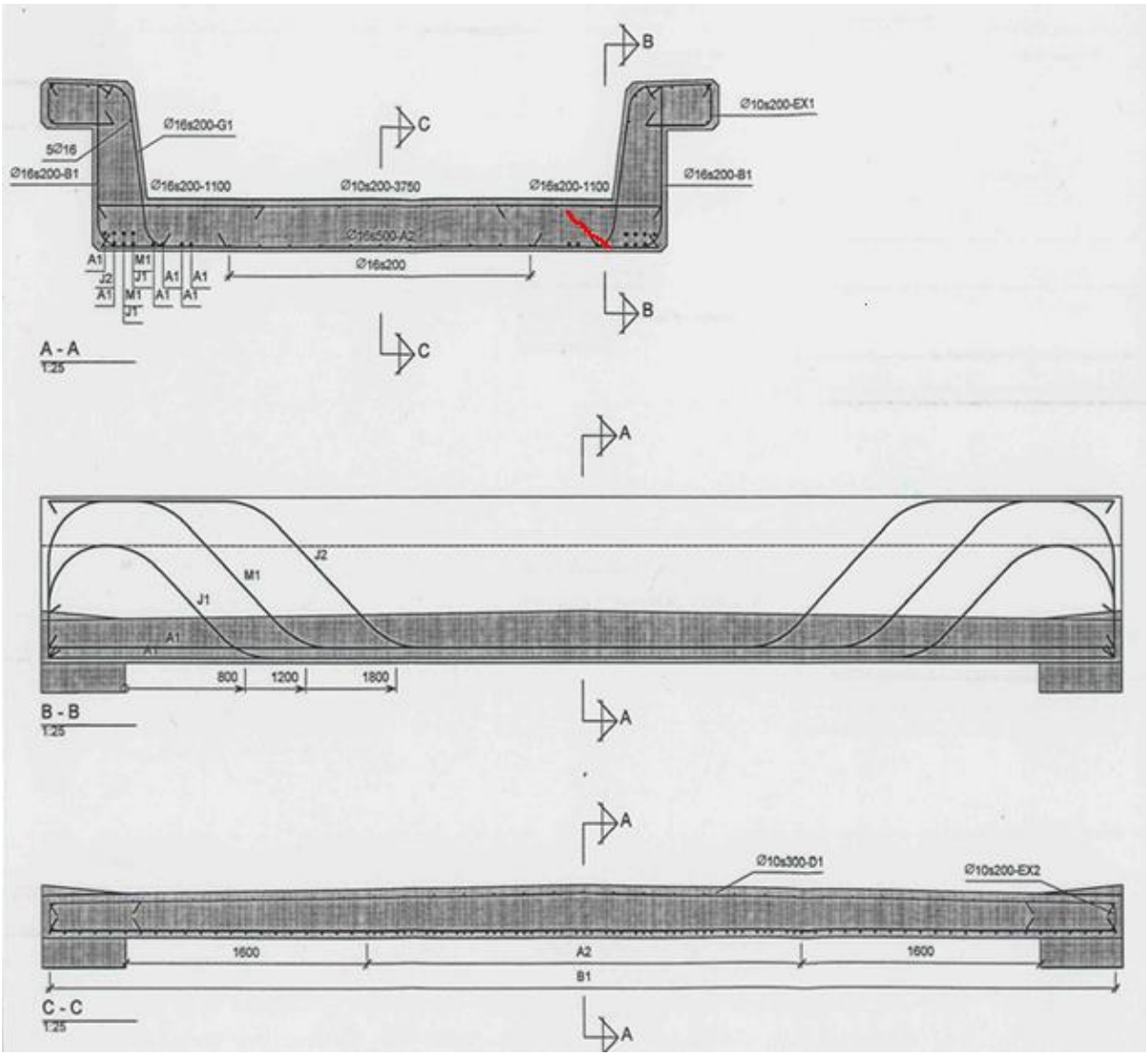

Fiure 3 - Cross section A-A (top) and elevations B-B and C-C (bottom) of a railway trough bridge tested at Luleå University of Technology (Paulsson et al. 1996, Thun et al. 2000). In the slab there is no vertical reinforcement so the shear transfer to the beams has to be taken by the concrete. A feared – but not materialized - shear crack is indicated in red close to the right support of the slab in section A-A. (1000 mm = 39 in., ϕ16 = #5).

Assessment versus test results

The tests showed that the fatigue capacity of the bridge was much higher than what was predicted by the codes, (Thun et al., 2000). Critical was the shear capacity in the connection of the slab to the longitudinal beams with no shear reinforcement in the slab. According to the Model Code (fib MC 2010, 2013) the number of possible shear stress cycles, N, can be written as a function of the ratio of the maximum shear force V_{max} (under relevant representative values of permanent loads including prestressing and maximum cyclic loading) and the design shear resistance attributed to the concrete $V_{ref} = V_{Rd,c}$ as:

$$\text{Log } N = 10\ (1 - V_{max}/V_{ref}) \qquad \text{Eq. (1)}$$

For V_{max} / V_{ref} = 0.5 we get $N = 10^5$ load cycles and for V_{max} / V_{ref} = 0.3 we obtain N = 10^7 load cycles. Monitoring has given that a bridge of this type experiences four axles (two bogies) as one load cycle. During a year with 8 trains per day, 68 wagons (each with 2 bogies) per train and 365 days we obtain 198,560 cycles ≈ 200 kc.

The shear load effect $V_E = V_{max}$ at the support of the slab consists of dead load V_{Eg} and train load V_{Eq} with values $V_E = V_{Eg} + V_{Eq}$ = 34 + 113 = 147 kN/m (10.2 kips/ft). For a concrete with a compressive strength of 40 MPa (5.8 ksi), we obtained with the Swedish code BBK94 (Thun et al. 2000), a shear resistance of $V_{ref} \approx$ 215 kN/m (14.8 kips/ft) and V_{max} / V_{ref} = 147/215 = 0.68 which gives $N = 10^{3.2}$ = 1.5 kc. If the concrete capacity is increased to 80 MPa (11.6 ksi), we obtain V_{max} / V_{ref} = 147/292 ≈ 0.5 and $N = 10^5$ = 100 kc which corresponds to about half a year of traffic. The value of V_{ref} varies in different codes depending on traditions and amount of longitudinal reinforcement. The test showed that the bridge could stand more than 6,000 kc without other than hairline cracks. A fatigue shear crack that might be detrimental is indicated at the right support of the slab in Figure 3 (top). The crack did not materialize. Probably, the longitudinal reinforcement has a positive influence by dowel action and by keeping the section tight together. The fatigue capacity of concrete is often estimated in a rather conservative way, while the reinforcement is more prone to fail in fatigue and is also modelled with better accuracy; see further discussion in Thun et al. (2011) and Elfgren (2015).

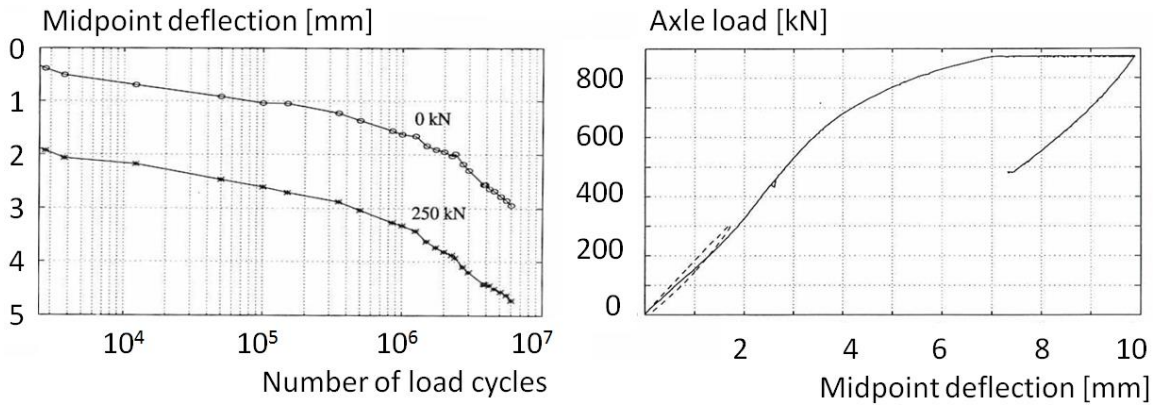

Figure 4 - Mid-point deflection. (a) - At 0 and 250 kN (57 kips) load for $6 \cdot 10^6$ load cycles with a maximum deflection of 4.8 mm (0.2 in). (b) - Final loading to 875 kN (200 kips) after 6 million cycles with 360 kN (82 kips) axle load. Dashed line shows preloading to 300 kN (68 kips). (10 mm = 0.39 in.)

ÖVIK TROUGH BRIDGE 2007– STRENGTHENED

Introduction

This test was scheduled as part of a demonstration of newly developed or upgraded tools for monitoring, assessment and upgrading of structures within a European project (Sustainable Bridges, 2007, Paulsson et al. 2016), see Figures 5 and 6. The studied bridge was a 50 year old RC railway trough bridge located in Örnsköldsvik (Övik) in northern Sweden. The bridge consisted of two outer beams supporting a slab in two spans (12 + 12 m, 39+39 ft), with a slight longitudinal curvature (R = 300 m = 984 ft) and with supports skewed at an angle of 17 degrees. It was taken out of service in 2005 and tested to failure in 2006 (Elfgren et al., 2008, Puruula, 2012).

Figure 5 - The tested railway bridge in Örnsköldsvik (Övik), Sweden, in a view from the West side showing the test setup. A cross-section is shown as an insert of one or the two beams with a height of 1,100 mm (3.6 ft) and a bottom reinforcement of 12,266 mm^2 (19sq.in.) steel bars and 1,800 mm^2 (2.8sq.in.) carbon fibre reinforced polyester (CFRP) bars. (100 mm = 3.9 in, 1000 mm^2 = 1.55 sq. in.).

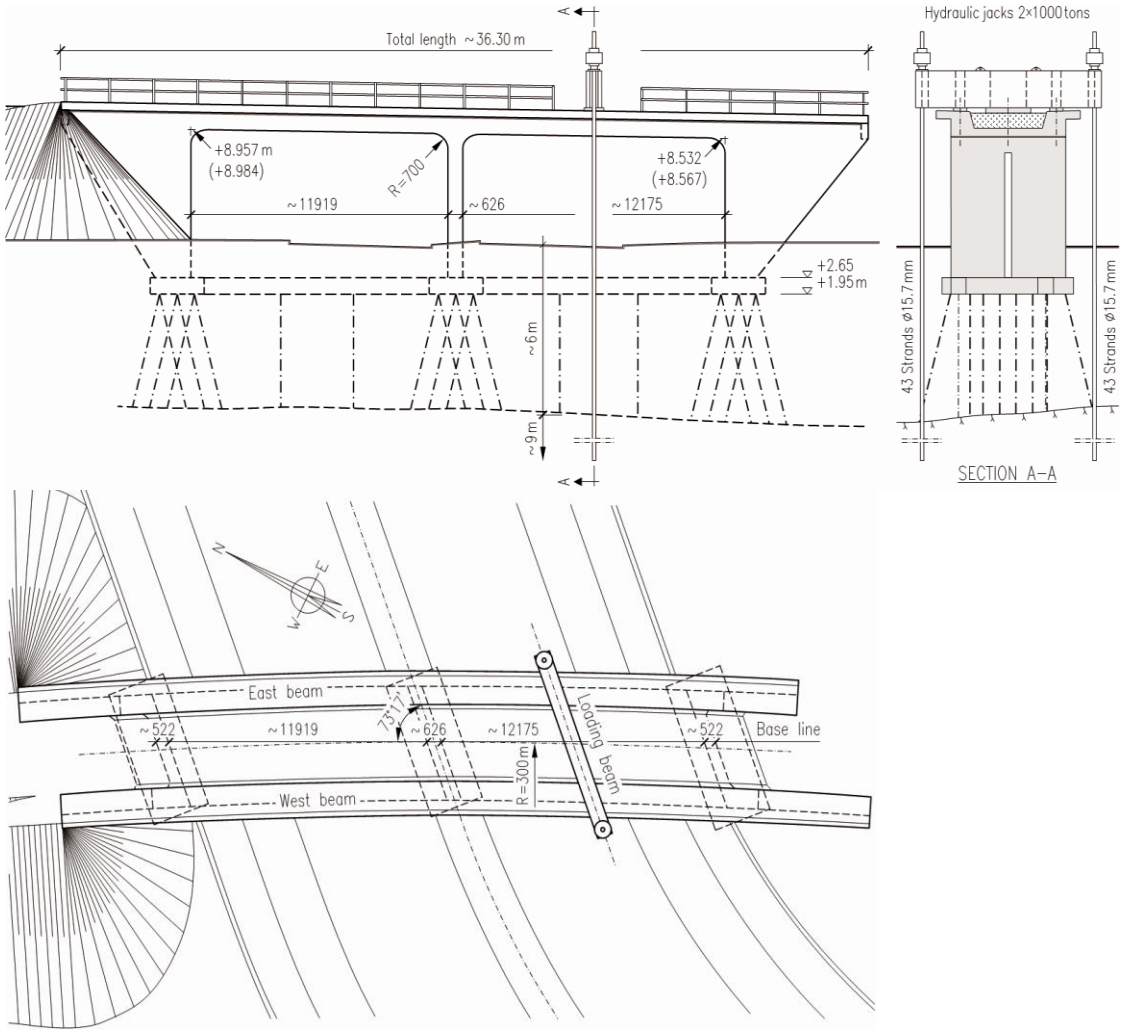

Figure 6 - Elevation, section and plan of the bridge together with the loading arrangement [mm]. Each of the two spans had a length of about 12 m (39 ft) and a width of 6 m (20 ft). The South landfill was removed before the test. A steel beam was placed in the middle of one of the two spans and was pulled downwards. (Elfgren et al., 2008).

Experimental Program

The bridge was designed for a 40 MPa (5.8 ksi) concrete and for steel reinforcement with yield strength of 400 MPa (58 ksi). However, the tested concrete had a higher mean compressive strength of 68.5 MPa (9.9 ksi). The reason for the higher concrete strength is, as for the previous bridge, coarse grinding of the cement, which prolonged the hydration process after the 28 days, when the original concrete was tested. The steel reinforcement tests showed yield strengths slightly above 400 MPa (58 ksi) and ultimate strengths up to 700 MPa (102 ksi). To obtain a shear failure (and avoid an uninteresting bending failure), the bridge was strengthened in bending before the final failure test with 18 (9 per beam) 10 m (32 ft) long near surface mounted (NSM) carbon fiber reinforced polymer (CFRP) bars, each with a 10×10 mm (0.39 × 0.39 in) cross section. The modulus of elasticity and the tensile strain at failure were 250 GPa (36 250 ksi) and 0.8 %, respectively.

The bridge was tested with two hydraulic jacks, placed on top of a loading beam. They exerted a downward force on the loading beam by pulling on steel tendons anchored in the bedrock to a depth of 9 m (30 ft), see Figures 5 and 6.

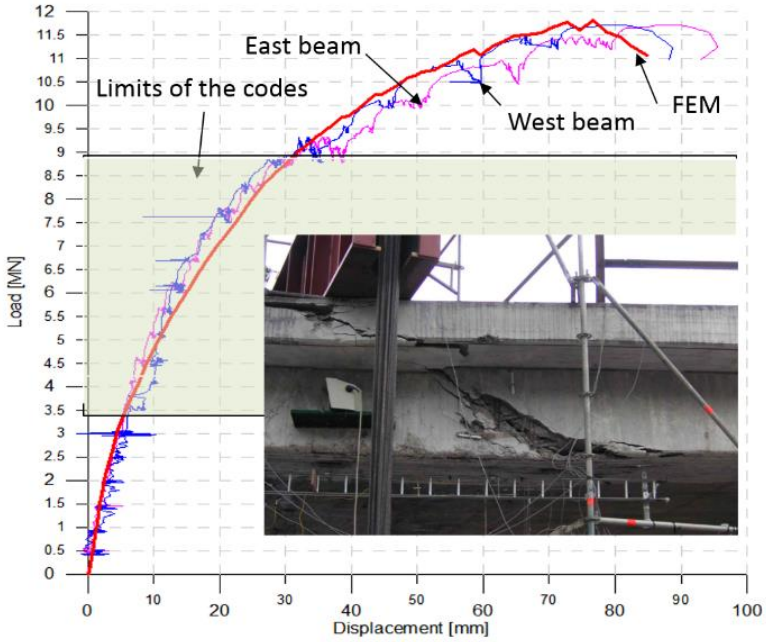

Figure 7 - Load-displacement curves as recorded and as calculated with codes and nonlinear FEM. Insert: crack pattern in the SE beam after failure. (11.7 MN = 2,630 kips; 100 mm = 3.9 in).

Assessment versus test results

The failure was relatively ductile, see Figure 7. The recorded failure load P was 11.7 MN (2,630 kips). The mechanism of failure was a simultaneous bond-bending-shear failure, resulting in the formation of flexural-shear cracks in both beams at an angle of about $\theta \approx 32°$. The NSM reinforcement played a major role in the failure process and enabled and initiated the shear-bending failure, see further below.

The bridge was modeled with a non-linear three-dimensional finite element model using (Brigade, 2011) based on Abaqus software. In the model, the number of separate parts was 1,650 (most of them discrete reinforcement bars), the number of elements was 152,460, the number of nodes was 164,003 and the number of variables was 511,317. Shell elements in the steel beam used for applying the load were of type S4R: linear quadrilateral, 4-node doubly curved shell, reduced integration, hourglass control. Solid elements in the concrete bridge were of type C3D8R: 8-node linear brick, reduced integration, hourglass control. Discrete reinforcement bars were modeled as wires, type 2-node linear 3-D truss elements. The material modeling (tension stiffening of the reinforcement and tensile properties of concrete) as well as boundary conditions (rotational capacity of supports) were important parameters in the calibration of the model.

At failure, high stresses between the CFRP reinforcement and the resin initiated a bond failure after yielding in the bottom longitudinal steel reinforcement. This increased the inclination of the concrete compression struts; see Figure 8, which gave higher stresses in the stirrups, as fewer stirrups had to carry the load. These stresses, mostly caused by the vertical shear forces but also to some extent by the torsion moment from the loads on the slab, ruptured the stirrups. The final capacity was reached for an applied mid span load of 11.7 MN (2,630 kips), see Figure 7.

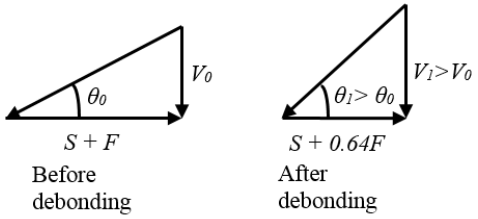

Figure 8 - Schematic figure of the effect of the decreasing force in the tensile reinforcement. Debonding of the FRP reinforcement reduced the tensile force $S+F$ in with 36 %, which increased the angle θ of the compression strut. S is the tensile force in steel reinforcement; F is the force in the FRP; V is the shear force; θ_0 is the angle of the compression strut before debonding; and θ_1 is the angle of the compression strut after debonding.

Load capacities calculated with code methods varied between 3.5 MN (798 kips) and 9 MN (2,052 kips). Gradually improved assessment methods have been applied from using simple linear elements to non-linear finite elements for yielding steel reinforcement bars and debonding CFRP bars, (Puurula, 2012, Puurula et al., 2015, 2016). The influence of torsion was not very large but still had an influence as in earlier tests on box girder bridges, (Scordelis et al. 1977, 1979, Elfgren, 2009). The applied methods for strengthening with near surface mounted carbon reinforced polymer bars are also discussed in (Mainline, 2014, ML-D1.3, 2015 and Täljsten et al., 2016).

An assessment of the load carrying capacity for train loads was also carried out. It showed that the Övik Bridge with the applied strengthening of the bridge slab with FRP bars could have sustained 6,5 times the axle load of 225 kN (56.2 kip) of the Swedish bridge code. Here statistical mean values were used of the material properties in the calculations (Puurula et al. 2016).

KIRUNA PRESTRESSED BRIDGE 2014

Background

A 55 year-old prestressed concrete girder bridge (see Figures 9 and 10) was taken out of service due to large ground deformations caused by mining activities. However, the bridge was still in very good condition with only minor damage observed and, thus, it was decided to further study the bridge in order to examine and develop methods for assessment. The study is reported in Ph D theses of (Nilimaa, 2015, and Bagge, 2017).

Figure 9 - View of the Kiruna bridge from north.

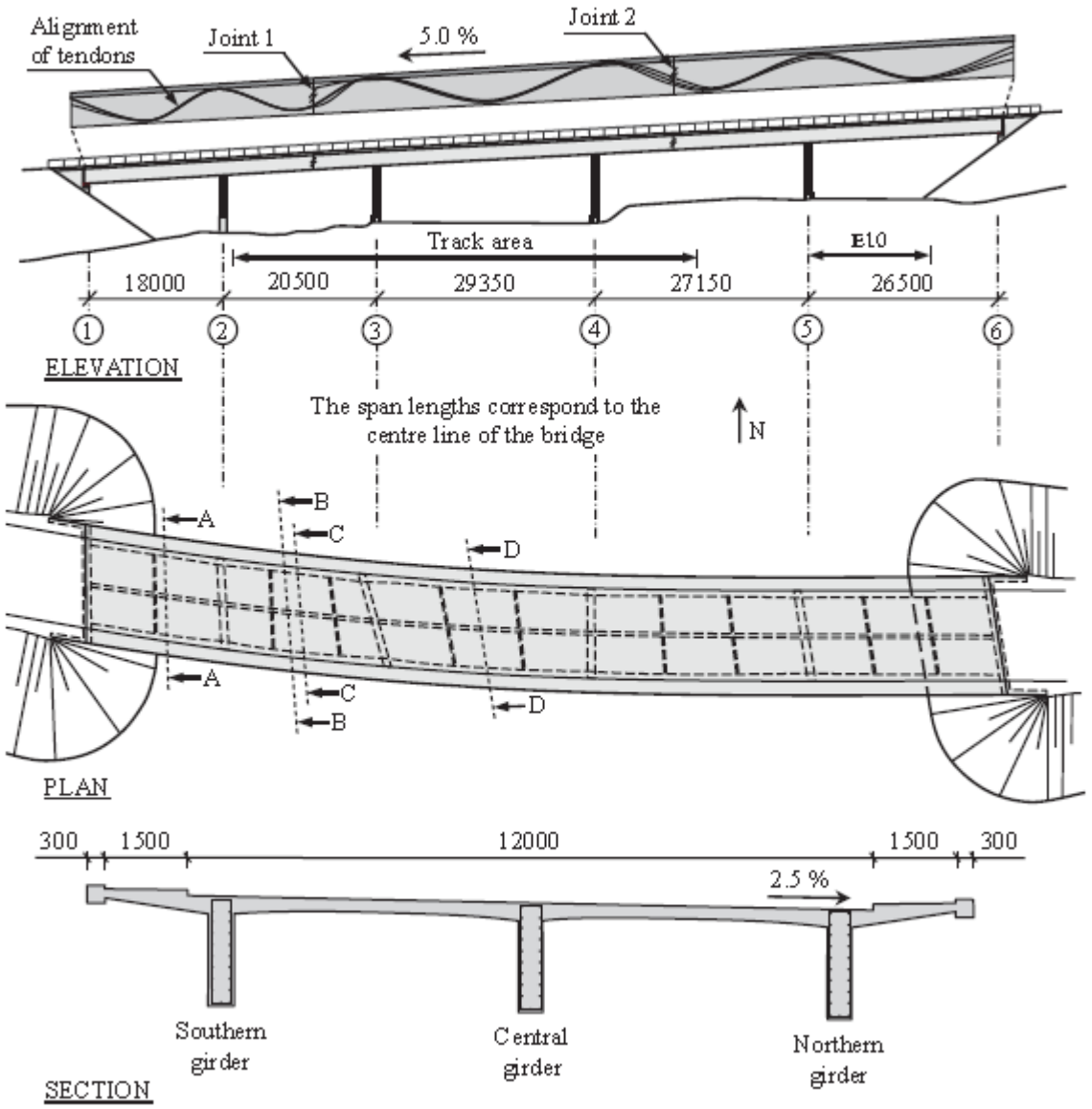

Figure 10 - Geometry of the Kiruna bridge. (10,000 mm = 32.8 ft).

The bridge was continuous over five spans with a total length of 121.5m (400 ft). The superstructure consisted of three girders (width: 0.41 – 0.65 m, 1.35-2.13 ft; height: 1.923 m = 6.3 ft) connected with a slab (width: 14.9 m = 48.9 ft, height: 0.22 – 0.30 m; 0.72-0.98 ft) with curbs on either side (width = height = 0.3 m = 1 ft) and was supported on columns and abutments. Four or six post-tensioned BBRV tendons, consisting of 32 strands (diameter: 6 mm = 0.24in), were used in the girders. Design of the bridge was based on a concrete compressive strength of 28.5 MPa (4.1 ksi); a non-prestressed yield strength of 400 MPa (58 ksi) for most of the bars; 600 MPa (87 ksi) for the longitudinal bars in the slab; and, for the prestressed steel a 0.2 % proof strength of 1,450 MPa (210 ksi) and an ultimate tensile strength of 1,700 MPa (247 ksi). Before the tests the settlements and deflections of the bridge had been studied for six years (Enochsson et al., 2011, Huang et al., 2016).

Experimental Program

An experimental program was designed for evaluation of the condition and the structural behaviour of the bridge. The girders were first with loaded in several cycles in order to investigate the bridge behaviour in the service stage. Thereafter a failure test of two of the girders was carried out, followed by a failure test of the bridge deck slab adjacent to the third girder still in function.

Assessment versus test results - Beams

The bridge girders were loaded in middle of the second span. Based on linear elastic analysis and local resistance models according to the European standard (CEN, 2005), the flexural capacity was reached adjacent to the mid-span at 9.1 MN (2,074 kips). However, the flexural capacity at the supports was not fully utilized and, thus, redistribution of internal forces can be expected. According to the European standard up to 30 % redistribution, in relation to the linear elastic distribution of internal forces, can be allowed for statically indeterminate structures without further verification of the deformation capacity of the plastic region. The approach taking redistribution into account, resulted in a shear failure at the support for a load of 10.4 MN (2,371 kips). In-situ tested material parameters were used in the calculations, leading to a considerably improved load-carrying capacity compared to the values used at the design of the bridge.

Figure 11 - Modelling of the Kiruna Bridge in stages following construction, service life, and testing procedures.

The further modelling of the bridge was made with linear and non-linear finite elements using the Atena System, (ATENA, 2017), see Figure 11.For the parts of the bridge simulated as exhibiting a linear behavior, beam elements (*CCIsoBeamBrick12_3D*) represented columns, girders, curbs and cross-beams, while shell elements (*CCIsoShellBrick*) represented foundations, deck slab and loading plates, and the components of the load distribution beams. In order to take the in-plane shear into account in the girders and cross-beams in the nonlinear region, the beam elements were replaced by continuum elements (*CCIsoBrick*). By having only one element across the width of the beams, the out-of-plane shear behavior could not be modelled. Moreover, continuum elements were used for the slab locally at the point of application of the external loads to the bridge, since the out-of-plane shear could be expected to be of importance in such a region. Due to the drastic increase in the number of elements needed to meet the requirements of the elements' aspect ratios, the use of continuum elements in the slab was limited to critical regions in order to reduce the computational effort required. Due to the size of the FE model and limited computational resources, it was preferable to vary the element sizes based on their importance for the structural behavior. Thus, the finest mesh was assigned to the region adjacent to the external loading where the final failure was expected, with gradually courser mesh used for the remaining nonlinear part, while even coarser mesh was used for the linear parts of the bridge outside the failure region. A mesh sensitivity study was carried out to ensure there was no major influence of mesh size on the outcomes of the simulations. The element sizes in the nonlinear region were halved in each direction, except for the region of the slab further refined at the point of load application, which already met the requirement that the maximal size of continuum elements should be half that of the maximal crack band width. The prestressed steel reinforcement tendons and NSM CFRP rods were modelled as discrete truss elements (*CCIsoTruss*). The non-prestressed reinforcement was generally modelled as smeared (or embedded) reinforcement in the concrete elements. However, in the region of highly stressed concrete, the longitudinal non-prestressed reinforcement was modelled with discrete truss elements in the girders and the cross-beams. Discrete truss elements were also used to represent both the longitudinal and transverse reinforcement in the slab, locally close to the external loading, as well as for the stirrups in the girders (for the entire span except for 4.0 m (13,1 ft) adjacent to the supports). The truss element sizes were consistent with the surrounding concrete elements.

In the test, the girders were first equally loaded up to a total load of 12 MN (2,736 kips), followed by increased load on the outer girder until failure at 13.4 MN (3,055 kips). After a drop of the load, the inner girder was further loaded to failure at 12.8 MN (2,918 kips), see Figure 12. The same failure mechanism was observed for the two girders. Extensive vertical and diagonal cracks were formed and both longitudinal non-prestressed reinforcement and vertical shear reinforcement yielded.

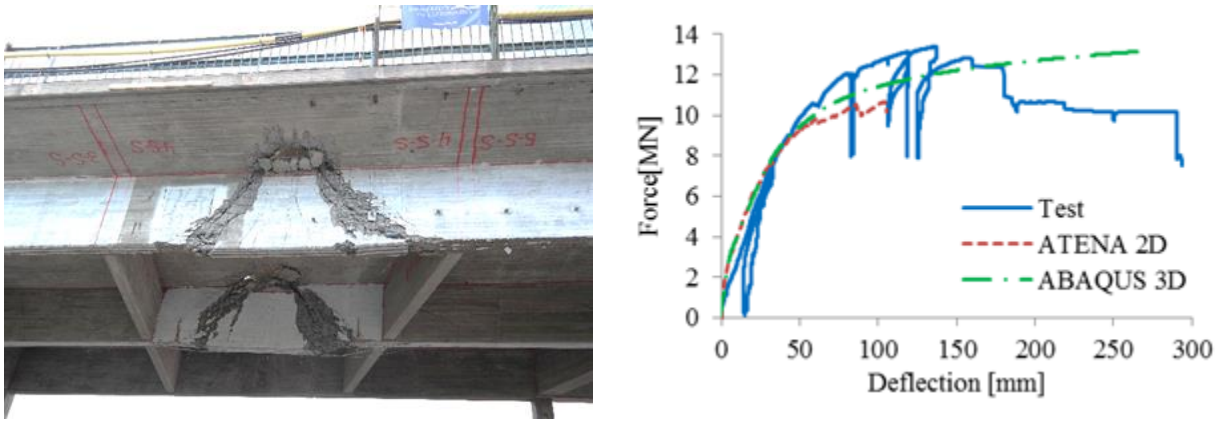

Figure 12 - Kiruna bridge girderfailure. (a) Photograph of the girders after test. (b)Load-deflection curves for the failure test of the bridge girders. (13.4 MN = 3,055 kips, 200 mm = 8 in).

In the final stage, the stirrups crossing the critical diagonal ruptured and simultaneously the loading plate punched through the slab as the girder could not take any more load, see Figure 12. In general, the structure behaved in a ductile manner and an appreciable residual load-carrying capacity remained after the test. Thus, a robust bridge structure can be concluded.

Comparison of the test result and the analytical calculations indicates difficulties to accurately predict the load-carrying capacity. Undoubtedly, redistribution of internal forces took place in the structure when the sections above the columns cracked and this should be taken into account in the assessment. The truss model for shear in the European standard (CEN, 2005) in combination with a linear elastic analysis with some redistribution of forces between supports and mid spans due to cracking, was not able to reflect the failure of the bridge; it indicated a bending failure instead of a shear failure. The load-carrying capacity was underestimated and the critical section was inaccurately located closer to the support than what took place in the test, where a high moment at mid span interacted with the shear and forced it to appear there.

Multi-level structural assessment

A method to gradually increase the quality of the numerical model was introduced. It corresponds to the enhanced Phase 3 in Figure 1 and is recommended by (Rijkswaterstaat, 2016). It follows Levels 2 and 3 in a proposed strategy based on ideas in (Plos et al., 2016); that is, a nonlinear analysis is carried out which can consider both flexural and shear failures. An example of possible increases in capacity is given at the end of the paper.

The increased quality, produced results much closer to the test values. Updated values were used for the boundary conditions of the columns (somewhat built in rather than hinged) and a somewhat lower concrete tensile strength f_{ct} and fracture energy G_F than what was originally assumed. By mistake, no tests were carried out to determine these properties, so they had to be extrapolated from tests of other similar concrete qualities.

Assessment versus test results – Bridge deck slab

The bridge deck slab was loaded in the middle of the second span with two loading plates (2.0 m (6.4 ft) apart) adjacent to the girder not previously loaded to failure. Punching of the loading plate and shear at the girder, assuming a simplified 45º shear distribution from the edge of the loading plate, have been regarded in principle according to the European standard, (CEN 2005), to determine the load-carrying capacity of the slab. Based on in-situ tested material parameters the one-way shear capacity of the slab relative to the nearby girder was critical and the predicted load-carrying capacity was 1.48 MN (337 kips).

The test resulted in a sudden, brittle failure of the slab at a load of 3.32 MN (757 kips), see Figure 13. The failure was formed around one of the loading plates and it has been classified as a combination of a shear and a punching failure, indicated to be initiated as shear failure at the girder, in principle the same failure mode as in the simplified analysis above. However, the simplified analytical model, giving less than half the actual tested value, is obviously very conservative and do not fully reflect the behaviour of the bridge deck slab. A refined analysis of the slab with the program Diana (TNO, 2015) with non-linear finite elements according to (Plos et al., 2016 and Shu et al., 2017) has given results closer to the tested value The slab was then modelled with shell and beam elements with nonlinear behavior of the materials included in the analysis. The prestressing as well as the ordinary reinforcements were also included in the model. A loading sub-structure was used in the model to enable a deformation-controlled loading procedure. The loading substructure was modelled with very stiff beam elements, and was designed to be statically determinate. The slab has also been analysed with (Atena, 2017) by (Eriksson & Karlsson, 2016, Hallgren et al., 2017) with good results.

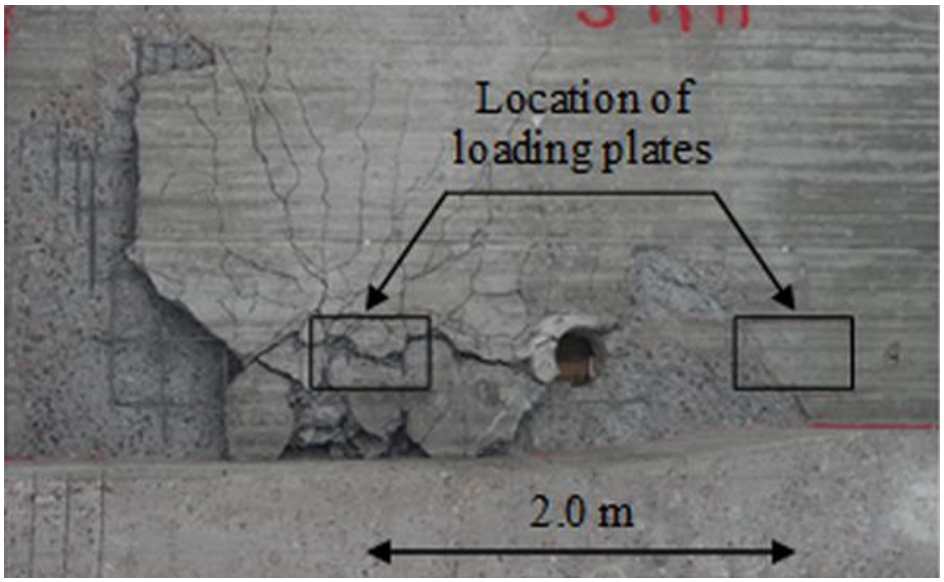

Figure 13 - Photograph of the Kiruna deck slab after test seen from below. The hole between the loading plates is for the cable transferring the applied load from the jacks to the bedrock under the bridge. (2 m = 6.6 ft)

Safety verification

To handle uncertainties associated with the assessed bridge, the structural assessment analysis must be used in combination with an appropriate safety concept. As well as the structural analysis, verification of the required level of structural safety can be carried out at several levels of increasingly complex approximation (fib MC 2010, 2013). In addition to the choice of safety concept, the level of safety is an important issue for bridge assessment and should take into account what is already known about the structure and economical, societal and environmental risks associated with it. The general condition to determine the load carrying capacity is given by:

$$R > E(G, P, Q) \qquad \text{Eq. (2)}$$

where R is the resistance, and E is the effect of permanent loads (G), prestressing (P), and variable loads (Q). This condition has to be satisfied for a certain level of probability defining the desired safety level. For verification of the failure mode captured in the structural analysis, the variables R and E in Equation (2) refer to structural resistance and effect, respectively; otherwise they refer to local resistance and action effects, respectively. According to (fib MC 2010, 2013), the verification of the required level of structural safety should follow a probability-based concept. The safety of the Kiruna bridge has been verified with different procedures with increasing complexity towards a full probabilistic analysis (Schneider &Vrouwenvelder, 2017):

- Partial Safety Factor, PSF, where partial coefficients are applied to the different materials and loads(as in the Euro codes),

- Global Resistance Safety Factor, GRSF, where partial coefficients are applied to the results of a (non-linear) numerical analysis
- Estimation of the coefficient of variance of the resistance *R*
- Improved estimation of the coefficient of variance of the resistance *R*
- Full probabilistic analysis of $G = R – E$.

For all the tested safety concepts the enhanced calculations gave more than 5 times higher values than the initial method. This is very big difference and there are several reasons for the low estimate of the initial method. The axle loads were only applied to one side of the bridge (the southern part) and transverse redistributions can be expected. The favorable impact of arching action for loads located close to the support was ignored, as well as the residual strength of the stirrups after initiated yielding (i.e. strain hardening). The local resistance model applied to the girders also shows a large scatter in the prestressed concrete members, members with a T-shaped cross-section and with low reinforcement ratios. In addition, the section used for capacity control plays an important role since shear forces are extreme at the supports. However, also the Övik bridge showed a very much higher capacity than it was originally designed for.

CONCLUSIONS

The results of tests to failure of three reinforced concrete bridges have been presented. The tests were carried out on decommissioned structures deemed for demolition. The analysis of the tested bridges gave the following conclusions:

- Numerical tools as linear and non-linear finite element methods have been shown to be useful instruments for assessment especially when combined with material testing and step-wise refinements from linear to non-linear modelling of bending, shear and bond.
- The tested structures had a considerable “hidden” capacity which can be missed during ordinary assessment processes and which is accounted for neither in standards nor in design guidelines. One reason is the high safety factors that are used both for loads and materials in the construction phase and which may not be necessary in an assessment process where geometry, materials and load may be better known.
- The concrete tensile strength and fracture energy are necessary in numerical modelling and more efforts should be taken to determine them in assessment of existing structures.
- Probabilistic methods can be applied successfully to improve the study of reliability and safety of existing structures
- The concrete fatigue capacity in shear was not as critical as the codes envisioned for the Lautajokk Bridge. Shear stresses are in the design phase often converted to tensile and compressive stresses and the tensile stresses are mostly carried with reinforcement or eliminated by prestressing. Concrete in compression seldom gives any fatigue problems.
- Strengthening with carbon fibre reinforced polymers (CFRP) worked well and the load-carrying capacity of the Övik bridge could be substantially increased. Non-linear finite element models of the bridge could be calibrated to model the behaviour in a good way. It was important to accurately model the tension stiffening in the reinforcement and the support conditions.
- Non-linear finite element methods could in the Kiruna Bridge be step-wise refined to model the prestressed bridge better and better. Large differences from normal code methods were obtained. They probably partly arose from redistribution of loads during the testing in the statically indeterminate structures, from conservative load-carrying models, increased values of material properties and the built-in properties of the supports.

Many unpredicted events can take place in “full scale” tests to failure. In the survey by (Bagge et al. 2017b) about 28% of the 40 full-scale tests on 30 bridges ended with a failure mode different to that predicted. In some cases, this was related to inaccuracies in the methods for determining the load-carrying capacity but, in the majority of cases, it

was caused by a lack of insight into aspects shown to be critical, particularly associated with the shear and punching capacities and the boundary conditions.

The paper shows that society may learn and may save money from the experiences from “full-scale” failure tests. It is therefore recommended that additional tests are to be carried out in order to further improve the understanding of existing bridges. The tests should as far as possible be based on realistic load cases, in order to optimize the outcome. As the tests are costly it is also important that planning, preparations and analysis are done in a careful way.

ACKNOWLEDGEMENTS

The partners in the European Project (Sustainable Bridges, 2007) were (by country): *Czech Republic:* Cervenka Consulting; *Denmark*: COWI A/S (Jens Sandager Jensen, WP 4 Leader); *Finland:* Finnish Road Administration, Finnish Rail Administration, University of Oulu, WSP Consulting – Kortes (Risto Kivilouma, WP 8 Leader) ; *France:* Société Nationale des Chemins des Fer Français, SNCF, Laboratoire Central des Ponts et Chaussées, LCPC (Christian Cremona, WP 7 Leader); *Germany:* Deutsche Bahn AG, Bundesanstalt für Materialforschung und prüfung, BAM (Ernst Niederleithinger, WP 3 Leader), Universität Stuttgart, Rheinisch-Westfälische Technische Hochschule; *Norway:* NORUT Technology A/S; *Poland:* PKP Polish Railway Lines,Wroclaw University of Technology (Jan Bien, WP 9 Leader); *Portugal:* Universidade do Minho; *Spain:* Universitat Politècnica de Catalunya, UPC; *Sweden:* Skanska Sverige AB (Jan Olofsson, Coordinator, and Hans Hedlund, Ass. Coordinator), Banverket - Swedish Rail Administration (Björn Paulsson, WP 2 Leader), Vägverket - Swedish Road Administration, LTU (Lennart Elfgren, Scientific Leader; Björn Täljsten WP 6 Leader), Chalmers University of Technology, Royal Institute of Technology, Lund University of Technology, Swedish Geotechnical Institute, Sto Scandinavia AB, Designtech AB; *Switzerland:* Eidgenössische Materialprüfungsanstalt, EMPA (Glauco Feltrin, WP 5 Leader), Ecole Polytechnique Federal de Lausanne, EPFL; *United Kingdom:*Network Rail (Brian Bell, WP 1 Leader), City University, and University of Salford.

The partners in the European Project (Mainline, 2014) were (by country): *Austria:* Graz University of Technology; *Czech Republic:* Skanska a.s.; *Denmark:* COWI; *France:* ARTTIC, Cerema/SETRA andUIC (Björn Paulsson, project coordinator); *Germany:* Deutsche Bahn Netz AG; *Hungary:* ; MÁV Magyar Államvasutak Zrt; *Portugal:* University of Minho; *Spain:* COMSA EMTE and Universitat Politècnica de Catalunya; *Sweden:* Damill AB, Luleå University of Technology (LTU, Technical Coordinator), and Trafikverket; *Turkey:* TCDD; *United Kingdom:* Network Rail Infrastructure Limited, Jacobs/Sinclair Knight Merz (SKM), TWI, and University of Surrey,

The authors gratefully acknowledge financial support from the European Union, Trafikverket, Network Rail, LKAB/HLRC, SBUF and LTU. They also thank colleagues and collaborators who have worked in the projects and the Swedish Universities of the Built Environment (LTH, Chalmers, KTH and LTU) for fruitful cooperation.

The experimental work and monitoring campaigns in Sweden were carried out in cooperation with staff of Complab at LTU.

REFERENCES

ACI 318 (2014). "Building code requirements for structural concrete and commentary." American Concrete Institute (ACI), Farmington Hills, MI, United States, 520.

ATENA (2017). Atena is a software for non-linear finite element analysis of reinforced concrete, see http://www.cervenka.cz/products/atena/

Bagge, Niklas (2017).Structural Assessment Pocedures for Exisisting Concrete Bridges. Experiences from failure tests of the Kiruna Bridge. Doctoral Thesis, Luleå University of Technology, ISBN 978-91-7583-879-3, 310 pp. Available at ltu.diva-portal.org/

Bagge, Niklas, Nilimaa, J., Blanksvärd, T., & Elfgren, L. (2014). Instrumentation and full-scale test of a post-tensioned concrete bridge. *Nordic Concrete Research, 51*, 63-83.

Bagge, N., Nilimaa, J., Blanksvärd, T., Täljsten, B., Elfgren, L., Sundquist, H., & Carolin, A. (2016). "Assessment and failure test of a prestressed concrete bridge." 5th International Symposium on Life-Cycle Civil Engineering, International Association for Life-Cycle Civil Engineering (IALCCE), Delft, Netherlands, Ed. by Bakker, Frangopol & van Breugel, London, Taylor & Francis Group, ISBN 978-1-138-02847-0, paper C134, Abstract p 194, Full paper on USB card pp 1958-1063.

Bagge, N., Nilimaa, J., & Elfgren, L. (2017a). "In-situ methods to determine residual prestress forces in concrete bridges." Engineering Structures, 135, 4152.

Bagge, Niklas; Popescu, Cosmin and Elfgren, Lennart (2017b), Failure tests on concrete bridges: Have we learnt the lesson? Structure and Infrastructue Engineering, Accepted for publication.

Brigade (2011): Brigade software is described on www.scanscot.com. It is based on the software Abaqus, see www.3ds.m/products/simulia/portfolio/abaqus/overview

CEN. (2005). Eurocode 2: Design of concrete structures - Concrete bridges - Design and detailing rules *SS-EN 1992-2:2005* (pp. 104). Brussels, Belgium: European Committee for Standardization (CEN).

Elfgren, Lennart (2009). Development of models for torsion of concrete structures in northern Europe. In Thomas T.C. Hsu Symposium: Shear and Torsion in Concrete Structures. ACI Fall 2009 Convention. ACI SP 265, Farmington Hills, MI, pp. 309–325.

Elfgren, Lennart (2015):Fatigue Capacity of Concrete Structures: Assessment of Railway Bridges. Research Report, Structural Engineering, Luleå University of Technology, 103 pp.Available at ltu.diva-portal.org/

Elfgren, Lennart, Enochsson Ola, Puurula Arto and Thun Håkan (2008). *Field Test of a Concrete Bridge in Örnsköldsvik*. Sustainable Bridges, Report SB-7.3, 2008, 406 pp. www.sustainablebridges.net

Enochsson, Ola; Sabourova, Natalia; Emborg, Mats & Elfgren, Lennart.(2011). Gruvvägsbron i Kiruna : Deformationskapacitet (Deformation Capacity of the Kiruna Bridge. In Swedish), Report, Luleå University of Technology.108 pp. Available at ltu.diva-portal.org/

Eriksson, Isabell and Karlsson, Niklas (2016). Non-Linear Assessment of a Concrete Bridge Slab Loaded to Failure. MSc Thesis, Royal Institute of Technology,KTH, Stockholm, Available at kth.diva-portal.org/

fib MC 2010 (2013). fib Model Code for Concrete Structures 2010, International Federation for Structural Concrete, fib. Berlin, Ernst & Sohn, ISBN 878-3-433-03061-5, 402 pp.

Hallgren, Mikael; Eriksson, Isabell & Karlsson, Niklas (2017): Numerical Simulations of a Concrete Bridge Deck Loaded to Failure. In: High Tech Concrete: Where Technology and Engineering meet, fib Symposium, Maastricht, Netherlands, 2017, Abstract p. 183, full paper on USB stick pp. 1898-1906.

Huang, Zheng; Grip, Niklas; Sabourova, Natalia; Bagge, Niklas; Tu, Yongming; and Elfgren, Lennart (2016). Modelling of damage and its use in assessment of a prestressed bridge. In *Proceedings of the 19th Congress of IABSE in Stockholm*,, pp 2093-2108. A longer version was also published 2016-04-30 as a Research Report, Division of Structural Engineering, Luleå University of Technology, 22 pp.Available at ltu.diva-portal.org/

ISO 16311-2 (2014). Maintenance and repair of concrete structures – Part 2: Assessment of existing concrete structures , International Organization for Standardization , 44p.

Mainline (2014). *MAINtenance, renewaL and Improvement of rail transport INfrastructure to reduce Economic and environmental impacts*. A European FP7 Research Project during 2011-2014. Some 20 reports are available at http://www.mainline-project.eu/

ML-D1.3 (2015). New technologies to extend the life of elderly rail infrastructure. Deliverable 1.3 in the EC-project MAINLINE, First ed. 2013, revised ed. 2015, 194 pp. http://www.mainline-project.eu/Results,7.html

Nilimaa, Jonny, Blanksvärd, T., Täljsten, B., & Elfgren, L. (2014). Unbonded Transverse Posttensioning of a Railway Bridge in Haparanda, Sweden. *Journal of Bridge Engineering*, 19(3).

Nilimaa, Jonny. (2015). *Concrete bridges: Improved load capacity.* Doctoral Thesis, Luleå University of Technology, Luleå, Sweden, 176 pp. Available atltu.diva-portal.org/

Nilimaa, Jonny, Bagge, N., Blanksvärd, T., & Täljsten, B.(2016). NSM CFRP Strengthening and Failure Loading of a Posttensioned Concrete Bridge. *Journal of composites for construction*, 20(3).

Olofsson, Ingvar, Elfgren, L., Bell, B., Paulsson, B., Niederleithinger, E., Jensen, J.S., Feltrin, G., Täljsten, B., Cremona, C., Kiviluoma, R., Bien, J. (2005). Assessment of European railway bridges for future traffic demands and longer lives – EC project "Sustainable Bridges",*Structure and Infrastructure Engineering* , Vol. 1, 2005, No 2, 93-100.

Paulsson, Björn; Töyrä, Björn; Elfgren, Lennart; Ohlsson, Ulf; Danielsson, Georg; Johansson, Håkan and Åström, Lars (1996): *30 ton på Malmbanan. Rapport 3.3 Infrastruktur. Forsknings- och utvecklingsprojekt avseende betongbroars bärighet*. (Static tests on four trough bridges and a laboratory fatigue test on one bridge. In Swedish), Banverket och Luleå tekniska universitet, 51pp + 5 Appendices. Available at http://ltu.diva-portal.org/

Paulsson, Björn; Töyrä, Björn; Elfgren, Lennart; Ohlsson, Ulf and Danielsson, Georg (1997): *Increased Loads on Railway Bridges of Concrete*. Advanced Design of Concrete Structures (Ed. By K Gylltoft et al), Cimne, Barcelona, 1997. pp 201-206 (ISBN 84-87867-94-4).

Paulsson, Björn; Bell, Brian; Schewe, Britta; Jensen, Jens Sandager; Carolin, Anders; and Elfgren, Lennart (2016). Results and Experiences from European Reserach Projects on Railway Bridges. *19th IABSE Congress Stockholm 21-23 September 2016: Challenges in Design and Construction of an Innovative and Sustainable Built Environment*, Zürich, 2016, pp. 2570 – 2578. ISBN 978-3-85748-144-4. Available at http://ltu.diva-portal.org/

Plos, Mario (1990). Skjuvförsök i full skala på plattrambro i armerad betong (Full-scale shear test on concrete slab frame bridge. In Swedish). *Report 90:3*, Chalmers University of Technology, Gothenburg, Sweden, 117 pp
.
Plos, Mario (1995). Application of fracture mechanics to concrete bridges. Finite element analyses and experiments. Ph.D. Thesis, Chalmers University of Technology, Gothenburg, Sweden.

Plos, Mario, Gylltoft, Kent, and Cederwall, Krister (1990). Full scale shear tests on modern highway concrete bridges.*Nordic Concrete Research*, 9, 134-144.

Plos, Mario, and Gylltoft, Kent. (1995). "Fracture mechanics analyses of the shear failure in a concrete bridge." *Nordic Concrete Research*, 16, 83-102.

Plos, Mario, Shu, J., Zandi, K. Z., & Lundgren, K. (2016). A multi-level structural assessment strategy for reinforced concrete bridge deck slabs. *Structure and Infrastructure Engineering*, 1-19.

Puurula, Arto (2012). *Load-carrying Capacity of a Strengthened Reinforced Concrete Bridge: Non-linear Finite Element Modeling of a Test to Failure. Assessment of Train Load Capacity of a Two Span Railway Trough Bridge in Örnsköldsvik Strengthened with Bars of Carbon Fibre Reinforced Polymers (CFRP)(2012)*. Doctoral Thesis, Luleå: Luleå University of Technology, 2012, 332 p.Available at ltu.diva-portal.org/

Puurula, Arto, Enochsson, O., Sas, G., Blanksvärd, T., Ohlsson, U., Bernspång, L., Elfgren, L. (2014). Loading to failure and 3D nonlinear FE modelling of a strengthened RC bridge. *Structure & Infrastructure Engineering*, 10(12), 1606-1619. 10.1080/15732479.2013.836546

Puurula, Arto, Enochsson, O., Sas, G., Blanksvärd, T., Ohlsson, U., Bernspång, L., Täljsten, B., Carolin, A., Paulsson, B., Elfgren, L. (2015). Assessment of the Strengthening of an RC Railway Bridge with CFRP Utilizing a Full-Scale Failure Test and Finite-Element Analysis, *J. Struct. Engineering*, ASCE, 2015, 141, D4014008, 11 p.

Puurula, Arto, Enochsson, O., Sas, G., Blanksvärd, Th., Ohlsson, U., Bernspång, L., Täljsten, B. and Elfgren, L. (2016). *3D non-linear FE analysis of a full scale test to failure of a RC Railway Bridge strengthened with carbon fibre bars*. 19th IABSE Congress Stockholm 21-23 September 2016: Challenges in Design and Construction of an Innovative and Sustainable Built Environment, Zürich, 2016, pp. 2527 – 2535. ISBN 978-3-85748-144-4.

Rijkswaterstaat (2016). "Guidelines for nonlinear finite element analysis of concrete structures." M. a. N. Hendriks, A. De Boer, and B. Belletti, eds., Rijkswaterstaat Centre for Infrastructure, 66.

Schneider, Jörg (1994): *Sicherheit und Zuverlässigkeit im Bauwesen. Grundwissen für Ingenieure*. (Safety in Civil Engineering. Basics for Engineers. In German) Unter Mitarbeit von Hans-Peter Schlatter. vdf Hochschulverlag AG an der ETH Zürich, 188p., ISBN 978-3-7281-2167-3. DOI 10.3218/2167-7,

Schneider, Jörg & Vrouwenvelder, Ton (2017). Introduction to Safety and Reliability of Structures. 3rd reviewed and extended Ed. (1st Ed. 1997). Structural Engineering Documents No 5, International Association for Bridges and Structural Engineering (IABSE), c/o ETH Zürich, Switzerland, 164 pp. ISBN 978-3-85748-131-2.

Scordelis, A. C., Larsen, P. K., & Elfgren, L. G. (1977). "Ultimate strength of curved RC box girder bridge." *Journal of the Structural Division*, ASCE, 103(8), 1525-1542.

Scordelis, A.C., Elfgren, L. & Larsen, P.K., (1979). Time-dependent behavior of concrete box girder bridges. *Journal of the American Concrete Institute*, 76(1), pp.159–177.

Shu, J., Bagge, N., Plos, M., Johansson, M., Yuguang, Y., & Zandi, K. (2017). "Shear and punching capacity of a RC bridge deck slab loaded to failure in a field test." *Journal of Structural Engineering*, (Submitted for publication)

Sustainable Bridges (2007). *Assessment for Future Traffic Demands and Longer Lives*. A European FP 6 Integrated Research Project during 2003-2007. Four guidelines and 35 background documents are available at www.sustainablebridges.net: *Inspection and Condition Assessment*, ICA, 259 p.; *Load and Resistance Assessment of Railway Bridges*, LRA,428 p.; *Guideline for Monitoring of Railway Bridges*, MON, 83 p.; *Guide for use of Repair and Strengthening Methods for Railway Bridges*, STR.139 p.

Thun, Håkan; Ohlsson, Ulf; Elfgren, Lennart (2000). Fatigue Capacity of Small Railway Concrete Bridges: Prevision of the Results of Swedish Full-scale Tests. Comparison and Analyses. Final Report to the European Rail Research Institute, ERRI D216, Structural Engineering, Luleå University of Technology, 99pp.http://ltu.diva-portal.org/

Thun, Håkan; Ohlsson, Ulf; Elfgren, Lennart (2011): *A deformation criterion for fatigue of concrete in tension*. Structural Concrete, Journal of fib, Volume 12, Issue 3, pp 187-197, September 2011.

TNO. (2015). *Diana finite element analysis, User'sManual -- Release 9.6. TNO DIANA BV.* Delft.

Täljsten, Björn (1994). Plate bonding strengthening of existing concrete structures with epoxy bonded plates of steel or fibre reinforced plastics. Ph.D. Thesis, Luleå University of Technology, Luleå, Sweden.

Täljsten Björn, Blanksvärd T. and Sas G. (2016). *Kompositförstärkning av betong* (Strengthening of Concrete Structures with Composites. In Swedish) Svensk Byggtjänst, Stockholm 2016. ISBN:978-91-7333-763-2, pp. 177.

UIC Code 778-4 (2009): Defects in railway bridges and procedures for maintenance. UIC Code 778-4 R, 2nd Ed International Union of Railways, UIC, Paris,32 p.

Wang, C., Wang, Z., Zhang, J., Tu, Y., Grip, N., Ohlsson, U., & Elfgren, L. (2016). "FEM-based research on the dynamic response of a concrete railway arch bridge." *19th Congress of IABSE Stockholm 2016: Challenges in Design and Construction of an Innovative and Sustainable Built Environment*, International Association for Bridge and Structural Engineering (IABSE), Stockholm, Sweden, 2472-2479.

AUTHOR BIOGRAPHICAL SKETCHES

Jonny Nilimaa is associate senior lecturer at Luleå University of Technology, Luleå, Sweden. He received his PhD from Luleå University of Technology in 2015.

Cristian Sabau, MACI**,** is PhD student at Luleå University of Technology, Sweden, and fellow within the European network for durable reinforcement (Endure), a Marie Skłodowska-Curie research fellowship programme (2013-2017).

Niklas Bagge is consultant bridge engineer with WSP, Luleå, Sweden. He received his PhD from Luleå University of Technology, Sweden, in 2017.

Arto Puurula is associate professor at Savonia University of Applied Sciences in Kuopio, Finland. He received his PhD from Luleå University of Technology, Sweden, in 2012.

Gabriel Sas is assistant professor at Luleå University of Technology, Sweden, and a Researcher at Norut Technology in Narvik. Norway. He received his PhD from Luleå University of Technology in 2011.

Thomas Blanksvärd is working with SKANSKA, Sweden, and as a part time associate professor of structural Engineering at Luleå University of Technology. He received his PhD from Luleå University of Technology in 2009.

Björn Täljsten is professor of structural engineering at Luleå University of Technology. He has been a Professor at Denmark University of Technology in Copenhagen and has also worked with SKANSKA and STO. He received his PhD from Luleå University of Technology in 1994.

Anders Carolin is senior bridge engineer at Trafikverket in Luleå, Sweden. He is active in Shift 2 Rail, a joint undertaking within the European Research Program Horizon 2020. He received his PhD from Luleå University of Technology, Sweden, in 2003.

Björn Paulsson is senior bridge engineer at Charmec Railway Centre in Gothenburg, Sweden. He was earlier at Trafikverket in Borlänge, Sweden, and at the International Union of Railways, UIC, in Paris, France. He received a PhD h. c. from Luleå University of Technology, Sweden, in 2015.

Lennart Elfgren, FACI, is senior professor of structural engineering at Luleå University of Technology, Sweden. He received his PhD from Chalmers University of Technology, Gothenburg, Sweden, in 1971. He is a corresponding member of ACI Committees 355 Anchorage to Concrete, 445 Shear and Torsion, and 446 Fracture Mechanics of Concrete.

High Magnitude Loading of Concrete Bridges

Jacob W. Schmidt, Philip S. Halding, Thomas W. Jensen, Svend Engelund

Synopsis: The motivation for full-scale testing of concrete bridges is significant, since it is deemed to solve some of the major challenges related to capacity evaluation of older concrete bridges combined with increasing load demands. A novel test rig was developed as a mean to evaluate the full-scale bridge response of concrete bridges spanning up to 12 m (39.4 feet). The test rig was fast to mount, applied the load accurately, and loaded the structures to a very high load magnitude. The bridges were loaded to maximum capacity of the test rig without cracking (approx. 100 tonne (220,000 lbs) axle loads). 3D scanning, LVDTs, distance lasers, and DIC cameras were applied to two of the bridges, as well as land surveying readings, in order to measure the structural behaviour during testing. The loading sequence worked well, and it was possible to measure deflections and strains. Using a wide-angle lens DIC-camera showed to be a promising method to measure strains, in-plane deformations and cracking during testing. Work regarding modelling in conjunction with monitoring is ongoing, to provide a more accurate way to evaluate the ultimate capacity of the bridges as well as stop criteria during full-scale testing.

Keywords: Full-scale testing, concrete bridges, test rig, advanced monitoring, Danish standard vehicles, structural response, modelling.

Jacob Wittrup Schmidt, is an associate professor at the Danish Technical University and have more than a decade of experience as bridge consultancy engineer specialist in the industry. His main research field concerns assessment of existing structures in the field of carrying capacity estimations- and multiple scale testing as well as strengthening using conventional- and FRP (Fiber reinforced polymer) materials. Additionally, he has performed full-scale load testing of several bridges.

Philip S. Halding, is Post Doc at the department of Civil Engineering at the Technical University of Denmark. His research regards holistic structural load testing of concrete bridges as well as related tests of sub-components combined with advanced monitoring methods. He is ACI reviewer.

Thomas W. Jensen is an Industrial PhD student at COWI A/S and at the department of Civil Engineering at the Technical University of Denmark. His research encompasses modelling of the load-carrying capacity of concrete bridges in conjunction with field-testing of existing bridges.

Svend Engelund is employed as chief specialist in the department "Transport Infrastructure, North" at COWI A/S in Denmark. He obtained his Ph.D in 1997 and has worked with condition assessment- and load carrying capacity evaluation of existing bridges for more than two decades. Additionally, he has performed full scale load testing of several bridges. His research interests are within reliability analysis of existing bridges and service life estimation of concrete structures.

INTRODUCTION

Many countries suffer from a traffic infrastructure where bridges are worn down, need capacity upgrading or even have to be demolished in order to meet today's demands to increasing traffic and high load magnitudes. Societies are therefore facing an extensive economic burden - A burden that can be reduced if technologies are developed to decrease uncertainties related to bridge capacity evaluations. Full-scale proof loading and destructive testing of concrete bridges is seen as one of the means to reveal the real capacity of different bridge types. Some of the first proof loadings were carried out already in the early 1910s, and different types of bridge tests have been performed in many locations until present date. However, the scopes, final outputs, theoretical approaches, and test procedures related to the full-scale test schemes of the tests vary significantly and can thus be difficult to compare. Dead loading, which is a gravity, or hydraulic force controlled loading, was mainly used in these projects.

Often such testing shows that the capacity is higher than expected in the tested structures, since uncertainties related to the overall structural behaviour, materials, modelling approach etc., are reduced.

However, the real ultimate capacity of the tested structure is often up to discussion since testing normally do not allow damage of bridges in service. Consequently, the margin between the predicted capacity and real ultimate capacity is unknown and can differ depending on the bridge type.
To the authors' knowledge, one of the earliest reported tests to a high load magnitude was conducted in 1913 on a flat arch bridge situated near the Rein in Germany (Elmont 1913). Pieces of steel was placed over an area of 16x26 feet (4.8x7.9 m) on the southern half of the bridge. The highest value of the compression stresses was reached via a concentrated load over the centre of one part of the arch. The magnitude was 2740 psi ((18.9 MPa) and the permissible stress was 560 psi (3.9 MPa). However, no indication of destructive failure was seen at that stage. The approximate weight of the used steel dead load was compared to a 23 tonne (50,700 lbs) steam roller (reference vehicle).

Later testing to failure of a concrete bridge was done in 1952 in the UK, where a three span pre-stressed concrete footbridge at the South Bank, was tested (Unknown 1952). Loading of this bridge was done by using dead loading. The bridge was first tested up to the design live (varying) load and afterwards tested with 50- and 100% overload, where full recovery (due to pre-stressing) was noted in both cases. Afterwards, loading was increased until failure. Failure occurred at a load level of approximately 2.4 times the design load, and the test lasted for approximately three days. Rösli (1963) was one of the first to apply loading by using hydraulic jacks. These were positioned between transverse loading steel beams and road surface on a three-span concrete bridge. Loading was conducted on the 23 m (75.5 feet) mid-span (side spans were 7.5 m (24.6 feet)) where the loading beam was anchored in the bedrock with threaded bars, which were mounted through holes in the bridge deck. It was reported that the ultimate failure load corresponded well to the predicted theoretical values.
Other researchers such as Bergström et al. (2009), Köppel and Vogel (1997), Plos (1995), Song et al. (2002) used similar ground anchor systems.

Gosbell and Stevens (1968) used a loading configuration on a one-span bridge with pre-stressed I-beams and in-situ cast concrete deck. A longitudinal supporting beam was anchored to the bed rock underneath the bridge. This beam had a length, which corresponded approximately to the width of the bridge and provided a fixed support for cables used in the full-scale test. The load configuration consisted of a cross beam above the bridge, attached to the cables near the ends, and loaded at the mid-point by a hydraulic jack. In this research it was stated that the ultimate punching shear was well predicted. However, a load over three times higher than the predicted cracking load was applied to initiate cracking, and no complete failure occurred at that state.

Goodpasture and Burdette (1973) used a load configuration, which simulated the different wheel pressures. A hole through the bridge deck enabled mounting of a bearing grill, which applied the load configuration. The one-span bridge was constructed in reinforced concrete and was a monolithic structure with T-beams. The measured bridge response was compared to theoretical- and AASHO methods, and it showed that the theoretical prediction was close to the measured value. The AASHO method showed a capacity, which was approximately half of the measured value. Jorgenson and Larson (1976) were some of the first to use loading beams in the longitudinal direction of the bridge span. They mounted the loading beams to the bridge piers and applied the hydraulic jacks between the loading beam and bridge surface. Later, this method was also used by Azizinamini (1994). Isaksen et al. (1998) load tested the mid-span of a three-span road bridge using a 6.9x12.5 m (22.6x41.0 feet) casing, which was filled with earth in order to simulate an evenly distributed rectangular load at the centre of the side-span of the bridge. A load corresponding to approximately 5.5 times the characteristic traffic load was reached. The use of hydraulic jacks was later adapted by Zhang et al. (2011, 2013), who placed a ballast box (as a substitute for ground anchors) underneath the bridge in which the loading beam was anchored via bolts. The bridge reached a much higher capacity than expected although the bridge was deteriorated. Additionally, similar testing, where

earth anchors were replaced with counterweight placed underneath the bridge, was conducted by Nanni et al. (1999) and Alkhrdaji et al. (2001). Lantsoght (2013) conducted testing on a multiple span concrete bridge (Ruytenschildt Bridgewhich) to investigate different failure types. A load spreader system was used to apply the desired load configuration. It was in this study concluded that the bridge had a sufficient flexural capacity.

Full-scale bridge testing conducted in Denmark and the ongoing research program

Only limited testing of bridges to failure or high magnitude loading have been done in Denmark. One Danish project in 1980 (Pedersen et al. 1980), tested a slab strip of a pre-stressed two-span bridge using hydraulic jacks, locally at mid-span. In addition, smaller projects, with static load on a one span bridge and a subcomponent (of an ASR (Alkali Silica Reaction) damaged bridge wing) tested on a full-scale bridge (Schmidt et al. 2014), were carried out.

Now, an ambitious research project was initiated in 2016 concerning full-scale testing of one span bridges with maximum span of 12 m (39.4 feet). One of the scopes in this project is to address some of the challenges seen in the literature, and consequently, contribute by solving some of these and thus propose a method to make full-scale testing a more commonly used tool in Denmark when evaluating the capacity of existing concrete bridges (mainly older bridges). The full-scale evaluation method is deemed to reveal if there is a higher load carrying capacity than anticipated by reducing the uncertainties related to the estimation of the structural behaviour.

The main milestones and related research questions in the project were therefore:

- Development of a full-scale test method: Is it possible to construct a test rig, which meets the demands to a high loading magnitude combined with a fast and precise in-situ full-scale test?
- Simplified monitoring: Is it possible to optimize advanced monitoring to a level, where measurements are performed in a fast- and simplified way, and at the same time reveal governing stop criterions?
- Calibration of theoretical models: Can advanced theoretical models be presented in a more abridged way, where it is calibrated, via input from in-situ testing, to the developed monitoring method?

Consequently, the first milestone was to develop a test rig, which could simulate the theoretical way of applying vehicle loads to a concrete bridge structure according to regulations by the Danish Road Directorate (2010). Based on the knowledges of the research team, experience from literature, and general demands to in-situ testing, it was decided to develop a test rig, which comply with a number of demands: A high magnitude load level (or testing to failure), a short test period, easy mounting, precise placing, and loading which is positioned identically to the one used in the Danish classification system (Danish Road Directorate, 2009).

LOADING PROCEDURE AND THE DANISH CLASSIFICATION SYSTEM

Administration and control of heavy vehicles in Denmark is handled through a unique bridge classification system, where both bridges and heavy vehicles are categorized in classes. Such classification is made according to Danish Road Directorate (2009) and is based on different sizes of "standard vehicles" with a defined load configuration. A heavy vehicle can pass the bridge if the bridge class is higher than the vehicle class. If the vehicle class is higher than the bridge class, the weight shall be reduced or re-arranged (to reach a lower class), otherwise an alternate route must be found. The Danish Road Directorate and engineering consultancies have developed a strategic road map based on this system, where heavy vehicles can drive safely. However, the number of heavy vehicles has increased significantly during the last decade, resulting in more restrictions and assignments of alternate routes as well as traffic delays. As a consequent, this is a huge- and increasing loss of time in traffic delays.

A plan view example of a load configuration is shown in Figure 1 with three lanes, two standard vehicles, and a fixed “traffic load”, p, distributed as a surface load. These traffic load configurations shall be placed as critically as possible (standard vehicle “A” in most critical lane) on the bridge to represent the worst loading case scenario according to (Danish Road Directorate, 2009). The standard vehicle B has a fixed size and weight, which corresponds to the least heavy vehicle (class 50) used from the classification system, Figure 2. The size and weight of standard vehicle “A”, combined with the other loads, must be within the limits of the load carrying capacity of the bridge. This means that the standard vehicle “A” provides the basis of a bridge class (the heavier a standard vehicle “A”, the larger a class). The width of the lanes dedicated to the “A”- and “B” vehicles are 3 m (9.8 feet) each, and the distance between the outer side tire faces is 2.6 m (7.9 feet) for vehicle classes up to class 100 and 2.8 m (9.2 feet) above class 100.

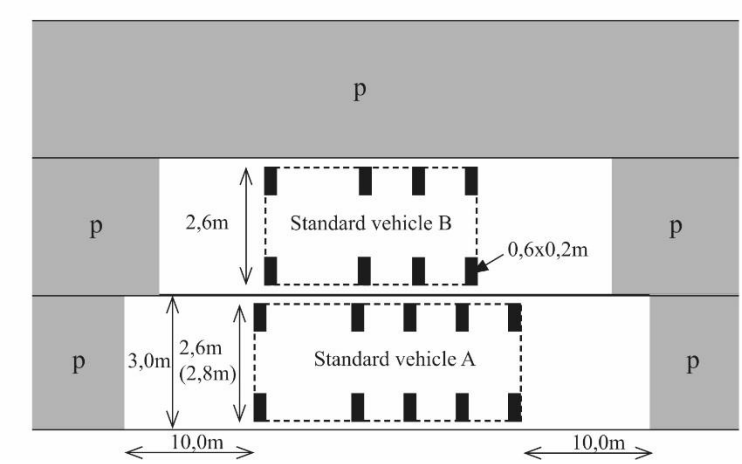

Figure 1 – Plan view of example of load configuration with standard vehicle "A" and "B", as well as uniformly distributed traffic load, p, (Danish Road Directorate, 2009) .

A class 50 (threshold between a conventional- and heavy vehicle), 100 (approximate classification magnitude used for existing old bridges), and highest class 500 vehicle axle configurations and related axle loads are shown in Figure 2. It is seen that the largest magnitude axle loads are on the rear axles. As the class of the standard vehicle increases, the number- and weight of the rear axles increase (class/rear axle load in tonne/rear axle load in lbs): 150/17.8/39200; 200/21.0/46300; 300/22.4/49400; 400/23.0/50700; 500/23.7/52200.

Each wheel load is rectangular and provides a local pressure on an area of 200 mm x 600 mm (7.9x23.6 inches). The uniformly distributed "traffic load" from Figure 1 is of magnitude 2.5 kN/m^2 (0.36 psi) including a dynamic amplification factor. As it is seen from Figure 2, the multiple axle distances at the rear location provide a configuration, where only a limited number of axle loads are acting on the bridge when the vehicle pass short span bridges. The classification system provided the basis for the load magnitudes and -configuration used, when the full-scale bridge test method, presented in this paper, was developed.

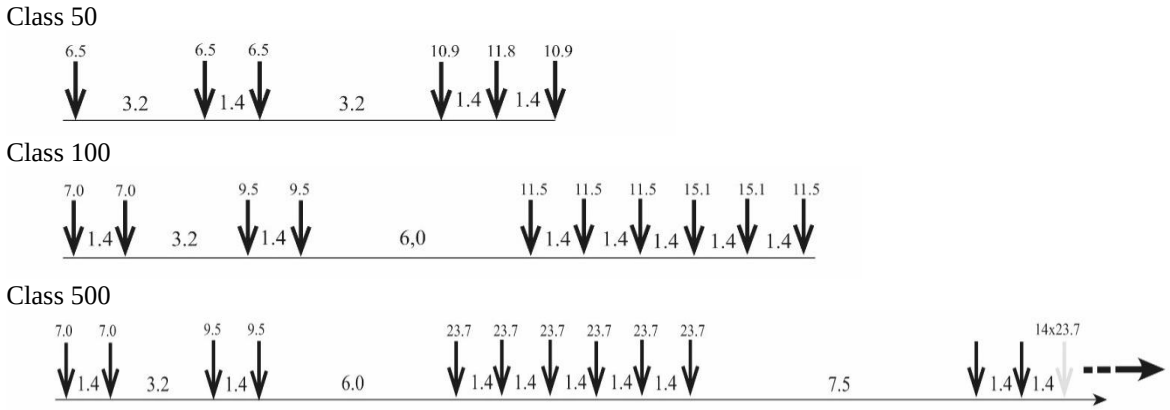

Figure 2 – Axle configuration of standard vehicles. Axle weight in tonne, distances in m (Danish Road Directorate, 2009).

THE FULL-SCALE TEST RIG

The novel full-scale test rig was constructed as a cradle system, where loading was applied using weights and hydraulic jacks combined, to generate a high magnitude load, Figure 3. This configuration provides a very flexible system, since dead load can be applied to a determined magnitude (which often depends on the nature of the failure mode) and the hydraulic actuators control the remaining load. The standard vehicle "B" is typically applied as dead load, but this depends on the application. Steel frames provide a load configuration according to the classification system, which correspond to the standard vehicle "A" and "B".

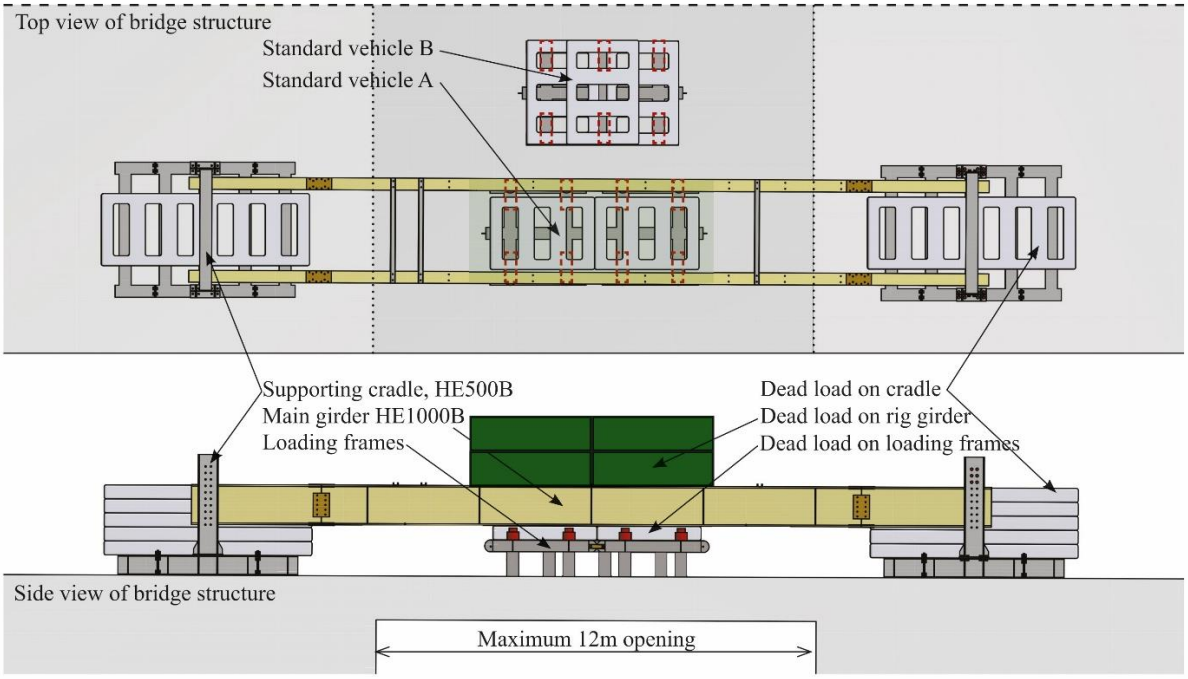

Figure 3 – Top and side view of loading rig where the standard vehicles "A" and "B" are placed in the most critical positions as required in the classification system.

Crane ballast weights, of 3.2 tonne (7100 lbs) and approximately HxWxL = 90 mm x 1850 mm x 2400 mm (3.5x72.8x94.5 inches), are placed on the frames to a desired, pre-determined level, and the hydraulic actuators are placed between the main HE1000B rig girder (standard I-girder with a height of 1000 mm (39.4 inches) and flange width of 300 mm (11.8 inches)) and the frames.

The frames for the standard vehicle "A" load, are constructed with axles in pairs and can be moved within the longitudinal direction of the test rig, whereas the standard vehicle "B" frame is constructed with three axles (corresponding to rear axles from a class 50 vehicle).

Two supporting cradle structures (constructed in HE500B, standard I-girder with a height of 500 mm (19.7 inches) and flange width of 300 mm (11.8 inches)) are positioned at each end of the main girders. The cradle structures are subject to a lifting force during testing, and the ballast weight on the cradles are modified to a level that correspond to the load applied during bridge testing plus approximately 10 tonne (22,000 lbs) at each cradle. This ensures that the cradles are stable and not lifted from the ground. Consequently, the cradle structures provide only limited weight on the adjacent area when the maximum test load is reached. They will safely decline to the original position, if structural failure or large rapid deformations occur during testing. Also, additional weights can be placed on the main HE1000B girders in order to reduce the applied dead load on the frames or to enable an even higher magnitude loading.

A hypothesized load/time curve is shown in Figure 4. The standard vehicle "B" is applied as the first level of dead load on the structure. Additional dead load is added to the standard vehicle "A" steel frames if desired. Loading from the hydraulic jacks is then added to the base dead load regimes (A, B, C….n) in each loading step. This setup provides a flexible high magnitude loading, where the load steps can be controlled and decided upon before testing but also during testing if required.

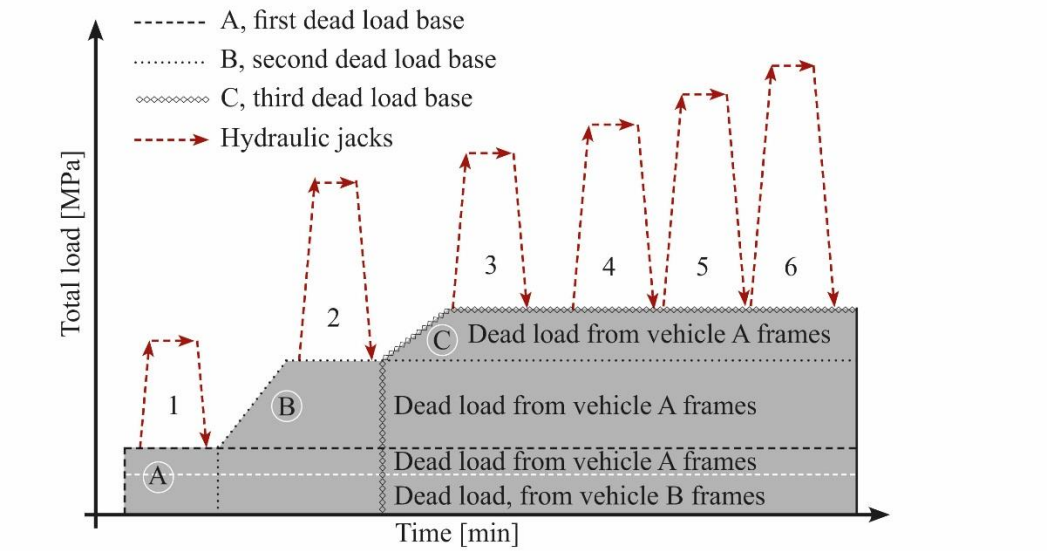

Figure 4 – Example of loading sequence with load peaks by hydraulic jacks, and increasing dead load.

Trial test loading procedure

A trial test was performed before testing of the full-scale bridges, see Figure 5. This test was executed to ensure that all parts of the loading rig fit well together, and to confirm that it was possible to perform loading sequence and magnitude as desired. The hydraulic jacks were positioned on top of each wheel location on all the frames to test if loading on six axles could be controlled separately. An EnerPac (2017) hydraulic controller pump unit performed a precise loading of the jacks. Loading of each step was performed through a predefined load magnitude, and it was limited by a decided deflection threshold. This loading system was chosen, since the applied wheel load should be accurate and controllable during testing.

Force controlled load alone is not desirable, since sudden failure could occur, if the bridge was weakened due to failure initiation. A deformation rate control of approximately 0.5 mm/sec (0.020 inch/sec) was added to ensure that the hydraulic pressure decreased if the bridge deflected too much during a load step. A purely deformation controlled loading system was also discussed, but such a system was not chosen since it could not provide a controllable wheel load.

Figure 5 – Trial testing of rig used as verification- and acceptance of the method before full-scale bridge testing

The test rig was constructed in a way which enabled the test equipment- and ballast to be transported to the test site, erected, dismantled and removed within one day. The test equipment and the ballast was delivered and removed on a number of flat-bed trucks. The erection and dismantling of the test equipment was performed using a mobile crane with a capacity of approximately 20 tonne (44,000 lbs) (with a maximum reach of 15 – 20 m (50 - 65 feet)). The total cost related to the delivery, erection, and removal of the test equipment and ballast at a given test site was approximately 30.000 € (exclusive monitoring, which is currently being optimized). This also includes rent of jacks and the equipment for controlling jacks. The cost greatly depends on the total weight of the ballast used during full-scale testing. In the presented full-scale testing, the weight of the ballast was 400 – 500 tonne (881,850 lbs - 1,102,311 lbs). It is deemed, that the cost will be significantly lower in proof loading applications since the ballast weight reduces.

TEST BRIDGES

The tested one-span bridges were located on the former main road between Herning and Holstebro in Denmark. After testing, they would be demolished and replaced due to construction of a new freeway. These circumstances enabled the opportunity to perform full-scale testing to a high magnitude load at a destructive level. The bridge types on this main road mainly consisted of OT-beam (overturned T-beam) bridges. Four bridges of this type were tested:

#1. Bridge 422-0-005, Underpass of Foldagervej (road) – 11 m span (36.1 feet)
#2. Bridge 422-0-009, Underpass of Rosmosevej (road) – 9 m span (29.5 feet)
#3. Bridge 422-0-004, Underpass of Løven Å (creek) – 5.9 m span (19.4 feet)
#4. Bridge 422-0-005, Underpass of Herningsholm Å (creek) – 10 m span (32.8 feet)

Figure 6 shows drawings from bridge #1, which is used as an example for all four bridges in regard to the structural build up, since they were almost similar.

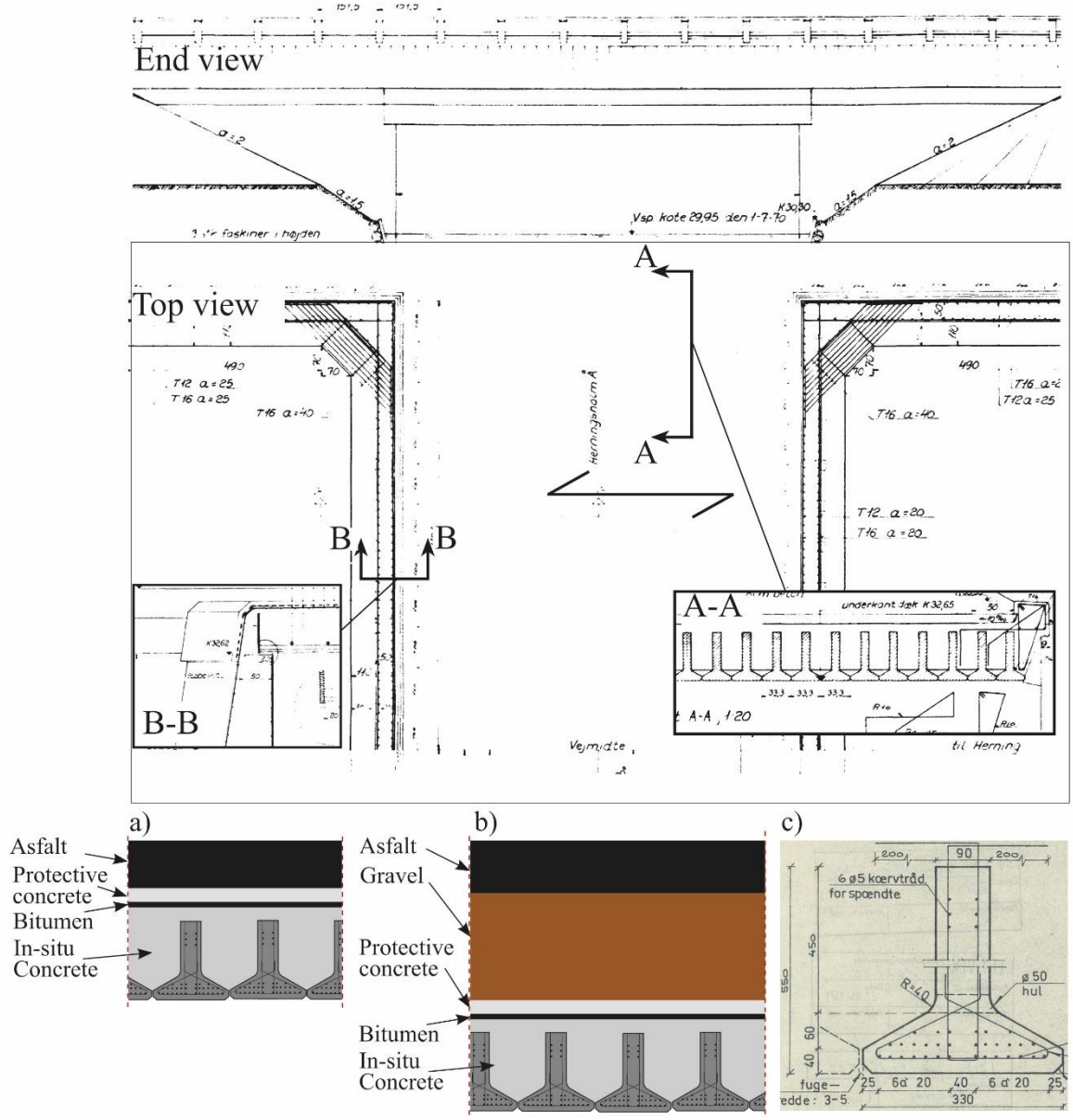

Figure 6 – End- and top view from bridge #1 as well as section view from original drawings. a) Build-up of cross section without gravel (not in scale), b) Build-up of cross section with gravel (not in scale) and c) OT-beam cross section.

The bridge deck was constructed with pre-stressed OT-beams with a height of 450 mm (17.7 inches) and a width of 330 mm (13.0 inches). The beams provided an in-situ mould in which regular concrete was cast. A bitumen

coating provided the insulation layer together with a 100 mm (3.94 inches) protective concrete layer. Asphalt was cast on top of the insulation layer. Bridge #3 and bridge #4 had a gravel layer between the protective concrete layer and the asphalt.

The following material parameters are from bridge #3. They do, in combination with the original drawings, provide the background for the initial capacity calculations of the bridges. It was stated that the strength of OT-beams had a characteristic compression cylinder strength of 45 MPa (6,500 psi), and that the pre-stressing strands 0.2 % yield tensile strength was 1500 MPa (220,000 psi) (The ultimate tensile strength was 1800 MPa (260,000 psi)). Compressive cylinder strength of the in-situ cast concrete, including the edge beams, had a characteristic value of 30 MPa (4,400 psi).

BRIDGE LOADING

Bridge #1 and bridge #2 were evaluated to be the most optimal bridges for testing, since they had relatively long spans (of 11 m (36.1 feet) and 9 m (29.5 feet) respectively) as well as available space above and below the bridge. Bridge #3 and bridge #4 were tested as well, but as pre-tests with a reduced maximum load, and limited monitoring. Loading of these bridges was also performed to verify the controlling, loading and general usability of the test rig. The aim of the testing of these bridges was to reach a high loading magnitude under full control. Subsequently, the rig was moved for testing of the main bridges: #1 and #2.

Loading configurations

The loading is based on the Danish classification system. Examples of the loading configurations on bridge #3 and bridge #4, and on bridge #1 and bridge #2 are seen in Figure 7. The load setup was positioned in the most critical lanes of the bridges.

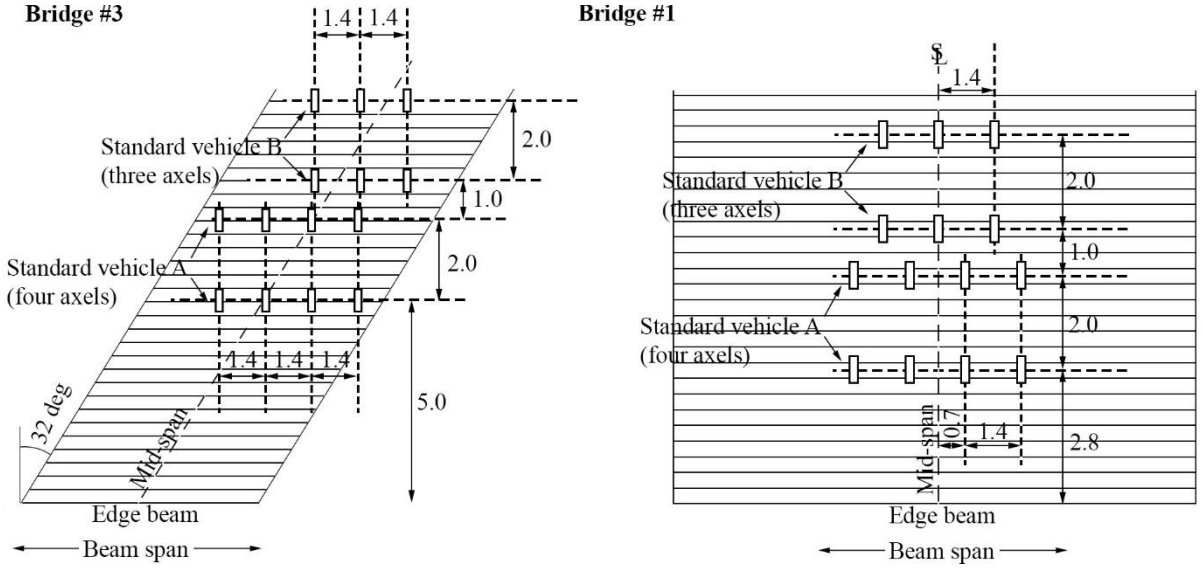

Figure 7 – Plan drawing of load setup with positions of wheel loads of trial bridge #3 and main bridge #1. Width of one OT-beam is 0.33 m (1.1 foot). Units in meters.

Approximately 100 tonne (220,000 lbs) dead load was placed on each cradle and additional weight in the test rig main girder was added to enable the high magnitude loading history on the bridge, Figure 8.

Figure 8 – Overview picture from testing performed on bridge #2

MONITORING

The main emphasis was on monitoring of bridge #1 and bridge #2, since access was possible both below and above the bridges, and they were evaluated to be the most optimal structures for this task. The initial monitoring on bridge #1 was placed as seen on the left in Figure 9a and consisted of: 12 distance lasers, 2 LVDTs (Linear Variable Differential Transformer), one wide-angle camera (used for DIC method), a surveyor, and load- and deformation output from the hydraulic jacks..

Monitoring equipment on bridge #2 was positioned as seen in Figure 9b and consisted of: 12 distance lasers, a laser scanning system, 6 LVDTs, 6 strain gages, a wide-angle camera for DIC, a surveyor, and load- and deformation outputs from the hydraulic jacks.

One of the ideas behind the monitoring methods, was also to provide knowledge concerning the applied systems and how they work in conjunction with the loading rig. This was deemed important, since in-situ monitoring can be very challenging due to environmental conditions (external noise, temperature, humidity, light etc.), access to the measurement points and limited time for testing.

Bridge #1 was tested under dry, calm conditions in the summer with a temperature around 20 C (68 F), while bridge #2 was tested under wet, cold and windy conditions in the wintertime with temperatures around 0 C (32 F).

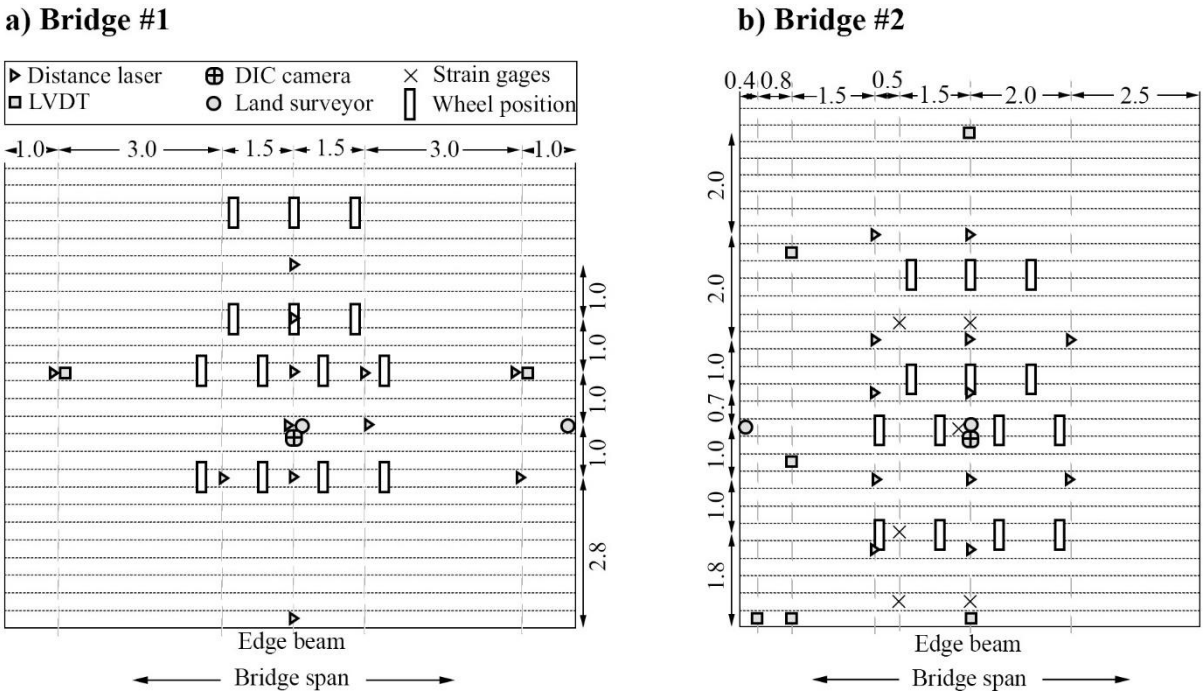

Figure 9 – Plan drawings with applied equipment of a) bridge #1 and b) bridge #2. Width of each OT-beam was 0.33 m (1.1 foot). Unit is meter.

Equipment specifications

The monitoring equipment used in the project can be divided into two groups: Equipment for measuring bridge deflections, and equipment for measuring strains and deformations on the concrete surface. The measurements were conducted in a way, which is deemed to open the opportunity for faster future testing, generate unique experience, and at the same time enable a basis for real time monitoring and remote access monitoring. The real-time method will enable diagnosing of the bridge during loading, where remote access ensures that monitoring and loading can be fully- and thus safely controlled externally. The monitoring systems are often time consuming to apply which means that an advanced system has to be optimized in order to reduce the mounting time and still provide consistent monitoring data.

Deflection measurements

A land surveyor performed measurements of bridge deflections at mid-span, and at the supporting wall in one side with precision of 0.1 mm. The purpose of the measurements was to have a reliable external reference to the other deflection measurement methods, and to keep track of the support settlements during the high magnitude loading.

The distance lasers were Leuze electronic (2017) ODSL 30 with analog output (4 to 20 mA), Figure 10b. The lasers were located underneath the bridge with the laser beam in plumb. In the test of bridge #1, the lasers were positioned in a pattern, which enabled a subsequent analysis of the bridge deflections, utilizing symmetry around mid-span. The points of measurement were carefully chosen in order to achieve the best possible basis to evaluate the cross distribution of the load, and the degree of fixation at the supports.

After the test on bridge #1, it was clear that the precision of the lasers (0.2 mm), in the in-situ environment, was too rough to achieve fulfilling measurements close to the supports, where the deflections were very small (up to 3 mm (0.12 inch)). Consequently, the distance lasers were primarily applied in the areas of larger deflection in the following test of bridge #2.

The high precision LVDTs were from Novotechnik (2017) with analog output (0 to 5 V). The precision (0.02 mm) is higher than that of the distance lasers, and therefore, these instruments were positioned closer to the supports, where the deflections were smallest. The measuring pin of this type of LVDT is in contact with the surface, and hence, the LVDT's housings were firmly attached to long rigid metal posts as seen in Figure 10a. In the test of bridge #1, two LVDTs overlapped with the distance lasers to be able to evaluate the instruments against each other.

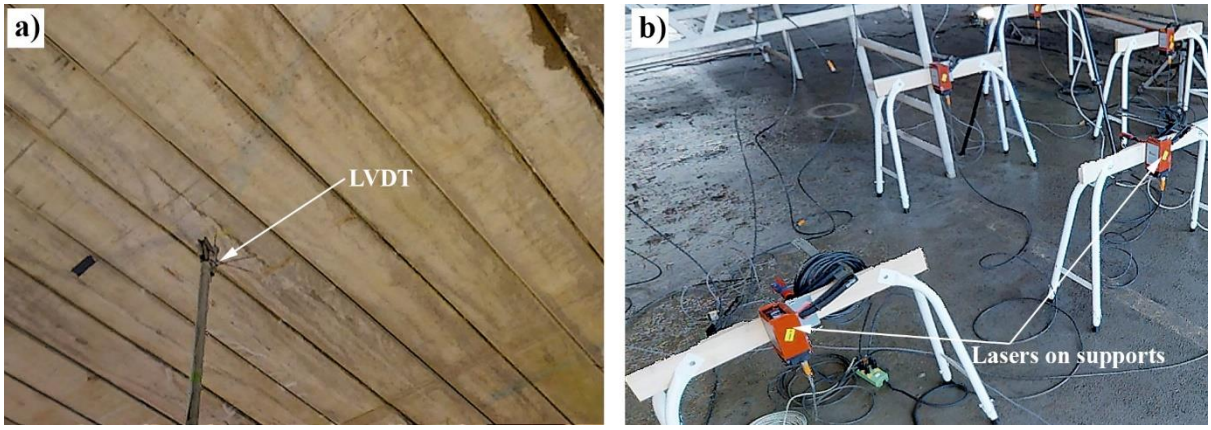

Figure 10 – a) Setup of LVDT positioned on top of rigid pole with pin in contact with concrete surface at bridge #2, and b) distance lasers at bridge #2.

Laser scanning

The Matterport (2017) laser scanning system was applied as a trial method to scan the test setup used for the full-scale testing to reproduce the test environment in virtual reality, and to be able to measure distances between points in the point cloud after the test. An illustration of this is seen in Figure 11a where a) shows a Matterport 3d laserscan with an overlay of a photograph. In Figure 11b, the same scan is shown with the actual points of the 3D point cloud, and an example of measured distance between two of the hydraulic jacks in the setup. The monitoring method also ensures that significant information concerning actual placing of loading points, monitoring points- and equipment, is saved in a detailed way.

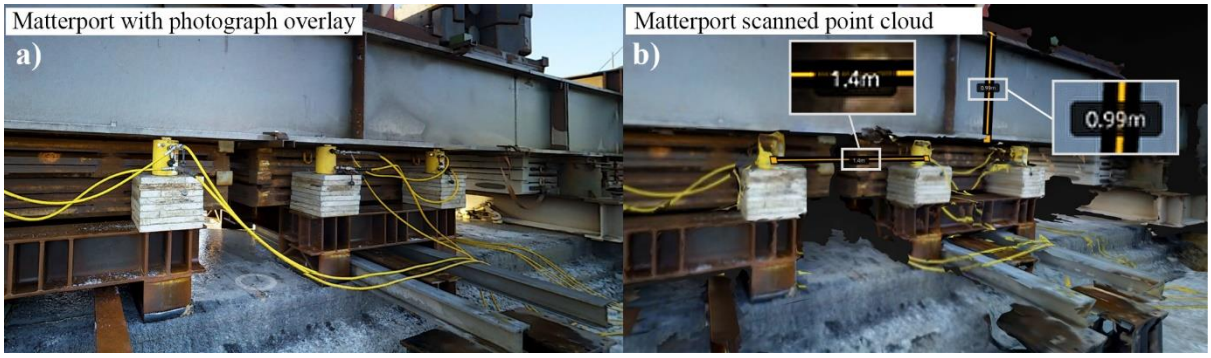

Figure 11 – 3d laser scan from the test rig with example of measured distances between points on hydraulic jacks and on HEB profile.

Horizontal strain and deformation measurements

A DSLR-camera was used to take photographs of the surface underneath the bridge deck in both tests, for later processing in DIC-software. The main novelty of this method relates to the use of a Canon 6d (2017) with a wide-angle lens (Canon EF 16-35mm f/2.8L II USM) which can measure on a much larger surface compared to conventional lenses. The key purpose was to register deformations and crack initiation during loading, but also to compare in-plane strains to strains found by strain gages.

Linear 50 mm (2.0 inches) strain gages from HBM (2017) (LY41-50/120) were applied to the surface of the concrete in the direction of the span in the test of bridge #2. The purpose was to get strain measurements directly from the surface in critical locations and hereby, to reveal the distribution of the applied load.

MONITORING RESULTS

Figure 12 shows output from the applied load on the two bridges during testing. It is seen that the test rig enabled stepwise increase of the dead load as well as a controlled loading by the hydraulic actuators. The jacks enabled the possibility to increase and reduce the loading magnitude as desired in the test plan.

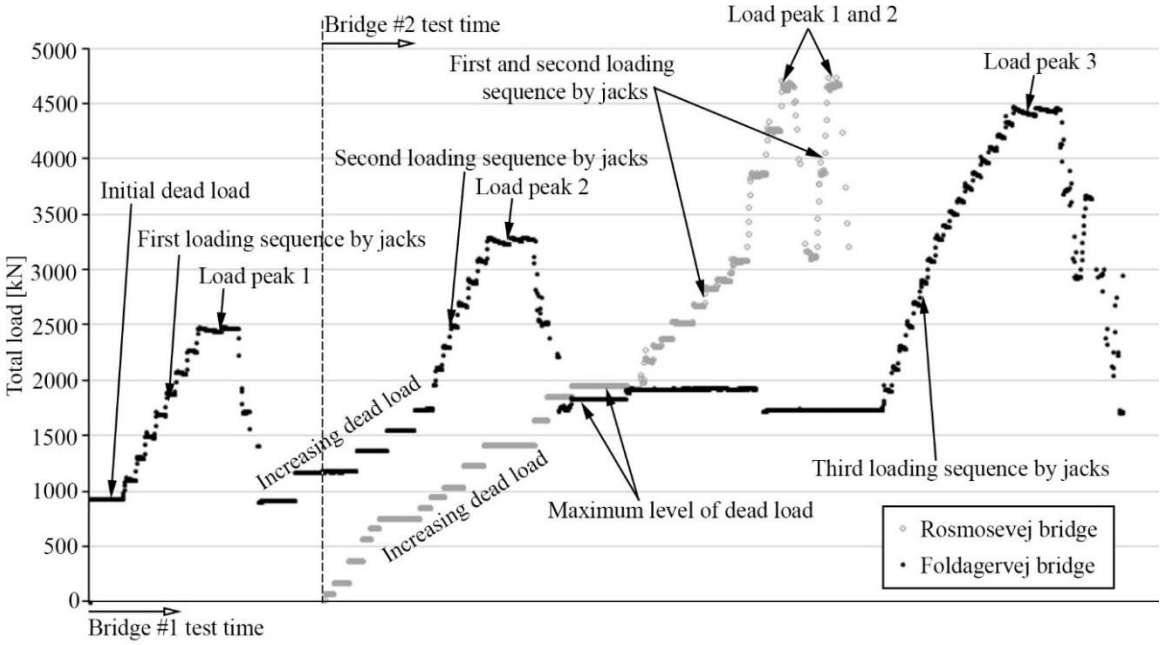

Figure 12 – Loading scheme of bridge #1 and bridge #2. Same time interval between measuring points.

The loading principle in Figure 4 was followed in the test of bridge #1. Initially, dead load was applied at a low magnitude, and then controlled loading by the hydraulic jacks further increased the total load to Load peak 1. After unloading the jacks additional dead load was applied, and subsequently, the jacks increased the total load to the level of Load peak 2. Potentially, this method could continue, but the maximum total load at Load peak 3 was (in this case) reached by using the hydraulic jacks without further increase of the dead load on the bridge.

Deformation measurements and loading magnitudes

In the test of bridge #1, the deformation at mid-span directly at the middle under standard vehicle "A", where the largest deflections were expected, was measured by land surveying instrumentation and laser. The load-deformation-relation is shown in Figure 13a. At the load level shown in the figure, a power cut occurred during the test. The outcome of that was a shutdown of the monitoring equipment including the lasers. After re-establishing the power, the lasers performed a self-calibration. Due to this calibration, the curve, of the laser directly under standard vehicle A, was translated by 1.4 mm (0.06 inches) from the curve from the surveyor. This error has been corrected in the figure. Similar errors of different magnitudes were seen for the other lasers as well. In the test of bridge #2, the curve Figure 13b, a power backup system was used to avoid a similar challenge. The difference in the maximum deflections for bridge #2 is due to a distance of approximately 1 m (3.3 feet) between the laser at mid-span and the land surveyor measuring point at mid-span. The 1 hour 45 min pause in the test of bridge #1 seem to have given a creep settlement of approximately 1 mm according to the laser measurement, which seems reasonable. The land surveyor did not record this settlement, which also underlines the importance of measuring the same parameters by multiple types of monitoring equipment.

In Figure 14 the bridge deflections are shown along the span and across the span. The curves could indicate that the deflections in the transverse direction of both bridges, was distributed across all recorded OT-beams.
Longitudinally, the deflections show that the beam response is almost symmetric which indicate that the load is placed correctly. Information from the measurement might reveal the level of fixation at the supports, which is currently being investigated.

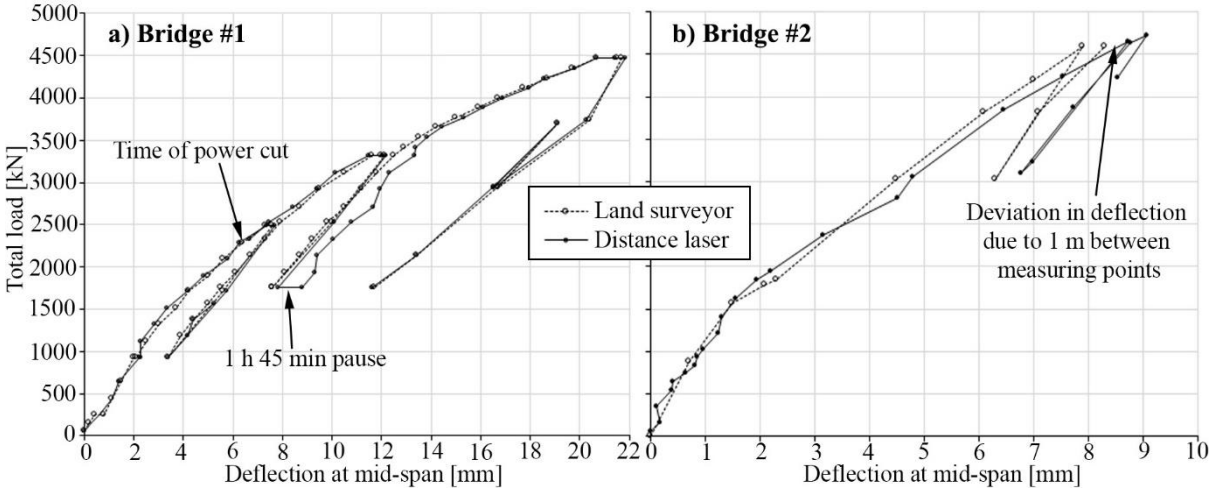

Figure 13 – Mid-span deflection laser vs land surveyor at mid-span from a) bridge #1 and b) bridge #2

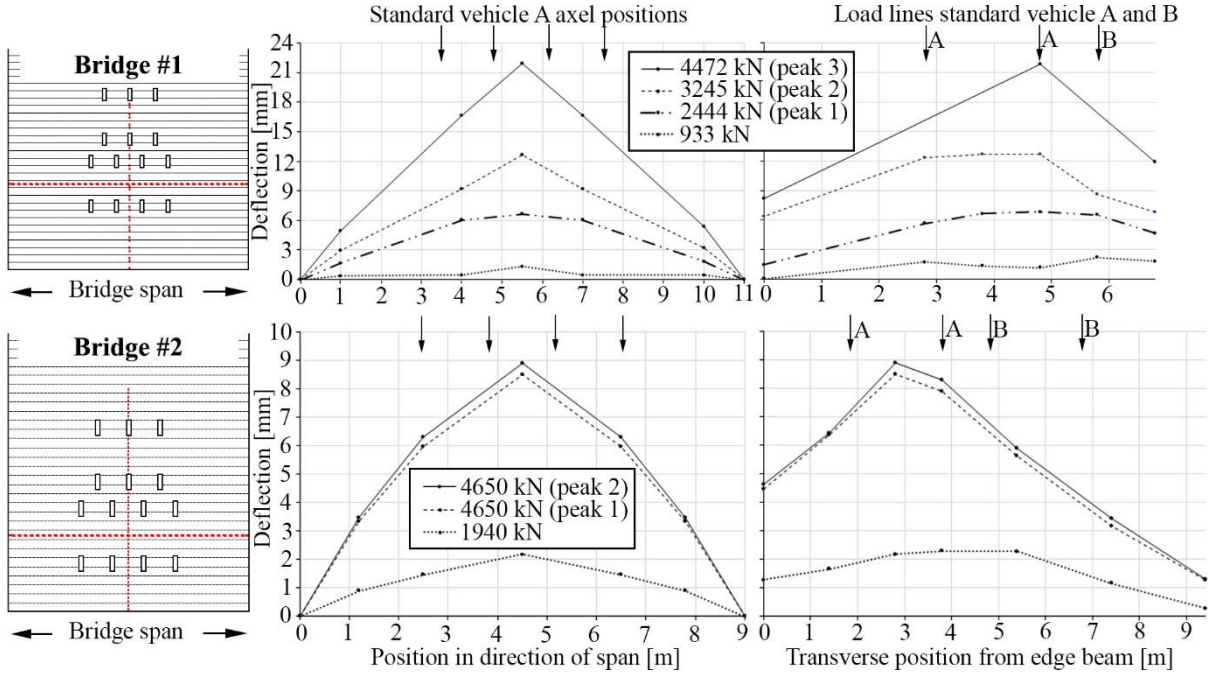

Figure 14 – Longitudinal and transverse deflections of bridge #1 and bridge #2 based on LVDT's, distance lasers, and land surveyor.

In the test of bridge #1 the largest deflection was 21.7 mm (0.85 inches) and was reached at a loading magnitude of 456 tonne (4482 kN or 1,010,000 lbs). The largest settlement during testing was 0.6 mm (0.024 inches) close to the second peak in the loading scheme and 0.8 mm (0.031 inches) after the maximum load at the third load peak. The highest loading magnitude was reached on bridge #2, where a maximum load of 473 tonne (4644 kN or 1,040,000 lbs)) was reached together with a corresponding maximum deflection of 9.1 mm (0.36 inches) at mid-span, and a support settlement of 0.6 mm (0.024 inches). Table 1 shows an overview of the maximum achieved values of loads and deflections in the tests.

Table 1 – Maximum loading magnitudes gained from experiments.

OT-beam bridges	Test date	Span [m]	Span [feet]	Maximum total load [Tonne – kN - lbs]	Maximum axle load [Tonne – kN - lbs]	Maximum deflection [mm – inches]
Bridge #1	September 2016	11.0	36.1	456.4 – 4482 – 1,010,000	95.9 – 942 – 211,000	21.8 – 0.86
Bridge #2	January 2017	9.0	29.5	481.2 – 4725 – 1,060,000	102.1 – 1003 – 225,000	9.1 – 0.36
Bridge #3	September 2016	5.9	19.4	391.2 – 3842 – 862,000	79.6 – 782 – 175,000	3.1 – 0.12
Bridge #4	January 2017	10.0	32.8	362.0 – 3555 –798,000	72.3 – 710 – 159,000	4.4 – 0.17

Only limited monitoring was applied to bridge #3 and bridge #4, where the surveyor measured deflections at mid-span and at the supports (the support settlement was for bridge #3 and bridge #4 also less than 1 mm (0.04 inches)). Reducing the amount of monitoring equipment was necessary due to a tight time plan, and the limited space underneath these bridges. This testing was also used as the first step of verifying the high magnitude load level, which was added to bridge #1 and #2. Also, the performance and general practical usability of the test rig was investigated in these full-scale tests.

DIC and strain measurements

The mid-span deflection curves showed that high magnitude loading was reached. The DIC-camera worked well and captured usable data-pictures during loading. The evaluation showed no visual cracking for neither bridge #1 nor bridge #2 for the given loads. The DIC-system did capture areas of highly increased strains, but due to the pre-compression of the beams, cracks did not initiate at the tested load levels. In Figure 15 longitudinal and transverse strain plot at load peak 3 (total load of 4482 kN (1,010,000 lbs)) of bridge #1 is given next to the reference photograph. The evaluation was performed in the DIC-software GOM Correlate (2017). The longitudinal strain plot shows an increase of strains across the whole monitored surface. Which seems to indicate an activation of a large number of OT-beams and thus an interaction between the beams at a high magnitude load level.

When looking at the plot of transverse strains in Figure 15 and 16, it is clear that the OT-beams separate in the joints, where no tensile strength is deemed available. Large deformations due to separation of elements on the measured surface seems to make it difficult for the DIC-software to recognize the subsets (of 40x40 pixels in the figure), and this is seen as areas of no colour along the joints in the figure. The strains found in the GOM correlate software deviated significantly from the surface strains found in the strain gage measurements. This was due to three factors: i) The distortion created by the camera lens, ii) the out-of-plane deflection of the monitored surface, and iii) the angle between camera and surface when applying a wide-angle camera to cover a large surface area. In Figure 16b the point distances found in three locations across a joint are compared, and the DIC system also shows fine precision in these types of measurements, though the actual values may deviate due to the above-mentioned factors.

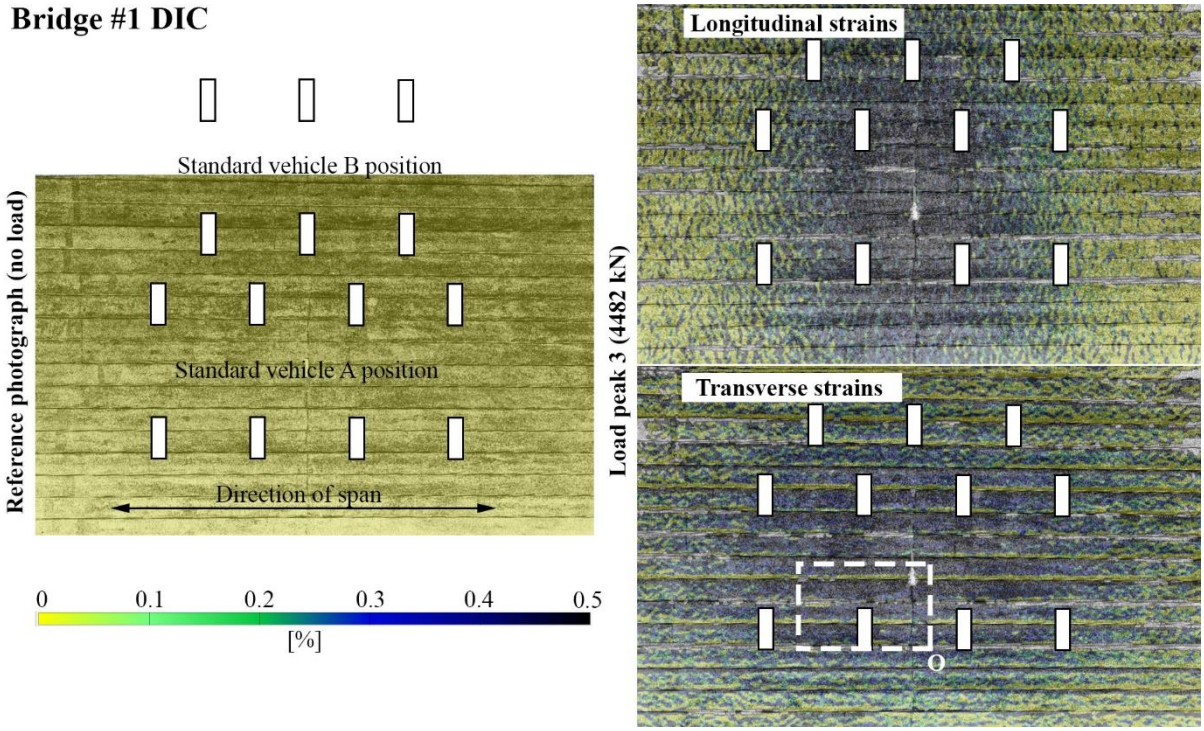

Figure 15 – Direct strain measurements from bridge #1 by DIC at maximum total load. Total area of measurement 8 m x 5 m (26.2x16.4 feet). Facet size 40 pixels. Close-up of highlighted rectangular is shown in Figure 16.

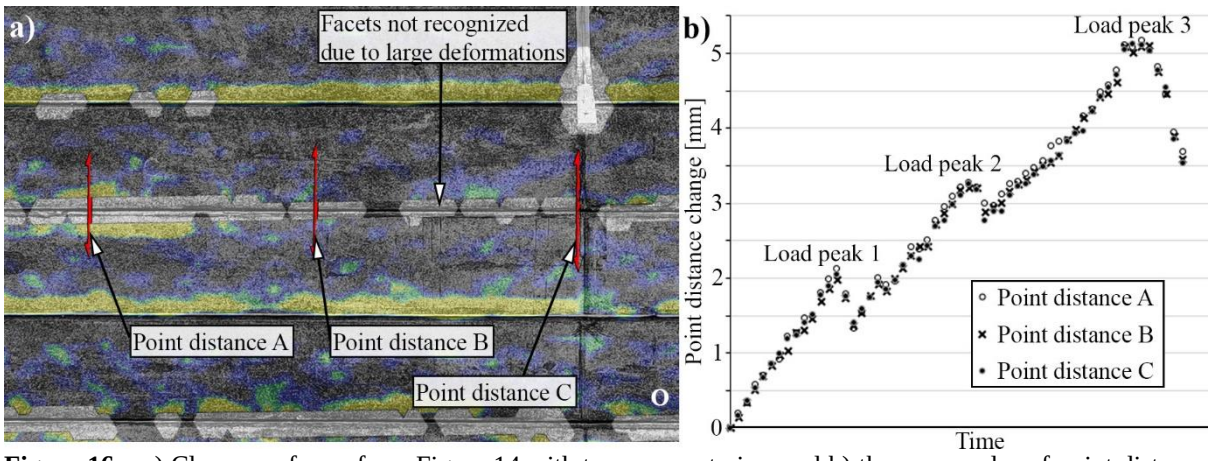

Figure 16 – a) Close-up of area from Figure 14 with transverse strains, and b) three examples of point distance development.

Three of the six strain gages mounted on bridge #2 worked as intended. The three functioning strain gages positioned at mid-span are plotted against the time in Figure 17. It is seen that the maximum surface strain is in the order of 0.023 %. In the area where SG2 is positioned, the surface strain found from the GOM correlate software was above 0.1 %. This discrepancy was due to above mentioned reasons with the DIC-system (results not corrected for lens distortion etc.), and an additional challenge with the wet surface condition experienced when testing bridge #2. All though this difference is present in this example, the DIC-system with wide-angle lens can provide a unique method to monitor strains, deformations and crack initiations (crack initiation measurements were verified in later testing of OT-bridge under same conditions).

The longitudinal strains found with the strain gages in Figure 17 for bridge #2 support the conclusion from the plot of longitudinal strains by DIC for bridge #1. The strains did not deviate much across the OT-beam bridges, and this could indicate that the applied loads were distributed well between the beams. Strain gage 3, positioned underneath standard vehicle "B", showed strains of approximately 75% of the strain at strain gage 2, positioned at the point of maximum deflection under standard vehicle "A". Furthermore, strain gage 1, positioned close to the edge beam, showed 90% of the strain at strain gage 2.

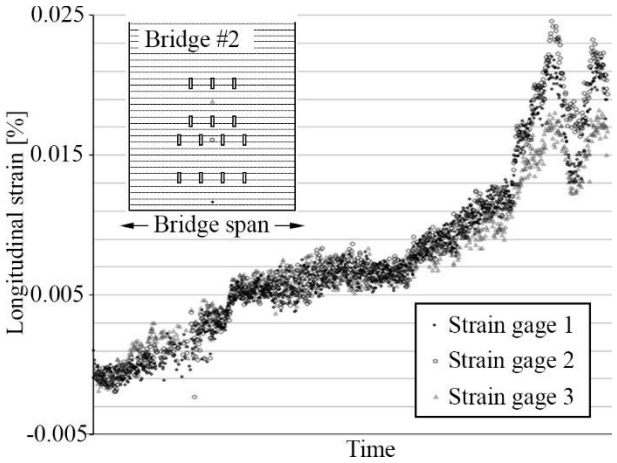

Figure 17 – Strains of strain gages 1, 2 and 3 in direction of span.

FUTURE CHALLENGES RELATED TO MODELING IN CONJUNCTION WITH MONITORING

A part of the research project is calibration of advanced theoretical models, which can be presented in a more abridged way, where the developed models are calibrated, via input from in-situ testing, to the developed monitoring method. When calculating the bridge class in accordance with the Danish classification system, it is seen that the ultimate capacity is used as a threshold for the bridge class. The governing failure mechanism and ability to provide an increased capacity result is, in the case of OT-beam bridges, deemed related mainly to the interfacial interaction between the structural elements, load separation and boundary conditions. However, the ultimate capacity found through a perfect plastic yield criterion does not reveal when damaging of the bridge occurs during testing. Thus, stop criteria has to be chosen in order to find the test limitations, which furthermore challenge the monitoring method. Consequently, the monitoring equipment is the mean to evaluate- and verify specific limits, where the specific bridge exceeds the damage threshold.

Ultimate capacity evaluation

The calculation of the ultimate moment capacity of concrete beams have been well defined for many years. The moment capacity can be based on perfect plasticity, which is provided by assuming a ductile bending failure mechanism. When this is the case, the calculated capacity often complies well with tested capacities. For concrete slabs with well-defined properties, the ultimate capacity can be calculated by assuming perfect plasticity and using limit analysis, which often complies well with the tested capacities.

However, some challenges arise when this method is used for an ultimate capacity evaluation of OT-beam cross-sections such asFigure 6. OT-beam cross-sections have top reinforcement placed orthogonal in the same layer, which could enable the opportunity to use the conic yield criterion. However, the bottom reinforcement of the slab is placed in different levels of the cross section, which differ from the assumptions in the yield criteria. Additionally, some of the challenges related to the theoretical evaluation due to the structural composition are: i) Voids between the precast beams at the bottom of the cross-section (these voids make it difficult to transfer the horizontal shear forces from the twisting moment through the lower bottom of the cross-section). (ii) The precast OT-beams have very limited shear reinforcement, and the in-situ concrete, cast between the precast beams, have no shear reinforcement. (iii) Interfaces between the precast beams and the in-situ concrete, which need to be considered when calculating the shear capacity in the transverse direction. (iv) Due to the lack of shear reinforcement and interfaces, the shear capacity needs to be considered when redistributing the internal forces. A new yield criterion is therefore under development, which combines the interaction between shear and moment. Work is now ongoing regarding calibration of this model to the monitoring output, which verifies the assumptions in the calculations in regard to boundary conditions, material parameters, interactions etc. The OT-beam modelling approach is developed to work in synergy with the used monitoring approach, but is also deem applicable for conventional evaluation of slab bridges, which is a future scope.

Stop criteria during testing

The ultimate capacity result has to be supported by a stop criterion, which decides when to stop a full-scale load-test, in order to prevent permanent damage of the bridge. Applied monitoring have shown the potential in verifying, if the structure behaves as predicted. This means that monitored information concerning boundary conditions, concrete cracking, deflections, and strains could provide reliable and relevant data about the structural behaviour including critical areas where failure potentially could occur. However, stop criteria can differ significantly depending on the bridge type, where the weakest positions of the bridge have to be found and

monitored. Being able to monitor the structural response during testing might provide confidence into the theoretical method, when they are calibrated together. The approach shown in this paper is, among the other objectives, developed to provide a method to evaluate the structural response and reveal the weakest areas of the structure. However, it is still an open question how short-term loading verify long term and fatigue effects, and how early brittle failures can be identified before they occur. These challenges are presently being investigated in the project.

CONCLUSION

The goal of developing a full-scale test rig for bridges up to 12 m (39.4 feet), which could apply a high magnitude load via an axle configuration, in accordance with the Danish classification system, was reached in the project. The novel test rig was shown to be fast to mount and provided a very accurate- and controllable load to the concrete OT-beam bridge structures. Consequently, every test was performed within one day. Four OT-beam bridges were tested, and two of these were loaded up to an axle load of approximately 100 tonne (220,000 lbs), which was the limitation of the test rig. No cracks were identified at that stage, however.

Distance lasers gave results of deflections with an accuracy of 0.2 mm. They corresponded well with the LVDT- and surveyor measurements, although the distance laser tolerance was larger than the other deformation measurement methods (LVDT: 0.02 mm, surveyor: 0.1 mm). The three deflection measurement methods worked well in combination. Measurements by land surveying instrumentation provided an extra reliable method to measure the mid-span deflections from a distance. 3D scanning provided a good tool for full-scale testing to reproduce the test environment in virtual reality and enabled distance measurements of the parts in the test setup.

A wide-angle high resolution DIC-camera was used and showed to be a promising method to measure strains, deformations and cracks initiations during testing. The wide-angle camera revealed a capability of measuring in-plane deformations and strains on a surface of 40 m^2. However, distortion created by the camera lens, and deviations due to out-of-plane deflection of the monitored surface, were deemed to affect the results, which were also seen in deviations between strains measured directly from DIC and foil strain gages. These effects are presently being evaluated more thoroughly and the results will be presented in future papers.

The monitoring equipment provided unique in-situ monitoring experience and seem to be one of the ways forward to determining stop criteria in future tests. The monitoring results from the given setup will be used, in conjunction with a theoretical evaluation of the ultimate capacity, to develop a threshold for the stop criteria, which is the next step of the project.

In addition, some challenges were related to the monitoring, which resulted in the lack of data from some of the monitoring devices. These related mainly to the weather conditions and time pressure. The wet surface made monitoring difficult and influenced the readings from lasers, DIC system and strain gauges. Preparation and structuring of the equipment, as well as calibration on site, was a challenging task due to a significant time pressure. However, the project team gained very important knowledge, which can be used when performing future full-scale in-situ testing.

ACKNOWLEDGEMENT

The financial support and assistance from the Danish Road Directorate is greatly acknowledged. Additionally, the assistance from the Danish crane firm BMS was invaluable, as well as the support from the technical staff at DTU Civil Engineering.

REFERENCES

Danish Road Directorate, EN 1991-2 DK NA:2009 - Annex A – Lastmodeller for klassificering og bæreevnevurdering, 2009.

Danish Road Directorate, 978-87-7060-359-1 – Broer. Vejledning til belastnings- og beregningsgrundlag, 2010.

Alkhrdaji, T.; Barker, M.; Chen, G.; Mu, H.; Nanni, A. and Yang, X., 2001, "Destructive and non-destructive testing of bridge J857, Phelps County, Missouri. Volume 1 - strengthening and testing to failure of bridge decks"

Azizinamini, A., 1994, "Old concrete slab bridges.1. Experimental investigations", *Journal of Structural Engineering-Asce*, V. 120, No. 11.

Bergström, M.; Täljsten, B. and Carolin, A., 2009, "Failure Load Test of a CFRP Strengthened Railway Bridge in Örnsköldsvik, Sweden", *Journal of Bridge Engineering*, V. 14, No. 5, pp. 300–308. https://doi.org/10.1061/(ASCE)BE.1943-5592.0000005

Canon Global, www.canon.com (accessed June 14, 2017)

Elmont, V. J., 1913, "Test-loading until breaking point of a 100-foot arch bridge", *Canadian Engineer*.

EnerPac, www.enerpac.com (accessed June 14, 2017)

GOM, www.gom.com (accessed June 14, 2017)

Goodpasture, D. W. and Burdette, E. G., 1973, "Full Scale Tests to Failure of Four Highway Bridges", *American Railway Engineering Association*, V. 74, No. 643, pp. 454–473.

Gosbell, K. B. and Stevens, L. K., 1968, "Test loading of a full scale bridge", In *A.R.R.B Proceedings*, V. 4, pp. 2018–2041.

HBM, www.hbm.com (accessed June 14, 2017)

Isaksen, H. R.; Kanstad, T. and Olsen, P.-E., 1998, "Prøvebelastning av bru nr 02-1234 Smedstua bru.

Jorgenson, J. L. and Larson, W., 1976, "Field Testing of a Reinforced Concrete Highway Bridge to Collapse, *Transportation Research Record*, No. 607, pp. 66–71.

Köppel, S. and Vogel, T., 1997, "Feldversuch Steilerbachbrücke", https://doi.org/10.3929/ETHZ-A-001853810

Lantsoght, E. O. L., 2013, "Shear In Reinforced Concrete Slabs under Concentrated Loads close to Supports", https://doi.org/10.4233/UUID:3C0045DC-66B2-4151-B778-C318A96B22BC

Leuze electronic, www.leuze.com (accessed June 14, 2017)

Matterport, www.matterport.com (accessed June 14, 2017)

Nanni, A.; Alkhrdaji, T.; Chen, G.; Barker, M.; Yang, X. and Mayo, R., 1999, "Overview of testing to failure of a highway bridge strengthened with FRP composites", In *4th International Symposium on FRP for Reinforcement of Concrete Structures (FRPRCS4)*, pp. 69–80.

Novotechnik, www.novotechnik.com. (accessed June 14, 2017)

Pedersen, E. S.; Nielsen, P. M. and Lyngberg, B. S., 1980, "Investigation and failure test of a prestressed concrete bridge". In *11th Congress - International Association for Bridge and Structural Engineering (iabse) Final Report*, pp. 849–854.

Plos, M., 1995, "Application of fracture mechanics to concrete bridges", Chalmers tekniska högskola. Avdelningen för betongbyggnad.

Rösli, A., 1963, "Die Versuche an der Glattbrücke in Opfikon", *Eidgenössische Materialprüfungs- Und Versuchsanstalt Für Industrie, Bauwesen Und Gewerbe*, V. 192, No. 85.

Schmidt, J. W.; Hansen, S. G.; Barbosa, R. A. and Henriksen, A., 2014, "Novel shear capacity testing of ASR damaged full scale concrete bridge", *Engineering Structures*, V. 79, pp. 365–374. https://doi.org/10.1016/j.engstruct.2014.08.027

Song, H.-W.; You, D.-W.; Byun, K.-J. and Maekawa, K., 2002, "Finite element failure analysis of reinforced concrete T-girder bridges", *Engineering Structures*, V. 24, No. 2, pp. 151–162. https://doi.org/10.1016/S0141-0296(01)00107-9

Unknown, 1952, "Destruction of the Prestressed Concrete Footbridge at the South Bank", *Civil Engineers Review*, V. 6, No. 8, pp. 330–334.

Zhang, J.; Peng, H. and Cai, C. S., 2011, "Field Study of Overload Behavior of an Existing Reinforced Concrete Bridge under Simulated Vehicle Loads", *Journal of Bridge Engineering*, V. 16, No. 2, pp. 226–237. https://doi.org/10.1061/(ASCE)BE.1943-5592.0000140

Zhang, J.; Peng, H. and Cai, C. S., 2013, "Destructive Testing of a Decommissioned Reinforced Concrete Bridge", *Journal of Bridge Engineering.* V. 18, No. 6, pp. 564–569. https://doi.org/10.1061/(ASCE)BE.1943-5592.0000408

Torsional Effects on Load Tests to Quantify Shear Distribution in Prestressed Concrete Girder Bridges

Benjamin Z. Dymond, Catherine E. W. French, Carol K. Shield

Synopsis: Torsion due to superimposed loads is often ignored in prestressed concrete bridge girders because it is considered negligible compared to other forces that control the structural design. However, during load testing of prestressed concrete girder bridges, shear strains due to torsion can be on the same order of magnitude as shear strains due to the vertical shear force resultant for superimposed loads. The inability to differentiate between the two types of shear strains may lead to inaccuracy when determining the vertical shear force distribution in statically indeterminate bridge structures. Rosette strain gages need to be placed on both sides of the girder web to differentiate between torsion and vertical shear to characterize the shear distribution. The need for this instrumentation configuration likely applies to other studies in the literature that have calculated shear force through the use of rosette strain gages on only one side of prestressed concrete girder webs in bridges. This paper discusses best practices to quantify shear distribution data. The study included tests and finite element modeling of laboratory and field bridges.

Keywords: concrete bridge, load testing, prestressed concrete, vertical shear strain, torsional shear strain, finite element model

INTRODUCTION

American Association of State Highway and Transportation Officials (AASHTO) requirements for the consideration of shear in prestressed concrete girders have changed considerably over the last 50 years. When some prestressed concrete girder bridges designed using older specifications are rated with current methods, the structures may rate poorly for shear. If bridges that rate poorly for shear do not show signs of distress under normal traffic conditions, they are often deemed to be in good condition and therefore the resulting shear rating may be neglected (AASHTO, 2011; Bradberry, 2015). Overly conservative shear distribution provisions were believed to be one reason that bridges can appear to be in good condition even though they rate poorly for shear (Dereli et al., 2010). To assess the accuracy of the AASHTO provisions, research was conducted by researchers at the University of Minnesota Twin Cities to investigate live load shear distribution in prestressed concrete girder bridges using experimental testing and numerical modeling methods. This paper focusses on the load testing methods used to quantify shear distribution and on the effect of torsion observed during the load tests.

Torsion in prestressed concrete bridge girders due to superimposed loads is often ignored because the low magnitude torque is considered negligible when compared to other forces that control the structural design. However, during load testing of prestressed concrete girder bridges in the laboratory and in the field (Dymond et al., 2016), the torsional shear stresses and vertical shear stresses due to the superimposed loads were of similar magnitude for some load cases. Previous research studies related to shear distribution in prestressed concrete bridge girders have not discussed the relative magnitudes of torsional shear stresses and vertical shear stresses (Millam and Ma, 2005; Cross et al., 2006; Cross et al., 2009). Cross et al. (2009) observed up to 25% difference in measured shear strains at the same location, depending on which side of the girder was instrumented. In the study conducted by Dymond et al. (2016), inability to differentiate between the two types of shear strains was shown to lead to potential inaccuracies in determining vertical shear forces and shear distribution from superimposed loads.

This paper also includes discussion of best practices to conduct load tests on *in-situ* bridges. These include the use of zero load readings (i.e., capturing data when the structure is unloaded) to account for strain changes due to temperature effects, repetition of load cases to account for error in truck positioning, and installing strain gages on both sides of the girder web to discern the effects of torsion. Challenges related to load test organization, efficiency, and coordination of the required participants are presented.

LOAD TESTING AND DATA COLLECTION METHODS

The load tests conducted by researchers at the University of Minnesota Twin Cities (Dymond et al., 2016) were intended to evaluate the distribution of shear forces in as-built prestressed concrete girder bridges at service load levels to assess system load carrying capacity more accurately. Particular challenges with the field tests included: coordinating use of Department of Transportation (DOT) sand-filled dump trucks to serve as the superimposed loads, coordinating traffic control and bridge closure for each load test, maximizing information collected from the bridge in a limited time frame, and appropriately utilizing a finite budget to collect as complete a data set as possible related to bridge load carrying capacity. During this project, field installation of strain gages and load testing of the structures each took an extended single business day to complete. This tight timeline required extensive pre-planning and coordination with the bridge owners. Up to 80 vibrating wire strain gages (VWSG) were installed on each structure the day prior to the load test. No additional calibration of the monitoring equipment was performed. With the limited number of gages, optimizing their placement to collect appropriate data was a challenge. Additionally, accessing the webs of the girders to mount the gages and precisely locating the gages was a challenge. The girder webs were high above the ground and often only accessible using a ladder. Multiple people on multiple ladders were required to precisely locate and install the gages with a jig at each location.

Selection of field testing instrumentation and loading configuration

To determine the loading required to generate measurable response in the bridges tested as part of this field study, calculation of the shear strains through the depth of a composite girder section was completed using linear elastic principles and mechanics of materials approaches. A single dump truck modeled with geometry and weight information described by Altay et al. (2003) was found to produce low magnitude shear strains (γ_{xy} of approximately 20-30 με). To increase the shear strain magnitudes, the decision was made to load the field bridges with two tri-axle DOT sand dump trucks parked back-to-back with the heavily loaded rear tandem axles as close as possible as shown in Fig. 1. The total weight of each truck (approximately 50 kips or 222 kN) and individual axle weights were recorded at certified truck scales before and after testing. When placed appropriately on the bridge, the back-to-back truck

loading produced larger shear strains and shear forces in any single girder compared to loading the bridge with one truck or two side-by-side trucks.

Fine resolution VWSGs capable of detecting strain changes of approximately 1-2 με due to static loading were required to capture small magnitude strains on the prestressed concrete bridge girders. The targeted minimum strain to be picked up on the horizontal, vertical, or diagonal legs of a strain gage rosette was approximately 5 με, which was approximately twice the expected resolution of the strain gages, accounting for the inherent noise. Sets of four VWSGs with a gage length of 6 in. (15.2 cm) formed a box-type rosette as shown in Fig. 2. This configuration allowed for linear interpolation of strain between the two horizontal gages such that, when incorporated with the single vertical and diagonal gage, three directions of a 45-degree rosette strain measurement were captured at mid-height of the box configuration. It was assumed that the vertical strain did not vary significantly over a small longitudinal distance. The box-type rosette was attached to a girder web so that the diagonal strain gage was parallel to the principal compressive stress from the applied load to maximize the reading. Strain gages in the box-type rosette were applied in a repeatable fashion to the web of the prestressed concrete girders using an instant epoxy adhesive, spray accelerator, and the jig shown in Fig. 2.

The neutral axis of the composite girder sections (where shear strain readings would be maximized) was typically in the girder top flange or at an elevation where the VWSG box-type rosette could not be attached to a flat vertical face (e.g., due to chamfer of the girder top flange). However, the shear strains were not anticipated to vary much through the height of the web due to the large top and bottom flanges. Placing the rosette near the bottom of the web provided large horizontal strain signal while not reducing the diagonal signals significantly from a location near the top of the web.

Location of instrumentation and trucks during field load tests

The majority of the load testing and instrumentation focused on the abutment end of each end span. Specifically, one corner of the end span, at the intersection of an exterior girder and abutment, was selected to be the focus corner for the instrumentation and load testing. During field tests, the box-type rosettes were typically placed on one side of the girder web on all girders in the end span to measure the transverse distribution of shear strain. The effects of torsion were unknown during field load testing and the desire for a large instrumentation grid with a limited budget dictated the VWSG placement on one side of the girder webs only. Strain gages were placed at various longitudinal locations on each girder to determine the shear strain distribution along the length of the span. These gage locations were related to the critical section for shear, taken as d_v from the support face (edge of sole plate or edge of bearing, whichever was closer to midspan). This type of rosette instrumentation grid, shown in Fig. 2, allowed for interpretation of strain at many longitudinal cross sections (typically $0.5d_v$, d_v, $2d_v$, and/or $4d_v$). For the bridges with four girders discussed in this paper, 20 box-type rosettes (four VWSGs each) were installed on each structure. The end of the span where testing was primarily conducted had box-type rosettes at $0.5d_v$, d_v, $2d_v$, and $4d_v$ (64 VWSGs), while the other end of the span had a box-type rosette at d_v on each girder (16 VWSGs).

Truck locations were chosen to study the influence of loading directly above girders versus in between girders, loading over interior versus exterior girders, and longitudinal position of loading. Trucks were transversely positioned in relation to the bridge girders and longitudinally positioned in relation to a transverse line of strain gage rosettes. Care was taken to avoid placing truck axles directly above a line of strain gages because of the disturbed region associated with the wheel loads. The strain profile through the depth of the cross section in the disturbed region may not be linear, as conventional Bernoulli beam theory is not applicable. Typically, the longitudinal location of back-to-back trucks was selected in an attempt to keep axles at least one girder depth away from a transverse line of gages. However, this was not always possible due to the length of the truck configuration and number of axles in the truck configuration compared to the length of the span and longitudinal location of the gages. Transversely, trucks were positioned over an interior girder so that each wheel line was equidistant from the centerline of the beam (straddling the interior beam). Trucks were also transversely located between girders (exterior-interior or interior-interior) so that the centerline of the trucks aligned with the centerline of the beam spacing (splitting two beams). The latter case is shown as an example in Fig. 3, where the trucks were placed longitudinally such that all tandem axles were beyond the d_v section of interest and not directly above any transverse lines of strain gages.

Strain measurements were gathered after the trucks were manually directed into position during load testing using chalk lines drawn on the bridge deck as a guide. The chalk lines corresponded to transverse locations of interest measured from the inside of the barrier and longitudinal locations of interest measured from the deck side of the expansion joint between the approach slab and bridge deck, as annotated in Fig. 1. The position of back-to-back trucks for each load test was set by first parking the lead truck in the appropriate location at the intersection of a transverse and longitudinal chalk line. The rear truck was then parked as close as possible to the lead truck in a back-to-back configuration (touching rear tailgates) along the same longitudinal line. Designation of lead and rear trucks are shown

in Fig. 3. Manually directing the trucks to each individual load test position and identifying the truck location on top of the deck relative to girders with chalk lines and a tape measure results in some error in positioning. To investigate the potential error, load tests with unique truck positions were often repeated two to three times and the multiple data sets were averaged.

The field bridge load testing protocol also included periodic "zero load readings," when strain gage data were collected with no truck or live traffic on the bridge. Zero load reading measurements were always taken prior to positioning the first trucks on the bridge and at the end of testing after all the trucks were removed from the bridge with intermittent zero load reading measurements taken throughout the course of a testing day. Engineering judgement was used when deciding the frequency of zero load readings, which was highly dependent on the cloud cover and slightly varied from bridge to bridge during this project. Typically, a block of four or five load tests were performed between zero load readings, which were taken approximately once per hour. If the cloud cover was consistent (completely cloudy or not cloudy) and temperature variation was approximately linear, the frequency of zero load readings was decreased, but if variation in cloud cover was anticipated throughout the course of a testing day, the frequency of zero load readings was increased. One bridge was tested at night to minimize the unpredictability related to solar radiation, but zero load readings were still taken on a frequent interval as the bridge deck temperature gradient changed while the deck cooled after sunset. The zero load reading data were used to isolate the mechanical strains due to the live loads during data processing.

Vibrating wire strain gage data processing

Field bridge data for each truck configuration or zero load reading were collected as a set of five measurements, corresponding to five separate cycles through all of the VWSG rosettes. Abnormally large strain variation within a five-cycle data set was minimized by discarding a maximum of two data points if they deviated from the five-cycle average by ±50 με. Average data points for each gage within each test were calculated from the remaining data. The resulting concrete mechanical strains included both temperature-induced mechanical strain from restrained movement due to temperature variation over the course of testing and load-induced mechanical strain from truck loading. Quantification of shear distribution is only dependent on the mechanical strain due to the applied live load, so it was important to separate the load-induced mechanical strain from the temperature-induced mechanical strain.

An example of the temperature-induced mechanical strain correction for the straight field bridge listed in Table 1 is discussed for two diagonal strain gages installed longitudinally on a girder at d_v and $2d_v$. The data used for the example strain correction were collected in the month of August. Samples of the VWSG data including both temperature- and load-induced mechanical strains are shown in Fig. 4, which also includes the eight zero load readings taken over the course of load testing. Zero load reading data in Fig. 4 generally did not align with a value of zero microstrain over the course of the day due to temperature-induced mechanical strains. Separation of the temperature-induced mechanical strain from the load-induced mechanical strain was done by subtracting an unloaded temperature-induced mechanical strain reading (Fig. 5) from the total mechanical strain (Fig. 4). The unloaded temperature-induced mechanical strain readings shown in Fig. 5 were calculated using a time-based linear interpolation between the zero load readings immediately before and after any given live load test. Mechanical strains due to the applied load only are shown in Fig. 6. Zero load reading data in Fig. 6 align with a value of zero microstrain over the course of the day. With this correction method, it was assumed that the temperature-induced mechanical strains varied linearly between zero load readings, which may not have always been the case. This is especially true just prior to or just after a peak zero load reading, when the maximum or minimum temperature-induced strains are not monotonic with time (e.g., due to the effects of cloud cover).

PRELIMINARY FIELD DATA EVALUATION

To check the accuracy and reliability of the field data, simple checks for static equilibrium were conducted. Select load cases with back-to-back trucks were investigated with statics and a beam-line analysis. In the beam-line analysis, the bridge was idealized as a one-dimensional structure along its length to determine the shear across a section of the bridge; each truck axle was idealized as a single point load incorporating the total axle weight. This type of simple check was only feasible because all of the girders in a bridge were instrumented at the same longitudinal locations (e.g., d_v, $2d_v$, $4d_v$). Using deformable body mechanics principles, the horizontal, diagonal, and vertical strains from the VWSG rosettes were used to calculate the shear strain on a vertical face, γ_{xy}. The shear strain was converted into a vertical shear force using the following elastic material relations: $\gamma_{xy} = \tau / G$ and $\tau = (VQ) / (It)$. In these relationships, τ was the shear stress; G was the shear modulus calculated using $G = E / (2+2\nu)$, where E was the modulus of elasticity calculated using the nominal concrete compressive strength and ν was an assumed Poisson's

ratio of 0.2; *V* was the applied vertical shear force at the longitudinal location of interest; *Q* was the first moment of the area about the neutral axis, where the area was taken between the extreme fiber and location in the cross section where shear stress was determined; *I* was the transformed centroidal moment of inertia of the entire composite cross-sectional area with the longitudinal deck steel, deck concrete, haunch, and prestressing strands transformed to girder concrete; and *t* was the width of the cross section at the elevation being considered.

Four load cases for the field bridge, whose characteristics are listed in Table 1, are presented here as an example. Within these load cases, the key parameters that varied included the longitudinal and the transverse location of the back-to-back trucks. The vertical shear force in each beam was calculated using information in Table 2 and summed at the d_v, $2d_v$, and $4d_v$ cross sections for comparison to beam-line analyses using statics. Results shown in Table 3 indicate that the load case where trucks were transversely positioned to straddle an interior girder matched simple beam-line analysis results better (percent difference values typically less than 20%) when compared to the load case where trucks were transversely positioned between two girders (percent difference values typically greater than 20%). The 41% difference at $4d_v$ for Case 2 with trucks straddling the first interior beam was an outlier. This value was attributed to a below average strain reading on the diagonal VWSG in the box-type rosette. The percent differences in either load case, especially with trucks transversely positioned between two girders, was attributed to torsion in the girders, which would create a scenario where the shear strain data obtained from each side of the web would not be equal as shown in Fig. 7.

Linear elastic finite element modeling (FEM) techniques, validated with laboratory test data, were used to provide further understanding of the shear strain behavior and discrepancies with basic statics observed in the field. Testing in the laboratory allowed for the use of additional resistive foil strain gages, which had insufficient resolution for the field application. In the laboratory, more localized loads were applied, which produced larger strain readings. Furthermore, dump trucks used during field load tests typically included three axles and ten tires per truck. Two trucks in a back-to-back orientation contained 20 individual contact points, which significantly spread the applied load of 100 kips (445 kN) over a larger area. This orientation also inherently created more complexity and potential for error compared to laboratory loading conditions where a load of 100 kips (445 kN) could be applied at a single contact area more definitively located in the context of the bridge geometry.

FEM VALIDATED WITH LABORATORY TESTING

Finite element modeling methods

With the advances in computer technology and modern FEM programs, it is possible to efficiently model and analyze bridge structures using a complete solid element model. This analytical approach may still be inefficient for use in design or rating of hundreds of individual bridges in a DOT inventory, but FEM provides an appropriate level of detail for comparison to experimental research results.

In this project, three-dimensional solid finite element models were created in Abaqus/Standard 6.11 (Dassault Systèmes, 2011) and validated with experimental data obtained from testing a full-scale laboratory bridge. The numerical models were used to develop an understanding of the complex structural behavior related to shear distribution and torsion of prestressed concrete girder bridges. Specifically, FEM provided the ability to compare measured strain data to FEM strain results rather than converting strain gage data to stress data, which required assumptions about the composite cross section, including the effective flange width dimension. The bridge superstructures modeled in Abaqus were divided into five parts, including: neoprene bearing pads, traffic barriers, end or intermediate diaphragms, bridge deck, and girders. All parts were meshed using eight node three-dimensional linear continuum elements with reduced integration. Characteristic element sizes were approximately 3 in. or smaller for bridge decks and approximately 2 in. or smaller for bridge girders, traffic barriers, and diaphragms. The mesh of each individual part was deemed satisfactory after verifying that no element had an aspect ratio greater than 2.5. The effects of prestressing and dead load were not included in the finite element models because the externally mounted rosette strain gages only captured the live load effects. Additional details regarding the FEM meshing, boundary conditions, and method of applying load can be found in the research report by Dymond et al. (2016).

Laboratory bridge geometry

A full-scale laboratory bridge was constructed in the Theodore V. Galambos Structural Engineering Laboratory at the University of Minnesota Twin Cities. This bridge was representative of end span structures in the DOT inventory that were designed in the 1960's, 1970's, and early 1980's. The bridge needed to fit within the available space, while ensuring that the applied load from a single 77 kip (343 kN) actuator would produce measurable shear strains in the elastic behavior range. In addition, it was required that a combination of three actuators producing a maximum load of 440 kips (1,957 kN) could induce ultimate shear failure in the bridge as discussed by Dymond et al.

(2016). Initial analysis indicated that the maximum bridge girder depth that could be tested to near ultimate strength in the bridge system, with appropriate over-strength factors, was 36 in. (91.4 cm). The laboratory bridge was constructed with the characteristics given in Table 1. The geometry and characteristics of the laboratory bridge were similar to the field bridge listed in Table 1.

Laboratory instrumentation and applied loading

The laboratory bridge instrumentation included VWSG box-type rosettes similar to those applied to the field bridges. Additionally, resistive foil strain gage rosettes were applied to the laboratory bridge on the opposite side of the girder web from the VWSGs at multiple longitudinal positions related to d_v. This configuration was used to capture the effects of torsion and to facilitate determination of the vertical shear force resultant in the section. Foil strain gages were much less expensive than the VWSGs, but they also inherently had a lower signal-to-noise ratio than the VWSGs. Use of foil strain gages was not desired during field load tests due to installation time constraints, the low magnitude applied load, and because they had different data acquisition requirements than the VWSGs. A significant portion of the laboratory bridge tests were conducted in the elastic range with a single actuator that applied its maximum available load (75 kips or 334 kN). This load value was also selected because lower load steps (e.g., 25 kips or 111 kN) did not provide large enough changes in strain (> 10 με) for clear detection by the foil strain gage rosettes. Larger load steps were excluded because additional load required multiple actuators and to avoid potential cracking in the structure (web-shear cracking was expected at approximately 200 kips or 890 kN).

Validation of FEM

Validation of the elastic FEM technique was completed using data from the controlled laboratory experiment before using the FEM techniques to understand the shear strain discrepancies observed in the field. Two acceptance criteria were used for girder shear strain validation purposes. First, the measured shear strain on either side of the girder web, γ_{xy}, calculated from VWSG box-type rosette data was compared to the FEM shear strain results at the same location, and differences between FEM and laboratory total shear strain values on each side of the web were deemed acceptable if they were below 8 με. This was the case for approximately 75% of the load positions and gage locations. Second, the shear strain due to the vertical shear force resultant (γ_{xy_shear}) was calculated as the average of γ_{xy} from both sides of the girder web and compared for both FEM results and laboratory data and positive or negative percent differences between the FEM and laboratory γ_{xy_shear} values below 10% were deemed acceptable. This was the case for approximately 75% of the load positions and gage locations. Outliers associated with the total strain differences greater than 8 με and γ_{xy_shear} percent differences greater than 10% were investigated and, generally, discrepancies were attributed to a larger than normal noise-to-signal ratio for a single linear strain gage within a rosette. Two validation scenarios with 75 kips (334 kN) applied load are presented in Table 4. More in-depth discussion regarding the FEM validation, with load cases and data from instrumentation beyond the scope of this paper, is contained in the report by Dymond et al. (2016). The validated FEM technique was used to verify the effect of torsion on the strain readings obtained during laboratory and field load tests.

THE EFFECTS OF TORSION

Two ratios were used to investigate the effects of torsion on the laboratory bridge data and the field bridge FEM results. The absolute value of the ratio of the torsional shear strain divided by the total shear strain, $|\gamma_{xy\_tor} / \gamma_{xy}|$, was calculated as a percentage for each face of the girder web at each location of interest. The shear strain due to torsion (γ_{xy_tor}) was calculated as the difference between the total shear strain, γ_{xy}, from either face of the girder web and the absolute value of the shear strain due to the vertical shear force resultant, γ_{xy_shear}. The $|\gamma_{xy\_tor} / \gamma_{xy}|$ ratio indicated two behaviors. First, it indicated the amount of torsional shear strain included in the total shear strain on either face of the girder web. In other words, a value of 50% would indicate that torsional shear strain was 50% of the total shear strain on one face of the girder web. These values gave an indication of the error associated with trying to quantify shear force (and shear distribution) by measuring shear strain on only one side of the girder web. Values over approximately 10% were likely to yield highly inaccurate shear distributions. Second, the smaller ratio of the torsional shear strain divided by the total shear strain at any location of interest (e.g., at d_v on an interior girder) indicated the side of the web where the effects of torsion and the effects due to the vertical shear resultant were additive. This additive behavior of shear stresses is illustrated in the foreground of Fig. 7.

The absolute value of the ratio of the shear strain due to torsion divided by the shear strain due to the vertical shear resultant, $|\gamma_{xy\_tor} / \gamma_{xy\_shear}|$, was calculated as a percentage for each location of interest. This ratio indicated the difference in relative magnitudes of the torsional shear strain and the shear strain due to the vertical shear resultant. In other words, a value of 100% (which stems from the value of 50% for the ratio of torsional shear strain divided by

total shear strain in the previous example) would indicate that the shear strain due to torsion was equal to the shear strain due to the vertical shear resultant. It should be noted that, for both of these ratios, if the magnitude of the shear strains are small the percentages could still be high, which would indicate significant torsional effects when the magnitude of strains are actually negligible.

Effects of torsion on laboratory bridge data

When force was applied directly above the girder at $4d_v$, the ratio of $|\gamma_{xy\_tor} / \gamma_{xy\_shear}|$ was approximately 4% in the loaded girder. The ratio of $|\gamma_{xy\_tor} / \gamma_{xy\_shear}|$ was 76% in the girder adjacent to the loaded girder, but the magnitude of shear strain due to the vertical shear resultant was smaller. The ratio of $|\gamma_{xy\_tor} / \gamma_{xy\_shear}|$ was in the range of 37-40% in both girders when load was applied between the interior and exterior girder as shown in Table 5. The effects of torsion observed in the laboratory bridge were significant ($|\gamma_{xy\_tor} / \gamma_{xy\_shear}| \approx 40\%$), but loading scenarios in the laboratory bridge (load applied with a single actuator in a small footprint) were different than those used to load test the field bridges (load applied with two back-to-back dump trucks that had ten individual tires per vehicle contacting the bridge deck in a large footprint). A FEM investigation of torsional effects in the field bridge was warranted to determine if torsion was important in the interpretation of the field data.

Effects of torsion on field bridge FEM results

When trucks were transversely oriented to straddle the first interior girder, the first interior girder had a minimum ratio of $|\gamma_{xy\_tor} / \gamma_{xy}|$ in the range of approximately 0-2% and torsional strains less than 1 με. Furthermore, the ratio of $|\gamma_{xy\_tor} / \gamma_{xy\_shear}|$ indicated that torsional shear strain was a very small percentage of the shear strain from the vertical shear resultant (2% or less). FEM results indicated that this loading scenario, with results shown in Table 6, had the lowest shear strain in the straddled girder due to torsion compared to all the other truck positions investigated in Dymond et al. (2016). The adjacent second interior girder exhibited more torsional response with ratios of $|\gamma_{xy\_tor} / \gamma_{xy\_shear}|$ in the range of 25-43% (torsional shear strains less than or equal to 6 με), but the magnitude of γ_{xy} was lower when compared to the first interior girder.

When the trucks were transversely positioned to split between the first and second interior girders, the interior girders had a minimum ratio of $|\gamma_{xy\_tor} / \gamma_{xy}|$ in the range of approximately 6-22%. The torsional shear strains ranged from 1 to 7 με in these cases as shown in Table 7. This higher magnitude torsional shear strain was expected with trucks placed between two interior girders when compared to the straddled girder load case. The ratio of $|\gamma_{xy\_tor} / \gamma_{xy\_shear}|$ indicated that torsional shear strain was, on average, 22% of the shear strain from the vertical shear resultant in the two interior girders. As expected, due to the symmetry of the loading case, the effect of torsion was approximately equal in both interior girders. The ratios of $|\gamma_{xy\_tor} / \gamma_{xy\_shear}|$ from the field bridge were typically smaller compared to similar ratios from the laboratory bridge, but the effects of torsion were still observed in the field bridge FEM results. The trucks still tended to twist the girders when one or more wheel lines was located between the girders even though truck axles provide more load distribution via the axle gage width and longitudinal spacing.

SUMMARY AND CONCLUSIONS

This paper presented several best practices for conducting load tests on as-built bridges to quantify shear distribution. As with any load test, coordinating the effort to make efficient use of time, space, and resources was critical. To capture high quality data, it was important to install fine resolution VWSGs on both sides of the girder web to capture small magnitude strains and differentiate between the effects of torsion and vertical shear. Trucks parked in a back-to-back configuration were utilized to maximize the applied live load shear, and load cases were repeated within the test protocol to minimize potential error related to truck positioning and data acquisition. Mechanical strains due to the live loads were isolated from the mechanical strain changes due to the environmental effects by using data captured when the structure was unloaded (zero load readings). This was done regardless of testing during the day or at night (when it was possible to minimize the unpredictability related to solar radiation).

The presence and magnitude of torsional shear strains was confirmed with data from a laboratory bridge and FEM results from a straight field bridge. The ratio of $|\gamma_{xy\_tor} / \gamma_{xy}|$ was often greater than 10% for the load case when trucks were split between girders, which indicated that the amount of torsional shear strain included in the total shear strain on either face of the girder web likely led to inaccurate estimations of shear distribution. In this study, it was not possible to determine the shear strain due to the vertical shear force resultant using the VWSG rosettes installed on the field bridges because the rosettes were only placed on one side of the girder webs. In order to differentiate between torsion and vertical shear, gages needed to be placed on both sides of the girder webs. This finding likely applies to other studies in the literature that have characterized shear distribution through the use of rosette strain gages on one side of a prestressed concrete girder web. The literature has a dearth of information regarding the effects of

torsion on the magnitude of shear strain in the webs of precast concrete I- and bulb-tee beam bridges. Cross et al. (2006 and 2009) noted, but did not account for, the potential effects of torsion after completing field tests and data processing.

The torsion induced in prestressed concrete bridge girders due to superimposed loads is frequently ignored during structural design because it is not the controlling force. The total shear strain, γ_{xy}, on one face of the girder web may be higher (additive) than on the other face (subtractive) owing to the nature of torsional and vertical shear stresses as shown in Fig. 7. Ignoring the effect of torsion may result in a conservatism or an unconservatism related to the combined effect of vertical shear stresses due to both torsion and the vertical shear force resultant. A larger shear strain may contribute to larger principal tensile stresses in the girder web that may lead to premature diagonal cracking of the girder web under service loads in bridge structures with a geometry and loading scenario prone to torsion. However, results from inspection of field bridges for diagonal web-shear cracks conducted by Dymond et al. (2016) suggested that the amount of live load present during load tests of these field bridges did not approach the principal tensile stress associated with diagonal web-shear cracking, even when considering torsion in the loading cases.

REFERENCES

Altay, A. K., Arabbo, D. S., Corwin, E. B., Dexter, R. J., and French, C. E. (2003). "Effects of Increasing Truck Weight on Steel and Prestressed Bridges." *Report No. MN/RC 2003-16*. Department of Civil Engineering, University of Minnesota, Minneapolis, MN, pp. 129.

American Association of State Highway and Transportation Officials (AASHTO) (2011). *The Manual for Bridge Evaluation*, 2nd Edition, Washington, DC.

Bradberry, T. E. (2015). Summary of Shear Rating Concrete Bridges in Texas. Personal communication.

Cross, B., Panahshahi, N., Vaughn, B., Petermeier, D., and Siow, Y. (2006). "Investigation of Select LRFD Design Factors through Instrumentation of Bridge Bearings." *Physical Research Report No. 152*, Southern Illinois University Edwardsville, Edwardsville, IL, pp. 349.

Cross, B., Vaughn, B., Panahshahi, N., Petermeier, D., Siow, Y. S., and Domagalski, T. (2009). "Analytical and Experimental Investigation of Bridge Girder Shear Distribution Factors." *Journal of Bridge Engineering*, 14(3), 154-163.

Dassault Systèmes (2011). "Abaqus," *SIMULIA*. Providence, RI.

Dereli, O., Shield, C., and French, C. (2010). "Discrepancies in Shear Strength of Prestressed Beams with Different Specifications." *Report No. MN/RC 2010-03*, Department of Civil Engineering, University of Minnesota, Minneapolis, MN, pp. 242.

Dymond, B. Z., French, C. W., Shield, C. K. (2016). "Investigation of Shear Distribution Factors in Prestressed Concrete Girder Bridges." *Report No. MN/RC 2016-32*, Department of Civil, Environmental, and Geo-Engineering, University of Minnesota, Minneapolis, MN, pp. 595.

Millam, J. L. and Ma, Z. (2005). "Single-Lane Live Load Distribution Factor for Decked Precast, Prestressed Concrete Girder Bridges." *Transportation Research Record 1928*, 142-152.

TABLES

Table 1—Laboratory and field bridge characteristics

Bridge Characteristic	Bridge Structure	
	Laboratory	Field
Year Built	2014	1970
AASHTO Design Specification Year	1991	1969
Average Daily Traffic	0	4,100
Span Length, ft (m)	32 (9.8)	42.6 (13)
Aspect Ratio (span length / bridge width)	0.94	0.78
Skew Angle (degrees)	0	0
Number of Girders	4	5
Girder Spacing, ft (m)	9 (2.7)	11.5 (3.5)
Girder Depth, in. (m)	36 (0.91)	
Girder Web Thickness, in. (cm)	6 (15.2)	
Nominal Girder Concrete Compressive Strength, ksi (MPa)	7.5 (51.7)	5 (34.5)
Deck Thickness, in. (cm)	9 (22.9)	8.25 (21.0)
Nominal Deck Concrete Compressive Strength, ksi (MPa)	4 (27.6)	

Table 2—Truck locations and axle weights used to generate beam-line shear results at VWSG locations

Description of Test and Truck Location*		Axle Label**	Axle Weight kip (kN)	Axle Distance from Support A ft (m)
Case 1: Back-to-back truck rear axles beyond d_v	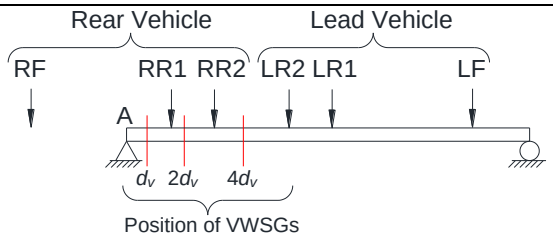	RF	16.1 (71.6)	—
		RR1	16.9 (75.2)	5 (1.5)
		RR2	16.9 (75.2)	3 (1.0)
		LR2	18.1 (80.5)	18 (5.3)
		LR1	18.1 (80.5)	22 (6.7)
		LF	14.0 (62.3)	37 (11.4)
Case 2: Back-to-back truck rear axles beyond $4d_v$	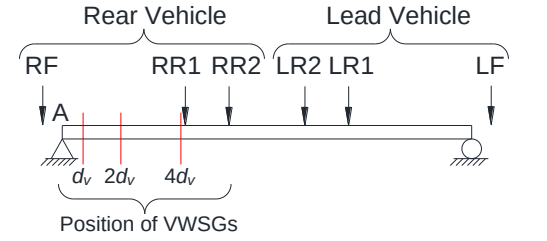	RF	16.1 (71.6)	—
		RR1	16.9 (75.2)	12 (3.7)
		RR2	16.9 (75.2)	16 (4.9)
		LR2	18.1 (80.5)	25 (7.6)
		LR1	18.1 (80.5)	29 (8.8)
		LF	14.0 (62.3)	—

* d_v = 2.83 ft (0.86 m) from the nearest support, span length = 42.6 ft (13 m)

** The first letter indicates vehicle (R = rear, L = lead) and the second letter indicates axle position within the vehicle (R = rear, F = front). Example: LR1 = lead truck, first rear axle

Table 3—Initial field data showing discrepancies between measured and analytical shear forces

Description of Test and Truck Location (reference Table 2)	VWSG Location[1]	Measured Shear[2] kip (kN)	Analytical Shear[3] kip (kN)	Percent Difference[4] %
Case 1 with trucks straddling the first interior beam	d_v	40 (177)	49 (219)	19
	$2d_v$	33 (149)	32 (144)	3
	$4d_v$	13 (60)	16 (69)	13
Case 1 with trucks splitting the first and second interior beams	d_v	33 (148)	49 (219)	32
	$2d_v$	26 (114)	32 (144)	21
	$4d_v$	11 (50)	16 (69)	28
Case 2 with trucks straddling the first interior beam	d_v	39 (172)	36 (160)	8
	$2d_v$	37 (167)	36 (160)	4
	$4d_v$	21 (95)	36 (160)	41
Case 2 and trucks splitting the first and second interior beams	d_v	26 (116)	36 (160)	28
	$2d_v$	29 (129)	36 (160)	19
	$4d_v$	26 (115)	36 (160)	20

[1] d_v = 2.83 ft (0.86 m) from the nearest support, span length = 42.6 ft (13 m)
[2] Measured = sum of girder shear forces calculated using field strain data at the VWSG locations
[3] Analytical = cross-sectional shear using beam-line statics
[4] Percent Difference = (Measured – Analytical) / (Analytical) * 100%

Table 4— Laboratory bridge girder shear strain (με) values from FEM results and strain gage rosette data used for FEM validation

Girder Web and Longitudinal Locations of Interest	FEM γ_{xy}	Rosette γ_{xy}	Percent Difference* %
75 k (334 kN) applied at point M at $4d_v$			
North side of interior girder web at d_v	35	38	9
South side of interior girder web at d_v	61	68	11
γ_{xy_shear}:	48	53	***10***
North side of exterior girder web at d_v	57	67	18
South side of exterior girder web at d_v	32	26	-19
γ_{xy_shear}:	45	47	***4***
75 k (334 kN) applied at point N at $2d_v$			
North side of interior girder web at d_v	99	115	16
South side of interior girder web at d_v	99	101	2
γ_{xy_shear}:	99	108	***9***

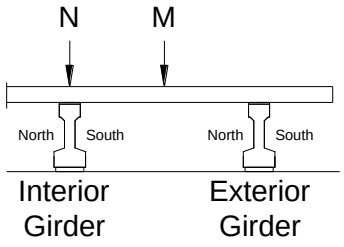

* Percent Difference = (Rosette – FEM) / (FEM) * 100%
γ_{xy_shear} = Average of North and South γ_{xy}

Table 5— Laboratory bridge girder shear strain data (με) and ratios indicating the effects of torsion with applied load at $4d_v$

Girder Web and Longitudinal Locations of Interest	γ_{xy}	γ_{xy_tor}	$\lvert\gamma_{xy\_tor} / \gamma_{xy}\rvert$ (%)	$\lvert\gamma_{xy\_tor} / \gamma_{xy\_shear}\rvert$ (%)
75 k (334 kN) applied at point M				
North side of interior girder web at d_v	26	-18	69	40
South side of interior girder web at d_v	61	18	***29***	
γ_{xy_shear}:	44			
North side of exterior girder web at d_v	57	16	***27***	37
South side of exterior girder web at d_v	26	-16	60	
γ_{xy_shear}:	42			
75 k (334 kN) applied at point N				
North side of interior girder web at d_v	58	-3	***4***	4
South side of interior girder web at d_v	63	3	4	
γ_{xy_shear}:	61			
North side of exterior girder web at d_v	29	13	***43***	76
South side of exterior girder web at d_v	4	-13	---	
γ_{xy_shear}:	17			
75 k (334 kN) applied at point S				
North side of interior girder web at d_v	5	-9	---	63
South side of interior girder web at d_v	22	9	***39***	
γ_{xy_shear}:	14			
North side of exterior girder web at d_v	67	-6	8	8
South side of exterior girder web at d_v	78	6	***7***	
γ_{xy_shear}:	73			

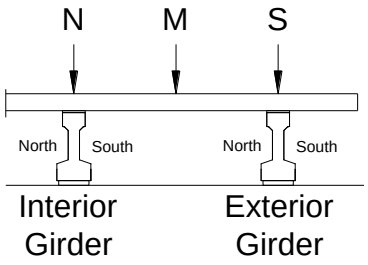

γ_{xy_shear} = Average of North and South γ_{xy}

$\gamma_{xy\_tor} = \gamma_{xy} - \lvert\gamma_{xy\_shear}\rvert$

Bold italics = minimum $\lvert\gamma_{xy\_tor} / \gamma_{xy}\rvert$

Table 6—Field bridge FEM girder shear strain results (με) and ratios indicating the effects of torsion with back-to-back axles beyond d_v and trucks straddling the first interior beam

Girder Web and Longitudinal Locations of Interest	First Interior Girder				Second Interior Girder			
	γ_{xy}	γ_{xy_tor}	$\lvert\gamma_{xy\_tor} / \gamma_{xy}\rvert$ (%)	$\lvert\gamma_{xy\_tor} / \gamma_{xy\_shear}\rvert$ (%)	γ_{xy}	γ_{xy_tor}	$\lvert\gamma_{xy\_tor} / \gamma_{xy}\rvert$ (%)	$\lvert\gamma_{xy\_tor} / \gamma_{xy\_shear}\rvert$ (%)
North side of web at d_v	32	0.5	2	2	20	6	***30***	43
South side of web at d_v	31	-0.5	***2***		8	-6	75	
γ_{xy_shear}:	31.5				14			
North side of web at $2d_v$	34	0.5	***1***	1	20	6	***25***	33
South side of web at $2d_v$	33	-0.5	2		9	-6	67	
γ_{xy_shear}:	33.5				15			
North side of web at $4d_v$	20	0	***0***	0	15	3	***20***	25
South side of web at $4d_v$	20	0	0		9	-3	33	
γ_{xy_shear}:	20				12			
γ_{xy_shear} = Average of North and South γ_{xy}			Average:	1			Average:	34

$\gamma_{xy\_tor} = \gamma_{xy} - \lvert\gamma_{xy\_shear}\rvert$

Bold italics = minimum $\lvert\gamma_{xy\_tor} / \gamma_{xy}\rvert$

Table 7—Field bridge FEM girder shear strain results (με) and ratios indicating the effects of torsion with back-to-back axles beyond d_v and trucks split between two interior beams

Girder Web and Longitudinal Locations of Interest	First Interior Girder				Second Interior Girder			
	γ_{xy}	γ_{xy_tor}	$\lvert\gamma_{xy\_tor} / \gamma_{xy}\rvert$ (%)	$\lvert\gamma_{xy\_tor} / \gamma_{xy\_shear}\rvert$ (%)	γ_{xy}	γ_{xy_tor}	$\lvert\gamma_{xy\_tor} / \gamma_{xy}\rvert$ (%)	$\lvert\gamma_{xy\_tor} / \gamma_{xy\_shear}\rvert$ (%)
North side of web at d_v	19	-6	32	24	32	7	***22***	28
South side of web at d_v	32	7	***22***		18	-7	39	
γ_{xy_shear}:	25				25			
North side of web at $2d_v$	20	-6	30	23	33	7	***21***	27
South side of web at $2d_v$	33	7	***21***		19	-7	37	
γ_{xy_shear}:	26				26			
North side of web at $4d_v$	16	-1	***6***	6	19	2	***11***	12
South side of web at $4d_v$	19	2	11		15	-2	13	
γ_{xy_shear}:	17				17			
γ_{xy_shear} = Average of North and South γ_{xy}			Average:	18			Average:	22

$\gamma_{xy\_tor} = \gamma_{xy} - \lvert\gamma_{xy\_shear}\rvert$

Bold italics = minimum $\lvert\gamma_{xy\_tor} / \gamma_{xy}\rvert$

FIGURES

Fig. 1—Back-to-back trucks positioned to maximize live load shear in the smallest rear tandem axle footprint

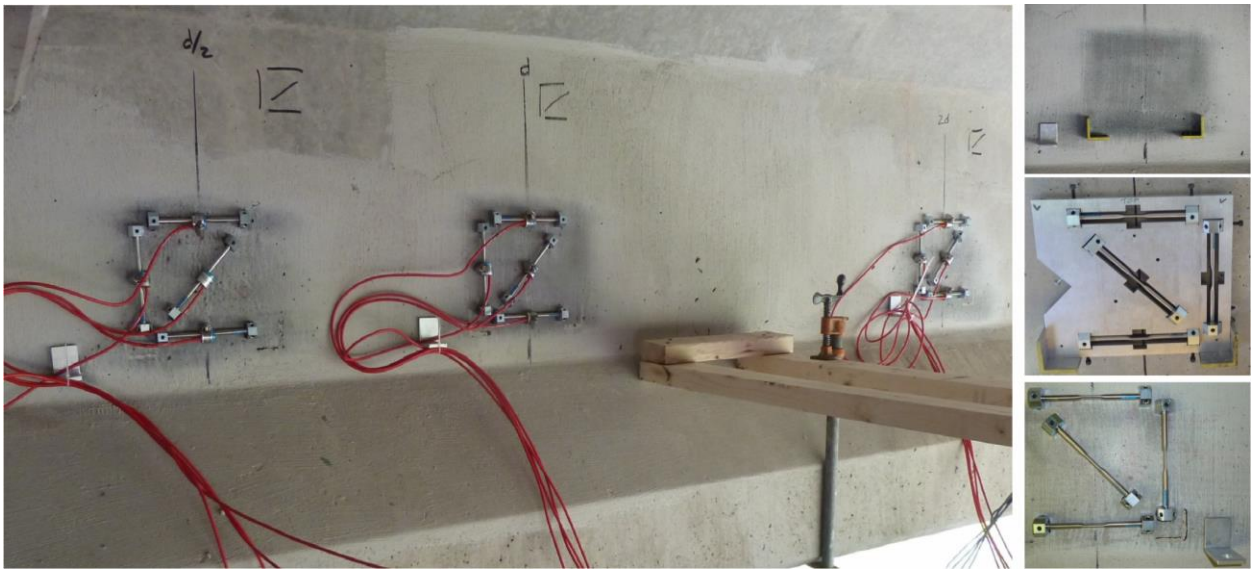

Fig. 2—Vibrating wire strain gage box-type rosettes installed at multiple longitudinal locations (left) using a jig (right) for repeatability

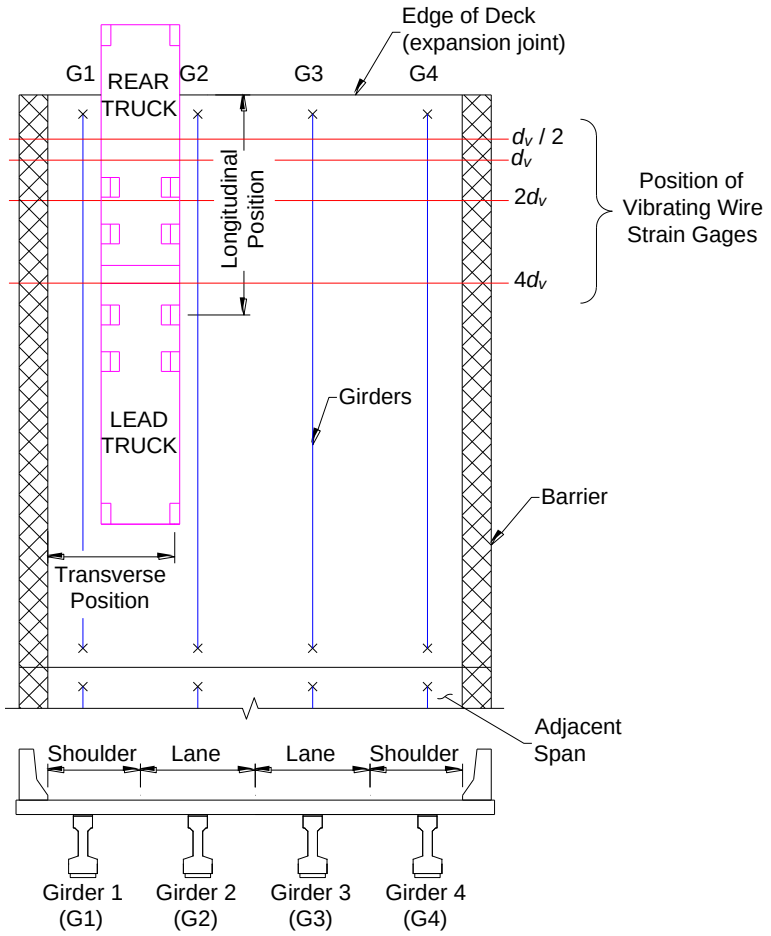

Fig. 3—Back-to-back truck configuration relative to rows of vibrating wire strain gages and girders

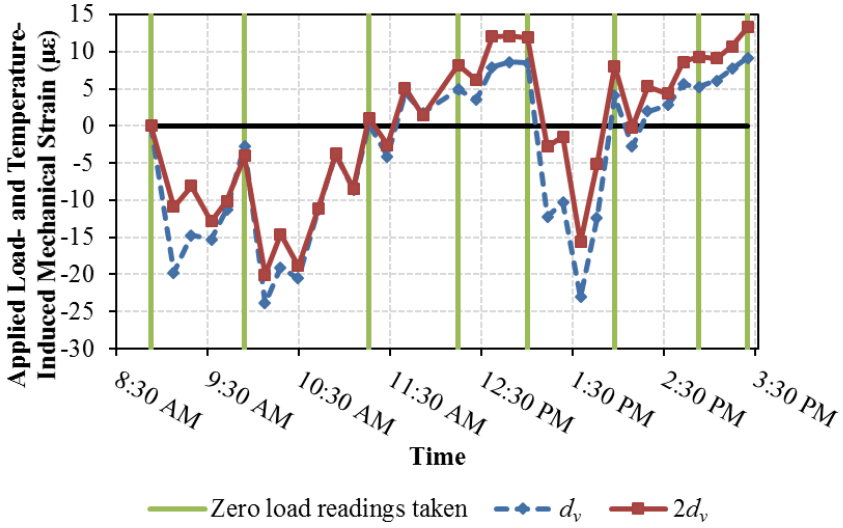

Fig. 4—Example of applied load- and temperature-induced mechanical strain at two cross sections

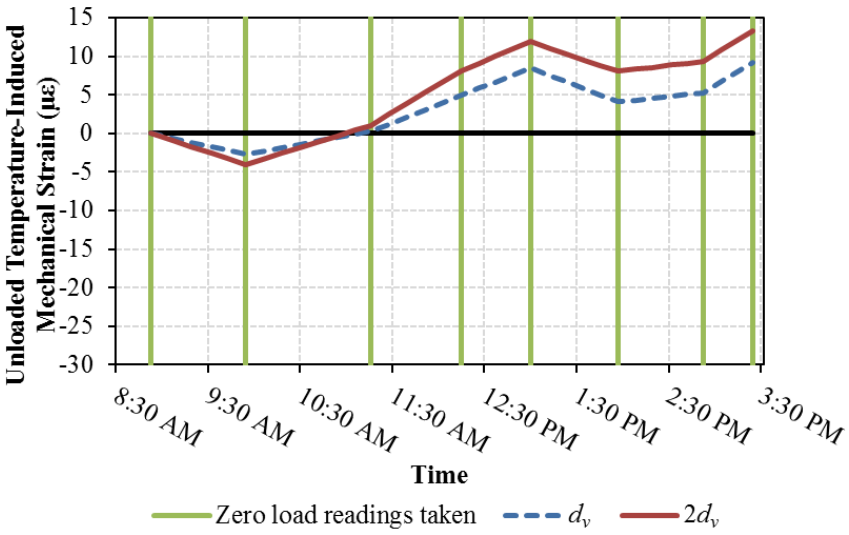

Fig. 5—Example of unloaded temperature-induced mechanical strain at two cross sections

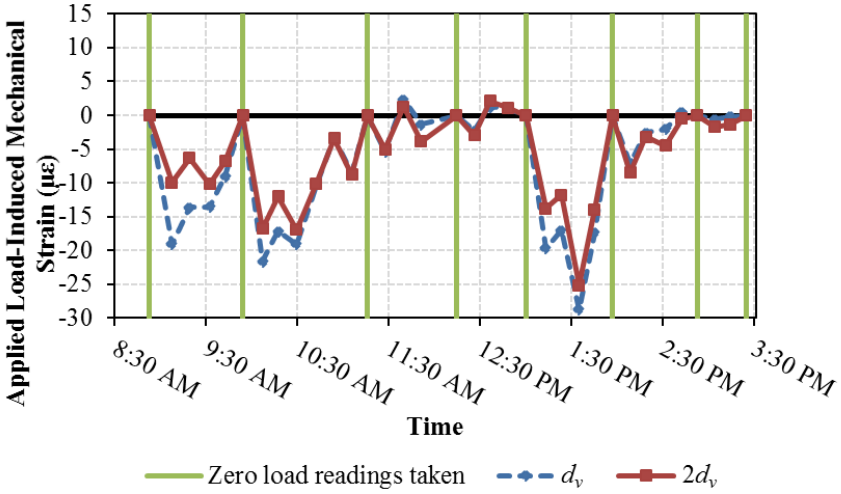

Fig. 6—Example of applied load-induced mechanical strain at two cross sections

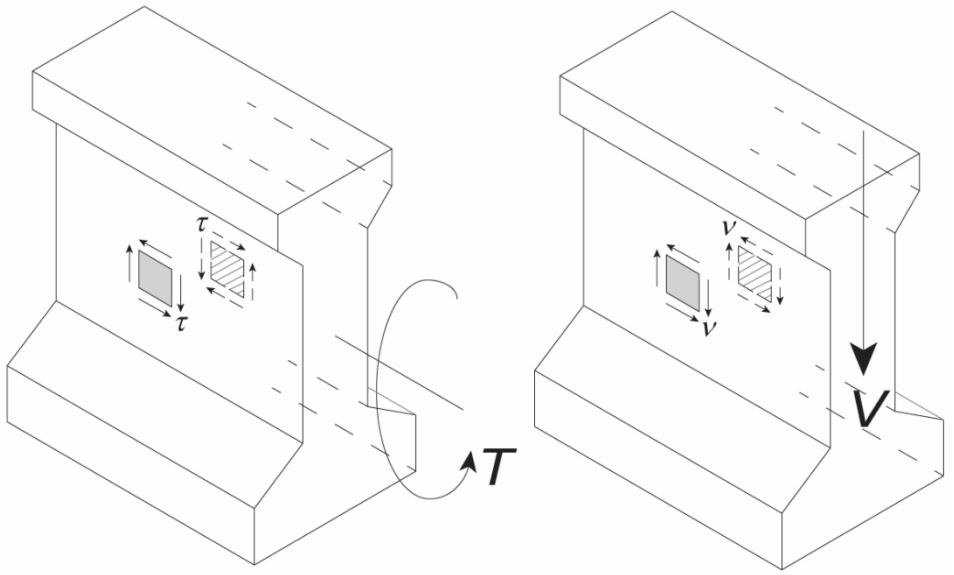

Fig. 7—Shear stresses due to torsion (left) and the vertical shear resultant (right) on both sides of the girder web; vertical stresses are additive in the foreground (shaded) and subtractive in the background (hatched)

Biographical sketches:

Ben Dymond is an Assistant Professor in the Department of Civil Engineering at the University of Minnesota Duluth. He is a member of ACI Committees 342 (Bridge Evaluation), 343 (Bridge Design), 423 (Prestressed), 123 (Research), and S802 (Teaching Methods and Materials). His research interests include design and analysis of concrete structural systems and their components, experimental investigations, and long-term structural monitoring.

Catherine French is a CSE Distinguished Professor in the Department of Civil, Environmental, and Geo- Engineering at the University of Minnesota Twin Cities. She is a member of several ACI technical committees including TAC, 318 (Building Code), and 352 (Joints). Her primary research areas involve the experimental investigation of reinforced and prestressed concrete infrastructure and structural systems subjected to earthquake loadings.

Carol Shield is a CSE Distinguished Professor in the Department of Civil, Environmental, and Geo- Engineering at the University of Minnesota Twin Cities. She is past chair of ACI committee 440 (FRP Reinforcement) and a member of 408 (Bond and Development of Steel Reinforcement) and 423 (Prestressed). Her primary research interests are in the use of composite materials in the infrastructure, prestressed concrete structures, and methods of seismic simulation.

Diagnostic Test for Load Rating of a Prestressed SCC Bridge

E.S. Hernandez and J.J. Myers

Synopsis: Self-consolidating concrete (SCC) has emerged as an alternative to build stronger structures with longer service life. Despite the advantages of using SCC, there are some concerns related to its service performance. The effect of a smaller coarse aggregate size and larger paste content is of special interest. It is fundamental to monitor the response to service loads of infrastructure employing SCC in prestressed concrete members. Bridge A7957 was built employing normal-strength and high-strength self-consolidating concrete in its main supporting members. The diagnostic test protocol implemented in this research included static and dynamic tests and the calibration of refined finite element models simulating the static loads acting on the structure during the first series of diagnostic tests. The main objective of this study centered on (a) presenting a diagnostic test protocol using robust and reliable measurement devices (including noncontact laser technology) to record the bridge's initial service response; and (b) obtaining the initial spans' performance to evaluate and compare the SCC versus conventional concrete girders' response when subjected to service loads. The initial response of the end spans (similar geometry and target compressive strength, but with girders fabricated using concrete of different rheology) was compared, and no significant difference was observed.

Keywords: assessment of bridge structures, diagnostic load tests, long-term monitoring, service evaluation of bridges.

ACI member **Eli S. Hernandez** is a PhD Candidate at Missouri University of Science and Technology, Rolla, Missouri. He received both his BS and his MS from Universidad de los Andes, Merida, Venezuela. He is an associate member of ACI Committee 435, Deflection of Concrete Building Structures and ACI Committee 342, Evaluation of Concrete Bridges and Bridge Elements. His research interests include fiber-reinforced polymers for strengthening applications and evaluation of bridges.

John J. Myers, Ph.D, P.E., F.ACI, F.ASCE, F.TMS, is a Professor and Associate Dean at Missouri University of Science and Technology, Rolla, MO. He received his BAE from Pennsylvania State University, University Park, PA. He earned both his MS and his PhD from the University of Texas at Austin, Austin, TX. He is the current Chair of ACI Subcommittee 440-L, FRP-Durability. His research interests include advanced concrete materials and fiber-reinforced polymers in strengthening applications.

INTRODUCTION

Since the late 1980s, self-consolidating concrete (SCC), a high-performance material that can flow easily into tight and constricted spaces without segregating, has been successfully employed for infrastructure projects in Europe, Japan, and Australia. The highly flowable feature of SCC results in better consolidation and placement, and fewer voids and honeycombing that creates a more condensed microstructure. For these reasons, SCC has become an effective alternative to build stronger infrastructure with longer service life[1-4]. Despite these main advantages of SCC, several concerns are related to its mechanical properties. The effect of the smaller coarse aggregate proportion and size in addition to a larger paste content employed to attain a flowable mixture is of special interest. Prestressed concrete (PC) members fabricated with SCC are expected to develop higher prestress losses (creep and shrinkage) and to undergo an increased in-service response due to its lower modulus of elasticity[5, 6]. Consequently, it is fundamental to monitor the in-service response of full-scale highway infrastructure employing self-consolidating concrete.

Field tests have largely demonstrated reserves of strength capacity of in-service bridges despite their visual condition and age. Sources that explain the difference are diverse and may be attributed to several in-situ parameters that are not considered during the design or strength evaluation of a bridge's structure. Load testing is a powerful approach used to assess the structural performance of bridges because it provides an in-service, as-built characterization of the bridge's performance. The AASHTO Manual for Bridge Evaluation[7] presents two test options: proof load tests and diagnostic load tests. Proof load tests are employed to obtain the maximum safe live load a bridge can withstand without undergoing inelastic deformations, while diagnostic load tests are used to better understand the service response of a bridge. Diagnostic tests are also employed to validate design assumptions and to corroborate the structure's response improvements due to field factors deemed as beneficial for the bridge's performance[8]. These factors have a direct influence in the estimation of the dynamic load allowance (impact factor) and lateral load distribution of a bridge, which affects its load rating.

The tasks conducted on this research included (1) static load tests; (2) dynamic load tests; and (3) the calibration of refined finite element models (FEM) simulating the static loads acting on the bridge superstructure during the first series of diagnostic tests. The main objective of this study centered on (a) presenting a diagnostic test protocol using robust and reliable measurement devices (including noncontact laser technology) to record the bridge's benchmark in-service response; and (b) obtaining the spans' performance to evaluate and compare the SCC girders' response to the conventional concrete girder's behavior when subjected to service loads.

RESEARCH SIGNIFICANCE

In the United States, the Federal Highway Administration and some State Departments of Transportation have made important efforts to employ self-consolidating concrete in infrastructure projects. Bridge A7957 was the first implementation project built by the Missouri Department of Transportation using normal-strength and high-strength self-consolidating concrete (NS-SCC and HS-SCC) in its main supporting members. The results presented herein are part of an ongoing research program whose main objective was to provide an implementation test bed and showcase the use of SCC in a field project. This stage of the research focused on monitoring and comparing the initial in-service response of the different spans of the bridge. It is hoped that the results presented herein can be used by researchers and engineers to further understand the initial in-service behavior of prestressed SCC members. In addition, it is expected that these results will help establish an experimental load rating benchmark of the PC girders to monitor changes in the long-term as their different concrete mixtures are exposed to the same environmental conditions and loads.

BRIDGE DESCRIPTION

Bridge A7957 is a three-span, continuous bridge with a 30-degree skew angle and a smooth surface condition (Fig. 1), fabricated with PC girders. The Nebraska University (NU) 53 PC girders [Fig. 1(c)] in each span were designed with concrete mixtures of different compressive strength[4, 9]. The girders in the first span are 30.48 m (100 ft) long and made of conventional concrete (MoDOT's Class A mixture) with a nominal compressive strength of 55.2 MPa (8,000 psi). Girders in the second span are 36.58 m (120 ft) long and were fabricated with a high-strength self-consolidating concrete (HS-SCC) mixture of 68.9 MPa (10,000 psi). The third span measures 30.48 m (100 ft) and employed normal-strength self-consolidating concrete (NS-SCC) with a target compressive strength of 55.2 MPa (8,000 psi). PC panels with a specified compressive strength of 41.4 MPa (6,000 psi) extend between the top flanges of the girders in the transverse direction and underneath a cast-in-place (CIP) reinforced concrete (RC) deck [Fig. 1(c)]. The CIP deck was cast with a 25% fly ash replacement mixture of portland cement concrete having a design strength of 27.6 MPa (4,000 psi). Two intermediate bents and two abutments support the superstructure [Figs. 1(a) and 1(b)]. The abutments and the second intermediate bent were cast with a concrete mixture using a 20% fly ash replacement of portland cement with a nominal compressive strength of 20.7 MPa (3,000 psi). The third intermediate bent was built using high-volume fly ash concrete (HVFAC) with a 50% fly ash replacement of portland cement and a specified compressive strength of 20.7 MPa (3,000 psi). Complete details about the girders production and the mixtures employed on this bridge have been documented elsewhere[4, 10].

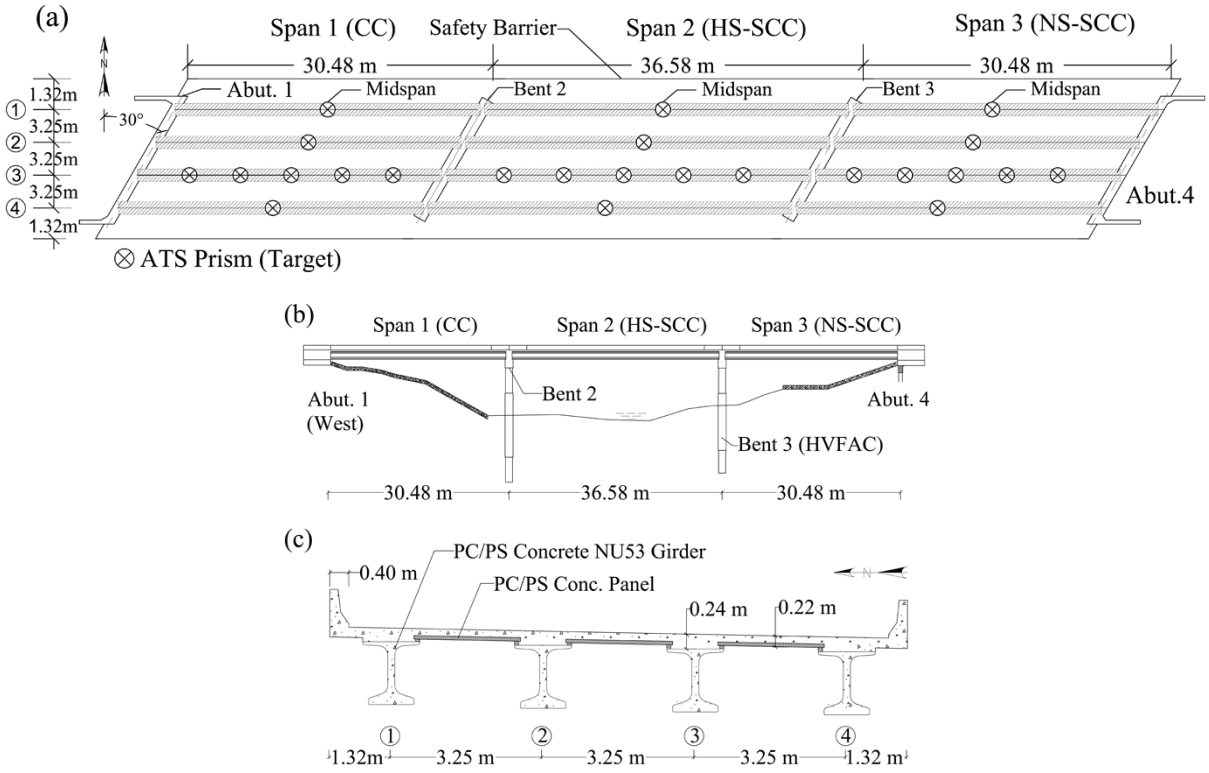

Fig. 1—Bridge A7957: (a) Plan view and ATS target (prism) locations; (b) elevation; (c) cross section. Conversion factor: 1 m = 3.28 ft.

TEST EQUIPMENT

The instrumentation was designed to collect (a) the static vertical deflection at midspan of girders 1–4 (spans 1–3) as shown in Fig. 1(a); (b) the static vertical deflection at several sections along girder 3 (spans 1–3); and (c) the vertical dynamic deflection at girder 3's midspan (only spans 1 and 3). The next sections present details about the non-contact laser equipment employed to collect data described in (a)–(c).

Automated total station

An automated total station (ATS), Leica TCA2003 (Fig. 2) with an accuracy of 1 mm (0.039 in.) ± 1 ppm (parts per million) for distance measurements and 0.5 arc-seconds (angular measurements) was employed to record the

girders' vertical deflection along girder 3's critical sections and at each girders' midspan during the first series of diagnostic tests. The ATS obtains three-dimensional (3D) coordinates of every target by measuring the horizontal and vertical angle as well as the distance between the ATS and target prisms. The instrument was configured to take three readings per target. This is done by four internal diodes installed to optically read a fine bar code set on a glass ring inside the Leica TCA2003. During monitoring, the equipment continuously read the bar codes on the horizontal and vertical planes by sending a laser ray that reflects on the targets mounted on the structure. The accuracy of the ATS has been reported to be ±0.1 mm (0.004 in.) in vertical deflection measurements[11]. Twenty-four critical locations were selected to monitor the superstructure response. Fifteen ATS prisms were deployed along the third girder at 1/6L, 1/3L, 1/2L, 2/3L, and 5/6L of each span. Three additional prisms were placed at the rest of the girders' midspan (1/2L) for each span [Fig. 1(a)]. MoDOT H20 dump trucks loaded the bridge superstructure[12] during the static tests as shown in Fig. 2(a). The prisms [Fig. 2(b)] have an internal magnet that keep them fixed to steel plates that were previously attached to the girders' bottom flange with an epoxy adhesive.

(a) (b) (c)

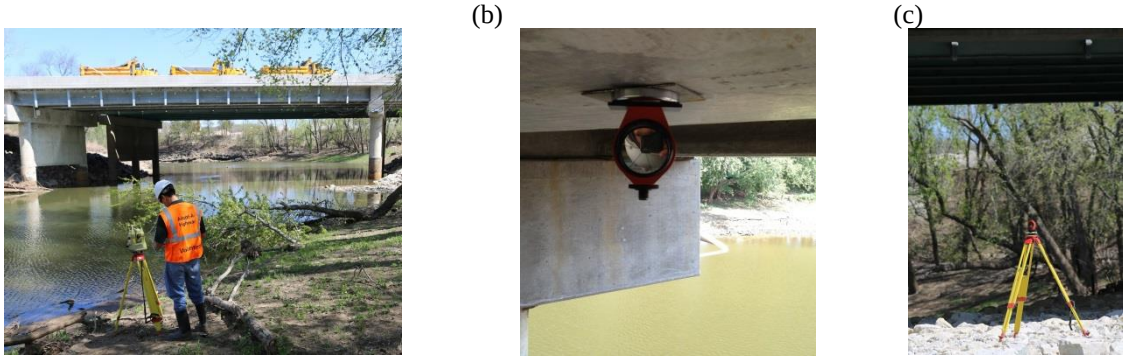

Fig. 2—Automated total station: (a) Leica TCA 2003; (b) target (prism); (c) reference target.

Remote sensing vibrometer

A remote sensing vibrometer (RSV-150) (Fig. 3) was utilized to collect the dynamic bridge response (vertical deflection) of the exterior spans' girder 3 (midspan sections). The RSV-150 has a bandwidth up to 2 MHz for nondestructive test (NDT) measurements and can detect the vibration and displacement of distant structures with limited access. The accuracy of the RSV-150 is ±0.025 mm (0.001 in.) when it records the dynamic response of a member.

Fig. 3—Remote sensing vibrometer (RSV-150).

DIAGNOSTIC TEST

Static and dynamic tests were performed on the superstructure of Bridge A7957. The static load tests were performed on three different dates (days 1-3 in Table 1) due to time restrictions. The dynamic tests were performed on day 3 (see Table 1). The following subsections describe the test procedures and load configurations planned to

obtain the maximum static and dynamic response of the bridge superstructure the authors have reported elsewhere[12-15].

Static load tests

Figure 4 presents the average trucks' dimensions and Figs. 5–6 show details of the static load configurations used to obtain the maximum bridge's response when a single lane or two lanes were loaded. For load stops 1–3, two lanes of trucks were driven from east to west. The trucks were parked separately at the center of spans 3, 2 and 1 [Fig. 5(a)–5(c)]. For stops 4–6 [Fig. 5(d)–5(f)], the trucks were driven from west to east, and parked separately at the center of spans 1, 2, and 3.

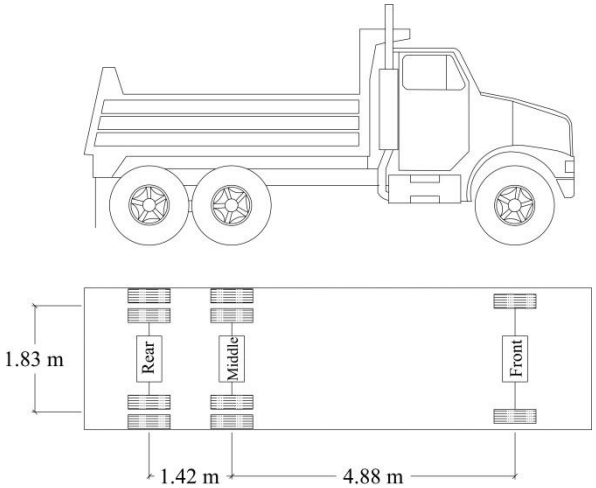

Fig. 4—MoDOT's H20 dump truck employed during diagnostic test. Conversion factor: 1 m = 3.28 ft.

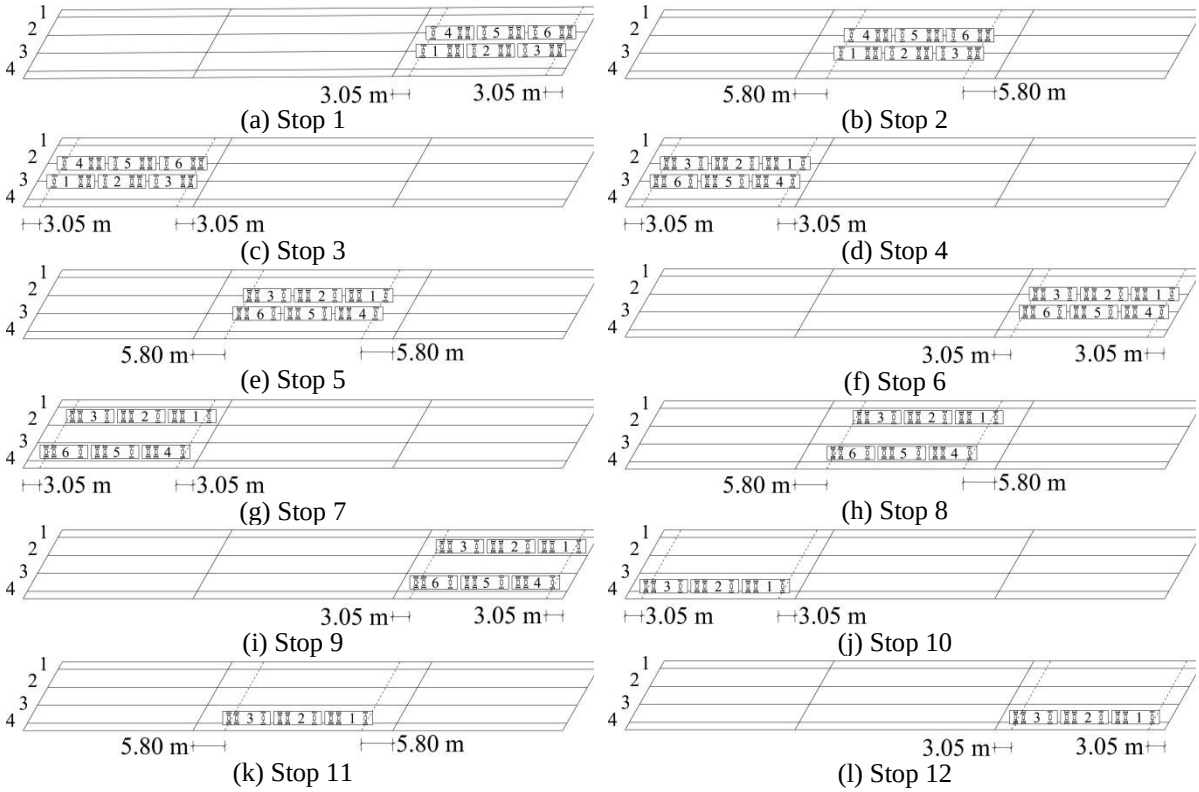

Fig. 5—Static load test configurations. Conversion factor: 1 m = 3.28 ft.

For these first six load stops, the center of the trucks' exterior wheels was separated 3.25 m (10.67 ft) from the safety barrier's edge, as illustrated in Fig. 6(a). For stops 7–9, the trucks were driven from west to east, as illustrated in Fig. 5(g)–5(i). The trucks' exterior axles were separated 0.60 m (2 ft) from the barrier's edge [Fig. 6(b)]. These first nine stops simulated two-lane load cases. For stops 10–12 [Fig. 5(j)–5(l)], a lane of three trucks

was driven from west to east along the south side of the bridge, and the trucks were separated 0.60 m (2 ft) from the barrier's edge [Fig. 6(c)]. The trucks' weights (as reported by MoDOT personnel) are listed in Table 1.

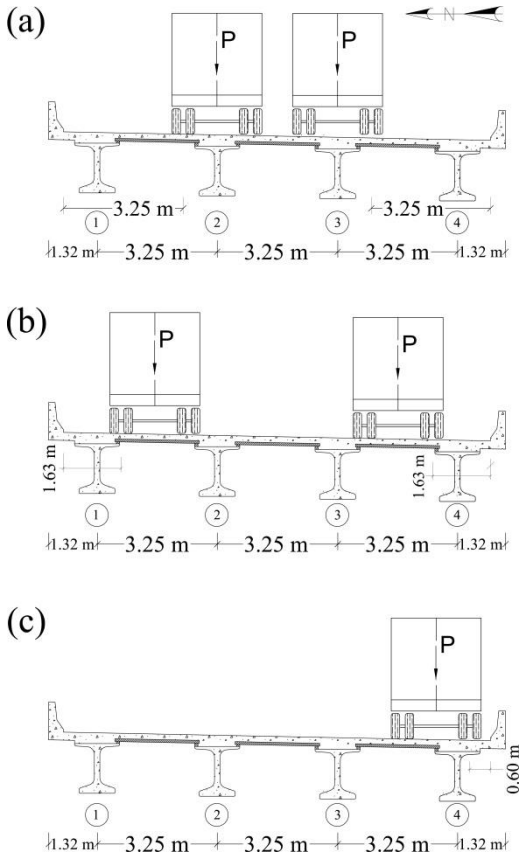

Fig. 6—Distance from trucks' exterior axle to barrier's edge: (a) Stops 1–6; (b) stops 7–9; (c) stops 10–12. Conversion factor: 1 m = 3.28 ft.

Table 1—Truck weights.

Test Day	Truck	Rear (kN)	Front (kN)	Total (kN)
1, 2*	1	158.2	74.0	232.2
1, 2*	2	161.6	57.2	218.8
1, 2*	3	150.3	56.0	206.3
1, 2*	4	178.0	75.3	253.3
1, 2*	5	170.2	77.9	248.1
1, 2*	6	166.4	71.6	238.0
3	1	164.6	61.1	225.7
3	2	180.3	70.8	251.1
3	3	169.1	70.4	239.5

Note: * Trucks remained loaded with the same weight on both days. Conversion factor: 1 kN = 0.2248 kip.

Dynamic load tests

A truck was driven at speeds ranging from 16 km/h (10 mi/h) to 97 km/h (60 mi/h) during different dynamic load tests (Fig. 4). During each test, the speed was kept constant starting with 16 km/h (10 mi/h). Then, the speed was increased at a rate of 16km/h (10mi/h) until the maximum speed of 96 km/h (60 mi/h) was attained for the last test. The maximum dynamic and static responses were compared to estimate the experimental dynamic load allowance. Experimental data was recorded with the RSV-150 at a sampling rate of 120 Hz. The truck was driven over the south side of the bridge (along the west–east and east–west directions), separated 0.60 m (2 ft) from the safety barrier's edge [Fig. 6(c)].

TEST RESULTS

Static load tests

The vertical deflections resulting from the load stops described above are given in Figs. 7–11. A preliminary examination of the data indicates the accuracy of the vertical deflection values estimated with the data recorded by the ATS. It is observed that the bridge's spans showed a continuous response to the load applied during the tests.

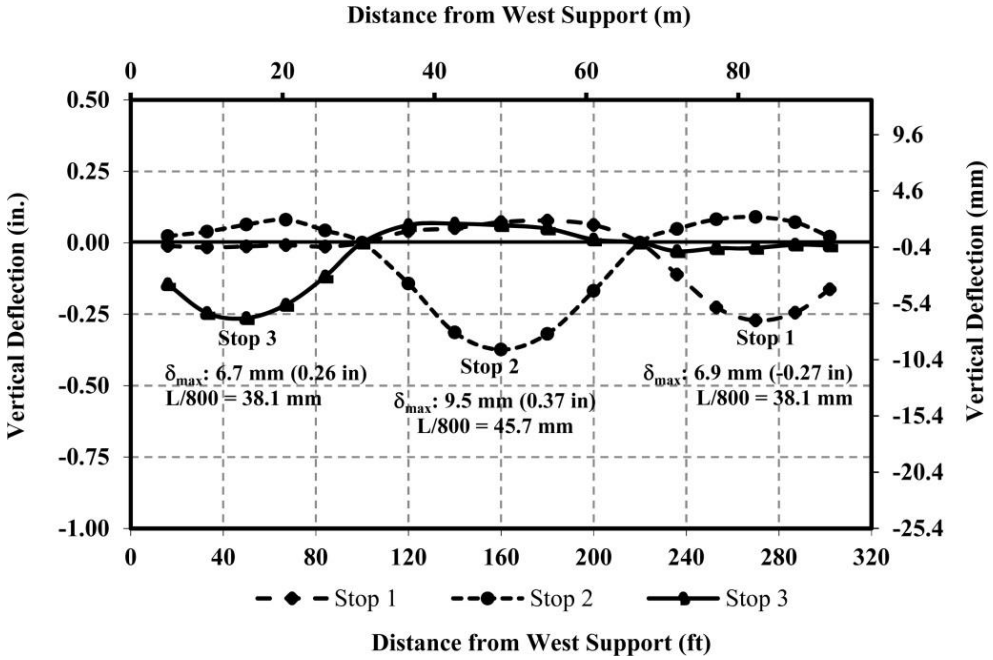

Fig. 7—Girder 3's vertical deflection (stops 1–3).

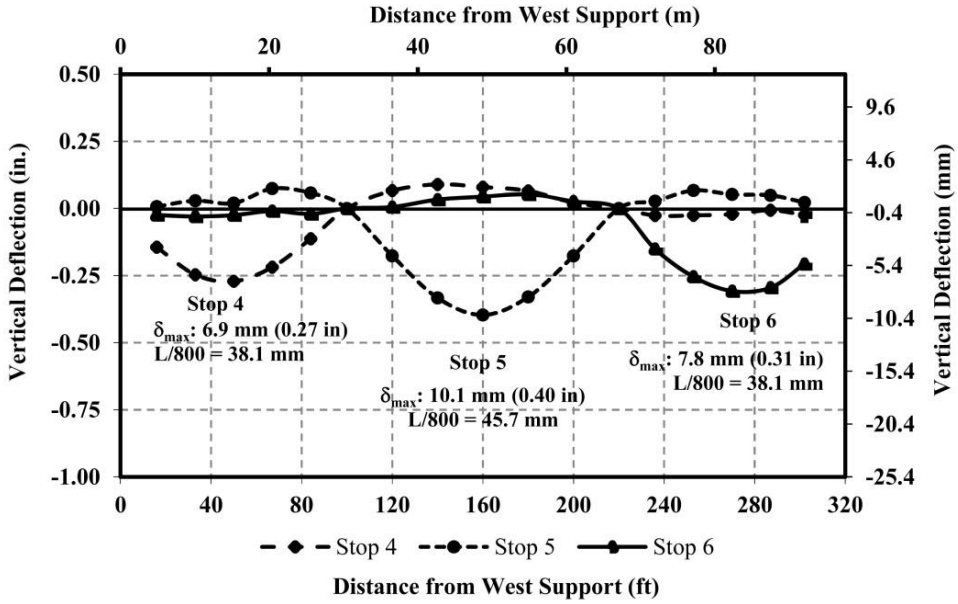

Fig. 8—Girder 3's vertical deflection (stops 4–6).

Figures 7–9 present the vertical deflections obtained along girder 3 for the stops 1–9 described above. The largest vertical deflection was obtained for span 2 (during stop 5) corresponding to a value of 10.1 mm (0.40 in.). This value was less than the maximum allowable live-load deflection of *L/800* = 45.7 mm (1.8 in.), recommended by current US bridge design codes[16, 17].

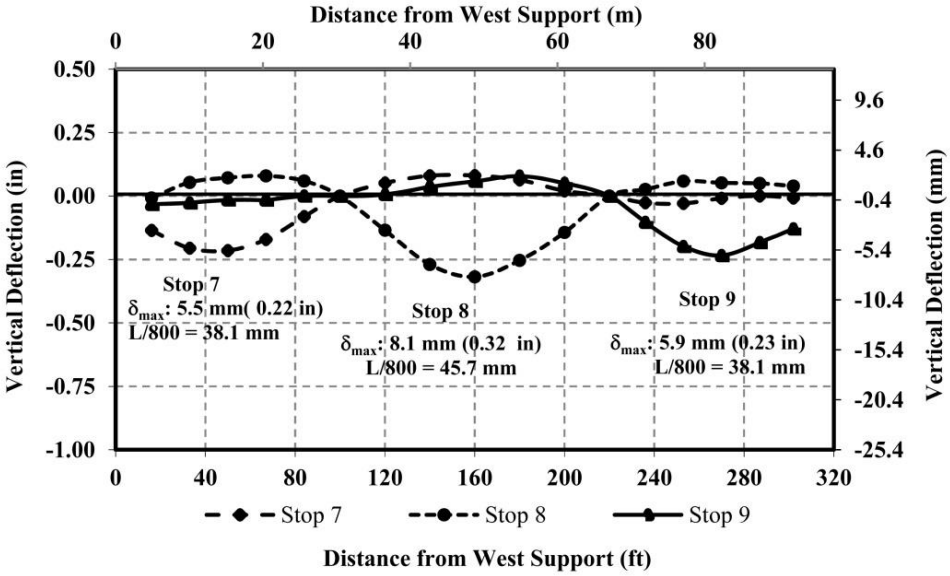

Fig. 9—Girder 3's vertical deflection (stops 7–9).

For load stops 10–12, vertical deflections were not recorded along girder 3. For these load stops, the vertical deflections were collected at the girders' midspan (across the bridge's transverse direction), and their values are shown in Figs. 10–11.

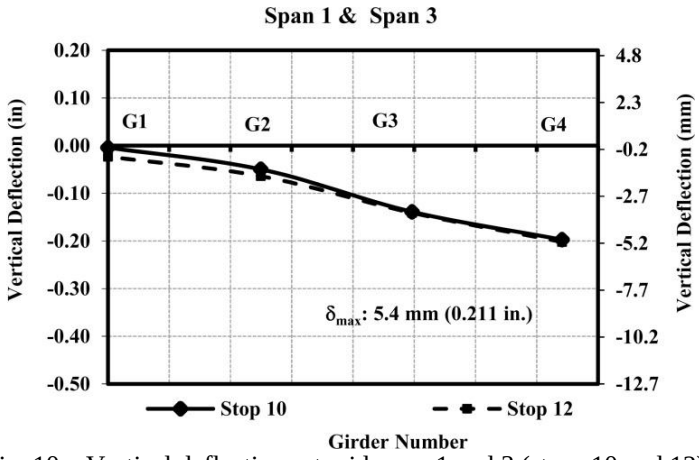

Fig. 10—Vertical deflections at midspans 1 and 3 (stops 10 and 12).

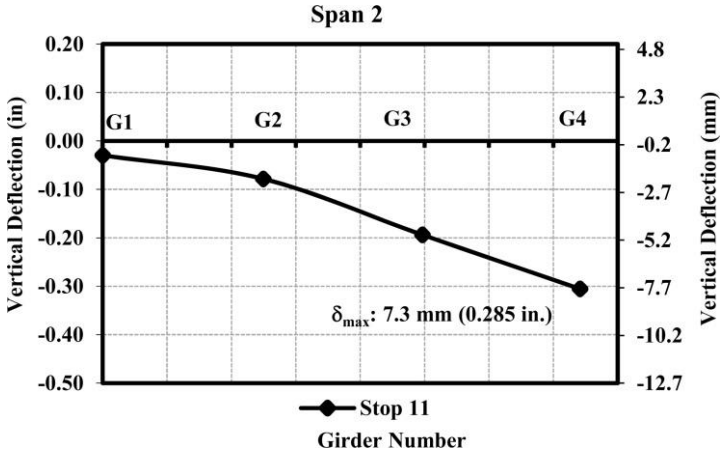

Fig. 11—Vertical deflections at midspan 2 (stop 11).

The experimental vertical deflections at the girders' midspan (along the transverse direction) obtained during load stops 1–12 are listed in Table 2. The error committed by the ATS when it collected data is listed within parentheses. In the case of two lanes loaded, comparable values were obtained corresponding to stops 1 and 3 (used to compare span 3 and 1's responses when the trucks were facing west), stops 4 and 6 (loading spans 1 and 3 when trucks were facing east, far from safety barriers), and stops 7 and 9 (loading spans 1 and 3, trucks facing east, closer to safety barriers). Larger deflections were obtained for the girders near the truck loads in the case of one lane loaded. For stops 10 and 12 (span 1 and 3's response), a larger difference ratio was observed when girders 1 and 2 of both end spans (1 and 3) were compared. This difference may be related to the accuracy of the ATS [±0.1 mm (0.004 in.) in vertical deflection measurements] that is close to the measured deflection values. When one lane was loaded (stops 10–12), the error committed by the ATS when recording girders 1 and 2's vertical deflection varied between 5% and 100% (Table 2, columns 3 and 4). This suggests that the magnitude of the loads applied during a diagnostic test should be large enough so that the span loaded directly undergoes vertical deflections larger than 2 mm. This level of load will ensure that the measurement error is kept below 5% when the ATS is employed to record data. In general, the girders' response in spans 1 and 3 (two lanes loaded) was within the same order of magnitude, implying that the spans' response during the first series of diagnostic tests was independent of the type of material used to fabricate the PC girders (i.e., conventional concrete and normal strength self-consolidating concrete). For load stops 1–9 (two-lane loads), the maximum error was below 2%.

Table 2—Vertical deflection at midspan (mm).

Stop	Span	δ_{G1} (mm)	δ_{G2} (mm)	δ_{G3} (mm)	δ_{G4} (mm)
Two Lanes Loaded					
1	3	4.2 (2%)	7.1 (1%)	6.9 (1%)	4.6 (2%)
2	2	6.3 (2%)	9.7 (1%)	9.5 (1%)	6.2 (2%)
3	1	5.1 (2%)	6.9 (1%)	6.7 (1%)	4.9 (2%)
4	1	4.2 (2%)	6.7 (1%)	6.9(1%)	4.4 (2%)
5	2	6.4 (2%)	9.8 (1%)	10.1 (1%)	6.4 (2%)
6	3	4.9 (2%)	8.4 (1%)	7.8 (1%)	5.2 (2%)
7	1	4.9 (2%)	5.1 (2%)	5.5 (2%)	5.7 (2%)
8	2	7.3 (1%)	7.8 (1%)	8.1 (1%)	7.6 (1%)
9	3	4.4 (2%)	5.5 (2%)	5.9 (2%)	5.9 (2%)
One Lane Loaded					
10	1	0.1 (100%)	1.3 (8%)	3.5 (3%)	5.0 (2%)
11	2	0.8 (13%)	2.0 (5%)	4.9 (2%)	7.7 (1%)
12	3	1.2 (8%)	2.1 (5%)	3.5 (3%)	5.4 (2%)

Note: Conversion factor:1 in = 25.4 mm.

Dynamic load tests

The dynamic load allowance (DLA) has been commonly defined as the ratio of the maximum dynamic and static responses regardless of whether the two maximum responses occur simultaneously[18, 19]. Equation (1) was employed to estimate the experimental DLA of Bridge A7957 as reported in[15]:

$$DLA^{exp} = \frac{{D_{dyn}}^{max} - {D_{sta}}^{max}}{{D_{sta}}^{max}} \quad (1)$$

where DLA^{exp} = experimental dynamic load allowance; ${D_{dyn}}^{max}$ = maximum dynamic (measured) vertical deflection (mm); and ${D_{sta}}^{max}$ = maximum static deflection (mm). Some researchers[19, 20] have stated that the maximum static response of a bridge can be obtained by (1) conducting a quasi-static test where vehicles move across the bridge at a low speed between 5–16 km/h (3–10 mi/h); (2) filtering the measured dynamic response with a low-pass filter to eliminate the dynamic components of signal; or (3) using finite element models (FEM) to calculate the static response when the vehicle weight and loading position are known. In this study, the first option was used to obtain Bridge A7957's DLA (i.e., the values of the ${D_{dyn}}^{max}$ and ${D_{sta}}^{max}$ were recorded with the RSV-150 and used to estimate the DLA^{exp}). Dynamic and quasi-static deflection values reported in[15] were used to obtain the DLA of Bridge A7957. Figure 12 shows the maximum static and dynamic vertical deflection recorded with the RSV-150 when the truck passed over the bridge at speed of 96 km/h (60 mi/h).

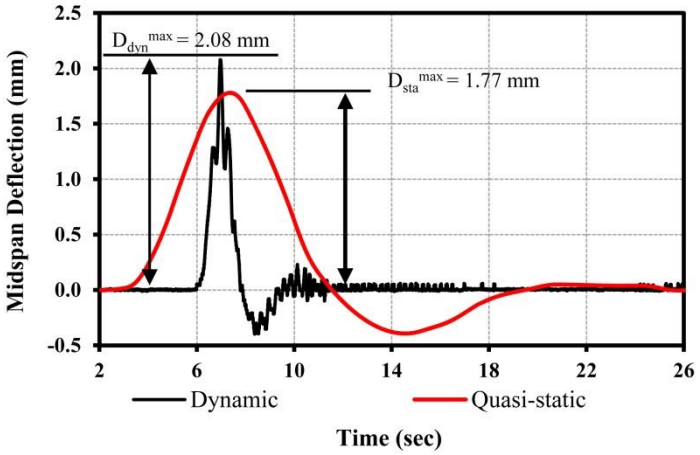

Fig. 12—Maximum static and dynamic vertical deflection. Conversion factor:1 in = 25.4 mm.

The bridge's static and dynamic maximum deflections recorded for the different speeds are listed in Table 3 (rows 3 and 4). Equation (2) was employed to estimate the experimental dynamic amplification factor, DAF^{exp}, listed in row 4 of Table 3:

$$DAF^{exp} = (1 + DLA^{exp}) \quad (2)$$

When the maximum experimental dynamic load allowance value ($DLA^{exp} = 0.175$) listed in Table 3 was compared to the AASHTO LRFD design value presented in[16], it was observed that the value proposed by AASHTO LRFD ($DLA = 0.33$) was conservative at this initial stage of Bridge A7957's service life. Differences between the experimental and analytical DLA values have repercussions in the assessment and load rating of a bridge structure. For instances, the remaining capacity of a bridge component obtained by means of an analytical load rating might be underestimated when the theoretical value is larger than the experimental DLA. These differences might be attributed to several in-situ factors that are not considered by the approach proposed in current design and evaluation codes[7]. The focus of bridge design specifications is to estimate the value of the dynamic load allowance based on several assumptions that cover a large spectrum of bridges fabricated with different materials, span lengths, and specific in-situ conditions. In this study, the experimentally obtained DLA values consider in-situ parameters that may improve the bridge's static and dynamic response such as unintended support constraints and continuity, skew angle, contribution of secondary bridge components, and soil-structure interaction. Other parameters such as the surface roughness of a bridge slab, have been recognized as one of the main causes of excitation in vehicle-induced bridge vibrations[21]. A poor road surface condition is a key factor in the underestimation of the DLA by current design and evaluation codes. However, the dynamic impact of moving traffic can be reduced if maintenance of the road surface is scheduled regularly. For this study, as the bridge road surface condition was smooth at the time of the load test, its influence was assumed to be unimportant. Moreover, the static and dynamic response of Bridge A7957's spans will vary in the long term as their PC girders (fabricated with conventional concrete and SCC) age or are subjected to overloads. The experimental protocol followed in this study is a useful tool that can be employed to update the DLA of the bridge at different stages of its service life and can provide an in-service, as-built characterization of the bridge's performance. Further research is necessary to isolate the influence of beneficial or detrimental in-situ parameters to the dynamic response of prestressed bridge structures.

Table 3—Dynamic load allowance.

	Truck Speed (km/h)					
	16	32	48	64	80	96
D_{sta}^{max} (mm)	1.77	1.77	1.77	1.77	1.77	1.77
D_{dyn}^{max} (mm)	1.77	1.79	1.79	1.77	2.03	2.08
DLA^{exp}	0.000	0.010	0.010	0.000	0.150	0.175
DAF^{exp}	1.000	1.010	1.010	1.000	1.150	1.175

Note: Conversion factor:1 in = 25.4 mm. 10 mi/h = 16 km/h.

FINITE ELEMENT MODELING (FEM)

The commercial finite element (FE) software ABAQUS[22] was used to develop 3D, linear, FE models of Bridge A7957 simulating each of the load stops depicted in Figs. 5–6. The bridge's geometry was created from construction documents and modeled with 20-node, three-dimensional solid elements (Fig. 13). The FE models simulated the bridge's geometry considering the primary members (CIP RC deck and PC girders) and secondary members (RC safety barriers and diaphragms). Each bridge component material was assumed to be linear elastic for the level of load applied during the tests. The modulus of elasticity (MOE) of the different bridge components were obtained by averaging the results of MOE tests conducted on companion specimens the same day of the tests. The MOE values of the different bridge component's materials employed to define the geometry of the bridge in ABAQUS are listed in Table 4 as reported in[4, 14]. Two different sets of MOE values were the model input, depending on whether the static load stop was conducted on days 1 and 2, or day 3 (Table 1). The boundary conditions (supports) were simulated as pin supports by (1) restraining the translation along the global axis *X* (i.e., $u_1 = 0$) of all the nodes located on a middle line (perpendicular to the global *X* axis) on the contact interface between the girders' bottom flange and supports (east and west ends); (2) restraining the translation along the global axis *Y* (i.e., $u_2 = 0$) of a node located at the center of the contact interface between the girders' bottom flange and supports; and (3) restraining the translation along the global axis *Z* (i.e., $u_3 = 0$) of all the nodes located on the contact interface between the girder's bottom flange and supports. The vertical deflection values presented elsewhere[12] were compared to FEM deflection results to calibrate the FEMs and to reproduce the bridge's initial in-service response with reasonable accuracy. The parameters used to calibrate the FE models included (1) real MOE values of the different bridge components employed to simulate the bridge's geometry; (2) adjusted support conditions to match FEM and experimental vertical deflections; and (3) secondary members (RC safety barriers and diaphragms) included in the FE models. The locations of the trucks over the slab deck and distances between the axles of the trucks were simulated as recorded for each load stop configuration. The truck axles' weight was simulated as concentrated forces applied at the locations where the trucks' wheels loaded the deck. Their values, as reported by MoDOT personnel, were previously presented (Table 1).

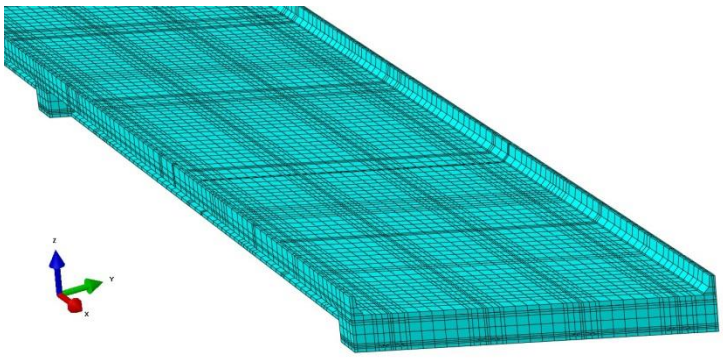

Fig. 13—Bridge A7957' FEM geometry.

Table 4—Modulus of elasticity of bridge's components (GPa).

Bridge Component	Test Days (1–2)	Test Day 3
Girders (span 1)	38.80	41.20
Girders (span 2)	39.30	42.25
Girders (span 3)	38.70	39.99
Safety Barrier	35.51	33.78
Deck and Diaphragm	31.03	31.03

Notes: Conversion factor:1 GPa = 145.04 ksi.

FEM RESULTS

Figures 14–17 present the vertical deflections obtained with the FEM simulations superimposed to the experimental results. The largest difference between the experimental and FEM deflections was close to 10% for all the interior girders. The difference might be attributed to two possible sources: first, a slight variation on the application of the truck load on each span; second, the accuracy of the ATS might have affected the measured deflections due to the level of load applied during the test. This difference will be monitored and corrected in future tests by taking caution regarding the location of the truck loads and level of load applied. In general, the FEM simulations represent the bridge's response for the different load configurations with a reasonable accuracy. These calibrated FEMs will be used to predict the response of the bridge in future diagnostic tests and to conduct "virtual" tests simulating the bridge's response of load stops that were not conducted in the field.

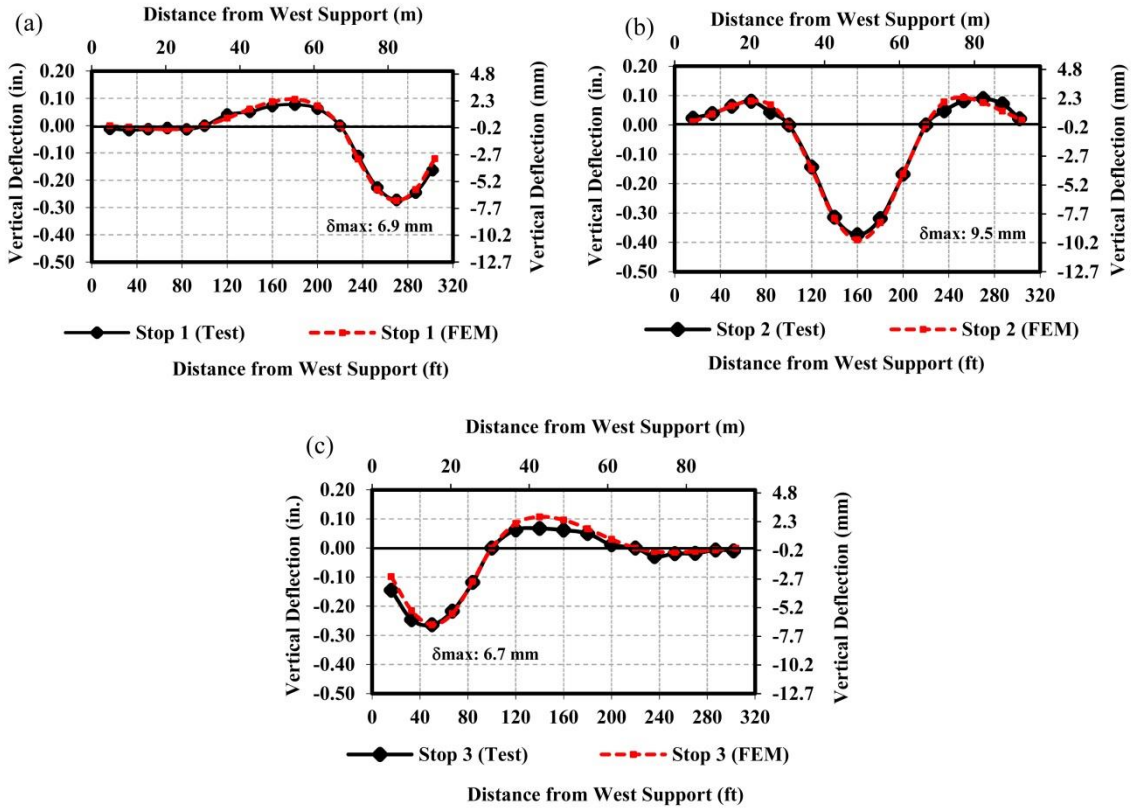

Fig. 14— Test vs. FEM results (stops 1–3).

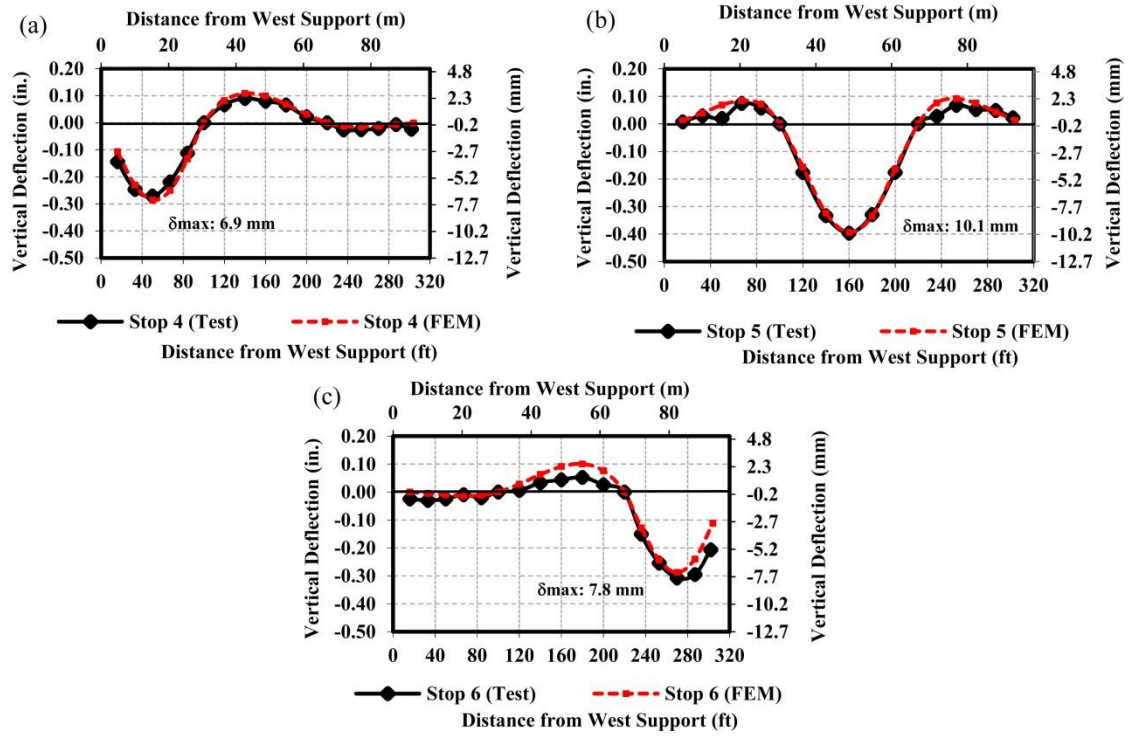

Fig. 15—Test vs. FEM results (stops 4–6).

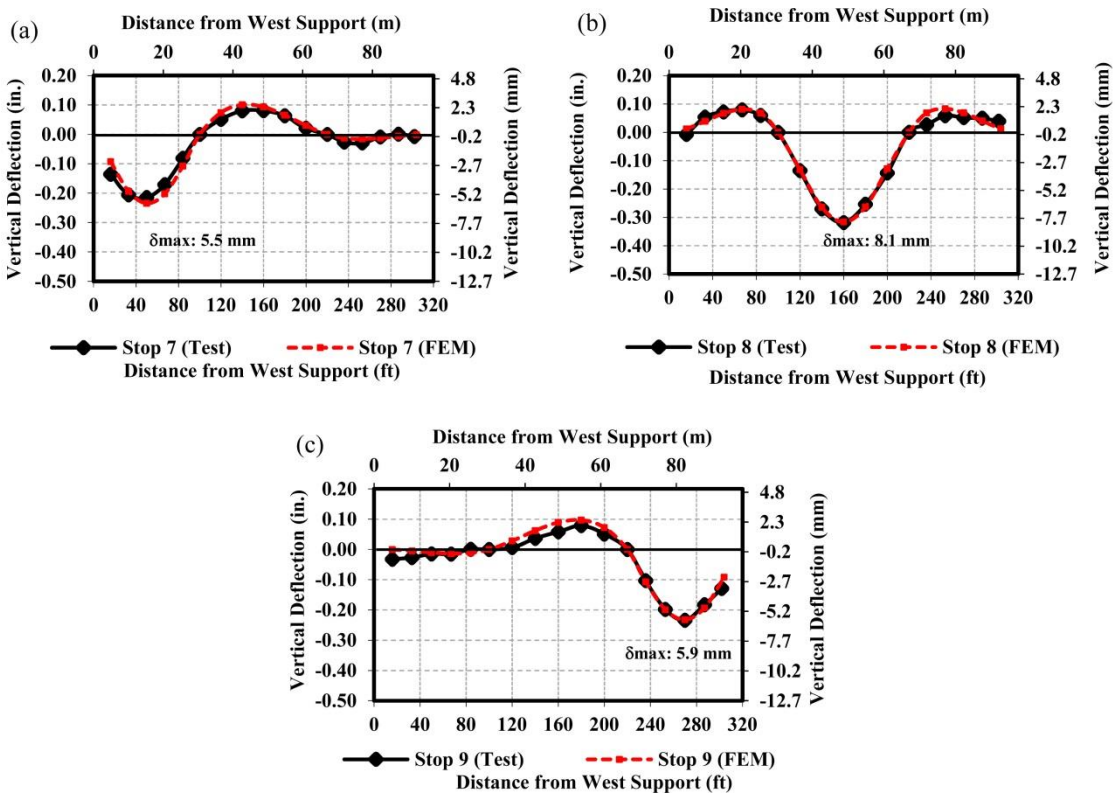

Fig. 16—Test vs. FEM results (stops 7–9).

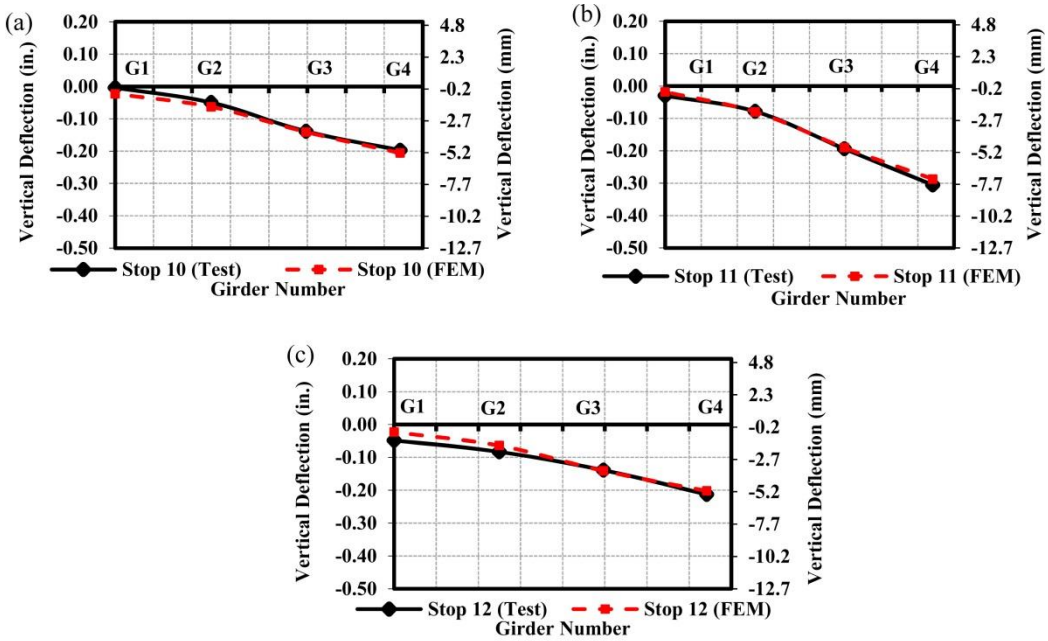

Fig. 17—Test vs. FEM results (stops 10–12).

SUMMARY AND CONCLUDING REMARKS

The Missouri Department of Transportation executed the first full-scale structure implementation of high-strength self-consolidating concrete (HS-SCC) on Bridge A7957. The first series of diagnostic tests was successfully conducted on Bridge A7957. Static tests were performed to compare the end spans' in-service response and to establish a benchmark of the different spans. These results will be employed to obtain an experimental load rating baseline of Bridge A7957. The structural performance of conventional concrete (span 1) and normal-strength self-consolidating concrete (span 3) PC girders was comparable, suggesting that the short-term structural performance

of NS-SCC and HS-SCC PC girders should not prevent its implementation in infrastructure projects. The first series of dynamic load tests were conducted on Bridge A7957 to experimentally establish its baseline dynamic response. The dynamic load allowance (DLA) of Bridge A7957 was obtained from field measurements, which was less conservative than the current value proposed by the AASHTO LRFD Bridge Design Specifications. The difference might be attributed to the presence of in-situ parameters that improve the bridge's response and are not considered by modern design and evaluation codes. Further research is necessary to isolate the influence of the beneficial or detrimental in-situ parameters to the dynamic response of prestressed bridge structures. In the long term, the static and dynamic response of Bridge A7957's spans will vary as the PC girders, fabricated with conventional concrete and SCC, age or are subjected to overloads. Therefore, it is recommended to continuously monitor and compare the spans' in-service performance to detect any change due to variations in the mechanical properties of the materials (i.e., modulus of elasticity and prestress losses). The experimental protocol followed in this study is a useful tool that can be employed to update the DLA of the bridge at different ages of its service life and can provide an in-service, as-built characterization of the bridge's static and dynamic performance. Finite element models of Bridge A7957 were developed and calibrated using experimental data collected during the different static load stops. The finite element models could represent the bridge's static response with an acceptable level of accuracy. These refined models will be used to predict the bridge's behavior in future diagnostic tests.

ACNOWLEDGEMENTS

The authors gratefully acknowledge the financial support provided by the Missouri Department of Transportation and the National University Transportation Center (NUTC) at Missouri University of Science and Technology.

REFERENCES

1. Ouchi, M., Sada-aki, N., Thomas, O., Hallberg, S.-E., and Myint, L., "Applications of Self-Compacting Concrete in Japan, Europe and the United States," ISHPC 2003, 2003.

2. McSaveney, L., Papworth, F., and Khrapko, M., "Self Compacting Concrete For Superior Marine Durability and Sustainability," *Concrete in Australia*, 37(2), pp. 59-64.

3. Keske, S.D., Miller, D.E., Barnes, R.W., and Schindler, A.K., "Live-Load Response of In-Service Bridge Constructed with Precast, Prestressed Self-Consolidating Concrete Girders," *PCI Journal*, 59(4), Fall 2014, pp. 63-76.

4. Hernandez, E.S. and Myers, J.J., "Use of Self-Consolidating Concrete and High Volume Fly Ash Concrete in Missouri Bridge A7957," *ACI SP 304–6*, 2015, pp. 85-100.

5. Myers, J.J., Volz, J., Sells, E., Porterfield, K., Looney, T., Tucker, B., and Holman, K., "Self-Consolidating Concrete (SCC) for Infrastructure Elements," *Report* No. cmr 13-003_A, Missouri University of Science and Technology, Rolla, MO, Aug. 2012, p. 204.

6. Khayat, K.H. and Mitchell, D., "Self-Consolidating Concrete for Precast, Prestressed Concrete Bridge Elements," *Report* No. NCHRP 628, Transportation Research Board, Washington, DC, 2009, p. 99.

7. American Association of State Highway and Transportation Officials (AASHTO). "The Manual for Bridge Evaluation (2nd Edition) with 2011, 2013, 2014 and 2015 Interim Revisions," Washington, DC, 2010.

8. Cai, C.S. and Shahawy, M., "Understanding Capacity Rating of Bridges from Load Tests," *Pract. Period. Struct. Des. Constr.*, Nov. 2003, pp. 209-216.

9. Hernandez, E.S., Griffin, A., and Myers, J.J., "Balancing Extended Service Life and Sustainable Concrete Material Usage in Missouri Bridge A7957," *Proceedings of the Structural Faults & Repair: European Bridge Conference (SF&R 2014)*, London, England, UK, Jul. 2014.

10. Myers, J.J., Hernandez, E.S., Alghazali, H., Griffin, A., and Smith, K., "Self-Consolidating Concrete (SCC) and High-Volume Fly Ash Concrete (HVFAC) for Infrastructure Elements: Implementation," *Report* No. Report cmr 16-011, Missouri University of Science and Technology, Rolla, Missouri, June 2016, p.

11. Merkle, W.J. and Myers, J.J., "Use of the Total Station for Load Testing of Retrofitted Bridges with Limited Access," *Proceedings of the Smart Structures and Materials 2004 - Sensors and Smart Structures Technologies for Civil, Mechanical, and Aerospace Systems,* San Diego, CA,

12. Hernandez, E.S. and Myers, J.J., "Field Load Test and Girder Distribution Factors of Missouri Bridge A7957," *Proceedings of the 2016 PCI Convention and National Bridge Conference,* Nashville, TN, March 2016.

13. Hernandez, E.S. and Myers, J.J., "Monitoring the Initial Structural Performance of a Prestressed Self-Consolidating Concrete Bridge," *Proceedings of the 8th International RILEM Symposium on Self-Compacting Concrete (SCC2016),* Washington, DC, May 2016.

14. Hernandez, E.S. and Myers, J.J., "Initial in-service response and lateral load distribution of a prestressed self-consolidating concrete bridge using field load tests," *Proceedings of the 5th International Symposium on Life-Cycle Civil Engineering (IALCCE 2016),* Delf, The Netherlands, October 2016.

15. Hernandez, E.S. and Myers, J.J., "Dynamic Load Allowance of a Prestressed Concrete Bridge Through Field Load Tests," *Proceedings of the SMAR 2017 Fourth Conference on Smart Monitoring, Assessment and Rehabilitation of Civil Structures,* Zurich, Switzerland, September 2017.

16. American Association of State Highway and Transportation Officials (AASHTO). "*LRFD bridge design specifications (6th Edition),*" Washington, DC, 2012.

17. American Association of State Highway and Transportation Officials (AASHTO). "*Standard specifications for highway bridges*," Washington, DC, 1992.

18. Bakht, B. and Pinjarkar, S.G., "Dynamic testing of highway bridges. A review," *Transportation Research Record 1223, Transportation Research Board, Washington, D.C.,* pp. 93-100.

19. Deng, L., Yu, Y., Zou, Q., and Cai, C.S., "State-of-the-art review of dynamic impact factors of highway bridges," *J. Bridge Eng.*, pp.

20. Paultre, P., Chaallal, O., and Proulx, J., "Bridge dynamics and dynamic amplification factors: A review of analytical and experimental findings," *Can. J. Civ. Eng,* 19(2), pp. 260-278.

21. Wang, T.L. and Huang, D., "Cable Stayed Bridge Vibration due to Road Surface Roughness," *Journal of Structural Engineering,* 118(5), pp. 1354-1374.

22. Dassault Systèmes Simulia Corp, "Abaqus Analysis User's Manual (Version 6.12)", Providence, RI, USA, 2012.

Extending the Life of Aged, Reinforced Concrete Arch Bridges through Load Testing and Monitoring

Jeffrey Weidner, John Prader, Nathaniel Dubbs, Franklin Moon,
A. Emin Aktan, John Taylor, and Clifford Skeens

Synopsis: The state of West Virginia is home to a substantial population of bridges that are in service well past their initial design lives. As these bridges have aged, and inevitably deteriorated, management has become a challenge. In 2006, The West Virginia Division of Highways (WVDOH) enlisted the help of Drexel University to develop an approach to managing these structures, with a particular focus on reinforced concrete bridges with little to no documentation. One such structure was the Barnett Bridge, located near Parkersburg, WV. This filled concrete arch bridge was built in 1929 with a 90 foot (27.4m) single span over a small creek. The bridge was posted due to challenges in accurately load rating the structure with only minimal historical documentation. Working side by side with WVDOH, and through a combination of load testing, repairs, and targeted long-term monitoring, the bridge was left in service. This paper presents the case study of the Barnett Bridge, from when it appeared in the local newspaper in 2008 as one of the bridges in the state with the lowest sufficiency rating, to present day where it still serves the surrounding area, with a focus on the proof load test that served as the cornerstone for the revitalization of this structure.

Keywords: Concrete Arch Bridge, Load Testing, Long-Term Monitoring, Model-Experiment Correlation, Structural Identification

ACI Member **Jeffrey Weidner** is an Assistant Professor in the Department of Civil Engineering at The University of Texas at El Paso in El Paso, Texas.

John Prader is a Project Engineer with Intelligent Infrastructure Systems in Philadelphia, PA

Nathaniel Dubbs is Practice Lead for Monitoring of Performance and Risk with Intelligent Infrastructure Systems in Philadelphia, PA.

Franklin Moon is a Professor and Undergraduate Director at Rutgers University.

A. Emin Aktan is the John Roebling Professor of Infrastructure Studies at Drexel University.

John E. Taylor is the Assistant Director of Contract Administration for the West Virginia Division of Highways.

Clifford Skeens is an employee of the West Virginia Division of Highways.

INTRODUCTION

In 2003, the state legislature of West Virginia approved Senate Bill 583 which authorized the designation of the Coal Resource Transportation System (CRTS) across the southern portion of the state. In 2005, CRTS was expanded to include additional counties. Routes which are designated as part of the CRTS are subject to gross vehicle weight permit load configurations up to 120,000 pounds (533kN). Once the program was implemented, the West Virginia Division of Highways (WVDOH) found that many of the approximately 6000 structures along these routes must be posted for loads less than the CRTS levels, and often less than standard legal loads. Often these posted structures were aged, deteriorated, concrete bridges lacking documentation.

In the subsequent five years, WVDOH allocated a portion of its research budget to solving the problem of bridges missing critical documentation, by enlisting the help of Drexel University. The Drexel team pursued two research objectives, listed below:

1. Develop and demonstrate a methodology for reliably establishing load ratings for aged bridges missing critical documentation through structural identification
2. Investigate screening approaches and experimental tools for classifying bridge populations in terms of relative risk of failure.

The latter objective served as the foundation for the development of the Targeted Hits for Modal Parameter Estimation and Rating (THMPR) system, which was awarded the 2016 Charles Pankow Award for Innovation from the American Society of Civil Engineers. This effort is outside the scope of this paper.

This paper will focus on the development of the methodology for reliably establishing load ratings for WVDOH for problematic structures via one application on an 80-year old concrete arch bridge. For this structure, the approach included material testing, finite element modeling, instrumentation, proof load testing, repairs to the structure, and long-term monitoring using a sparse, affordable instrumentation system. The full application presents a comprehensive approach to decision-making under uncertainty, using a host of tools and technologies in conjunction with one another to gather the evidence required to inform these decisions and allow WVDOH to move ahead confidently with their plans.

Background of the Barnett Bridge

The Barnett Bridge is a single span concrete arch structure located in Mineral Wells, WV which for context is near Parkersburg, WV, near the border with Ohio. The structure is not part of the CRTS, but was lumped in the research program because of some special considerations, discussed below.

The bridge was built in 1929. The main span of the bridge is 90 feet in length (27.4 m), crossing the Tygart Creek. The form of the structure is a filled arch, which means that the main structural component, the arch, is covered by a layer of fill which is boxed in by spandrel walls and the deck. The main arch component varies in thickness between 17 inches and 100 inches (43 cm and 254 cm).

The structure was retrofitted to arrest spandrel wall movements that were reportedly visible to the naked eye. The retrofit consisted of tie-backs anchored to the main arch and tensioned to the spandrel wall. The movements were arrested, but WVDOH was burdened with the need to frequently inspect the walls. The connection between the spandrel walls and the arch ring was also heavily deteriorated, which called into question the ability of the structure to contain the fill, which directly supported the roadway.

Barnett Bridge was the primary access point to an industrial area off of I-77. In 2004, the Average Daily Traffic (ADT) peaked at 15,000 vehicles per day. The condition and age of the bridge led to the decision to post the structure lower than the state legal limit of 80,000 lbs (355.9 kN). The detour was approximately 16 miles (25.7 km), stifling industry in the area to which the bridge serves. The intention was to bypass the bridge, and remove it from service. In 2008, the window of operation for the structure was five years. Many options were being considered to stretch the operational life of the structure to cover the five-year window, with cost estimates ranging up to $5 million dollars for a temporary structure to bypass the bridge. Today the bridge remains in operation, thanks primarily to efforts of this project to address performance concerns through a broad assessment approach centered on proof load testing.

Assessment Approach for Aged Concrete Structures Missing Documentation

One approach for assessing structural systems is through the paradigm of structural identification, or St-Id. St-Id stemmed from system identification as first highlighted by Liu in 1978[1]. Since then, the authors have been involved in numerous St-Id applications. In 1997, Aktan et al presented a comprehensive assessment of St-Id by looking independently at the experimental and analytical challenges of modal testing on a typical highway bridge[2,3], and decades later provided an assessment of the state of the art in 2000 and 2016[4,5]. Moon et all focused on tying St-Id projects to decision-making[6,7]. Dubbs looked at multiple model approaches to St-Id[8,9] and addressed a specific long-span bridge performance vibration question[9]. Weidner presented a case study of three bridge tests focused on safety and performance assessment through St-ID[10] and a led a comprehensive St-Id effort as part of an international bridge study[11]. Other selected St-Id applications include Brownjohn et al[12] which critically explored the challenges to the experimental side of St-Id, Sanayei et al[13] which detailed a comprehensive integration of sensing, nondestructive testing and finite element modeling for bridge evaluation, and Smith[14] which explored the role of uncertainty in St-ID. Yarnold et al presented a demonstration of St-Id based on temperature as the forcing function[15]. In 2013, ASCE released a report titled “Structural Identification of Constructed Systems: Approaches, Methods and Technologies for Effective Practice of St-ID,” lending their support to the methodology[16]. Note that there is a substantial body of literature concerning load testing that is not explicitly focused on St-Id, and is therefore not referenced here.

St-Id is a six-step process, with the overarching goal of correlating experimental data with a simulation model in order to make informed decisions. The six steps are conceptualization, a priori modeling, experiment design and execution, data reduction and analysis, model-experiment correlation, and simulation.

For this effort, more specifically the following were focus points:

(1) Determination if the structure is a candidate for load testing, and if yes…
(2) Careful field assessment of the structure both from the operational standpoint as well as the proof load testing standpoint.
(3) Material sampling and testing, in conjunction with various nondestructive evaluation.
(4) Development of a finite element model, inclusive of existing conditions, to be used for proof load testing predictions.
(5) Execution of a proof load test that not only visibly demonstrates the load carrying capacity of the structure, but also provides information for model calibration.
(6) Refined load rating based on a calibrated model, which is then available for future analyses.
(7) Monitoring for future operations

This paper will present the details of these assessments, focusing on proof load testing, and the subsequent management decisions that stemmed from the experiment and monitoring.

Determination of Load Testing Suitability

The AASHTO Manual for Bridge Evaluation (MBE) provides guidance for two types of load testing; diagnostic testing and proof testing. Diagnostic testing is conducted at lower load levels, and is designed to verify "certain response characteristics of the bridge, its response to loads, the distribution of loads, or to validate analytical procedures or mathematical models," according to the MBE 8.1.2[17]. Proof load tests are meant simply to prove that the structure can carry a given load while remaining linear-elastic. Prior to selecting the type of test to be conducted, the basic question of whether the bridge is a suitable candidate for load testing must be addressed. Table 1 lists the reasons provided in MBE for which a bridge may be considered a poor candidate for load testing, and the evaluation of these criteria for the Barnett Bridge.

Table 1 — Assessment of Load Testing Appropriateness

MBE Criteria (AASHTO MBE 8.6)	Barnett Bridge Assessment
The cost of testing reaches or exceeds the cost of bridge strengthening	The cost of the test likely approached or exceeded the cost of repairs. WVDOH was balancing several competing cost items including a stopgap solution until the nearby bypass was complete, installing repairs, and a complete shutdown. Given the existing funding mechanism and the other competing financial challenges, the cost was justified.
Pretest evaluation shows that the load test is unlikely to show the prospect of improvement in load-carrying capacity	The load posting was reflective, in itself, of the uncertainty surrounding this bridge. It was difficult to say, in an a priori sense, that the rating would improve enough.
According to calculations, the bridge cannot sustain the lowest level of load	The uncertainty plays a role here, as the expected failure mechanism of failure of a spandrel wall is not the same as predicting overload of a girder, but there was no indication that the bridge could not sustain the lowest level of load.
There is a possibility of sudden failure	Failure of the spandrel wall would be a sudden failure. However, it would likely not be a complete failure of the structure. Also, spandrel wall movement was directly measureable, and therefore worth the risk of proceeding with the test.
Load tests may be impractical due to access difficulties or site traffic conditions	Given the horizon of five years of operation for the structure until completion of the bypass, the effect on traffic and the site-specific challenges, though substantial, were worth addressing.

Table 1 indicates that, on the surface, Barnett Bridge was a poor candidate for testing. This is highlighted because the authors wish to show the versatility of load testing, and the approaches taken to ensure a safe and reliable test when detrimental conditions exist. Even if a bridge such as Barnett does not appear to be a good candidate for load testing, other extenuating circumstances such as the need to keep an older bridge in service, may make load testing and St-ID an attractive candidate to mitigate risk, reduce uncertainty and assist an owner with a problem structure. Each step of the assessment discussed below can be viewed through the lens of conducting a load test safely and reliably. Together, WVDOH and the researchers elected to pursue a load testing approach, within a structural identification framework, as it provided the most likely positive outcome in the safest and most affordable manner possible.

Initial Field Assessment

By necessity, many load rating efforts are based on review of documentation. The engineer rarely is afforded the opportunity to be on site and observe the bridge. When load testing is chosen as a means to establish a load rating, this field visit becomes absolutely critical. The insight into the performance of the bridge and the logistics of testing at that site are invaluable.

The initial field visit to Barnett Bridge was conducted in February 2008. Access to the structure was limited for the initial visit because recent rains had raised the level of the Tygart Creek up approximately ten feet. Water level was immediately identified as a primary challenge for proof load testing, given the desire to have instrumentation beneath the structure. Underside access is a challenge even when the creek level is not elevated. WVDOH proposed installing a pair of girders, braced to the integral parapet, on which a manual traveler system would be installed. This would provide access for instrumentation installation as well as future repairs. The dual purpose helped to alleviate the cost burden of this access system, which WVDOH felt was warranted given the issues with traffic interruption on this structure.

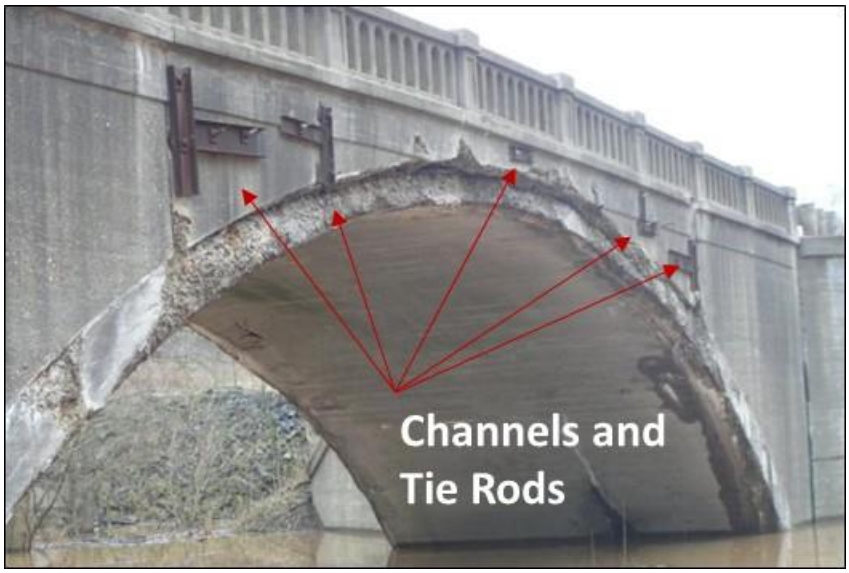

Figure 1 — Barnett Bridge in February 2008

The bridge, from the February 2008 visit, is shown in Figure 1. Extensive deterioration to the arch ring is visible, particularly at the pinnacle of the arch. In Figure 1, the channels and anchor rods from the prior repair as well as the spandrel walls are visible. The site visit revealed the susceptibility of the bridge site to flooding. The underside of the arch shows minor spalling and efflorescence, except at the edges where more extensive deterioration is visible.

In April 2008, one month before the field testing was scheduled to commence, the Parkersburg News and Sentinel newspaper ran a story focused on the upcoming bridge work, identifying Barnett Bridge as problem structure, and highlighting the bridge's current sufficiency rating of 7. The sufficiency rating was assigned based on National Bridge Inventory data and visual inspection. This type of coverage exacerbated the already difficult situation resulting from the posting.

EXPERIMENT

Typical load ratings make use of nominal properties based on original drawings, as-builts, relevant specifications, or other documentation. For the approach described herein, there was substantial uncertainty about the bridge construction and material properties due to the lack of design plans or drawings. In cases like this, spending some time and money to obtain field measurements of material properties can support refined rating, model calibration, and ultimately, comfort and confidence during proof load testing. For Barnett, material sampling allowed the team to not only get better information about material properties of the main concrete and steel elements, but also to understand

what the cross-section of the bridge looked like, inclusive of the fill. WVDOH collected samples from the structure for material testing. Nine cores were taken from the driving surface down through the arch ring. Seven of the nine cores were taken along the length of the roadway at a spacing of ten feet (3 m), centered on the arch, covering a total of 60 feet (18.3 m) in bridge length. The remaining two cores were taken at 20 feet (6.1 m) from the center of the bridge, in the transverse direction from the main longitudinal line of cores, at a spacing of six feet (1.83 m). All cores were four inches (10.2 cm) in diameter, and the maximum depth was approximately 12 feet (3.66 m). Care was taken to keep the cores intact, as each core has four distinct layers; mainly the wearing surface, concrete deck, fill material, and the arch ring. While the deck and wearing surface layers were of a constant thickness at 8 inches and 10 inches (20.3 cm to 25.4 cm), respectively, the fill material varied from six inches to 86 inches (15.2 cm to 218 cm) depending on the core location. The arch ring thickness also varied. A sample core is shown in Figure 2.

Figure 2 — Sample Core Extracted from the Barnett Bridge

Concrete cylinders were tested in compression per ASTM C39/C39M-05e2[18], and a petrographic analysis was conducted on the concrete. Cylinder compressive strength ranged from 6,000 to 12,000 psi (41,368 kPa to 82,737 kPa), with a mean of 9100 psi (62,742 kPa) and a standard deviation of 2066 psi (14,245 kPa). The variation of compressive strength may be due to differences in compaction and curing. The petrographic analysis indicated a similar concrete mix throughout the bridge, including both the deck and the arch ring. In addition, rebar samples were taken from the structure as well. Small samples taken from cores were used for chemical analysis of the steel, while larger samples were taken from areas of spalling on the bridge. These samples were machined down and tested for tensile strength per ASTM E8/E8M-04[19]. The machined samples had an average yield stress of 42 ksi (289,580 kPa) with a standard deviation of 5.8 ksi (39,990 kPa). These material properties were used as input for the finite element model that was developed for design of the proof load test. Rebar layouts were estimated using pachometer scanning once the traveler system was in place.

Finite Element Modeling and Instrumentation Design

AASHTO MBE includes the content related to nondestructive load testing developed in NCHRP Project 12-28(13)A[20] and presented in NCHRP Research Results Digest Number 234 from November 1998. For the Barnett Bridge Test, the NCHRP Research digest was referenced, but for the sake of simplicity, the MBE will be referenced herein. Neither document explicitly requires the development of a finite element model as a required step for load testing. However, the authors believe that finite element models are invaluable as experimental design tools as well as post-test interpretation tools. Further discussion of this topic is provided in the proof load testing section.

Many iterations of finite element models were explored for this project. Simplified models were considered first, including a “slice” model and a beam-frame model that represented a portion of the full structure. These models were found to be inadequate to represent the complex behavior of the soil fill. In the end, a three-dimensional solid model, shown in Figure 3, was utilized. Though it was slower computationally, the additional flexibility of the model form

was desired. The model was built in ABAQUS and contained 36,000 elements for a total of 415,000 degrees of freedom.

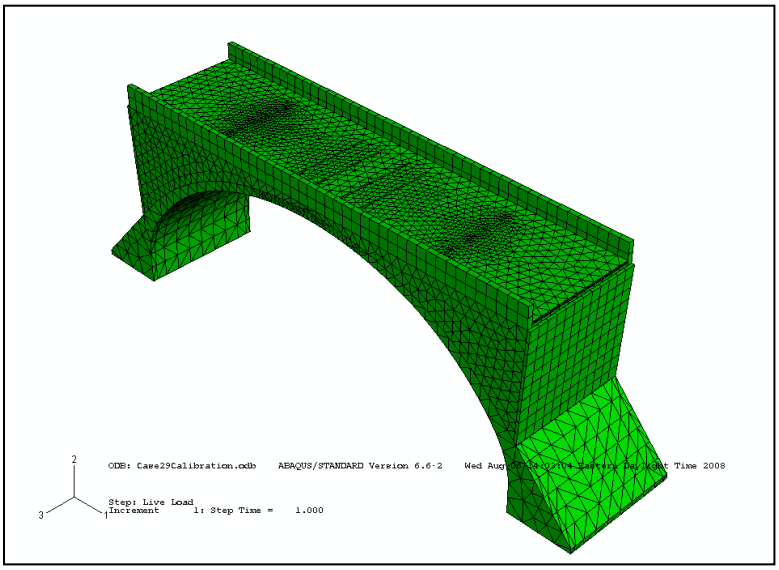

Figure 3 — Finite Element Model Utilizing Solid Elements

Prior to testing, the model was used to investigate instrumentation design requirements. Sensors were selected based on expected output due to anticipated loads that would be applied during testing. The goal was to ensure that the responses would be captured by the selected instrumentation with sufficient resolution.

Measurements consisted of vertical and lateral displacements and longitudinal rebar strains of the arch ring and tilt of the spandrel walls.

Rebar strains were measured using one inch (2.54 cm) quarter bridge strain gages that were spot welded to the rebar. The layout of these sensors is shown in Figure 4. The rebar strains were installed by chipping away concrete with a hammer drill and grinding down the rebar to create a flat, clean surface for installation. The research team felt this was important because of the condition of the surface concrete on the underside of the arch ring which would have called into question any surface sensors. Tilt sensors were mounted to the spandrel walls. The general layout of the instrumentation was in transverse lines at the ¼, ½ and ¾ position along the span, also known as transverse line C, line E and line G. Displacement sensors were not located at the ¾ position (line G), as this was in the deepest portion of the creek. Three longitudinal strain sensors each were installed at Line C and Line G, and seven longitudinal strain sensors were installed at Line E. Sensor E4 was centered on the bridge, with E1-E3 spaced at 36” (91.4 cm) OC in the upstream direction, while E5-7 were spaced at 36” (91.4 cm) OC in the downstream direction.

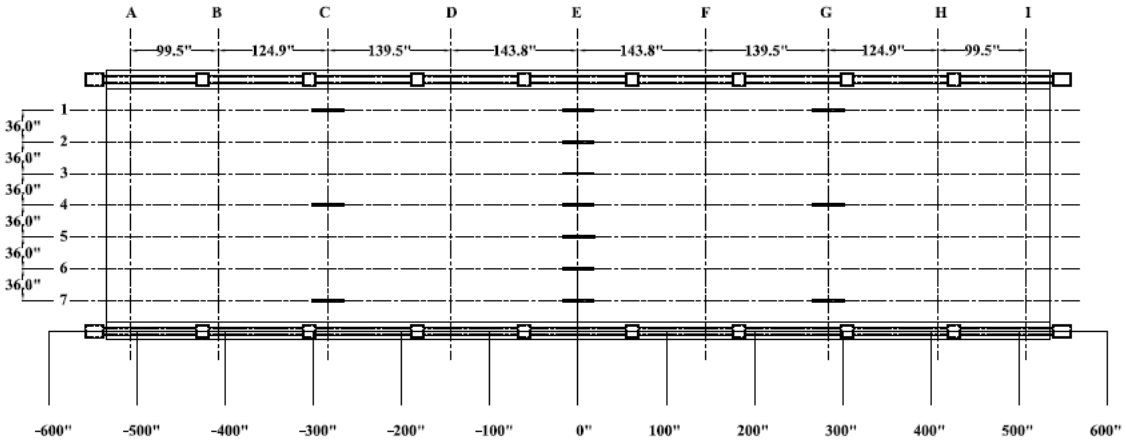

Figure 4 — Layout of Longitudinal Steel Strain Gages where Line 1 is Upstream (1 inch = 2.54cm)

The sensors selected for displacement measurement were the TML CDP Displacement Transducers, with a range of 25mm a sensitivity of $500x10^6$ strain/mm. The layout of the displacement sensors is shown in Figure 5. In order to protect the displacement sensors from the water, posts were installed in the riverbed by WVDOH, to which the sensors were mounted. Weights were then hung from the structure and the displacement of these weights was measured with the displacement sensor. Lateral displacement of the arch at the base was referenced to a post as well.

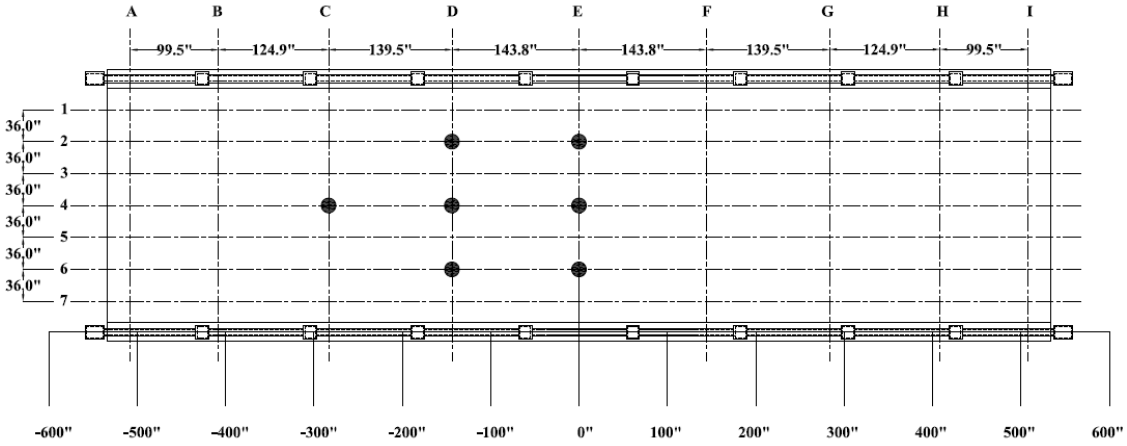

Figure 5 — Layout of Vertical Displacement Sensors where Line 1 is Upstream (1 inch = 2.54cm)

Proof Load Testing

Both proof load testing and diagnostic load testing were considered for Barnett Bridge. In the end, proof load testing was selected. The justification for this is as follows:

- The structure is shrouded in uncertainty due to a lack of as-built documentation, a heterogeneous construction method (i.e., the fill material), substantial deterioration, presence of a retrofit, and difficulty in analytically predicting load distribution and path.
- The five-year horizon for the structure shifted the mindset from a long-term management to a stopgap approach, meaning that the focus was on showing that bridge could carry load for five years, and the operating rating required to do so. The existing operating rating was 35 tons.

- The spandrel wall performance could not be readily extrapolated using diagnostic load testing data as it is non-linear.

The two requirements for stopping a proof load test are that the required proof load (per AASHTO MBE) plus a margin of safety is reached, or that the structure behaves nonlinearly. The former is easy to track during testing, as each load stage is planned out. The latter is more difficult. In order to check the linearity of the structure, two factors must be tracked. First, after each load stage, does the structure return to its initial position? Second, are the responses vs. load level plots linear? These are particularly challenging because the final load stage is most likely to be the stage where the structure exhibits some nonlinearity.

For the Barnett Bridge, the target Proof load was calculated using AASHTO MBE equation 8.8.3.3.2-2 which states:

$$L_T = X_{pA} L_R (1 + IM)$$

where:
L_T = Target Proof Load
L_R = Unfactored Live Load for Rating Vehicle and Lanes
IM = Dynamic Load Allowance
X_{pA} = Target Adjusted Live Load Factor

The target adjusted live load factor takes into account numerous factors including condition, redundancy, traffic, ratability, and inspection quality, outlined in Section 8.8.3.3.1 in the AASHTO MBE. The target proof load was determined to be 408 kips (1814 kN). The size of the structure, and the availability of loading vehicles ended up limiting the proof load to 400 kips (1779 kN). WVDOH provided four trucks capable of carrying 100 kips (445 kN) of load each, if loaded very carefully. WVDOH also created a loading site approximately one half of a mile (0.8 km) from the bridge to facilitate intermediate load stages, which is critical to tracking linearity of the structure. The loading progress went from one-quarter full, to half full, to three-quarter full, and finally completely full. The respective load values were 200k, 260k, 320k, and 400k (890 kN, 1156 kN, 1423 kN, and 1779 kN). Within a given load stage, the trucks would be positioned facing away from the bridge on either side and backed on to the bridge one at a time while monitoring responses. The final 400k (1779 kN) load stage is shown in Figure 6. Note that the fill is piled well above the top of the truck bed. Also note the presence of the girders and the traveler platform.

Figure 6 — Barnett Bridge under the 400k Load Stage

Figure 7 shows the loading versus displacement behavior of three sensors at the midspan line of the structure. Recall that sensor E2 is upstream, E4 is under the geometric center of the structure, and E6 is downstream (farthest from the

point of view in Figure 4). There is a slight nonlinearity of the midspan displacement versus the load. However, the structure returned to the initial zero position after the load was removed, and there were no signs of visible distress. The nonlinearity is attributed to differences in the load positioning within the trucks and the distribution of the load at the higher load levels due to the interaction of deck slab, fill, and arch ring. Per MBE specifications the proof load was complete and the test proved the bridge could carry the rating load without distress.

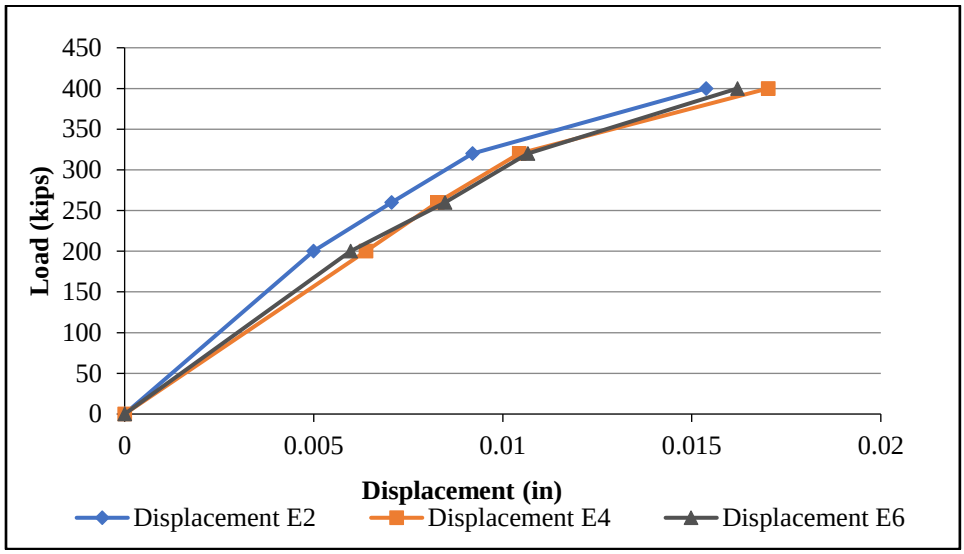

Figure 7 — Load versus Displacement at Midspan (1 inch = 2.54cm; 1 kip = 4.45 kN)

Model-Experiment Correlation

After experimental data is collected, the previously developed model can and should be updated. There are numerous methods for updating a model, including automated and manual approaches. The general approach of these manual methods is simply adjusting model parameters and evaluating if the resulting model was "better." The original Barnett Bridge model was updated using manual methods to better represent the experimental results meaning parameters were distributed and scaled based on heuristics, then the model was executed and checked against the experimental results. Numerous distributions of deterioration (through concrete modulus variation) in the arch ring were manually explored, as well as asphalt and fill properties, boundary conditions, and connectivity between the spandrel walls, the parapets, the deck and the arch ring. The material properties are shown in Table 2, and the distribution in the model in Figure 8. The location and boundaries of the different concrete and fill parameters were determined through a visual inspection of the structure and iterative analysis of model results. In the end, the most influential parameter was the connectivity between the deck and parapet, shown in Figure 9.

Table 2 — Material Properties for Calibrated Model

Value	Concrete	Semi-Weak Concrete	Weak Concrete	Asphalt	Fill-1	Fill-2
Modulus ksi (kN/m^2)	5700 (39300)	3500 (24131)	1000 (6895)	2000 (13789)	100 (689)	1000 (6895)
Poisson	0.18	0.18	0.18	0.3	0.4	0.2
Color	Orange	Green	Purple	Light Purple	Teal	Yellow

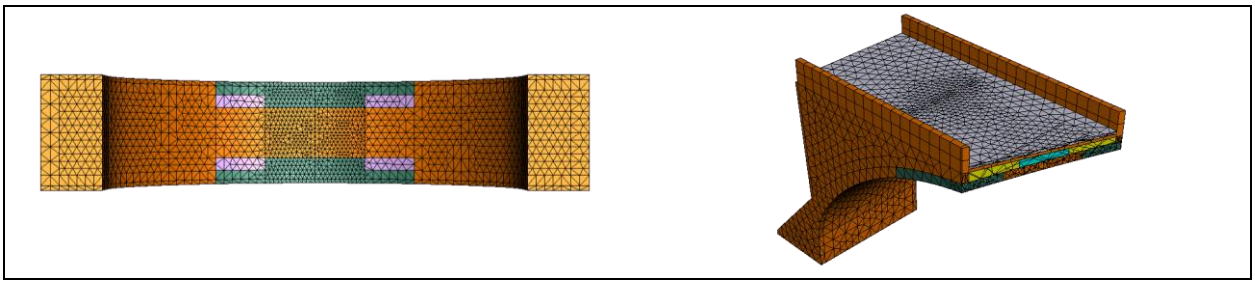

Figure 8 — Material Property Distribution for Calibrated Model

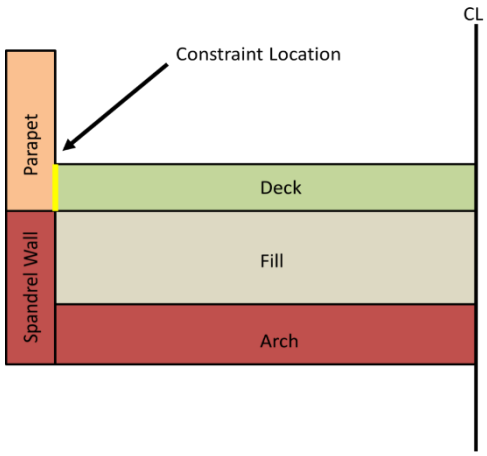

Figure 9 — Critical Constraint Location

Forcing this connectivity greatly improved the model results as compared to the experiment. Figure 10 shows a comparison of displacement across the arch at the quarter point and midpoint at the 400k (1779 kN) load stage. The model represents the global behavior of the bridge well.

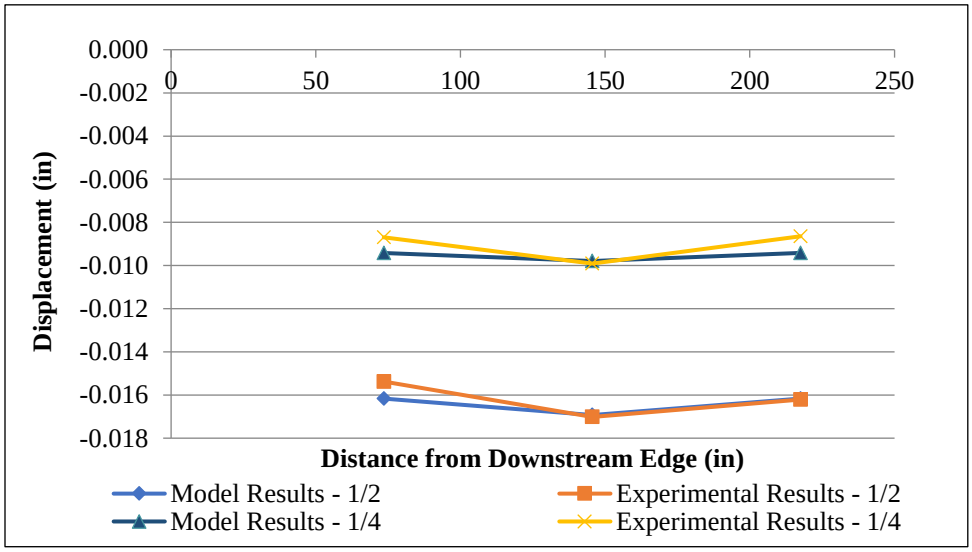

Figure 10 — Comparison of Model and Experiment at 400 kip (1779 kN) Load Stage (1 inch = 2.54cm)

While the model was not technically required to update the load posting, considering the proof load level was met, WVDOH and the research team felt that to comfortably leave the bridge in service for five years, the proof load test alone was not adequate. In essence, any load test is representative of the bridges' behavior that day. With time, any number of factors may cause the bridge to change – most notable deterioration. As Barnett was exhibiting deterioration at the interface between the spandrel walls and the arch ring, these component interfaces were seen as extremely critical. Correlation with the model was best when the model showed strong connections between components. Therefore, it was decided that repair efforts should focus on keeping the connection between the deck, parapet, spandrel walls and arch ring in the best shape possible.

Repairs and Monitoring

WVDOH made several repairs to the structure. The repairs focused primarily on the arch ring and spandrel wall connection. All deteriorated concrete was chipped away and replaced. Where required, new rebar were drilled and anchored into the arch ring and the spandrel wall. The repairs, in progress indicated by the oval, can be seen in Figure 11. Additionally, the driving surface was stripped and replaced, creating a smoother ride and better protection from intrusion of water.

Figure 11 — Repair of the Arch Ring in Progress

Despite the presence of the repairs, WVDOH and the research team were concerned about movement of the spandrel walls over the remaining life of the structure. A simple, affordable long-term monitoring system was designed to monitor these movements. The system consisted of four vibrating wire tiltmeters mounted to the spandrel walls, one in each quadrant of the bridge. The wires were run to a set location at the side of the structure that could be accessed periodically by WVDOH personnel. The sensors were interrogated by WVDOH periodically for four years after the repairs were completed. WVDOH intended to collect data monthly, but often missed a month or more at a time. The system is shown in Figure 12. The tilt data for the spandrel walls is shown in Figure 13. All four quadrants showed a period of unrecovered movement from installation in November 2008 through the end of 2009. The average value for tilt movement was 0.05 degrees, which equates to 0.01 inches/foot of length ($8.3e^{-4}$ cm/m). This movement, while apparently permanent, is very small. Starting in 2010, three of the four sensors tended to show seasonal cyclic variation of a similar, small range, while the fourth sensor returned to its original position. In all cases, the observed movement was not substantial enough to warrant any concern about the integrity of the spandrel walls or their connection to the arch ring.

Figure 12 — Long-Term Tilt Monitoring System

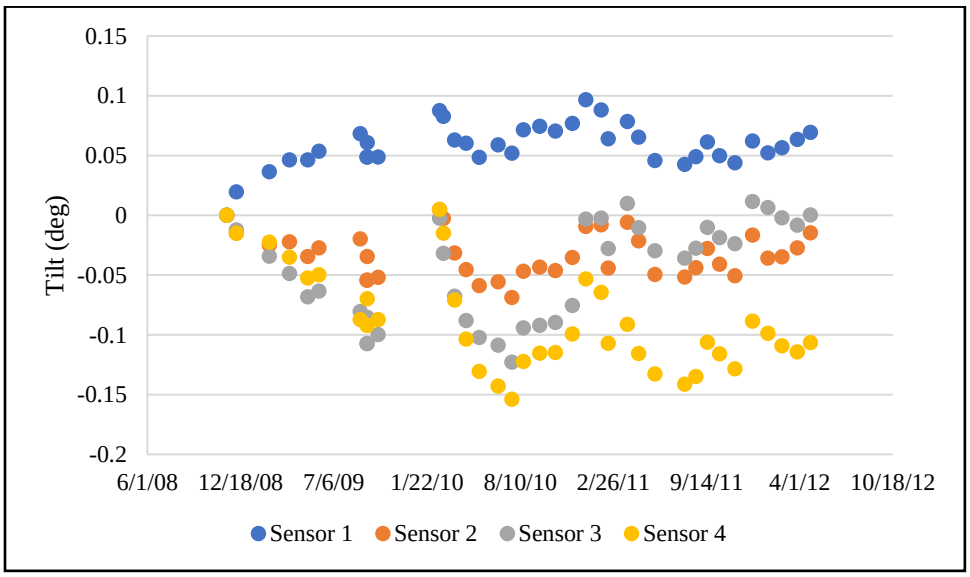

Figure 13 — Long-Term Monitoring of Spandrel Wall Tilt

Management Timeline

The prior section presented an overview of the results of a proof load test of a complex concrete structure with deterioration. What makes this case particularly interesting is the situation surrounding the bridge. The testing occurred in 2008. By 2011, construction of a bypass to the northeast of the bridge was underway, and by 2013, the bridge was completely bypassed, as shown in Figure 14.

Figure 15 shows the timeline of the end of service life for the Barnett Bridge including the relevant data for decision making. In 2005, the operating rating was decreased to around 45 tons (400 kN), then again in 2007, when the bridge was subsequently posted. At the same time, it can be seen that the average daily traffic for the bridge was increasing to its maximum value of over 15,000 vehicles per day. Of that, WVDOH estimated that 5% were trucks, many of which would have had to have been rerouted. The load test is indicated by the first black dotted vertical line. Immediately after the test, repairs began, and the monitoring system was installed in the late fall, indicated by the second vertical line. At this time, the rating was recalculated and the posting was removed. At the end of the five-year

window the bypass was completed, and there is a correspondingly large drop in ADT, which continues precipitously to less than 200 vehicles per day currently. The bridge remains in service currently.

Figure 14 — Construction of the Bypass (Circled) Relative to Barnett Bridge (Starred)

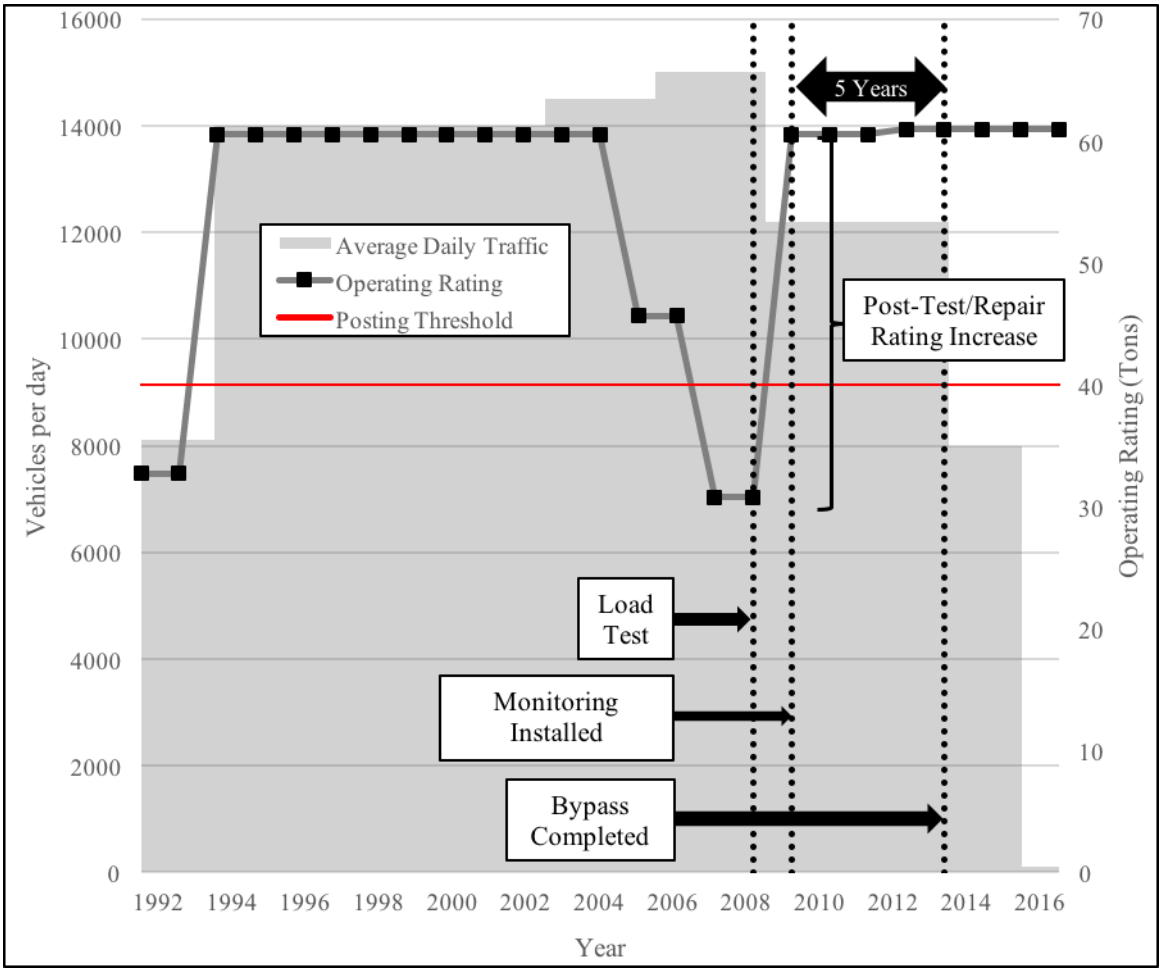

Figure 15 — End of Service Timeline for the Barnett Bridge (1 ton = 8.90 kN)

CONCLUSIONS

The focus of this effort was to develop an approach to load rating for problematic structures for WVDOH. This effort centered on proof load testing of a reinforced concrete arch. The scope of the project spanned from initial visits to the bridge in February 2008, through completion of a bypass and observations of the effects of the bypass in 2016. The load testing was part of a structural identification effort that included material sampling, finite element modeling, model-experiment correlation, and long-term monitoring. This project highlights several key issues related to load testing and how and when it is applied.

1. Load testing played a critical role in the management decision timeline for the Barnett Bridge, but the entire process as a whole gave WVDOH the confidence to implement the plan described herein. The testing, modeling, and monitoring, when combined, painted a complete picture of the bridges' current condition, and allowed WVDOH to observe the efficacy of the repairs they implemented.
2. AASHTO MBE identifies several characteristics of "unsuitable" bridges for load testing. The Barnett Bridge presents a situation where the structure could be considered unsuitable by these standards, but that was very much a candidate for load testing. This discrepancy is only visible when the entire operational and management situation was considered. In the context of expensive, temporary replacements, excessively long detours, and an imminent bypass, the cost of load testing was justified, as was the elevated risk.
3. Finite element plays a critical role in load testing. The authors concede that the MBE does not require a finite element model to conduct a load test and ultimately change a load rating/posting, instead simply requiring an analysis and leaving much to the judgement of the engineer. Many bridge managers and departments of transportation do not see the value in the model as well. However, for this test, a model was required to design the experiment and understand the results. The computational cost of models is going down every day, with some engineering firms building simple models in a near-automated fashion. Moving past the aversion to finite element modeling opens the door load testing on structures that would otherwise not be candidates. In this case the model was used to make sense of the experimental data, to calculated refined load ratings, and to explore scenarios of interest.

REFERENCES

1. Liu, S. and J. Yao (1978). "Structural Identification Concept." ASCE Journal of the Structural Division. 104(ST12): 1845-1858.

2. Aktan, A. E., et al. (1997). "Structural Identification for Condition Assessment: Experimental Arts." Journal of Structural Engineering 123(12): 1674-1684.

3. Aktan, A. E., et al. (1998). "Structural Identification: Analytical Aspects." Journal of Structural Engineering 124(7): 817-829.

4. Aktan, A. E., et al. (2000). The State of the Art in Structural Identification of Constructed Facilities. S. Doebling and C. Farrar, ASCE: 223.

5. Aktan, A. E., et al. (2016). "Leveraging Technology for Infrastructure Condition and Performance Assessment." Frontiers in Built Environment 2(36).

6. Moon, F. L., et al. (2009). Structural Identification of Various Constructed Systems to Inform Decisions. Don't Mess with Structural Engineers: Expanding Our Role, ASCE.

7. Moon, F. L., et al. (2010). Infrastructure Decision-Making based on Structural Identification. Structures Congress 2010, ASCE.

8. Dubbs, N. and F. Moon (2015). "Comparison and implementation of multiple model structural identification methods." Journal of Structural Engineering 141(11): 04015042.

9. Dubbs, N. and F. Moon (2016). "Assessment of Long-Span Bridge Performance Issues through an Iterative Approach to Ambient Vibration–Based Structural Identification." Journal of Performance of Constructed Facilities 30(5): 04016029.

10. Weidner, J., et al. (2009). Structural Identification of Bridges to Assess Safety and Performance. Structures 2009: Don't Mess with Structural Engineers, ASCE.

11. Zhou, Y., et al. (2012). Structural Identification Study of International Bridge Based on Multiple Reference Impact Study. 15th World Conference on Earthquake Engineering. Lisbon, Portugal.

12. Brownjohn, J., et al. (2008). Structural Identification of Constructed Systems: Experimental Considerations. Structures Congress 2008: Crossing Borders.

13. Sanayei, M., et al. (2012). "Instrumentation, Nondestructive Testing, and Finite-Element Model Updating for Bridge Evaluation Using Strain Measurements." Journal of Bridge Engineering 17(1): 130-138.

14. Smith, I. (2010). "Structural Identification with Correlated Uncertainties." Engineering Structures.

15. Yarnold, M., et al. (2012). "Evaluation of a long-span steel tied arch bridge using temperature-based structural identification." International Association for Bridge Management and Safety, Stresa.

16. ASCE (2013). Structural Identification of Constructed Systems: Approaches, Methods and Technologies for the Effective Practice of St-ID.

17. AASHTO (2011). The manual for bridge evaluation. Washington, DC, American Association of State Highway and Transportation Officials.

18. ASTM C39 / C39M-05e2, Standard Test Method for Compressive Strength of Cylindrical Concrete Specimens, ASTM International, West Conshohocken, PA, 2005, www.astm.org

19. ASTM E8-04, Standard Test Methods for Tension Testing of Metallic Materials, ASTM International, West Conshohocken, PA, 2004, www.astm.org

20. National Cooperative Highway Research Program (NCHRP) (1998). Manual for Bridge Rating Through Load Testing, Transportation Research Board, Washington D.C.

CONVERSION FACTORS—INCH-POUND TO SI (METRIC)*

To convert from	to	multiply by
	Length	
inch	millimeter (mm)	25.4E†
foot	meter (m)	0.3048E
yard	meter (m)	0.9144E
mile (statute)	kilometer (km)	1.609
	Area	
square inch	square centimeter (cm^2)	6.451
square foot	square meter (m^2)	0.0929
square yard	square meter (m^2)	0.8361
	Volume (capacity)	
ounce	cubic centimeter (cm^3)	29.57
gallon	cubic meter (m^3)‡	0.003785
cubic inch	cubic centimeter (cm^3)	16.4
cubic foot	cubic meter (m^3)	0.02832
cubic yard	cubic meter (m^3)‡	0.7646
	Force	
kilogram-force	newton (N)	9.807
kip-force	newton (N)	4448
pound-force	newton (N)	4.448
	Pressure or stress (force per area)	
kilogram-force/square meter	pascal (Pa)	9.807
kip-force/square inch (ksi)	megapascal (MPa)	6.895
newton/square meter (N/m^2)	pascal (Pa)	1.000E
pound-force/square foot	pascal (Pa)	47.88
pound-force/square inch (psi)	kilopascal (kPa)	6.895
	Bending moment or torque	
inch-pound-force	newton-meter (Nm)	0.1130
foot-pound-force	newton-meter (Nm)	1.356
meter-kilogram-force	newton-meter (Nm)	9.807

To convert from	to	multiply by
	Mass	
ounce-mass (avoirdupois)	gram (g)	28.34
pound-mass (avoirdupois)	kilogram (kg)	0.4536
ton (metric)	megagram (Mg)	1.000E
ton (short, 2000 lbm)	megagram (Mg)	0.9072
	Mass per volume	
pound-mass/cubic foot	kilogram/cubic meter (kg/m^3)	16.02
pound-mass/cubic yard	kilogram/cubic meter (kg/m^3)	0.5933
pound-mass/gallon	kilogram/cubic meter (kg/m^3)	119.8
	Temperature§	
deg Fahrenheit (F)	deg Celsius (C)	$t_C = (t_F - 32)/1.8$
deg Celsius (C)	deg Fahrenheit (F)	$t_F = 1.8t_C + 32$

* This selected list gives practical conversion factors of units found in concrete technology. The reference source for information on SI units and more exact conversion factors is "Standard for Metric Practice" ASTM E 380. Symbols of metric units are given in parentheses.

† E indicates that the factor given is exact.

‡ One liter (cubic decimeter) equals 0.001 m^3 or 1000 cm^3.

§ These equations convert one temperature reading to another and include the necessary scale corrections. To convert a difference in temperature from Fahrenheit to Celsius degrees, divide by 1.8 only, i.e., a change from 70 to 88 F represents a change of 18 F or 18/1.8 = 10 C.